Mode of occurrence and behaviour of mineral matter in fine coal rejects during thermal treatment

K Mphahlele

orcid.org/ 0000-0003-2677-3928

Thesis accepted in fulfilment of the requirements for the degree Doctor of Philosophy in Engineering with Chemical Engineering at the North-West University

Promoter: Prof JR Bunt

Co-promoter: Dr RH Matjie

Graduation: October 2024

DECLARATION

I, **Katlego Mphahlele**, hereby declare that this thesis entitled: “Mode of occurrence and behaviour of mineral matter in fine-coal rejects during thermal treatment”, submitted in fulfilment of the requirements for the degree Doctor of Philosophy in Engineering with Chemical Engineering, is my own work, except where acknowledged in the text and has not been submitted to any other tertiary institution in whole or in part.

Signed at Potchefstroom on the 30th day of May 2024

…….

Katlego Mphahlele

DEDICATION

In loving memory of my beloved grandfather, MV Mphahlele, and cherished friend, SV Khumalo, whose lives were sadly claimed by Covid-19. Your presence illuminated my journey through the complex paths of my academic pursuit, and your undying support and encouragement fuelled my passion to chase greatness.

Grandfather (*Rakgolo*),

You were more than just a pillar of wisdom, but also a beacon of resilience and courage. You taught me the importance of perseverance and the pursuit of knowledge. You never once doubted my journey and even in your grave, I still draw from your gentle words of guidance, and undying love as my greatest inspiration.

Friend (*Nja yam*)

Your infectious laughter and boundless enthusiasm brought joy to every moment we shared. Your brilliance and curiosity were contagious and have ignited in me a passion for academic exploration and discovery.

Though you are no longer physically with us, your spirits remain eternally woven into the fabric of my being, the remnants of which can be traced in the pages of this thesis. It is with profound gratitude and a heavy heart that I dedicate this work to you both. May your legacies endure, guiding me as I navigate the challenges ahead, and may your memories be a source of strength and inspiration for all who were fortunate enough to have experienced life with you in it.

In loving memory of MV Mphahlele and SV Khumalo,

PREFACE

Format of thesis

This thesis is formatted in accordance with the academic rules of the North-West University approved on November 22nd, 2013, where rule **A.5.4.2.7** states: “Where a candidate is permitted to submit a thesis in the form of a published research article or articles, or as an unpublished manuscript or manuscripts in article format and more than one such article or manuscript is used, the thesis must still be presented as a unit, supplemented with an inclusive problem statement, a focused literature analysis and integration and with a synoptic conclusion, and the guidelines of the journal concerned must also be included.”

Rule **A.5.4.2.8** states: “Where any research article or manuscript and/or internationally examined patent is used for the purpose of a thesis in article format to which other authors and/or inventors than the candidate contributed, the candidate must obtain a written statement from each co-author and/or co-inventor in which it is stated that such co-author and/or co-inventor grants permission that the research article or manuscript and/or patent may be used for the stated purpose and in which it is further indicated what each co-author's and/or co-inventor's share in the relevant research article or manuscript and/or patent was.”

Rule **A.5.4.2.9** states: “Where co-authors or co-inventors as referred to in A.5.4.2.8 above were involved, the candidate must mention that fact in the preface and must include the statement of each co-author or co-inventor in the thesis immediately following the preface.”

Format of numbering and referencing

A note should be made that the manuscript's general outline was adapted to ensure consistency and uniformity in formatting, referencing style, and figures and table numberings throughout the thesis. The author guidelines of the specific journals, as provided by the editor-in-chief of each journal, were adhered to. As a result, the published version of the manuscript may appear in different formatting than what is presented in this thesis. However, the technical content and heading of the manuscripts were not modified from the submitted and/or published versions, and only minor spelling and typographical errors were corrected. The reference list was included at the end of each chapter.

Supplementary information

Where necessary, relevant supplementary data were included in this thesis's Appendices section.

Nomenclature

The description of the nomenclature (notations/symbols, Greek symbols, and relevant abbreviations) was included in the text, following the guidelines of the published and accepted papers unless stated otherwise. It should be noted that notations/symbols and Greek symbols may vary between chapters, following the format of the published papers.

Letter of consent

To whom it may concern,

The listed co-authors hereby give consent that **Katlego Mphahlele** may submit the following manuscript(s) as part of his thesis entitled: Mode of occurrence and behaviour of mineral matter in fine-coal rejects during thermal treatment, for the degree Philosophiae Doctor in Chemical Engineering, at the North-West University:

Mphahlele, K., Matjie, R.H., Bunt, J.R. and Janse van Vuuren, A., 2024. Effect of fluxing inorganic element-bearing acetate composite on the distribution of pyrolytic products from Highveld partially oxidised fine-coal reject and its beneficiated residue. Fuel, 371, 131891. https://doi.org/10.1016/j.fuel.2024.131891.

Mphahlele, K., Matjie, R.H. and Bunt, J.R., 2023. Catalytic effect of reactive extraneous mineral composites on char and tar distribution during pyrolysis of Highveld partially oxidised fine-coal reject and its beneficiated residues. ACS omega, 8, pp.36479-36492. https://doi.org/10.1021/acsomega.3c05462

Mphahlele, K., Matjie, R. H., Bunt, J. R., and Uwaoma, R. C., 2023. Properties and reactivity of two oxidised and unoxidised South African Highveld fine-coal rejects and their density-separated fractions. International Journal of Coal Preparation and Utilisation, 43, pp.1451−1477. https://doi.org/10.1080/19392699.2023.2221634

(This letter of consent complies with rules **A5.4.2.8** and **A.5.4.2.9** of the academic rules, as stipulated by the North-West University).

…… 25/05/2024

John R. Bunt Date

… … 25/05/2024

Ratale H. Matjie Date

…… 28/05/2024

Romanus C.Uwaoma Date

28/05/2024

Arno Janse van Vuuren Date

List of publications

Journal articles.

Mphahlele, K., Matjie, R.H., Bunt, J.R. and Janse van Vuuren, A., 2024. Effect of fluxing inorganic element-bearing acetate composite on the distribution of pyrolytic products from Highveld partially oxidised fine-coal reject and its beneficiated residue. Fuel, 371, 131891. https://doi.org/10.1016/j.fuel.2024.131891.

Mphahlele, K., Matjie, R.H. and Bunt, J.R., 2023. Catalytic effect of reactive extraneous mineral composites on char and tar distribution during pyrolysis of Highveld partially oxidised fine-coal reject and its beneficiated residues. ACS omega, 8, pp.36479-36492. https://doi.org/10.1021/acsomega.3c05462

Mphahlele, **K.**, Matjie, R. H., Bunt, J. R., and Uwaoma, R. C., 2023. Properties and reactivity of two oxidised and unoxidised South African Highveld fine-coal rejects and their density-separated fractions. International Journal of Coal Preparation and Utilisation, 43, pp.1451−1477. https://doi.org/10.1080/19392699.2023.2221634

Conference proceedings/presentations

Mphahlele, K., Matjie, R.H. and Bunt, J.R., 2023. Catalytic effect of reactive extraneous mineral composites on char and tar distribution during pyrolysis of Highveld partially oxidised fine-coal reject and its beneficiated residues. In *40th Annual International Pittsburgh Coal Conference 2023, PCC 2023.*

Mphahlele, K., Matjie, R. H., Bunt, J. R., & Uwaoma, R. C. 2023. Chemical, mineralogical, physical, petrographic properties and reactivity of two South African fine coal refuses. In *19th International Symposium on Waste Management, Resource Recovery and Sustainable Landfilling*, CISA Publisher, Italy.

ACKNOWLEDGEMENTS

I am deeply grateful to Prof John R. Bunt, Dr Ratale H. Matjie and Dr Romanus Uwaoma for their excellent guidance, invaluable advice, and unwavering dedication throughout this study. Your support and expertise have significantly contributed towards this research and its outcomes.

An extension of appreciation is made to the following individuals and organisations/institutions for their significant contribution to the success of this study:

- Dr Xolisa Gosa and Napo Ntsasa of Mintek ACD Group for their technical assistance and provision of the acid washing facilities for this study.
- Willem Swanepoel of Bureau Veritas laboratory in Centurion for his assistance in performing proximate, ultimate, total sulphur, forms of sulphur and calorific value analyses of the samples used in this study.
- Prof Nikki Wagner and Dr Liberty Kapesi of the University of Johannesburg are thanked for their assistance with Petrography and Raman analyses, respectively.
- Dr Arno Janse van Vuuren of the Nelson Mandela University for his assistance with HR-TEM feasibility and analysis
- Morne Van Zyl of SGS for his assistance with, sample collection, density separation and performing proximate, ultimate, total sulphur, forms of sulphur and calorific value analyses of the raw and density separated samples.
- Belinda Venter of North-West University for conducting X-ray fluorescence analysis and Dr Sabine Verryn of XRD Analytical and Consulting cc for their expertise in conducting X-ray diffraction analysis of various samples.
- Moses Lelaka of Setpoint laboratories for assistance with the analysis of the leachates from various inorganic element dissolution procedures.
- Dr Roelf Venter of the North-West University School of Chemical and Minerals Engineering for his assistance with Gas Chromatography and simulated distillation analysis.

- Adrian Brock, Jan Kroeze and T Motlhabane of the North-West University, School of Chemical and Minerals Engineering for technical assistance with the Fischer Assay rig.

- Simone Peacock of the coal research group at the NWU for her contribution with administrative work.

- René Bekker, Philip Mofokeng, and Elias Mofokeng of the NWU School of Chemical and Minerals Engineering for their technical assistance with laboratory work

- Special thanks are extended to my mother, grandmother, siblings, nephew, and the rest of my family for their unwavering patience, encouragement, and support. Your love and support have been my anchor during challenging times, and I am profoundly grateful for your presence in my life.

- To my dear friends Magae Masenya, Moketla Rammala, Tshepiso Malete, Madimetja Chauke, Baatseba Ramushu, Ntombifuthi Hlatswayo and Matase Malahlela, your understanding and support have been invaluable throughout this journey. Your friendship has been a source of strength and comfort; I am deeply thankful for that.

- I am grateful for the financial support provided by the National Research Foundation (NRF) free-standing bursary MND200715544211/UID: 136078 and the South African Research Chairs Initiative (SARChI) of the Department of Science and Technology and National Research Foundation of South Africa (Coal Research Chair Grant No. 86880). Opinions, findings, conclusions or recommendations expressed in any publication generated by the NRF-supported research is that of the author alone, and the NRF accepts no liability whatsoever in this regard.

ABSTRACT

The use of coal as a primary energy source remains of interest globally due to its contribution to economic development and the affordable and reliable energy. However, the depletion of coal reserves and increased energy demand highlight the need to valorise coal wastes such as fine-coal rejects (FCR). In addition, conventional disposal of FCR poses significant threats to human health and the environment due to emissions of H_2S, SO_2, CO_2, heavy metals/metallic inorganic elements such as cadmium and arsenic, as well as volatile organic compounds (VOCs) arising from pyrite-associated spontaneous combustion and the interaction of organic sulphur and calcium within the FCRs. Direct utilisation of FCR in conventional boilers and gasifiers with high ash yield, high moisture content, and fine particle size may create downstream problems such as slagging, fouling, and erosion during utilisation. This is especially true if the transformational behaviour of the mineral matter (ash forming part of coal) is not fully understood.

Discerning the FCR mineral matter has the potential to allow for the utilisation of FCR in conventional boilers and gasifiers as a co-feed to traditional feedstocks. This can extend coal energy security, minimise coal waste handling costs and alleviate/mitigate environmental challenges associated with FCR disposal. These benefits may be achieved by better understanding the mode of occurrence of mineral matter and its behaviour during thermal treatment.

This research investigates the potential for utilisation of South African FCR in gasification and pyrolysis processes and aims to address environmental concerns and reduce disposal costs associated with this coal waste. Previous studies have focused primarily on unoxidised FCRs, particularly steam-station coals (labelled STEM in this study), and neglecting the partially oxidised FCRs, such as those from thermal-export plants (labelled TEP in this study) and their beneficiated fractions. This investigation comprehensively characterised and compared two types of South African FCRs, one from TEP and the other from STEM. The FCRs exhibited properties similar to those of feed coals for gasification and combustion, with notable differences in the mineral matter and vitrinite proportions and the alkali index, which is higher in the TEP sample. Thermogravimetric-gasification experiments demonstrated higher reaction rates and carbon conversion for the TEP sample, indicating its superior reactivity compared to the STEM sample. Raman and X-ray diffraction analyses revealed the presence of aromatic and aliphatic hydrocarbons and mineral matter in the FCRs, contributing positively to coal gasification reactivity.

An exploration of the mode of occurrence of mineral matter in FCR was also conducted by employing density-separation, chemical fractionation, and demineralisation techniques. This approach divided FCR mineral matter into different modes of occurrence, including extraneous minerals and inherent mineral matter (ion-exchangeable cations, salts of carboxylic acids and submicron minerals). The influence of extraneous minerals was studied by blending FCR and its density-separated, chemically fractionated, and demineralised residues with a composite of reactive oxides (MgO and Fe_2O_3) and a hydrated oxide mineral ($Ca(OH)_2$). The results indicated an enhanced activation energy during pyrolysis, resulting in increased carbon conversion. Cleat minerals and extraneous minerals catalysed pyrolysis reactions, facilitating the cracking of heavy tars to lighter fractions. However, the presence of oxygen in the reactive oxides hindered deoxygenation reactions, affecting pyrolysis efficiency.

The study also investigated the effects of carboxylate salts on FCR pyrolysis, particularly ferrous acetate, magnesium acetate and calcium acetate as Fe^{2+}/Mg/Ca-acetate composite. The results revealed the catalytic potential dependency on FCR carbon conversion on inherent mineral matter and its association with the dominant maceral groups. Adding carboxylate salts led to enhanced decomposition rates, carbon conversion, and the formation of sulphur-bearing phases and nano-carbonates, which influenced tar yield and gas composition.

Overall, this research provides valuable insights into the reactivity and mode of occurrence of mineral matter in FCR, offering a foundation for their utilisation in gasification and pyrolysis applications. Understanding these properties makes it possible to mitigate disposal costs, health hazards, air pollution, and fines volume accumulation of FCR, thereby promoting their sustainable utilisation in the energy sector.

Key terms: Fine-coal rejects, Gasification, Mode of occurrence, Pyrolysis, Mineral matter, Activation energy, Environmental impact.

LIST OF ABBREVIATIONS

Abbreviation	Definitions
^{13}C NMR	Carbon 13 solid-state nuclear magnetic resonance
a.d.b	Air dried basis
a.f.b.	Ash free basis
AAEM	Alkali and Alkaline earth metals
AAEMIE	Alkali and alkaline earth metallic inorganic elements
AI	Alkali index
AM	Amorphous material
ARD	Acid-rock drainage
ASTM	American Society for testing and Materials
B/A	Base/Acid ratio
CC	Carbon crystal
CCSEM	Computer-controlled scanning electron microscopy
CSC	Carboxylate salt composite
CV	Calorific value
DTF	Drop-tube furnace
FC	Fixed carbon
FCR	Fine-coal rejects
FTIR	Fourier transform infrared spectroscopy.
GC-MS	Gas chromatography-mass spectrometry
HREE	Heavy rare earth elements
HRTEM	High resolution transmission microscopy
ICP	Inductively coupled plasma
ISO	International organisation for standardisation
LTA	Low-temperature ashing
MM	Mineral matter
MSWI	Municipal solid waste incinerator
OS	Oil sludge
PM	Particulate matter

Abbreviation	Definitions
PM2.5	Fine particulate matter particles are less than 2.5 microns
PSD	Particle size distribution
QEMSCAN	Quantitative Evaluation of Minerals by Scanning Electron Microscopy
REE	Rare earth elements
ROSH	Reactive oxide and hydroxide
SA	South African
SEM	Scanning electron microscope
SEM-EDX	Scanning electron microscopy energy dispersive X-ray spectroscopy
SGS	General Society of Surveillance
STEM	Steam plant
TEM	Transmission emission
TEP	Thermal Export plant
TESCAN TIMA	Tescan Integrated Mineral Analyser
TGA	Thermogravimetric analyser
TIMA	TESCAN Integrated Mineral Analysis
VM	Volatile matter
VOCs	Volatile organic compounds
XRD	X-ray diffraction
XRF	X-ray fluorescence

TABLE OF CONTENTS

DECLARATION ..... **I**

DEDICATION ..... **II**

PREFACE ..... **III**

ACKNOWLEDGEMENTS ..... **VIII**

ABSTRACT ..... **X**

LIST OF ABBREVIATIONS ..... **XII**

CHAPTER 1 INTRODUCTION **1**

1.1 Background and Motivation **1**

1.2 Problem Statement **4**

1.3 Hypothesis **5**

1.4 Aim and Objectives **5**

1.5 Scope and Outline of the Thesis **6**

Chapter References **8**

CHAPTER 2 LITERATURE REVIEW **12**

2.1 Coal and Coal Pyrolysis Overview **13**

2.2 Significance of Mode of Occurrence of Mineral Matter in Coal and Fine-coal Rejects **13**

2.3 Mineral Matter Liberation and Coal Pre-treatment **14**

2.4 Extraneous Minerals **20**

2.5 Influence of Extraneous Minerals on Coal Pyrolysis **22**

2.5.1 Effect of Extraneous Quartz 22

2.5.2 Effect of Extraneous Kaolinite 22

2.5.3 Effect of Extraneous Dolomite 23

2.5.4 Effect of Extraneous Calcite 24

2.5.5 Effect of Extraneous Pyrite 25

2.5.6 Inherent Mineral Matter 26

2.5.7 Non-mineral Inorganic Elements 26

2.5.8 Bound by Organic Matter/Organically Associated Inorganic Elements 27

2.6 Influence of Inherent Mineral Matter on Coal Pyrolysis 29

2.7 Conclusions 33

2.8 Summary of Key Findings 34

CHAPTER 3 PROPERTIES AND REACTIVITY OF TWO OXIDISED AND UNOXIDISED SOUTH AFRICAN HIGHVELD FINE-COAL REJECTS AND THEIR DENSITY-SEPARATED FRACTIONS 49

3.1 Introduction 51

3.2 Materials and Methods 53

3.2.1 Sample Collection and Preparation 53

3.2.2 Density Separation Experiments 54

3.2.3 Char Preparation 55

3.2.4 Particle Size Distribution (PSD) Analysis 55

3.2.5 Coal Composition 55

3.2.6 XRD Analysis 56

3.2.7 Raman Analysis 56

3.2.8 Petrographic Analysis 56

3.2.9 TGA 57

3.2.10 Reactivity Analysis 57

3.3 Results and Discussion 57

3.3.1 Coal Washability Characteristics 57

3.3.2 PSD Analysis 59

3.3.3 FCR Composition 59

3.3.4 XRF Analysis 63

3.3.4.1 Ash Compositional Analysis Results 63

3.3.4.2 Ash Properties by Empirical Indices 65

3.3.5 XRD Analysis 66

3.3.6 Raman Analysis 69

3.3.7 Petrographic Analysis 72

3.3.7.1 Rank Determination 72

3.3.7.2 Microlithotypes 74

3.3.8 Thermogravimetric Analysis (TGA) 74

3.3.8.1 Analytical Pyrolysis 74

3.3.8.2 Reactivity of Prepared FCR Chars 76

3.4 Conclusions 78

3.5 Acknowledgements 79

Chapter References 80

CHAPTER 4 CATALYTIC EFFECT OF REACTIVE EXTRANEOUS MINERAL COMPOSITE ON CHAR AND TAR DISTRIBUTION DURING PYROLYSIS OF HIGHVELD

PARTIALLY OXIDISED FINE-COAL REJECT AND ITS BENEFICIATED RESIDUES. 86

4.1 Introduction 88

4.2 Materials and Methods 91

4.2.1 FCR Sampling and Preparation 91

4.2.2 Density Separation 91

4.2.3 Demineralisation Experiments 91

4.2.4 Chemical Fractionation Procedure 91

4.2.5 Preparation of Blends of Coal and ROSH Composites 91

4.2.6 Pyrolysis Experiments 92

4.2.7 Proximate, Calorific Value (CV), Ultimate, XRF, XRD, BET Surface Area, GC/MS, and Activation Energy Analyses 94

4.3 Results and Discussion 95

4.3.1 Coal and Char Compositions 95

4.3.2 XRF Analysis 97

4.3.3 XRD Analysis 99

4.3.4 Chemical Fractionation Procedure 102

4.3.5 Pyrolytic Product Yields 104

4.3.5.1 Char Yield 104

4.3.5.2 Tar Yields 109

4.3.5.3 Tar Composition 109

4.3.5.4 Simulated Distillation 112

4.3.6 Activation Energy 113

4.4 Conclusions 116

4.5 Acknowledgements 117

Chapter References 118

CHAPTER 5 EFFECT OF FLUXING INORGANIC ELEMENT-BEARING ACETATE COMPOSITE ON THE DISTRIBUTION OF PYROLYTIC PRODUCTS FROM HIGHVELD PARTIALLY OXIDISED FINE-COAL REJECT AND ITS BENEFICIATED RESIDUE 123

5.1 Introduction 124

5.2 Materials and Methods 127

5.3 FCR Sampling and Preparation 127

5.4 Preparation of Blends of Coal and Ca/Fe^{2+}/Mg-acetate Composite 127

5.5 Pyrolysis Experiments 127

5.6 Analytical Methods and Sample Characterisation 128

5.7 Results and Discussion 129

5.7.1 Proximate, Ultimate, and ICP Analyses 129

5.7.2 XRD Analysis 132

5.7.3 HRTEM Analysis 136

5.7.4 Organic Matrix Analysis 137

5.7.4.1 GC-MS scan (Solvent Extraction) 137

5.7.4.2 FTIR Analysis 138

5.7.5 ^{13}C Nuclear Magnetic Resonance 139

5.7.6 TGA 140

5.7.7 Pyrolytic Product Yields 144

5.7.7.1 Tar Composition 145

5.7.7.2 Gas Composition 147

5.8 Conclusions 148

5.9 Acknowledgements 150

Chapter References 151

CHAPTER 6 SUMMARY OF CONCLUSIONS AND RECOMMENDATIONS 157

6.1 Concluding Remarks 157

6.1.1 Mode of Occurrence of Mineral Matter 157

6.1.2 Pyrolysis and CO_2-Gasification Reactivity 158

6.1.3 The effects of Reactive Oxides and Hydroxide Composite 158

6.1.4 The effects of Carboxylate Salts on Pyrolysis 159

6.1.5 Achievements of Objectives and Aims 160

6.2 Contribution to Science 160

6.3 Prospects and Recommendations 161

ANNEXURES A: CHAPTER 3 SUPPLEMENTARY DATA 163

ANNEXURES B: CHAPTER 4 SUPPLEMENTARY DATA 172

ANNEXURES C: CHAPTER 5 SUPPLEMENTARY DATA 183

ANNEXURES D: DEMINERALISATION AND CHEMICAL FRACTIONATION PROCEDURES 190

ANNEXURE E: KINETIC TRIPLET DERIVATIONS 192

LIST OF TABLES

Table 2-1: A summary of typical analytical techniques used to determine and discern mineral matter occurrence. 17

Table 2-2: A list of major minerals found in SA coals [24-28]. 21

Table 2-3: Summary of literature findings on the effects of inherent mineral matter on coal pyrolysis. 30

Table 3-1: Proximate analysis results for FCR samples. 60

Table 3-2: Ultimate results of FCR samples, along with their corresponding density-separated fractions (wt. % a.d.b.) 61

Table 3-3: Forms of sulphur in the FCR samples and distribution across their corresponding density-separated fractions. 62

Table 3-4: Chemical composition of ashes of FCR samples and their corresponding density fractions. 63

Table 3-5: Chemical ash properties of the FCR samples along with their corresponding density-separated fractions. 65

Table 3-6: Mineralogical compositions and crystal carbon size of the FCR samples and their corresponding density-separated fractions. 67

Table 3-7: Raman fitted peak parameters for the FCR samples and their density-separated fractions. 71

Table 3-8: Thermal degradation characteristic parameters of the FCR samples under inert environment at 30 °C/min. 75

Table 4-1: Proximate and ultimate results FCR, beneficiated fractions, acid-washed residues, ROSH blends and their corresponding chars. 96

Table 4-2: Chemical composition for FCR, beneficiated fractions, acid-washed residues and ROSH blends along with their corresponding chars. 98

Table 4-3: Mineral composition for FCR, beneficiated fractions, acid-washed residues, ROSH blends, and corresponding chars. 101

Table 4-4: Leachability of inorganic elements in FCR by de-ionised water, 1 M $NH_4CH_3CO_2$ and 1 M HCl Solutions. 103

Table 4-5: BET Surface area results for FCR, beneficiated fractions, acid-washed residues and ROSH blends and their corresponding chars. 104

Table 4-6: List of possible reactions taking place during pyrolysis of FCR, beneficiated fractions, acid-washed residues, and ROSH blends. 108

Table 4-7: Activation energy distribution for FCR and its beneficiated fractions and ROSH

Table 5-1: Proximate and ultimate results for FCR, FCRD, Sl1.9D and their blends with CSC, and their corresponding chars. 130

Table 5-2: ICP results of the ashes for FCR, FCRD, Sl1.9D and their blends with CSC and their corresponding chars. 132

Table 5-3: Proportions of crystalline and amorphous phases of the CSC blends and Sl1.9 D, and their chars. 135

Table 5-4: Mineral-element matrix based on HRTEM spectra counts for FCR. 137

Table 5-5: GC-MS scan results for FCR and its pyrolytic char. 138

Table 5-6: Structural parameters obtained by 13C NMR of FCR and FCR Char. 140

Table 5-7: Pyrolysis characteristic parameters for CSC blends and Sl1.9D. 143

LIST OF FIGURES

Figure 2-1: A schematic drawing of a typical coal particle..... 16

Figure 2-2: Film-like mineral phases of REE phosphates (light) in the coal ash. Subbituminous B coal: *1*— rare-earth phosphate minerals (light) in the coal ash; *2*—inclusion of rare-earth phosphate minerals in film-like material (adapted from [79]). 28

Figure 3-1: Schematic diagram of a horizontal tube furnace used for pyrolysis. 55

Figure 3-2: Washability characteristics of two FCR samples at 100% passing 1 mm 58

Figure 3-3: Particle size distribution results for the TEP and STEM samples (Cum.STEM = Cumulative distribution of particle sizes in the STEM sample..... 59

Figure 3-4: Distribution of chemical properties of FCR samples and their density-separated fractions. 61

Figure 3-5: Raw Raman spectra for the FCR samples (a) and the deconvoluted Raman spectra for the STEM sample (b) and TEP sample (c). 70

Figure 3-6: Petrographic analysis results for the TEP and STEM samples, a.) field of view of the STEM sample showing banded vitrinite and inertinite, b.) field of view of the TEP sample showing distributed macerals and liberated MM and c.) distribution of macerals in the FCR samples and their corresponding density fractions (mmf-MM free basis). 73

Figure 3-7: Distribution of microlithotypes in the FCR samples by petrographic analysis a) TEP sample and b) STEM sample. 74

Figure 3-8: TG and derivative thermogravimetry (DTG) thermographs of the FCR

Figure 3-9: Comparison of gasification progression for chars prepared from the FCR samples and their corresponding density-separated fractions: a) conversion vs time, b) normalised gasification rate characteristics for the TEP sample, c) rate of conversion vs conversion and d) normalised gasification rate characteristics for the STEM sample..... 77

Figure 4-1: A schematic of the modified Fischer assay experimental rig used to conduct the pyrolysis experiments [18]. 92

Figure 4-2: Diffractograms of a.) FCR and demineralised FCR along with their ROSH blends and b.) the chars of FCR and demineralised FCR along with their ROSH

Figure 4-3: Product Distribution during Pyrolysis of FCR and Its Beneficiated Fractions, FCR/FCR D and ROSH Blends at 500 °C. 105

Figure 4-4: Distribution of chemical compounds during pyrolysis of FCR and its beneficiated fractions and ROSH blends at 500 °C. 111

Figure 4-5: Crude fractions distribution of tars obtained during pyrolysis of FCR and its beneficiated fractions and ROSH blends at 500 °C. 113

Figure 5-1: A schematic diagram of the sampling and preparation and experimental

Figure 5-2: Diffractograms of FCR, FCRD, SI1.9D, their blends with CSC, and their corresponding chars. 134

Figure 5-3: HRTEM (a&b) images of FCR showing nano-mineral particles and selected detection spots and (c&d) the spectra of 2 points presenting major elements..... 136

Figure 5-4: FTIR spectra of (a) FCR, FCRD and SI1.9D chars, and (b) FCR+CSC, FCRD+CSC and SI1.9D+CSC chars obtained at 500 °C..... 139

Figure 5-5: The (a & c) thermogravimetry and (b&d) derivative thermogravimetry plots for the CSC blends and SI1.9D..... 141

Figure 5-6: Yields of (a) char, (b) tar, (c) gas and (d) change in product yield from pyrolysis of CSC blends and SI1.9 D. Note: ∆Y – change in product yield (e.g., ∆Y_char=Y_(char FCR+CSC)-Y_CharFCR). 145

Figure 5-7: Distribution of chemical compounds in pyrolytic tars of CSC blends and

Figure 5-8: Distribution of non-condensable gases during pyrolysis of CSC blends and

CHAPTER 1 INTRODUCTION

1.1 Background and Motivation

In 2019, coal was the second-largest source of primary energy, generating around 27% of the global energy demand [1]. Although the focus has recently shifted towards renewable energy sources such as solar, wind, and biofuels, coal is still very useful for the economic development of nations and the generation of affordable and reliable energy. According to British Petroleum plc.[1] global coal recoverable reserves are estimated to last at least 132 years, with South Africa having coal reserves estimated to last 39 years at the current consumption-production rate. This indicates a potential for continued coal utilisation in South Africa and other major coal consumers worldwide due to its availability, reliability, and economic benefits. However, environmental challenges such as emissions of SO_x, NO_x, and CO_2 [2–4] are major drawbacks of this technology [5].

Progress has been made regarding CO_2 capture, reduction of H_2S, SOx and NOx emissions by applying technologies such as CO_2 sequestration, H_2S conversion to elemental sulphur by Stretford^{TM} solutions [6,7], flue gas desulphurisation and selective catalytic reduction [3,7–10]. These advances represent steps towards clean coal utilisation technologies. However, the lack of environmentally viable disposal methods for fine-coal rejects or coal discards remains a challenge for all coal-producing and utilising nations.

The term “fine-coal rejects” refers to coal particles smaller than 1 mm generated as an inevitable by-product during coal mining, beneficiation, and transportation [11]. Globally, approximately 60 billion tonnes of fine-coal rejects are discarded annually, including around 60 million tons a year generated in SA, due to their poor solid fuel properties, i.e. high moisture content which negatively affects their heating value (CV), rendering them unsuitable for utilisation in thermochemical processes [12, 13].

The current disposal methods involve storage in tailings dams or stockpiles, both of which have several associated drawbacks, such as land scarcity, the formation of acid mine drainage (AMD), spontaneous combustion, and emission of dust particles into the environment [14–16]. Furthermore, the economic and environmental non-viability of these methods presents an opportunity to explore improved disposal and valorisation techniques.

According to Matjie et al. [17] and Isaac and Bada [18], fine-coal rejects possess chemical properties similar to those of feed coals, but generally also contain more ash-forming minerals

due to their liberation and concentration into the finer size ranges, resulting in their classification as high-ash yield coals. Coal comprises various types of mineral matter such as minerals, mineraloids, organically associated inorganic elements, non-mineral inorganics, and macerals of vitrinite, inertinite and liptinite groups [17, 19]. These constituents of coal undergo chemical decomposition and/or transformation during thermochemical treatment, whereby the transformation of the inorganic fractions leads to ash formation. Extraneous minerals may attach to the molten solution during thermal treatment and form heterogeneous clinkers [20]. These clinkers can cause deposition issues and encapsulate fine carbon particles, resulting in lower carbon conversion [17, 21]. On the other hand, the inherent mineral matter in the carbon matrix could react with the carbon matrix or each other through distinct reaction pathways, forming intermediate products having a catalytic propensity during thermal treatment [22–24].

Considerable research has been conducted on the behaviour of extraneous minerals, macerals and organically associated inorganic elements present in caking coals during thermochemical treatment, serving as caking inhibitors, in-situ sulphur capturing mediums, catalysts or reaction inhibitors [25–30]. Ahmad et al. [31], Zhao et al. [32], Liang et al. [33], and Yu et al. [34] evaluated the effect of inherent mineral matter on the reactivity of pyrolytic intermediate products and composition of the final products during pyrolysis by comparing demineralised and untreated foreign coals. Similar studies on foreign feed coals have been comprehensively summarised by Roets [35]. The results from these studies indicate that inherent mineral matter present in feed coals has a catalytic effect, which remains active in the char even at elevated pyrolysis temperatures. However, under oxidising conditions, aluminosilicates start to form due to the interaction of meta-kaolinite or free silica with CaO (a fluxing mineral) at elevated temperatures, thus reducing the thermal reduction of the carbon matrix as was reported in studies on Chinese Zhundong and Xiao-long coals [22,33].

On the other hand, Liu et al. [27], Wei et al. [36] and Yao et al. [37] added potassium, sodium, magnesium, and calcium as either acetates, oxalates, or nitrates to demineralised and untreated Chinese feed coals, along with some oxides of iron, nickel, cobalt, germanium, calcium, and magnesium to study their effects during thermal treatment. Additionally, Hippo et al. [38] and Klopper et al. [39] conducted similar work on American and South African (SA) feed coals, respectively. Significant results indicated the formation of intermediate products such as K-O-C, HCOO− and −ONa groups [40, 41], which were found to enhance the reactivity of the chars under gasification conditions, following the order: K > Na ≈ Ca > Fe > Mg [38].

These inorganic materials are commonly added in their pure forms or as individual metallic or non-metallic oxides to demineralised, raw, and modelled coal mixtures. However, this approach

could be misleading, as these materials exist in coal as mixtures of various modes of occurrence of mineral matter, which could interact during thermochemical processing to form active intermediate artefacts [24]. Work has been reported on the performance of high percentage ash yield (AY) coal, and the beneficiation of fine-coal rejects and Highveld coal as potential export-grade steam coal with a percentage ash yield (AY) below 10% [17,42]. However, there remain opportunities to understand better the reactivities and transformational potential of mineral matter, particularly regarding their modes of occurrence. This understanding could influence coal blending strategies when preparing feed coals for boilers and gasifiers.

The following knowledge gaps have been identified during a comprehensive literature survey on fine-coal rejects and the effects of mineral matter pertaining to processing thermochemical plants.

- Comprehensive analysis and comparison of typical SA Highveld fine-coal reject samples and insights into their pyrolysis and gasification behaviours have not been reported.
- Studies on the catalytic effects of blends of reactive oxides and/or hydroxide composite of major SA coal extraneous minerals present in the fine-coal rejects on the pyrolysis product efficiencies and gasification reactivities have not been addressed in the literature.
- Studies into the catalytic effects of blends of salts of carboxylic acid composites and fine-coal reject, and its beneficiated residues, relating to major SA coal inherent minerals, on the pyrolysis product efficiencies and gasification reactivities have not been explored in the literature.

As a result, a study was proposed to evaluate the catalytic effects of two composites: one composed of salts of carboxylic acids, representing a fraction of inherent mineral matter, and the other simulating reactive intermediate products of extraneous minerals. The properties of two SA Highveld fine-coal rejects were evaluated comprehensively, and one was selected for further investigation. These composites were added to the fine-coal rejects, their density-separated fractions, chemically fractionated residues, and demineralised residues. The research aimed to elucidate the interactions and impacts of these composites on coal properties.

For the simulation of reactive intermediate products of extraneous minerals, a composite consisting of calcium hydroxide ($Ca(OH)_2$), magnesium oxide (MgO), and hematite (Fe_2O_3) was used to represent the reactive intermediate products of extraneous minerals. Another composite containing calcium (Ca), magnesium (Mg), and ferrous (Fe^{2+}) acetates simulated salts of carboxylic acids was also investigated to simulate organically associated inorganic elements.

The study employed a combination of chemical (Inductively Coupled Plasma (ICP), X-ray fluorescence (XRF), proximate and ultimate) analyses, physical (High-resolution transmission electron microscopy (HRTEM) and Brunauer-Emmett-Teller (BET)) as well as mineralogical analyses (Raman spectroscopy, X-ray diffraction (XRD)), petrology and thermogravimetric analysis (TGA). These analyses provided insight into the distinct nature of the two SA Highveld fine-coal rejects. Furthermore, the properties of the density-separated coal fractions, chemically fractionated and demineralised residues, and their blends with either a composite of salts of carboxylic acids or reactive oxides and hydroxides and corresponding chars prepared using the North-West University Fischer Assay set-up were examined.

The pyrolytic products obtained from this study underwent a series of analyses, including petrographic examination, gas chromatography-mass spectrometry scan (GC-MS scan), solid-state nuclear magnetic resonance (^{13}C NMR), gas chromatography-mass spectrometry (GC-MS), simulated distillation (SimDist) and Fourier transform infrared spectroscopy (FTIR).

1.2 Problem Statement

Feeding fine-coal rejects directly into conventional gasifiers without understanding the behaviour of all the mineral matter present may create problems in the plant. These include the formation of clinkers, erosion, slagging and fouling deposits, and corrosion of reactor internals, resulting in plant shutdowns.

Associations of clay minerals and calcite, dolomite and pyrite are commonly associated with sintering and deposition problems. However, these associations could also have a catalytic effect on the pyrolysis and gasification reactions.

The practice of generalising coal mineral matter overlooks the diverse modes of occurrences of mineral matter, which may behave differently under pyrolysis and gasification conditions. This knowledge is critical if fine-coal rejects are to be valorised. The usual approach of adding mineral matter as individual metallic and non-metallic oxides to raw and treated feed coals must be clarified. This is because mineral matter exists in coal as mixtures of inherent mineral matter, extraneous mineral matter, organically associated inorganics, non-mineral inorganics, and submicron cleat minerals. No studies have been conducted on the effect of adding blends of reactive oxides and hydroxide composite of major coal minerals and their corresponding salts of carboxylic acids composite as inherent mineral matter to fine-coal rejects.

1.3 Hypothesis

The following hypotheses are formulated:

- The addition of reactive oxides and hydroxide composite of extraneous mineral matter ($Ca(OH)_2$-MgO-Fe_2O_3) as a blend to fine-coal rejects and its density-separated fractions, may impede carbon conversion but promote in-situ capturing of CO_2 and sulphur gases during pyrolysis and gasification.
- A composite of Ca^+, Mg^+ and Fe^{2+} acetates, as salts of carboxylic acids (organically associated inorganic elements) and fine-coal rejects, and their density-separated fractions, demineralised, and chemical fractionated residues, may promote carbon conversion and produce pyrolytic chars with higher gasification reactivities and high pyrolysis thermal efficiencies.

1.4 Aim and Objectives

Aim: To evaluate the influence of the mode of occurrence of mineral matter on the reactivity and product efficiencies of fine-coal rejects and their density-separated fractions, demineralised and chemical fractionated residues during pyrolysis and gasification.

The specific objectives of the study are to:

- Perform density separation, chemical fractionation, and demineralisation of fine-coal rejects.
- Perform comprehensive characterisation of fine-coal rejects and their density-separated fractions/demineralised fine-coal reject/chemical fractionated fine-coal reject employing petrographic, chemical, and mineralogical analyses.
- Evaluate the effect of reactive oxides and hydroxides of extraneous minerals on the yields and composition of the products derived from the pyrolysis of their blends containing fine-coal rejects and their beneficiated residues.
- Evaluate the effect of salts of carboxylic acids representing inherent mineral matter on the yields and composition of the products obtained from the pyrolysis of their blends with fine-coal rejects and their beneficiated residues.

1.5 Scope and Outline of the Thesis

Chapter 1: Introduction

Chapter 1 provides a concise overview of the context, thereby providing relevant background and state-of-the-art of FCR processing, beneficiation, and the catalytic effect of mineral matter. It also addresses potential strategies to alleviate environmental issues associated with the disposal of fine-coal rejects. The problem statement, the hypothesis and the aims and objectives of the study are also described in this chapter.

Chapter 2: Literature Review

An overview of coal and coal pyrolysis, the significance of the mode of occurrence of mineral matter and their classification are briefly discussed in this chapter. A review of existing literature on the influence of mineral matter as catalysts during thermochemical processing is reported in this chapter. Factors affecting the reactivity of coal and fine-coal rejects, particularly the composition and yields of products produced from pyrolysis and gasification, are evaluated by comparing and surveying previously conducted work. The effect of mineral matter and the mode of occurrence is addressed. A summary of the conclusions made from the literature and future aspects is also included in this chapter.

Chapter 3: Manuscript 1

This manuscript presents the research methodology utilised and discusses the findings obtained from the sampling, preparation, and detailed characterisation of two fine-coal rejects samples from (1) a thermal export plant (TEP) and (2) a steam station sample (STEM), both from the Highveld Coalfield in South Africa. Density-separated fractions derived from these samples were also characterised using both advanced and conventional analytical techniques.

Chapter 4: Manuscript 2

The effect of extraneous mineral matter via the addition of composites of reactive oxides and hydroxide minerals ($Ca(OH)_2$-MgO-Fe_2O_3) to the TEP fine-coal reject sample, its density-separated fractions, and demineralised and chemically fractionated residues are reported in this paper. The blends were analysed using various conventional and advanced techniques and subjected to pyrolysis experimentation. The findings from the characterisation and pyrolysis experiments are reported on in this manuscript. Comparisons of the yields and compositions of the derived chars and tars are also discussed.

Chapter 5: Manuscript 3

In this paper, the effect of a composite addition of Ca^{2+}, Mg^{2+}, and Fe^{2+} acetates as salts of carboxylic acids, simulating inherent mineral matter on the yields and composition of pyrolytic products (chars, tars, and gases) derived from the TEP fine-coal reject samples is reported. The density-separated fractions and the demineralised residues derived from the utilisation of the NWU Fischer assay pyrolysis set-up is also described. The degradation profiles of fine-coal rejects, and their density-separated fractions during pyrolysis were also studied using a thermogravimetric analyser (TGA). The results are described in this manuscript.

Chapter 6: Conclusions and Recommendations

Chapter 6 summarises the conclusions drawn from this study and the contributions made to science and engineering. Recommendations for future studies are made.

Chapter References

[1] British Petroleum. BP Statistical Review of World Energy 2020. 2020.

[2] Jeffrey R, Falcon R, Kinghorn A. The benefits and challenges associated with coal in South Africa. Cornerstone 2014; 2:66–70.

[3] Hajari A, Atanga M, Hartvigsen JL, Rownaghi AA, Rezaei F. Combined flue gas clean-up process for simultaneous removal of SOx, NOx, and CO_2 - A techno-economic analysis. Energy and Fuels 2017; 31:4165–72.

[4] Mphahlele K. Characterisation of streams and performance evaluation of the Co-pyrolysis of sewage sludge and lignite for bio-oil production [M-Tech Dissertation]. Vanderbijlpark, South Africa: Vaal University of Technology; 2020.

[5] Uwaoma RC. Pyrolysis and gasification of coal residues derived from tetralin liquefaction of South African density-separated coal [PhD thesis]. Potchefstroom, South Africa: North-West University; 2020.

[6] Connell JA, inventor; Nrg Inc, assignee. Method for removing hydrogen sulfide from hydrocarbon gas streams without pollution of the atmosphere. United States patent US 3,864,460. 1975 Feb 4.

[7] Ndou M, Matjie R, Mahlamvana F, Neomagus H, Bunt J, Mphahlele K. Effect of the $V^{5+}$to V^{4+} molar ratio on H_2S absorption and conversion to elemental sulphur. Industrial & Engineering Chemistry Research. 2021; 60:1505–16.

[8] Shelef M. Selective catalytic reduction of NOx with N-free reductants. Chemical Reviews. 1995; 95:209–25.

[9] Shukla R, Ranjith P, Haque A, Choi X. A review of studies on CO_2 sequestration and caprock integrity. Fuel. 2010; 89:2651–64.

[10] Koech L, Rutto H, Lerotholi L, Everson RC, Neomagus H, Branken D, et al. Spray drying absorption for desulphurisation: a review of recent developments Clean Technologies and Environmental Policy. 2021; 23:1665–86.

[11] Tambwe O, Kotsiopoulos A, Harrison STL. Desulphurising high sulphur coal discards using an accelerated heap leach approach. Hydrometallurgy. 2020; 197:105472.

[12] Bunt JR, Neomagus HWJP, Botha AA, Waanders FB. Reactivity study of fine discard coal agglomerates. Journal Analytical and Applied Pyrolysis. 2015; 113:723–8.

[13] Uwaoma RC, Strydom CA, Matjie RH, Bunt JR, Okolo GN, Brand DJ. Pyrolysis of tetralin liquefaction derived residues from lighter density fractions of waste coals taken from waste coal disposal sites in South Africa. Energy and Fuels. 2019; 33:9074–86.

[14] Department of Environmental Affairs. National waste information baseline. Pretoria: 2012.

[15] Muzenda E. Potential uses of South African coal fines: a review. University of Johannesburg. 2014.

[16] Moyo A, Filho JA, Harrison S, Broadhurst J. Characterising the environmental risks of coal preparation wastes: A study of fine coal slurry waste and discards from South African collieries. In: Wolkersdorfer CH, Sartz L, Weber A, Burgess J, Tremblay G, editors. Mine Water – Risk to Opportunity. Pretoria: IMWA; 2018. p. 417–24.

[17] Matjie RH, Li Z, Ward CR, Kosasi J, Bunt JR, Strydom CA. Mineralogy of furnace deposits produced by South African coals during pulverised-fuel combustion tests. Energy and Fuels. 2015; 29:8226–38.

[18] Isaac K, Bada SO. The co-combustion performance and reaction kinetics of refuse derived fuels with South African high-ash coal. Heliyon. 2020; 6:e03309.

[19] Gupta R, Wall T, Baxter L, editors. Impact of mineral impurities in solid fuel combustion. New York, USA: Springer Science & Business Media; 2007

[20] Matjie RH. Sintering and slagging of mineral matter in South African coals during the coal gasification process [PhD thesis]. Pretoria, South Africa: University of Pretoria; 2008.

[21] Wang X, Xu Z, Wei B, Zhang L, Tan H, Yang T, et al. The ash deposition mechanism in boilers burning Zhundong coal with high contents of sodium and calcium: A study from ash evaporating to condensing. Applied Thermal Engineering. 2015; 80:150–9.

[22] Ma Z, Bai J, Li W, Bai Z, Kong L. Mineral transformation in char and its effect on coal char gasification reactivity at high temperatures, part 1: Mineral transformation in char. Energy and Fuels. 2013; 27:4545–54.

[23] Schobert HH. Catalytic and chemical behavior of coal mineral matter in the coal conversion process. Clean Utilisation of Coal. 1992:65–73

[24] Suárez-Ruiz I, Crelling JC. Applied coal petrology: the role of petrology in coal utilization. Oxford, UK: Academic press; 2008.

[25] Everson RC, Neomagus HWJP, Kaitano R, Falcon R, Alphen C van, du Cann VM. Properties of high-ash char particles derived from inertinite-rich coal: 1. Chemical, structural and petrographic characteristics. Fuel. 2008; 87:3082–90.

[26] Van Dyk JC, Benson SA, Laumb ML, Waanders B. Coal and coal ash characteristics to understand mineral transformations and slag formation. Fuel. 2009; 88:1057–63.

[27] Liu L, Liu H, Cui M, Hu Y, Wang J. Calcium-promoted catalytic activity of potassium carbonate for steam gasification of coal char: Transformations of sulphur. Fuel. 2013; 112:687–94.

[28] Keller M, Arjmand M, Leion H, Mattisson T. Interaction of mineral matter of coal with oxygen carriers in chemical-looping combustion (CLC). Chemical Engineering Research and Design. 2014; 92:1753–70.

[29] Coetzee S. The caking and swelling of South African large coal particles [PhD thesis]. Potchefstroom, South Africa: North-West University; 2015.

[30] Tsemane MM, Matjie RH, Bunt JR, Neomagus HWJP, Strydom CA, Waanders FB, et al. Mineralogy and Petrology of Chars Produced by South African Caking Coals and Density-Separated Fractions during Pyrolysis and Their Effects on Caking Propensity. Energy and Fuels. 2019; 33:7645–58.

[31] Ahmad T, Awan IA, Nisar J, Ahmad I. Influence of inherent minerals and pyrolysis temperature on the yield of pyrolysates of some Pakistani coals. Energy Conversion and Management. 2009; 50:1163–71.

[32] Zhao H, Wang B, Li Y, Song Q, Zhao Y, Zhang R, et al. Effect of chemical fractionation treatment on structure and characteristics of pyrolysis products of Xinjiang long flame coal. Fuel. 2018; 234:1193–204.

[33] Liang D, Xie Q, Wei Z, Wan C, Li G, Cao J. Transformation of alkali and alkaline earth metals in Zhundong coal during pyrolysis in an entrained flow bed reactor. Journal of Analytical and Applied Pyrolysis. 2019; 142:104661.

[34] Yu J, Guo Q, Ding L, Gong Y, Yu G. Study on the effect of inherent AAEM on char structure evolution during coal pyrolysis by in-situ Raman and TG. Fuel. 2021; 292:120406.

[35] Roets L. The effect of mineral addition on the pyrolysis products derived from typical Highveld coal [Master's dissertation]. Potchefstroom, South Africa: North-West University, 2014.

[36] Wei L, Cui B, Guo L, Sun Y. Effect of sodium on three-phase nitrogen transformation during coal pyrolysis: A qualitative and semi-quantitative investigation. Fuel Processing Technology. 2021:213:106638.

[37] Yao Q, Ma M, Liu Y, He L, Sun M, Ma X. Pyrolysis characteristics of metal ion-exchanged Shendong coal and its char gasification performance. Journal of Analytical and Applied Pyrolysis. 2021; 155:105087.

[38] Hippo EJ, Jenkins RG, Walker PL. Enhancement of lignite char reactivity to steam by cation addition. Fuel. 1979; 58:338–44.

[39] Klopper L, Strydom CA, Bunt JR. Influence of added potassium and sodium carbonates on CO_2 reactivity of the char from a demineralised inertinite rich bituminous coal. Journal of Analytical and Applied Pyrolysis. 2012; 96:188–95.

[40] Takarada T, Tamai Y, Tomita A. Effectiveness of K_2CO_3 and Ni as catalysts in steam gasification. Fuel. 1986; 65:679–83.

[41] Wang J, Yao Y, Cao J, Jiang M. Enhanced catalysis of K_2CO_3 for steam gasification of coal char by using $Ca(OH)_2$ in char preparation. Fuel. 2010; 89:310–7.

[42] Bunt JR. Development of a fine coal beneficiation circuit for the Twistdraai Colliery. Master's dissertation, University of Cape Town, Cape Town, South Africa; 1997.

CHAPTER 2 LITERATURE REVIEW

This chapter provides an overview of coal and the process of coal pyrolysis, the significance of the mode of occurrence of mineral matter, techniques for liberating mineral matter, and pre-treatment of coal. The chapter describes the classification of coal mineral matter into extraneous and inherent segments. A comprehensive discussion based on previous work on the influence of major extraneous minerals present in SA coals and the influence of inherent mineral matter and their relevance during thermal treatment follows. The review is concluded by highlighting a summary of findings obtained from this literature review. An argument is made to consider the effects of modes of occurrence of mineral matter on the composition and yields of products produced from pyrolysis.

2.1 Coal and Coal Pyrolysis Overview

Coal is a sedimentary rock that comprises complex structures made up of macerals (organic elements) and mineral matter (inorganic elements). These elements exist in coal in a wide variety of associations, concentrations, and modes of occurrence. The term "modes of occurrence" in coal refers to the various ways in which minerals are distributed within the coal matrix. These modes can include whether minerals are uniformly dispersed throughout the coal or concentrated in specific layers or bands. In addition to the organic constituents present, the behaviour, fate, and effects of the inorganic elements present in coal establish the suitability of coal for thermochemical processing, along with the design and types of reactors that can utilise it. Pre-treatment of coal and post-treatment of coal-derived products may be necessary due to the nature of the coal inorganic matrix. South African run-of-mine sub-bituminous and bituminous coals comprise up to 50 wt. % mineral matter, often necessitating pre-treatment for improved energy efficiency [1].

Understanding the presence, behaviour, fate, and effects of coal constituents has been of interest to researchers since the inception of coal technology. It is generally agreed [2-4] that pyrolysis, as an initial stage of gasification and combustion, plays a pivotal role towards carbon conversion efficiencies. As a result, pyrolysis has been adopted to evaluate the behaviour and suitability of coal feedstocks for thermochemical processes. The four major products obtained during the pyrolysis of coal include tar, gas, pyrolytic water and char. The coal macerals, moisture, volatile matter, ash yield, and ash compositions have been explored extensively to estimate the behaviour of coal during thermochemical processing. These advancements have led to the development of empirical methods to predict slagging, reactivity, and carbon conversion, along with software applications to estimate ash fusibility under equilibrium conditions [5]. However, these applications need to consider the different modes of occurrence of mineral matter, which results in inaccuracies in conceptualisation. This chapter compares, integrates, and interprets findings from the last two decades. The focus is mainly on the significance of the mineral matter and the mode of occurrence of mineral matter, the mineral matter liberation and coal pre-treatment, the classification of mineral matter in coal, and the influence of inherent and extraneous mineral matter on coal pyrolysis. The chapter includes a summary of the conclusions.

2.2 Significance of Mode of Occurrence of Mineral Matter in Coal and Fine-coal Rejects

Coal mineral matter affects reaction mechanisms, ash formation and ash characteristics, energy recovery, and coal grindability. It also has environmental pollution implications. For instance, the discrete mineral particles associated with other coal components during gasification can form heterogeneous clinkers with detrimental process issues [6]. The generated ash may be unsuitable

for use in cement production, leading to high disposal costs and causing environmental nuisance [7]. On the other hand, these coal ashes may be a source of high-value metallic inorganic elements and hard minerals (anorthite ($Ca_2Al_2Si_2O_8$) and quartz (SiO_2)). Depending on the shape and size of these mineral particles, they can pose erosion, fouling, and slagging issues. However, they may also catalyse gasification and liquefaction reactions [8, 9].

All these factors depend on the type of mineral matter and its mode of occurrence. Mineral matter in coal can be broadly categorized based on its origin and association with the coal matrix. The two primary types are inherent minerals and extraneous minerals. Extraneous minerals may be in the form of ultra-fine material (discrete particles of minerals) on the surface of coal, originating from coal contamination by floor or roof strata during mining operations. On the other hand, Inherent mineral matter refers to non-mineral inorganic elements and submicron minerals associated with macerals encapsulated in the carbon matrix [10] [17].

As a result, coal mineral matter is classified as inherent or extraneous to differentiate its mineral types and behaviour during utilisation. For example, the formation of mullite and cristobalite at high temperatures is mainly a result of the transformation of extraneous kaolinite and quartz, which are not associated with the extraneous fluxing minerals. Fluxing minerals are specific types of minerals that can lower the melting point of the surrounding materials during thermo-chemical processes (pyrolysis, gasification and combustion), leading to the facilitation of ash fusion and flow. These are often minerals such as pyrite (FeS_2), siderite ($FeCO_3$), limestone ($CaCO_3$) and dolomite ($CaMg(CO_3)_2$) which are used in industrial processes to aid in the smelting and refining of metals from coal-derived ash.

However, anorthite can be formed at elevated temperatures due to the interaction of either inherent or extraneous dolomite, pyrite, calcite and siderite and extraneous kaolinite or inherent kaolinite under oxidising conditions [11] [10]. Understanding the proportions and effects of mineral matter and their mode of occurrence is important for efficient coal utilisation. Density separation, chemical fractionation, and demineralisation have played a significant role in coal mineral matter studies. The following section expands on these techniques and describes how they can be used to isolate specific mineral matter for further study.

2.3 Mineral Matter Liberation and Coal Pre-treatment

Figure 2-1 is a schematic diagram illustrating a typical coal particle. It depicts the association of the carbon matrix with inherent mineral matter. Ash formation during coal gasification/combustion at T>800 °C is controlled by reactions occurring at the particle level [12] [18]. As a result, it is

important to liberate mineral matter for better understanding on their behavior. Extraneous, minerals can be easily separated from the carbon-rich fraction through physical methods such as density separation or froth flotation [13] [14]. Density and gravity separation techniques produce a by-product (tailings or sink fraction) containing low proportions of carbon phases. Although this technique is practised worldwide as a coal beneficiation technique to improve the economic feasibility of coal utilisation, more research is needed to discern extraneous mineral behaviour. The physical separation of mineral matter from the organic matrix of coal has been of interest due to its importance in understanding the liberation propensity of coal mineral matter and the production of carbon-rich coal. Kumar and Rawat [14] [15] defined froth flotation as a process whereby the separation of solid particles is based on the differences in hydrophobicity. Density separation is defined as techniques that separates lower-density particles from higher-density particles at a specific separating density, regardless of their physical properties [15] [16]. Dry beneficiation, a type of density separation, using an air table has also been explored, significantly reducing mineral matter in the clean coal product [16] [12]. Research has also been conducted to improve the quality of coal through washing and beneficiation processes, with the use of solvents such as Tetrahydrofuran showing promising results in reducing the percentage of ash yield during laboratory studies [17] [11]. Filtration, surface-based and centrifugation separation methods have been studied to find viable ways for coal mineral matter removal [17] [11]. A coal mineral physical separation device has been proposed, which includes vibrating motors and filters for efficient separation [18] [13]. Liberation models have been developed to evaluate the behaviour of different mineral groups in coal, with some minerals easily liberated through grinding while others remain attached to coal particles. These physical separation techniques are effective mainly for the removal of extraneous minerals.

The removal of inherent mineral matter from coal can be achieved with dissolution techniques using lixiviants such as water, ammonium acetate, hydrochloric acid, and hydrofluoric acid. Using different lixiviants indicates the associations and mode of occurrence of the mineral matter present in coal. On the other hand, the inherent mineral matter is not liberated by density and gravity separation techniques, and its interaction with extraneous minerals may hinder the actual effects of extraneous minerals present during utilisation. As a result, demineralisation with strong mineral acids such as hydrochloric and hydrofluoric acids is preferred for the almost complete separation of organic and inorganic phases comprised in coal. However, Strydom et al. [19] and Song et al. [20] cautioned that these acids only slightly affect the remaining coal carbon matrix. Also, these techniques do not allow for an understanding of the mode of the occurrence of mineral matter.

For instance, water removes ions and cations associated with pore waters; ammonium acetate dissolve carboxylic acid salts. Hydrochloric acid dissolves hydroxides, oxides, carbonates, and inherent submicron minerals. For complete dissolution of extraneous and inherent mineral matter, extraction with highly concentrated solutions of hydrochloric and hydrofluoric acids can be used [13] [14].

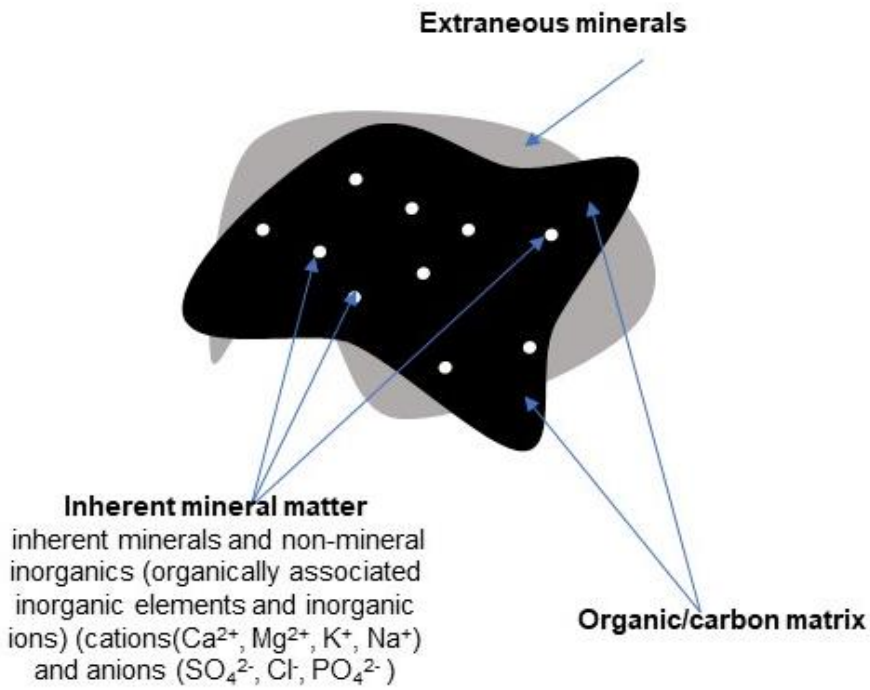

Figure 2-1: A schematic drawing of a typical coal particle.

As a result, chemical fractionation (selective leaching), which involves sequential leaching of mineral matter by using lixiviants such as ammonium acetate, water, and hydrochloric acid, targets specific mineral matter based on their modes of occurrence [17,10,21]. As a result, a combination of these techniques can provide insight into the behaviour, mode of occurrence, and proportions of mineral matter present in coal. Typical analytical techniques helpful in determining different modes of occurrence of mineral matter are listed in Table 2-1.

Table 2-1: A summary of typical analytical techniques used to determine and discern mineral matter occurrence.

Techniques	Extraneous minerals	Inherent minerals	Non-mineral inorganics	Remarks
Quantitative X-ray diffraction (XRD)	X	x		A non-destructive analytical technique for the determination of total crystalline and amorphous phases in coal/ores/metals. However, this technique may underestimate non-minerals. Quantification of minerals is done using the Rietveld method [5, 22].
Electron microscope and microprobe analysis (HRTEM and SEM)	X	x		Used for performing qualitative and quantitative analyses of coal constituents and to determine the elemental composition of the individual macerals in each coal sample, minerals and glass phases in coal ash. Assessment of coal quality and rank, coal petrology and mineralogy can also be aided by the results obtained from electron microscope and microprobe analysis [24].
Low-temperature plasma ashing/asher (LTA)	X	x	x	Determine the mineral matter percentage in the coal samples. Isolate the minerals for XRD analysis, including clay fraction by decomposition of organic matter in an oxygen plasma at 120 - 150°C [18, 25, 26].
Infra-red spectrometry	X	x	x	This technique can be used for qualitative analysis of coal mineral matter. Interference by macerals and minerals sharing functional groups is possible, which makes low-temperature ashing (LTA) essential for more accurate mineral determinations [27].

Techniques	Extraneous minerals	Inherent minerals	Non-mineral inorganics	Remarks
Inductively coupled plasma	X	x	x	It can be used to quantify the proportion of non-mineral inorganics and the total concentration of inorganic elements by selective leaching of different mineral matter in raw coal or ashes obtained from the LTA or loss on ignition (LOI) method [28]. This technique relies on the complete dissolution of coal ash in the digestion of lixiviant(s) [14, 28].
Petrography	x	x		It is used to determine the types and proportions of maceral groups as well as maceral morphology in coals, and the rank by vitrinite reflectance. The analysis of microlithotypes can provide mineral-mineral and mineral-maceral associations with estimations of quartz, clay minerals, pyrite and carbominerite quantities [29, 30].
X-ray fluorescence spectrometry				It is a non-destructive technique used to identify and quantify the concentrations of inorganic elements present in solid, powdered and liquid samples. This technique can analyse inorganic elements from analyzing elements from Sodium (Na) to Uranium (U) (accuracy for lighter elements such as Na is limited, even with the use of standards) from 1 ppm to 100% concentrations in coal ashes obtained from the LTA or LOI method [18, 31]. Although this technique does not determine

Techniques	Extraneous minerals	Inherent minerals	Non-mineral inorganics	Remarks
Quantitative Evaluation of Minerals by Scanning Electron Microscopy (QEMSCAN)	x	x	x	This technique integrates the concepts of SEM and petrography to evaluate mineral-maceral association by bulk mineralogy, particle properties, mineral liberation and mineral association [23].
Raman spectroscopy	x	x		This technique can be used to analyse the chemical structure, phase and polymorphy, crystallinity and molecular interactions of coal. The graphitic and defective carbon structures can be determined by the deconvolution of the Raman spectra of coal samples [33, 34].

2.4 Extraneous Minerals

The term extraneous minerals refer to discrete mineral particles attached to the coal surface by static forces. Their origin is associated with the contamination of coal by floor and roof strata during coal formation and mining operations. During gasification, these discrete coal particles may attach to a molten solution of aluminium silicate minerals to form heterogeneous clinkers, which may lead to severe blockages [35, 36]. Physical separation processes such as water washing (wet-screening), gravity separation, and density separation are employed to separate these discrete mineral particles from the carbonaceous fraction prior to utilisation. Despite these mitigation efforts, completely removing extraneous minerals without using strong inorganic acids and bases is impossible [14, 37]. As coal quality varies widely across different regions and seams, the level of extraneous minerals can fluctuate, demanding tailored solutions for each coal source. For instance, South African coals are heavily contaminated with extraneous minerals and comprise only a small fraction of inherent mineral matter. By contrast, foreign brown coals are comprised almost entirely of inherent mineral matter [38].

Coal beneficiation methods and understanding the behaviour of extraneous minerals have been of interest to researchers [39-42]. In addition, the drive toward cleaner and more efficient coal utilisation technologies in a circular economy demands an understanding of extraneous minerals. Table 2-2 presents a list of common minerals present in SA coals as reported in previous studies [39-43].

Table 2-2: A list of major minerals found in SA coals [39-43].

Mineral	A	B	C	D	E
Method of analysis	**XRD**	**CCSEM**	**XRD**	**QEMSCAN**	**QEMSCAN**
Quartz (SiO_2)	15-22	12	1-7.5	2.8	1.5
Kaolinite ($Al_2Si_2O_5(OH)_4$)	44-52	25	18-20.2	26.9	8.6
Dolomite ($CaMg(CO_3)_2$)	6-15	4	0.5-9.5	-	4.7
Calcite ($CaCO_3$)	1-10	2	1.5-3.2	0.4	2.3
Illite ($K\ H_3O)\bullet(Al, Mg, Fe)_2\bullet(Si\ Al)_4\bullet O10\bullet[(OH)_2\ (H_2O)]$	-	-	1.2-3.5	-	0.8
Microcline ($KAlSi_3O_8$)	-	-	-	0.2	0.3
Muscovite ($KAl_2(F, OH)_2$)	-	-	0.1-4.1	0.4	0.8
Pyrite (FeS_2)	1-3	4	0.3-1.6	0.4	3.9
Siderite ($FeCO_3$)	-	-	-	1.2	0.2
Anatase (TiO_2)	1-3	-	0.2	-	-
Rutile (TiO_2)	-	-	0-0.1	0.1	0.1
Goyazite [$SrAl_3(PO_4)_2(OH)_5.(H_2O)$]	1-3	-	-	-	-
Bassanite[a] ($CaSO_4 \cdot 1/2H_2O$)	1-3	-	-	-	-
Graphite (C)	-	-	0.4-2.8	-	-
Apatite $Ca_5(PO_4)$	-	-	-	0.3	0.7

XRD - X-ray diffraction, CCSEM – Computer-controlled scanning electron microscopy, QEMSCAN - Quantitative Evaluation of Minerals by Scanning Electron Microscopy, a – derived during the interaction between organic sulphur and organic Ca and S from inherent pyrite and organic sulphur, coal A – Highveld , coal B – Highveld, Coal C – Witbank, Coal D – Waterberg, coal E – KZN

2.5 Influence of Extraneous Minerals on Coal Pyrolysis

The South African Sasol Lurgi MK-IV dry-bottom fixed-bed gasifiers typically comprise four reaction zones, namely the drying, pyrolysis, gasification, and combustion zones when gasifying local bituminous coal. These are identical to commercial North Dakota gasifiers that operate on lignite. The study by Mangena et al. [44] describes North Dakota lignite samples and mineral matter transformational behaviour across these zones. During the pyrolysis of coal at temperatures above 400 °C, minerals such as kaolinite start to undergo dehydroxylation, leading to meta-kaolinite formation. A series of solid-state reactions may occur at this stage to yield diverse ash particles. For instance, meta-kaolinite may interact with Ca, Mg, and/or Fe to form Ca, Mg, and/or Fe- aluminosilicates [45, 46].

Quantifying the proportions of extraneous minerals in coals from different mines and origins and classifying the presence of different extraneous minerals is crucial. The characterisation of extraneous minerals will aid in studying their transformation and interaction with the carbon matrix. It has ignited much research interest globally. Complete separation of extraneous minerals from high-ash coals such as SA Highveld coals is impractical, if not impossible. The current literature, therefore, focuses on studies that have utilised the in-situ addition of minerals representing typical coal minerals of an extraneous mode of occurrence.

Extraneous minerals in SA coals consist mainly of quartz, kaolinite, dolomite, and calcite [36, 47-49]. Lower proportions and traces of pyrite, illite, gypsum, and other minerals are present in these coals. For the sake of brevity in this review, only the significant minerals, quartz, dolomite, kaolinite, calcite, and pyrite, will be considered. Pyrite is considered due to its high propensity to affect pyrolysis reactions [50, 51]. The rest are considered due to their high proportions in SA coals.

2.5.1 Effect of Extraneous Quartz

Although quartz is a major mineral in SA coals, pure extraneous quartz particles are inert under pyrolysis conditions [42, 52]. As a result, they act mainly as a diluent to the carbon matrix and report to the char unaltered. Quartz may also exist in coal as included grains associated with kaolinite, calcite and illite [53].

2.5.2 Effect of Extraneous Kaolinite

Under inert conditions, extraneous pure kaolinite particles and kaolinite associated with fluxing elements or fluxing element-bearing minerals may undergo partial dehydroxylation at 400 °C to

form meta-kaolinite [54]. The water rejected during this process may be involved in the in-situ water gas shift reactions, consequently changing product composition and reaction mechanisms. As the reaction temperature increases above 900 °C to 1150 °C, pseudo mullite is formed, and mullite occur at 1200°C. These high abrasive index minerals are formed from meta-kaolinite [6]. Additionally, Ca/Mg/K/Fe/Na-aluminosilicates may be formed from the interaction of meta-kaolinite and Ca, Mg, Fe, K and/or Na [55, 56]. Hlatshwayo et al. [57] linked mullite formation to abrasion and erosion in plant equipment. In the presence of potassium, kaolinite may prevent or reduce caking of coal by up to 90 wt. % by acting as an oxygen donor during pyrolysis at 600 °C, resulting in the formation of illite, sanidine, nepheline, microcline, and muscovite [58]. During combustion, sodium species can volatilise and report to the fly ash [45], but in the presence of extraneous kaolinite, capturing of water-soluble Na and reduction of Na particulate matter with particle diameter <2.5µm ($PM_{2.5}$) may take place. Extraneous kaolinite can react with intermediate volatile mineral vapours, such as Ca and Na, inhibiting their partitioning into ultrafine $PM_{2.5}$ during combustion at 900-1500 °C [59]. This reaction modifies the ash melting behaviour and promotes the capture of ultrafine PM onto coarse particles [60].

The composition and yields of pyrolytic tars, chars and non-condensable gases are also affected by the presence of extraneous kaolinite. For instance, the evolution of low molecular weight tars is suppressed by kaolinite at 450 °C [61] due to the adsorption of these tar fragments on the surface of kaolinite [55]. Kaolinite increases the yield of pyrolytic tars as pyrolysis temperatures increase. At the same time, a slight change in the proportions of C_4-C_8 is possible due to the scission of C_{al}-C_{al} and C_{al}-C_{ar} bonds [61]. Furthermore, coal fluidity may increase while the ratio of CH_3 to CH_2 may decrease in the char [61]. At lower pyrolysis temperatures, the presence of kaolinite produces chars with reduced contents of VM, which correlates with an increased yield of pyrolytic tars at 500 °C [62]. Additionally, Roets et al. [63] indicated that the addition of kaolinite was associated with the cracking of tar to form increases yields of H_2 and thereby increase the overall gas yield. This finding coincides with the temperature range wherein kaolinite transforms to meta-kaolinite [54].

2.5.3 Effect of Extraneous Dolomite

Extraneous dolomite has been found to have various effects during coal pyrolysis. Malaysian Dolomite has shown potential as a deoxygenation catalyst, producing high-quality biofuel with desirable hydrocarbon content [64]. According to Hafriz et al. [65], natural dolomite (representing extraneous dolomite) can be used as a catalyst to promote the cracking of anthracene oil, resulting in the formation of more valuable products. Extraneous dolomite has also been investigated for high-temperature desulphurisation of coal-derived gases, showing effective

removal of H_2S but with limitations in the presence of water vapour [66]. Additionally, dolomitic limestones have been evaluated for flue gas desulphurisation, showing little effect of impurities on the calcination and desulphurisation processes [67]. These studies highlight the potential of dolomite in various catalytic and desulphurisation processes but also indicate the need to consider the specific conditions and limitations associated with its use.

The decomposition of pure dolomite under pyrolysis conditions takes place at 700 °C to form CaO and MgO [68]. Roets et al. [62] observed no significant differences in the nitrogen contents of the chars, but extraneous dolomite facilitated nitrogen removal in the chars at 750 °C and 900 °C. Interestingly, the sulphur fixation by dolomite is active at 500 °C. The CaO derived from extraneous dolomite decomposition can react with heterocyclic nitrogen forms in the char (char-N) to form interstitial species such as CaC_xN_y and $CaO_xC_yN_z$ at 850 °C [62, 69]. Sulphur fixation, on the other hand, can be associated with the formation of CaS and $CaSO_3$ by the interaction of H_2S and sulphur dioxide (SO_2) with CaO [70]. Unlike extraneous kaolinite, the reaction atmosphere has a much higher impact on dolomite decomposition [71]. At around 500 °C, dolomite does not affect tar yield, but its effects start being significant at T> 750 °C due to its higher decomposition temperature [68]. Roets et al. [63] have reported a decrease in tar yield due to secondary tar cracking and re-polymerisation, catalysed by calcium, which provides a nascent crosslink site in coal. Subsequently, this mechanism enhances the coordination of carboxyl and hydroxyl groups through hydrogen bonds [72]. It has also been reported that calcium oxide can decrease the release of pyrolysates at 700-900 °C due to its associated decrease in the fluidity temperature, sulphur and nitrogen capturing [73–75]. Dolomite also reduces the yield of H_2, while its effect on CO yield is temperature-dependent [63]. The addition of calcium oxide in the pyrolysis process of oil sludge (OS) can capture sulphur-containing gases, reducing their release during thermochemical processing [75]. Furthermore, the presence of calcium oxide in the pyrolysis of OS allows for the purification of pyrolysis gas from hydrogen sulphide (H_2S) and reduces the sulphur content in the liquid products [76]. Calcium oxide also plays a role in reducing the release of nitrogen-containing gases such as NH_3 and HCN during coal pyrolysis by catalytically enhancing the fracture and combination of chemical bonds [77].

2.5.4 Effect of Extraneous Calcite

Calcite has been found to have different effects on product distribution during pyrolysis depending on the specific conditions and materials being studied. In the presence of coal, the addition of calcite or lime reduces the yield of hydrocarbon products at high temperatures. It increases the yield of CO, likely due to lime-catalysed secondary cracking reactions and base catalysis of phenolic group decomposition [78]. Calcite decomposition takes place at around 800 °C, resulting

in the formation of quick lime (CaO) and CO_2 [79]. The presence of CaO formed from calcite decomposition reduces sulphur-containing compounds (H_2S and sulphur dioxide (SO_2)) by sulphur fixation [80]. In addition, it is known to significantly influence the yields and composition of pyrolytic products, even at low loading ratios (less than 10 wt. %). During the coal coking process, CaO can promote the transformation of HCN to NO, while reducing the nitrogen content in the solid residue [81]. During catalytic pyrolysis of brown coals, the formation of light aromatic hydrocarbons is promoted by the CaO-supported Fe-Ca catalyst while the yields of water and gas are reduced [82]. However, in the pyrolysis of oil shale kerogen, calcite appears to inhibit the formation of oil, while minerals like montmorillonite and gypsum promote oil formation and minimise residual products [83]. Additionally, in the pyrolysis of corn stalks, adding a high amount of CaO leads to a decrease in non-condensable gas yield and an increase in H_2 concentration, indicating catalytic effects on the pyrolysis process [84]. Although some of the literature is not on coal pyrolysis, the consensus is that the effect of calcite on product distribution during pyrolysis can vary depending on the specific system and conditions being studied.

2.5.5 Effect of Extraneous Pyrite

The behaviour of extraneous/discrete pyrite particles during coal pyrolysis involves its transformation and decomposition processes. These processes are controlled by sulphur availability, diffusion rate, and the availability of oxygenated and hydrogenated functional groups during pyrolysis [85]. For instance, in the presence of a hydrogen donor such as tetrahydronaphthalene or H^+ in the activated complex, the conversion of the coal organic matrix can be enhanced via pyrite reduction reaction pathways. Chen et al. [86] illustrated that these hydrogen donation effects on pyrite decomposition are significant for indigenous hydrogen (such as hydrogen associated with coal carbon matrix), while oxygenated compounds may compete with pyrite for hydrogen. As a result, the latter's tendency may minimise the conversion of pyrite into organic sulphur. This behaviour would lead to a low char yield, higher carbon conversion, tar yield, and the yield of gas products, such as H_2, CH_4 and C_2Hx, during coal pyrolysis because pyrite catalyses the bond dissociation reactions of the coal carbon matrix [87].

From a transport phenomenon point of view, the smaller coal particles associated with pyrite tend to facilitate the formation of low-sulphur (FeS) phases along with elemental iron in char [88]. Interestingly, the presence of the organic matrix further promotes the conversion of FeS to form traces of SO_2 at 350-570 °C. The intermediate pyrolytic char can interact with residual pyrite to form pyrrhotite, and this reaction is more pronounced at 920 °C. It is noteworthy that the decomposition of pure pyrite particles occurs at 500 °C [52]; only pyrite particles contaminated

with carbon particles may start to decompose at 350 °C. The following pyrite decomposition reactions presented in Reaction 1 and Reaction 2 have been adapted from Chen et al. [86].

At 0.1 MPa and temperatures below 950 °C under a nitrogen atmosphere

Reaction 1

$$FeS_2 \rightarrow FeS_{1.2} \rightarrow FeS$$

At 3 MPa and temperatures below 800 °C under a nitrogen atmosphere

Reaction 2

$$FeS_2 \rightarrow FeS_{1.34}$$

2.5.6 Inherent Mineral Matter

2.5.7 Non-mineral Inorganic Elements

Non-mineral inorganic elements in coal can be classified into two groups: those of intimate, organic association (i.e. exchangeable cations dissolved in pore waters) and those of organic association (i.e., carboxylate salts). The intimate and organic associations of these inorganic elements within the macerals, the carbon matrix, are because of the multiple mechanisms, such as metalation, chelation, and carboxylation reactions that occurred during coal formation [89]. These different associations of non-mineral inorganic elements in the organic fraction of coal undergo different reaction pathways and the formation of artefact minerals during gasification, pyrolysis and combustion processes [48, 90, and 91]. These artefact minerals, such as mullite, anorthite, and amorphous aluminosilicate, may pose downstream handling problems by eroding and abrading plant components. At the same time, the intermediate artefacts (calcium oxide, magnesium oxide and pyrrhotite) formed by the interaction of non-mineral inorganics with each other or with nearby minerals may either catalyse or impede some reactions. In addition, the composition of non-mineral inorganic elements varies from seam to seam due to different geochemical and geophysical processes that took place during coalification and with coal age (decreasing from lignite to anthracite). The strengthening of covalent and hydrogen bonds with the ageing of coal leads to the rejection of weak organo-metallic bonds via demetalation and deceleration reactions due to their incompatibility with the evolving organic structures [89]. As a result, geographical location and coal age need to be considered when determining the suitability of coal for thermochemical utilisation. This further emphasises the importance of fully discerning the composition of coals from different seams.

2.5.8 Bound by Organic Matter/Organically Associated Inorganic Elements

Alkali and alkaline earth minerals (AAEM) such as calcium (Ca), magnesium (Mg), sodium(Na) and potassium (K), along with rare earth elements (REE) such as lanthanum (La), cerium (Ce), praseodymium (Pr), neodymium (Nd), promethium (Pm), samarium (Sm), europium (Eu), gadolinium (Gd), scandium (Sc), yttrium (Y), highly rare earth elements (HREE) such as terbium (Tb), dysprosium (Dy), holmium (Ho), erbium (Er), thulium (Tm), ytterbium (Yb), lutetium (Lu), and scandium (Sc), and toxic elements, are typically organically associated with coal macerals and nano clay minerals. The modes of occurrence of REEs in coal macerals vary depending on the coal types and the stage of the coalification process. In low-rank coals, REEs are primarily associated with the coal organic matrix, particularly humic substances. As coal undergoes coalification, the REEs gradually transition from primary organic compounds to primary minerals, such as authigenic minerals (pyrite, calcite, dolomite, kaolinite, illite, quartz, siderite and smectite), anthracite, and graphite [92]. In bituminous coals, REEs are found in different solid fractions, including water-soluble, exchangeable, acid-soluble, reducible, and oxidisable fractions [93]. The mobility of REEs is associated with exchangeable, oxidisable, and acid-soluble fractions. At the same time, non-extractable REEs are likely held in refractory apatite phases and primary REE-phosphates [93]. The modes of occurrence of REEs in coal macerals provide insights into their behaviour during coal processing. They can guide extraction techniques for REE recovery from coal-related materials [94].

The use of advanced techniques such as Scanning Electron Microscopy with Energy Dispersive X-rays (SEM-EDX), Transmission electron microscopy (TEM), and TESCAN Integrated Mineral Analysis (TIMA) can confirm the presence and mode of occurrence of these elements in coal [95]. However, the low and trace concentrations present in coal make their accurate quantification challenging [96]. Figure 2-2 illustrates typical REE phosphates association in sub-bituminous rank B coal ash from the Azeiskoe coalfield [94]. As a result, ICP analysis of the aqueous solution obtained from acid digestion solution of the coal ash is often adopted for REE quantification [95]. Matjie [36] has reported that not more than 0.2% of organically associated inorganic elements are present in SA Highveld feed coals fed to gasifiers, while Li et al. [89] reported up to 1.5% of organically associated inorganic elements in low-ranked Chinese coals. Regardless of their low concentrations, organically associated inorganic elements influence reactivities and the nature of products obtained during pyrolysis, gasification, and combustion [97]. As a result, their quantification and understanding of the reaction mechanisms under different conditions are vital for the efficient utilisation of coal in thermochemical processes.

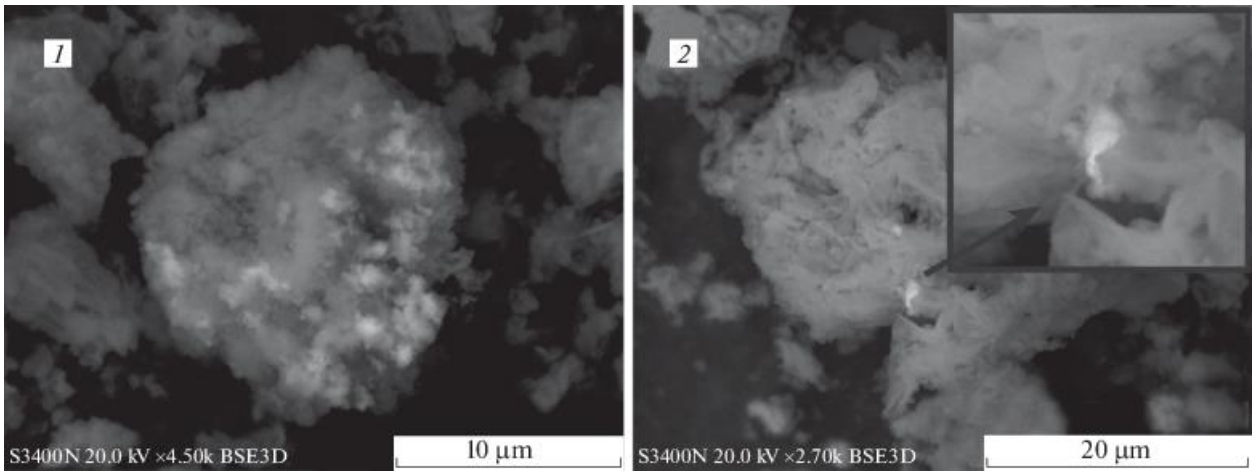

Figure 2-2: Film-like mineral phases of REE phosphates (light) in the coal ash. Subbituminous B coal: *1*— rare-earth phosphate minerals (light) in the coal ash; *2*—inclusion of rare-earth phosphate minerals in film-like material (adapted from [79]).

During the gasification process, the organically associated inorganic elements, especially the fluxing elements such as Mg, Na, Ca, and Fe), interact with meta-kaolinite ($2SiO_2.Al_2O_3$) from the transformation of inherent kaolinite to form slags and clinkers [98-100]. A detailed slag model has been established to understand the formation and flow of molten slag in a water-cooled membrane wall pulverised coal gasifier, providing insights into wall heat transfer and reactor operation [101]. This was necessary because the slags and clinkers are formed due to ash deposition, and they cause problems such as heat transfer limitations and corrosion and erosion of reactor internals. However, the organically associated inorganic elements have also been reported to catalyse the pyrolysis and gasification reactions [102]. The cations of fluxing inorganic elements such as Ca^{2+}, K^{+}, Fe^{2+}, and Na^{+}, which are non-mineral inorganics, are commonly found in the pore waters of coal. There is no clear discernment of their propensity to initiate slag and clinker formation or to the effect of fluxing elements found in pore waters vs organic matter. Additionally, silicates, aluminosilicates, and Ca-Fe and Fe oxides can have catalytic actions during carbon gasification, enhancing the reactivity of the slag [103].

The accumulation of REE, HREE, and toxic elements in the gasifier ashes, surrounding soils and air is indisputable and may be related to health issues [97]. For instance, studies conducted near the Plomin thermal power plant in Croatia show that the ashes emitted from the plant influenced the REE composition of the surrounding soils, with higher REE levels recorded in recent ash samples [104, 105]. A study was also conducted near a municipal solid waste incinerator (MSWI) and found that the concentrations of potentially harmful elements in soil were influenced by wind direction, with higher concentrations in the area northwest of the MSWI [106]. The accumulation

and fate of toxic elements in soils can occur over long operation times, and it is essential to monitor these levels and understand contributing parameters, especially when processing high REE and HREE-rich coals.

2.6 Influence of Inherent Mineral Matter on Coal Pyrolysis

Coal pyrolysis is a fundamental stage in combustion and gasification. It is profoundly influenced by the presence of inherent mineral matter. Inherent mineral matter encompasses a diverse range of inorganic elements and compounds that are inherently rooted within the coal matrix. Consequently, these minerals can interact with each other and with the coal carbon matrix and affect the reaction kinetics, product distribution, and carbon conversion efficiency. As a result, understanding the complex dynamics of inherent mineral matter during coal pyrolysis is essential for optimising coal utilisation technologies and addressing environmental challenges associated with coal combustion and gasification. This subsection provides a brief assessment of the influence of inherent mineral matter on coal pyrolysis. It provides insight into its effectiveness in the thermal decomposition of coal and the characteristics of pyrolysis products. A summary of the findings of the literature on the effect of inherent mineral matter is presented in Table 2-3.

The effect of alkali and alkaline earth metallic (AAEM) species on coal pyrolysis has been studied in the provided papers. It has been reported that metal chlorides such as KCl, $ZnCl_2$, and $MnCl_2$, including AAEM chlorides (i.e., Ca and K), have a catalytic effect on coal pyrolysis, influencing the production of hydrogen, methane, and tar during the process [70, 107]. Although the catalytic mechanisms of chlorinated AAEM have been extensively discussed, the specific effects of transition metal ions (such as Co^{2+}, Ni^{2+}) and of KCl, $ZnCl_2$, and $MnCl_2$ on coal pyrolysis are still unclear [108, 109]. The presence of organically associated inorganic Na-acetate can act as a catalyst for char gasification, affecting the reactivity of the coal [110]. However, the dispersion and chemical forms of AAEM species on the char surface play a significant role in their catalytic potency. For instance, the accumulation of Na on the surface of the char during pyrolysis leads to the formation of Na-containing clusters within gasification zones, which have higher catalytic activities than finely dispersed Na-containing species. This accumulation of Na on the pore surface enhances the char reactivity, resulting in increased specific reactivity values of the chars. However, at higher char conversion levels, the heterogeneity of the char structure becomes a limiting factor. The highly condensed/graphitised carbonaceous matter tends to concentrate in the char, leading to lower reactivity values. There needs to be more than the dispersion of Na to maintain high char reactivity at high conversion levels due to the heterogeneity of the char structure [108].

Table 2-3: Summary of literature findings on the effects of inherent mineral matter on coal pyrolysis.

Author	Aim	Results
Quyn et al. [110]	Studied the catalytic effects of NaCl and Na carboxylates in Victorian brown coal on char reactivity.	NaCl and sodium carboxylates have different catalytic effects on char reactivity. Na-exchange coal showed increased reactivity with increasing pyrolysis temperature. Chemical form and dispersion of Na in char govern catalytic effects.
Xu et al. [111]	Investigated Na volatilisation during pyrolysis and its catalytic effects and loading saturation level in char. This was achieved by physically impregnating NaCl into coal.	The volatilisation of Na during pyrolysis is an important factor in catalyst loading saturation. Peak pyrolysis temperature affects the release of Cl and distribution of Na in char. The catalytic activity of Na depends on the char/carbon structure.
Yang et al. [80]	Studied the effects of different forms of sodium, chlorine, and sulphur on volatilisation and deposition.	Acid elution treatment significantly reduces Na deposition in coal. Cl is more competitive than S in enhancing Na-bearing compound deposition. The addition of CaO captures volatile Cl atoms and reduces NaCl deposition. Water-and ammonium acetate-soluble Na content in chars is low due to their higher volatilisation. Interactions between Na-bearing compounds and coal matrix affect Na deposition.

Author	Aim	Results
Liu et al. [107]	Investigated catalytic effects of KCl, $ZnCl_2$, and $MnCl_2$ on lignite pyrolysis by acid washing and Mn, Zn and K chloride addition	Mn, Zn and K chlorides have little effect on the structure of coal. The inherent mineral matter has a catalytic effect on the pyrolysis process. Mn, Zn and K chlorides enhance CH_4 production but impede CO production. The catalytic mechanism of KCl was different from $MnCl_2$ and $ZnCl_2$.
Wei et al. [112]	Examined trace elements volatilisation during oxidative pyrolysis of coal from southwest Guizhou Province in China	As, Sb, Pb, Zn, Cd, and Cr are moderately volatile trace elements at higher temperatures, but As, Sb, Pb, Zn, Cd, and Cr are highly volatile below 450°C Arsenic exhibits high release at 900-1000°C due to association with sulphide. The volatility of trace elements correlates with the mode of element occurrence
Kuo et al. [113]	Studied mineral matter and temperature affect the conversion of carboxylic acids in brown coals.	Clays and quartz impede diffusion and suppress the formation of certain compounds. Cations catalyse the decomposition of carboxylic dimers and promote the formation of anhydrides and RCOOAr.
Li et al. [114]	Investigate the effects of Ca^{2+} species on direct liquefaction of lignite	Exchangeable Ca^{2+} in coal inhibits the direct liquefaction process. Ca^{2+} loaded by physical mixing has less detrimental effects on oil yield. Discrete calcium salts have negligible influence on the liquefaction process.

Author	Aim	Results
Liang et al. [115]	Studied the transformation of alkali and alkaline earth metals (AAEMs) in Zhundong coal during pyrolysis	Na content in coal char initially increased, then decreased, and finally increased. Pyrolysis temperature affects the occurrence modes and distribution of AAEMs K, Mg, and Ca contents in coal char changed slightly before 700 °C and increased continuously after 700 °C. Water-soluble sodium and exchangeable sodium decrease with increasing pyrolysis temperature. Insoluble potassium content remains relatively unchanged. HCl-soluble magnesium and calcium decompose and form insoluble silicates or aluminosilicates.
He et al. [116]	Studied the effects of alkali and alkaline earth metals (AAEM) on Fe-catalysed coal pyrolysis	The enhanced catalytic effect of AAEM on Fe catalyst was in the order of Na > K > Ca > Mg. High H_2 selectivity and low yield towards CO_2 were observed. AAEM promote the reduction of Fe species and dispersion of Fe particles. AAEM combined with an oxygen-containing functional group generated CeO-AAEM and COO-AAEM.

On the other hand, calcium species are usually associated with aromatic carbons, which results in the maximum specific reactivity of coal with such associations [110]. During the early stages of gasification, the concentration of catalyst on the char surface increases, leading to an increase in reactivity. However, at later gasification stages, changes in the overall char structure become significant. The preferential removal of smaller aromatic ring systems and the persistence of cross-linking structures hinder the access of catalysts and oxygen to the interior carbons, resulting in a decrease in reactivity. Therefore, the poor dispersion of calcium-based catalysts on the char surface at later gasification stages is mainly responsible for the decrease in reactivity [117].

2.7 Conclusions

A literature review study was conducted to evaluate the state of the art of coal mineral matter, mode of occurrence, and their effects during pyrolysis. This conclusion highlights the significance of coal pyrolysis and the mode of occurrence of mineral matter, the diversity of analytical and physical techniques following their different basic principles and functions used for characterisation and classification studies, and the importance of understanding mineral matter behaviour for optimising coal processing. Understanding coal pyrolysis and mineral matter is crucial for optimising thermochemical processes and reactor designs because mineral matter significantly impacts reaction mechanisms, ash formation, energy recovery, and environmental implications. Inherent mineral matter undergoes complex reactions influenced by its mode of occurrence. Extraneous minerals influence pyrolysis reactions and product yields; for instance, quartz acts as an inert diluent, while kaolinite influences water gas shift reactions, subsequently affecting the gas composition. The presence of extraneous minerals alters pyrolysis product composition and yields, necessitating future studies to elucidate their effects on coal pyrolysis, especially major coal minerals. Dolomite shows efficacy in various processes but may be limited by water vapour, while calcite and dolomite decomposition impact product distribution and sulphur removal. CaO derived from calcite plays diverse roles in pyrolysis, influencing product formation, although calcite's effect on pyrolysis varies depending on conditions, inhibiting tar formation. Pyrite's behaviour is controlled by sulphur availability. It influences pyrolysis kinetics and product distribution, with its decomposition affecting pyrolysis kinetics and product distribution.

Evidently, the use and integration of multiple analytical techniques such as LTA-XRD, XRF, ICP, Raman and HRTEM is essential for accurate discernment of the mode of occurrence of mineral matter and its quantification in coal. While XRD provides qualitative and quantitative results on the proportions of crystalline and amorphous phases, XRF and ICP is used to complement these results by providing quantitative elemental analysis results of coal ash

samples, which is used for stoichiometry verifications. ICP is essential for analysing aliquots from chemical fractionation tests, which aid in discernment of the mode of occurrence of mineral matter by selective leaching. Raman spectrometry offers mapping and single point analysis of organic as well as mineralogical analysis while HRTEM high-resolution visualisation of nanoscale mineral phases and non-mineral inorganic intimately associated with coal carbon matrix. These tools are vital for understanding coal's reactivity in pyrolysis, gasification and combustion processes.

A summary of the key findings is presented below.

2.8 Summary of Key Findings

- The study of coal pyrolysis and mineral matter is crucial for optimising thermochemical processes and reactor designs by using a combination of selected analytical techniques.
- Mineral matter in coal significantly affects reaction mechanisms, ash formation, energy recovery, and environmental pollution implications.
- Various techniques, including density separation, chemical fractionation, and different advanced and conventional analytical methods, are employed to discern mineral matter in coal.
- Inherent mineral matter, comprising non-mineral inorganic elements and organically associated elements, undergoes complex reactions during coal processing.
- The mode of occurrence of mineral matter, whether extraneous or inherent, plays a crucial role in coal behaviour and processing outcomes.
- A comprehensive understanding of mineral matter in coal is essential for efficient coal utilisation in thermochemical processes.
- Coal pyrolysis is a critical stage in thermochemical processing, with extraneous minerals exerting significant influence on reaction mechanisms and product outcomes.
- Understanding the transformation and interaction of extraneous minerals during coal pyrolysis is crucial for optimizing process efficiency and product quality.
- Quartz, kaolinite, dolomite, calcite, and pyrite are prominent extraneous minerals in South African coals, each impacting pyrolysis reactions differently.
- Extraneous minerals such as quartz act as inert diluents, while kaolinite undergoes dehydroxylation, forming metakaolinite and influencing water gas shift reactions.
- The presence of extraneous minerals affects the composition and yields of pyrolytic tars, chars, and non-condensable gases, altering process kinetics and product selectivity.

- Future studies should focus on elucidating the mechanisms underlying the effects of extraneous minerals on coal pyrolysis and exploring strategies to optimise process performance considering mineral variability.
- Studies suggest dolomite's efficacy in cracking anthracene oil and the desulphurisation of coal-derived gases. However, its effectiveness may be limited by water vapour presence.
- Decomposition of dolomite at 700 °C yields CaO and MgO, facilitating nitrogen and sulphur removal in chars through the formation of interstitial species.
- Dolomite's impact on tar yield, hydrogen, and carbon monoxide production is temperature-dependent, with significant effects observed at temperatures exceeding 750 °C.
- Calcite influences product distribution during pyrolysis, reducing hydrocarbon yields and promoting CO production due to lime-catalysed secondary cracking reactions.
- Decomposition of calcite at around 800 °C forms CaO, which reduces sulphur-containing compounds through sulphur fixation and influences pyrolytic product yields and composition.
- CaO derived from calcite decomposition plays diverse roles in coal pyrolysis, including the transformation of HCN to NO, the reduction of nitrogen content, and the enhancement of compressive strength and light aromatic hydrocarbon formation.
- However, calcite's effect on pyrolysis product distribution varies depending on the specific system and conditions studied, with instances of inhibition of oil formation observed in some cases.
- Pyrite's behaviour during coal pyrolysis involves transformation and decomposition processes controlled by sulphur availability, diffusion rate, and the presence of hydrogen donors.
- Pyrite reduction reaction pathways, facilitated by hydrogen donation, enhance the conversion of coal organic matrix, leading to lower char yield, higher carbon conversion, and increased tar and gas product yields.
- Pyrite catalyses bond dissociation reactions of the coal carbon matrix, promoting the formation of low sulphur-containing phases such as FeS and elemental iron in char.
- The presence of an organic matrix further promotes the conversion of FeS to SO_2, with the decomposition of intermediate pyritic char to pyrrhotite becoming more pronounced at higher temperatures.
- Decomposition of pure pyrite particles occurs at higher temperatures, while contamination with carbon particles lowers decomposition temperature, affecting pyrolysis kinetics and product distribution.

Chapter 3, comprises a manuscript titled "*Properties and reactivity of two oxidised and unoxidised South African Highveld fine-coal rejects and their density-separated fractions*", detailing the properties of two fine-coal reject samples. One sample has experienced oxidation, while the other one is unoxidised. Density separation is performed, and the density fractions from this process are characterised by several analytical techniques relating to mineralogical, petrographic, physical and chemical composition (see Table 2-1). The chemical fractionation and demineralisation of the fine-coal reject samples were employed to study the distinctive nature of coal mineral matter, and the results obtained are also reported.

Chapter References

[1] Nyoni S, Bwalya M, Chimwani N. Beneficiation potential of a low-grade coal from the Emalahleni (Witbank) coalfield. Physicochemical Problems of Mineral Processing. 2020; 56:849-859.

[2] Tang X, Pu W, Chen Q, Liu R, Yang Y. An experimental investigation on hydrogen generation from in-situ gasification by pyrolysis. International Journal of Hydrogen Energy. 2024 Jan 2; 49:1019-27.

[3] Pretorius GN, Bunt JR, Gräbner M, Neomagus H, Waanders FB, Everson RC, Strydom CA. Evaluation and prediction of slow pyrolysis products derived from coals of different rank. Journal of analytical and applied pyrolysis. 2017; 128:156-67.

[4] Dang J, Xie Q, Liang D, Wang X, Dong H, Cao J. The fate of trace elements in Yanshan coal during fast pyrolysis. Minerals. 2016; 6(2):35.

[5] Rautenbach R, Strydom CA, Bunt JR, Matjie RH, Campbell QP, Van Alphen C. Mineralogical, chemical, and petrographic properties of selected South African power stations' feed coals and their corresponding Density-separated fractions using float-sink and reflux classification methods. International Journal of Coal Preparation and Utilisation. 2019; 39:421–46.

[6] Matjie RH, Li Z, Ward CR, French D. Chemical composition of glass and crystalline phases in coarse coal gasification ash. Fuel. 2008; 87:857–69.

[7] Singh N, Shehnazdeep, Bhardwaj A. Reviewing the role of coal bottom ash as an alternative of cement. Construction and Building Materials. 2020; 233:117276.

[8] Matjie RH, Li Z, Ward CR, Kosasi J, Bunt JR, Strydom CA. Mineralogy of furnace deposits produced by South African coals during pulverised-fuel combustion tests. Energy and Fuels. 2015; 29:8226–38.

[9] Huang Z, Li Y, Lu D, Zhou Z, Wang Z, Zhou J, et al. Improvement of the coal ash slagging tendency by coal washing and additive blending with mullite generation. Energy and Fuels. 2013; 27:2049–56.

[10] Ramudzwagi M, Tshiongo-Makgwe N, Nheta W. Recent developments in beneficiation of fine and ultra-fine coal-review paper. Journal of Cleaner Production. 2020; 276:122693.

[11] Rautenbach R, Matjie R, Strydom C, Bunt J. Transformation of inherent and extraneous minerals in feed coals of commercial power stations and their density-separated fractions. Energy Geoscience. 2021; 2:136–47.

[12] Ward CR. Analysis and significance of mineral matter in coal seams. International Journal of Coal Geology. 2002; 50:135–68.

[13] Raghoo M. The volatilisation of aluminium and silicon species from a Highveld coal [PhD thesis]. Potchefstroom, South Africa: North-West University 2010.

[14] Kumar, S. and Rawat, V. Froth flotation of refuse coal fines and process optimization using 2D surface plots. Journal of Central South University. 2016; 23:2520-2525.

[15] Maré E, Beven B, Crisafio C. Developments in nonmagnetic physical separation technologies for hematitic/goethitic iron ore. In Lu, L., editor. Iron Ore: Mineralogy, Processing and Environmental Sustainability. 2015 p. 309-338.

[16] Jambal D, Kim BG, Jeon HS, Lee JH. Physical separation using an autogenous medium on coal. Separation Science and Technology. 2017; 52:958–64.

[17] Prudich ME, Henry JD. Surface chemistry applications in mineral matter removal from coal-derived liquids. In: Gregory DB, Yuli MG, editors. Interfacial Phenomena in Coal Technology, Boca Raton: CRC Press; 2022, p 425–46.

[18] Wang KC, Alvarez J; Seminis Vegetable Seeds Inc, Liquid density separation system US20150238974A1, January 2015.

[19] Grieco EM, Baldi G. Predictive model for counter-current coal gasifiers. Chemical engineering science. 2011; 66:5749–61.

[20] Strydom CA, Bunt JR, Schobert HH, Raghoo M. Changes to the organic functional groups of an inertinite rich medium rank bituminous coal during acid treatment processes. Fuel Processing Technology. 2011; 92:764–70.

[21] Song Q, Zhao H, Jia J, Yang L, Lv W, Gu Q, et al. Effects of demineralisation on the surface morphology, microcrystalline and thermal transformation characteristics of coal. Journal of Analytical and Applied Pyrolysis. 2020; 145:104716.

[22] Rietveld HM. A profile refinement method for nuclear and magnetic structures. Journal of Applied Crystallography. 1969; 2:65–71.

[23] Liu, Y., Gupta, R., Sharma, A., Wall, T., Butcher, A., Miller, G., Gottlieb, P. and French, D. Mineral matter–organic matter association characterisation by QEMSCAN and applications in coal utilisation. Fuel. 2005; 84(10):1259-1267.

[24] Reed SJ. Electron microprobe analysis and scanning electron microscopy in geology. Cambridge University Press; 2005

[25] Wang B, Liu M. Ashing temperature of lignite and mineral transition sequence. Journal of Geochemical Exploration. 2018; 193:41-51.

[26] Ward CR. Mineral matter in Australian bituminous coals. Proceedings - Australian Institute of Mining and Metallurgy Australas, Smith J (eds.), Melbourne, Australia, 1978. p. 265-270.

[27] Pansu M, Gautheyrou J. Mineralogical Analysis by Infra-Red Spectrometry. Handbook of Soil Analysis: Mineralogical, Organic and Inorganic Methods. 2006:133-65.

[28] Iwashita A, Nakajima T, Takanashi H, Ohki A, Fujita Y, Yamashita T. Effect of pretreatment conditions on the determination of major and trace elements in coal fly ash using ICP-AES. Fuel. 2006; 85(2):257-63.

[29] Falcon, R. M. S. and Snyman, C. P. (1986) 'An introduction to coal petrography: Atlas of petrographic constituents in the bituminous coals of Southern Africa', The Geological Society of South Africa, Review. 1989; 2:1-27

[30] Wagner N, Eble C, Hower J, Falcon R. Petrology and palynology of select coal samples from the Permian Waterberg Coalfield, South Africa. International Journal of Coal Geology. 2019; 204:85-101.

[31] Matjie RH, French D, Ward CR, Pistorius PC, Li Z. Behaviour of coal mineral matter in sintering and slagging of ash during the gasification process. Fuel Processing Technology. 2011; 92:1426–33.

[32] Norrish K, Hutton JT. An accurate X-ray spectrographic method for the analysis of a wide range of geological samples. Geochimica et Cosmochimica Acta. 1969; 33:431–53.

[33] Raman C. V. and Krishnan K. S. A new type of secondary radiation. Nature. 1928; 121: 501–502.

[34] Potgieter-Vermaak S, Maledi N, Wagner N, Van Heerden JH, Van Grieken R, Potgieter JH. Raman spectroscopy for the analysis of coal: a review. Journal of Raman Spectroscopy. 2011; 42(2):123-9.

[35] Van Dyk JC, Baxter LL, Van Heerden JHP, Coetzer RLJ. Chemical fractionation tests on South African coal sources to obtain species-specific information on ash fusion temperatures (AFT). Fuel. 2005; 84:1768–77.

[36] Matjie RH. Sintering and slagging of mineral matter in South African coals during the coal gasification process [PhD thesis]. Pretoria, South Africa: University of Pretoria; 2008.

[37] Bokanyi L, Csöke B. Preparation of clean coal by flotation following ultra fine liberation. Applied Energy. 2003; 74:349-58.

[38] Dai S, Hower JC, Finkelman RB, Graham IT, French D, Ward CR, Eskenazy G, Wei Q, Zhao L. Organic associations of non-mineral elements in coal: A review. International Journal of Coal Geology. 2020; 218:103347.

[39] Matjie RH, French D, Ward CR, Pistorius PC, Li Z. Behaviour of coal mineral matter in sintering and slagging of ash during the gasification process. Fuel Processing Technology. 2011; 92:1426–33.

[40] Matjie RH, Li Z, Ward CR, Bunt JR, Strydom CA. Determination of mineral matter and elemental composition of individual macerals in coals from Highveld mines. Journal of the Southern African Institute of Mining and Metallurgy. 2016; 116:169–80.

[41] Tsemane MM, Matjie RH, Bunt JR, Neomagus HWJP, Strydom CA, Waanders FB, et al. Mineralogy and petrology of chars produced by South African caking coals and Density-Separated Fractions during pyrolysis and their effects on caking propensity. Energy and Fuels. 2019; 33:7645–58.

[42] Roets L. The effect of mineral addition on the pyrolysis products derived from typical Highveld coal [Master's thesis]. Potchefstroom, South Africa: North-West University; 2014.

[43] Van Dyk JC, Benson SA, Laumb ML, Waanders B. Coal and coal ash characteristics to understand mineral transformations and slag formation. Fuel. 2009; 88:1057–63.

[44] Mangena SJ, Bunt JR, Waanders FB, Baker G. Identification of reaction zones in a commercial Sasol-Lurgi fixed bed dry bottom gasifier operating on North Dakota lignite. Fuel. 2011; 90:167–73.

[45] Xiao R, Wang Y, Zhang Y, Xiong Z, Zhang J, Zhao Y. Effect of kaolinite additive on water-soluble sodium release and particle matter formation during Zhundong coal combustion. Fuel. 2023; 333:126422.

[46] Wu H, Zhang Y, Chen W, Liu Z, Zhang T, Sun Q, et al. Experimental research on the characteristics of ash in oxy-fuel combustion. Fuel. 2020; 263:116799.

[47] Mphahlele K, Matjie RH, Bunt JR, Uwaoma RC. Properties and reactivity of two oxidized and unoxidised South African Highveld fine-coal rejects and their density-separated fractions. International Journal of Coal Preparation and Utilisation. 2023; 43:1451–77.

[48] Rautenbach R, Matjie RH, Strydom CA, Bunt JR, Ward CR, French D, et al. Evaluation of mineral matter transformations in low-temperature ashes of South African coal feedstock samples and their Density-separated cuts using high-temperature X-ray diffraction. International Journal of Coal Preparation and Utilisation. 2020; 40:320–47.

[49] Krull S. Analytical Chemistry. InTech. 2012. Available from https://doi.org/10.5772/3086.

[50] Zhang S, Rajendran S, Henderson S, Zeng D, Xiao R, Bhattacharya S. Use of pyrite cinder as an iron-based oxygen carrier in coal-fuelled chemical looping combustion. Energy and Fuels. 2015; 29:2645–55.

[51] Cao Y, Chen W, Yuan Y, Wang T, Sun J. Gas generation and Its carbon isotopic composition during Pyrite-Catalysed pyrolysis of shale with different maturities. Processes. 2022; 10:2296.

[52] Xu H, Guo X, Seaman LA, Harrison AJ, Obrey SJ, Page K. Thermal desulphurisation of pyrite: An in-situ high-T neutron diffraction and DTA-TGA study. Journal of Materials Research. 2019; 34:3243–53.

[53] Ward CR. Analysis, origin and significance of mineral matter in coal: An updated review. International Journal of Coal Geology. 2016; 165:1–27.

[54] Cheng H, Li K, Liu Q, Zhang S, Li X, Frost RL. Insight into the thermal decomposition of kaolinite intercalated with potassium acetate: An evolved gas analysis. Journal of Thermal Analysis and Calorimetry. 2014; 117:1231–9.

[55] Punjak WA, Shadman F. Aluminosilicate sorbents for control of alkali vapours during coal combustion and gasification. Energy & Fuels. 1988; 2:702–8.

[56] Mphahlele K, Matjie RH, Bunt JR. Catalytic Effect of Reactive Extraneous Mineral Composites on Char and Tar Distribution during Pyrolysis of Highveld Partially Oxidised Fine-Coal Reject and Its Beneficiated Residues. ACS Omega. 2023; 8:36479–92.

[57] Hlatshwayo TB, Matjie RH, Li Z, Ward CR. Mineralogical characterisation of SASOL feed coals and corresponding gasification ash constituents. Energy and Fuels. 2009; 23:2867–73.

[58] Matjie R, Bunt J, Stokes W, Bijzet H, Mphahlele K, Uwaoma R, et al. Interactions between Kaolinite, Organic Matter, and Potassium Compounds at Elevated Temperatures during Pyrolysis of Caking Coal and Its Density-Separated Fractions. Energy and Fuels. 2021;35:13268–80.

[59] Xu Y, Liu X, Wang H, Zeng X, Zhang Y, Han J, et al. Influences of in-furnace kaolin addition on the formation and emission characteristics of PM2.5 in a 1000 MW coal-fired power station. Environmental Science & Technology. 2018; 52:8718–24.

[60] Prempeh K, Chequer L, Badalyan A, Bedrikovetsky P. Effects of kaolinite on fines migration and formation damage. Proceedings - SPE International Symposium on Formation Damage Control 2020. 2020-February.

[61] Meng F, Gupta S, Yu J, Jiang Y, Koshy P, Sorrell C, et al. Effects of kaolinite addition on the thermoplastic behaviour of coking coal during low temperature pyrolysis. Fuel Processing Technology. 2017; 167:502–10.

[62] Roets L, Strydom CA, Bunt JR, Neomagus HWJP, Niekerk D Van. The effect of acid washing on the pyrolysis products derived from a vitrinite-rich bituminous coal. Journal of Analytical and Applied Pyrolysis. 2015; 116:142–51.

[63] Rotes L, Bunt JR, Neomagus HWJP, Strydom CA, Van Niekerk D. The effect of added minerals on the pyrolysis products derived from a vitrinite-rich demineralised South African coal. Journal of Analytical and Applied Pyrolysis. 2016; 121:41–9.

[64] Lu Q, Zhang N, Yang Q, Li Y, Cao Q, Liu S, et al. Influence of calcium promoter on catalytic pyrolysis characteristics of iron-loaded brown coal in a fixed bed reactor. Journal of the Energy Institute. 2020; 93:695–710.

[65] Hafriz RSRM, Salmiaton A, Yunus R, Taufiq-Yap YH. Green Biofuel Production via Catalytic Pyrolysis of Waste Cooking Oil using Malaysian Dolomite Catalyst. Bulletin of Chemical Reaction Engineering & Catalysis. 2018; 13:489–501.

[66] Liang P, Yu J, Zhang Y, Jiao T, Qin X. Effects of natural dolomite catalysts on cracking anthracene oil. Energy and Fuels 2017; 31:11765–72.

[67] Ay Ş, Atakül H, Sarioğlan A, Akgün F, Işik-Gülsaç I, Çetin Y, et al. Hot gas clean-up with dolomites: Effect of gas composition on sulphur removal activity. The Canadian Journal of Chemical Engineering. 2015; 93:1643–50.

[68] Reifenstein AP, Kahraman H, Coin CDA, Calos NJ, Miller G, Uwins P. Behaviour of selected minerals in an improved ash fusion test: quartz, potassium feldspar, sodium feldspar, kaolinite, illite, calcite, dolomite, siderite, pyrite and apatite. Fuel. 1999; 78:1449–61.

[69] Tsubouchi N, Ohtsuka Y. Formation of N_2 during pyrolysis of Ca-loaded coals. Fuel 2002; 81:1423–31.

[70] Wang W, Lemaire R, Bensakhria A, Luart D. Review on the catalytic effects of alkali and alkaline earth metals (AAEMs) including sodium, potassium, calcium and magnesium on the pyrolysis of lignocellulosic biomass and on the co-pyrolysis of coal with biomass. Journal of Analytical and Applied Pyrolysis. 2022; 163:105479.

[71] Zhang Y, Zhang Z, Zhu M, Cheng F, Zhang D. Decomposition of key minerals in coal gangues during combustion in O_2/N_2 and O_2/CO_2 atmospheres. Applied Thermal Engineering. 2019; 148:977–83.

[72] Ahmad T, Awan IA, Nisar J, Ahmad I. Influence of inherent minerals and pyrolysis temperature on the yield of pyrolysates of some Pakistani coals. Energy Conversion and Management. 2009; 50:1163–71.

[73] Khan MR. A literature survey and an experimental study of coal devolatilisation at mild and severe conditions: influences of heating rate, temperature, and reactor type on products yield and composition. Fuel. 1989; 68:1522–31.

[74] Lin X, Yang S, Chen X, Zheng P, Wang Y, Zhang S. Effects of calcium on the evolution of nitrogen during pyrolysis of a typical low rank coal. International Journal of Coal Science & Technology 2020; 7:397–404.

[75] Liu S. Research on the effect and dynamics of calcium oxide on pyrolysis behavior of medium and low-rank coal. Journal of Physics: Conference Series 2023. 2023; 2527:012058.

[76] Chu Z, Gong Z, Zhang H, Wang Z, Liu L, Wang Z, et al. Pyrolysis characteristics and kinetics analysis of oil sludge with CaO additive. Environmental Technology. 2022; 43:4493–503.

[77] Varbanov PS, Walmsley TG, Klemeš JJ, Seferlis P, Khaskhachikh V, Gerasimov G, et al. Study of oil sludge pyrolysis in the presence of calcium oxide. Chemical Engineering Transactions. 2019; 76.

[78] Franklin HD, Peters WA, Cariello F, Howard JB. Effects of calcium minerals on the rapid pyrolysis of a bituminous coal. Industrial and Engineering Chemistry Process Design and Development. 1981; 20:670–4.

[79] Fursov SG, Meltyukhov M V, Lyashenko SA. The pyrocarbon, gas phase densification of the catalytic carbon formations (CCFs), obtained on iron. Problems of Atomic Science and Technology. 2023; 45: 123-130.

[80] Yang Y, Lin X, Chen X, Guo W, Wang Y, Zhang J, et al. Investigation on the effects of different forms of sodium, chlorine and sulphur and various pretreatment methods on the deposition characteristics of Na species during pyrolysis of a Na-rich coal. Fuel. 2018; 234:872–85.

[81] Zheng J, Gu Y. Thermodynamic research on the effect of CaO on the transformation of arsenic and sulphur in coal in different pyrolysis atmospheres. Energy Science & Engineering. 2022; 10:3108–24.

[82] Oni BA, Sanni SE, Ibegbu AJ, Tomomewo OS, Dike HN. Pyrolytic-gasification of biomass and plastic accompanied with catalytic sequential tar reformation into hydrogen-rich gas. Journal of the Energy Institute. 2023; 109:101287.

[83] Hu M, Cheng Z, Zhang M, Liu M, Song L, Zhang Y, et al. Effect of calcite, kaolinite, gypsum, and montmorillonite on huadian oil shale Kerogen pyrolysis. Energy and Fuels. 2014; 28:1860–7.

[84] Li B, Yang H, Liu B, Wei L, Shao J, Chen H. Influence of Addition of a High Amount of Calcium Oxide on the Yields of Pyrolysis Products and Noncondensable Gas Evolving during Corn Stalk Pyrolysis. Energy and Fuels 2017; 31:13705–12.

[85] Zhao HL, Bai ZQ, Yan JC, Bai J, Li W. Transformations of pyrite in different associations during pyrolysis of coal. Fuel Processing Technology. 2015; 131:304–10.

[86] Chen H, Li B, Zhang B. Decomposition of pyrite and the interaction of pyrite with coal organic matrix in pyrolysis and hydro-pyrolysis. Fuel. 2000;79:1627–31.

[87] Geng H, Li L, Li G, Wei Y, Fan H, Jin L, et al. Pyrolysis behaviors of coal-related model compounds catalysed by pyrite. Fuel. 2020; 262.

[88] Zhao H, Bai Z, Bai J, Guo Z, Kong L, Li W. Effect of coal particle size on distribution and thermal behaviour of pyrite during pyrolysis. Fuel. 2015; 148:145–51.

[89] Li Z, Ward CR, Gurba LW. Occurrence of non-mineral inorganic elements in macerals of low-rank coals. International Journal of Coal Geology. 2010; 81:242–50.

[90] Liu Y, Cheng L, Zhao Y, Ji J, Wang Q, Luo Z, et al. Transformation behaviour of alkali metals in high-alkali coals. Fuel Processing Technology. 2018; 169:288–94.

[91] Si T, Hong D, Li P, Guo X. The migration and transformation of sodium carboxylate during Zhundong coal pyrolysis and combustion: A ReaxFF simulation study. Journal of Analytical and Applied Pyrolysis. 2021; 156:105098.

[92] Dai S, Finkelman RB, French D, Hower JC, Graham IT, Zhao F. Modes of occurrence of elements in coal: A critical evaluation. Earth-Science Reviews. 2021; 222:103815.

[93] Bauer S, Yang J, Stuckman M, Verba C. Rare Earth Element (REE) and critical mineral fractions of central appalachian coal-related strata determined by 7-step sequential extraction. Minerals. 2022;12:1350.

[94] Arbuzov SI, Finkelman RB, Il'enok SS, Maslov SG, Mezhibor AM, Blokhin MG. Modes of Occurrence of Rare-Earth Elements (La, Ce, Sm, Eu, Tb, Yb, Lu) in Coals of Northern Asia (Review). Solid Fuel Chemistry 2019; 53:1–21.

[95] Zuma MC, Nomngongo PN, Mketo N. Simultaneous determination of REEs in coal samples using the combination of microwave-assisted ashing and ultrasound-assisted extraction methods followed by ICP-OES analysis. Minerals. 2021; 11:1103.

[96] Song Y, Zhao Y, Ginella A, Gallagher B, Sant G, Bauchy M. Predicting Rare Earth Elements Concentration in Coal Ashes with Multi-Task Neural Networks Materials Horizons 2022; 11:1448

[97] Wall TF. Mineral matter transformations and ash deposition in pulverised coal combustion. In: International Symposium on Combustion. 1992; 24:1119–26.

[98] Rhines JM, Mill KC, Putland FH. The physical properties of slags formed during coal gasification. High Temperatures High Pressures. 1985; 17:173–83.

[99] Li F, Fan H, Fang Y. Exploration of slagging behaviours during multistage conversion fluidised-bed (MFB) gasification of low-rank coals. Energy and Fuels. 2015; 29:7816–24.

[100] ten Brink HM, Hamburg G, Eenkhoorn S. Slagging in entrained-flow gasification and low-NOx firing conditions. In: Williamson J. editor, The impact of ash deposition on coal fired plants: Proceedings of the Engineering Foundation Conference Held at the St. John's Swallow Hotel, Solihull, England (1st ed.). Routledge 2022. p.113–122.

[101] Jiang S, Zhou Q, Ge ZH, Chen W, Xing JW, Zhang W Bin, et al. Model development and numerical investigation of the slag formation in an entrained-flow gasifier. In: Journal of Physics: Conference Series 2023; 2442:012039.

[102] Ram LC, Masto RE, Srivastava NK, George J, Selvi VA, Das TB, et al. Potentially toxic elements in lignite and its combustion residues from a power plant. Environmental Monitoring and Assessment. 2015; 187:1–14.

[103] Wu S, Huang S, Wu Y, Gao J. Characteristics and catalytic actions of inorganic constituents from entrained-flow coal gasification slag. Journal of the Energy Institute. 2015; 88:93–103.

[104] Fiket Ž, Medunić G, Kniewald G. Rare earth elements distribution in soil nearby thermal power plant. Environ Earth Sci. 2016; 75:1–9.

[105] Medunic G, Fiket Z, Kniewald G. Rare earth elements distribution in soil nearby Plomin thermal power plant (Croatia), Proceedings of 27th IAGS, Bowell RJ, Cox M.(eds), Tucson, USA, 2015. p.1-9.

[106] Han Y, Xie H, Liu W, Li H, Wang M, Chen X, et al. Assessment of pollution of potentially harmful elements in soils surrounding a municipal solid waste incinerator, China. Frontiers of Environmental Science & Engineering. 2016; 10:1–11.

[107] Liu L, Kumar S, Wang Z, He Y, Liu J, Cen K. Catalytic effect of metal chlorides on coal pyrolysis and gasification part I. Combined TG-FTIR study for coal pyrolysis. Thermochimica Acta. 2017; 655:331–6.

[108] Li X, Hayashi JI, Li CZ. Volatilisation and catalytic effects of alkali and alkaline earth metallic species during the pyrolysis and gasification of Victorian brown coal. Part VII. Raman spectroscopic study on the changes in char structure during the catalytic gasification in air. Fuel. 2006; 85:1509-17.

[109] Yao Q, Ma M, Liu Y, He L, Sun M, Ma X. Pyrolysis characteristics of metal ion-exchanged Shendong coal and its char gasification performance. Journal of Analytical and Applied Pyrolysis. 2021; 155:105087.

[110] Quyn DM, Wu H, Hayashi JI, Li CZ. Volatilisation and catalytic effects of alkali and alkaline earth metallic species during the pyrolysis and gasification of Victorian brown coal. Part IV. Catalytic effects of NaCl and ion-exchangeable Na in coal on char reactivity. Fuel. 2003; 82:587–93.

[111] Xu L, Liu H, Zhao D, Cao Q, Gao J, Wu S. Transformation mechanism of sodium during pyrolysis of Zhundong coal. Fuel. 2018 Dec 1; 233:29-36

[112] Wei X, Zhang G, Cai Y, Li L, Li H. The volatilisation of trace elements during oxidative pyrolysis of a coal from an endemic arsenosis area in southwest Guizhou, China. Journal of analytical and applied pyrolysis. 2012 Nov 1; 98:184-93.

[113] Kou JW, Bai ZQ, Bai J, Guo ZX, Li W. Effects of mineral matter and temperatures on conversion of carboxylic acids and their derivatives during pyrolysis of brown coals. Fuel Processing Technology. 2016 Nov 1; 152:46-55.

[114] Li X, Bai ZQ, Bai J, Zhao BB, Li P, Han YN, Kong LX, Li W. Effect of Ca^{2+} species with different modes of occurrence on direct liquefaction of a calcium-rich lignite. Fuel Processing Technology. 2015 May 1; 133:161-6.

[115] Liang D, Xie Q, Wei Z, Wan C, Li G, Cao J. Transformation of alkali and alkaline earth metals in Zhundong coal during pyrolysis in an entrained flow bed reactor. Journal of Analytical and Applied Pyrolysis. 2019; 142:104661.

[116] He R, Deng J, Deng X, Xie X, Li Y, Yuan S. Effects of alkali and alkaline earth metals of inherent minerals on Fe-catalysed coal pyrolysis. Energy. 2022; 238:121985.

[117] Radovic RL, Walker Jr LP, Jenkins GR. Importance of catalyst dispersion in the gasification of lignite chars. Journal of Catalysis. 1983; 82:382-94.

CHAPTER 3 PROPERTIES AND REACTIVITY OF TWO OXIDISED AND UNOXIDISED SOUTH AFRICAN HIGHVELD FINE-COAL REJECTS AND THEIR DENSITY-SEPARATED FRACTIONS

K, Mphahlele, R. H. Matjie, J. R. Bunt, R.C. Uwaoma.

In this chapter, oxidised and unoxidised South African fine-coal reject samples were obtained from the Highveld Coalfield and subjected to chemical mineral matter dissolution and density separation. This was conducted to discern the mode of occurrence of mineral matter in the two fine-coal reject samples. A comprehensive characterisation study using advanced and conventional analytical techniques allowed for this discernment.

This manuscript is published in the International Journal of Coal Preparation and Utilisation, 2022; volume 43, Pages 1451-1477. https://doi.org/10.1080/19392699.2023.2221634

Abstract

Fine-coal reject samples (FCR) derived from the South African (SA) feed-coal preparation plants are unsuitable for gasification/combustion applications due to their physical size and coal properties. In this novel investigation, two SA FCRs were taken from a thermal export plant (TEP) and a steam station (STEM) for a coal-property comparison and pyrolysis/gasification reactivity study. H_2S/SO_2/CO_2/Cadmium/Arsenic/volatile organic compounds (VOCs) emissions/dust/particulate-matter pollution, linked to the pyrite-spontaneous combustion and the interaction of organic sulphur and calcium in FCRs, are serious threats to the global human-health and atmospheric environment. Numerous investigations focused primarily on SA unoxidised FCR (STEM sample, as labelled in this study) rather than on oxidised FCR (labelled as TEP sample in this study) and beneficiated fractions. Furthermore, no Raman/X-ray diffraction (XRD)/density-separation/thermogravimetric results for the TEP (40-400 µm; 83% recovery) and STEM (111-500 µm; 20% recovery) samples have been previously reported. FCRs and their beneficiated fractions were characterised by both conventional and advanced coal analyses. Results indicate that the FCRs have similar properties compared to gasification/combustion feed coals except for higher mineral matter content (39% versus 29%), higher vitrinites (43% versus 24%) and higher alkali index (8 versus 5) in the TEP sample. Thermogravimetric-gasification experiments illustrate higher reaction rates and higher carbon conversion for the TEP sample than for the STEM sample. Raman/XRD detected aromatic/aliphatic hydrocarbons/minerals, contributing positively to the coal reactivity. Based on their reactivity, results provide a baseline for FCRs utilisation in pyrolysis/gasification applications.

Keywords: Gasification, char reactivity, fine-coal rejects, mode of occurrence, Mineral-matter

3.1 Introduction

Utilizing coal and advancements in coal mining technologies involving mechanised coal mining operations and beneficiation of run-of-mine (ROM) coal to export grade thermal coal, along with coal handling, crushing, and transportation, has led to the generation of FCR samples. These FCR samples are unsuitable for direct utilisation in conventional gasifiers and boilers due to their fine (<1 mm) and ultra-fine (<0.25 mm) nature, high moisture content, high sulphur content, and high ash yield [1]. Conventionally, they are disposed of into slime dams and stockpiles, which create environmental pollution and cause thermal energy loss [2].

During the storage of coal fines in stockpiles or slime dams, pyrite (FeS_2) oxidises in the presence of water and oxygen to form ferrous ions (Fe^{2+}), ferric ions (Fe^{3+}), sulphates (SO_4^{2-}) and acidic ions (H^+) [3]. A higher proportion of Fe^{3+} increases with an increase in the pH of the slurry water (pH = 4.5). The cyclic pyrite oxidation and the increasing Fe^{3+} ion concentration through acid-rock drainage (ARD) reactions produce more acids to contaminate the environment. The co-disposal of coal waste rock with coal-fines waste can potentially assist in preventing the ARD reactions by reducing excess amounts of oxygen and water to pyrite surfaces [3]. The possible cyclic oxidation reactions between pyrite and O_2 and H_2O during the spontaneous combustion of coal fines are as follows (Reactions 1-3; [3]):

$$\mathrm{FeS_2} + \frac{7}{2}\mathrm{O_2} + \mathrm{H_2O} \rightarrow \mathrm{Fe^{2+}} + 2\mathrm{SO_4}^{2-} + \mathrm{H^+} \quad (1)$$

$$\mathrm{Fe^{2+}} + \frac{1}{4}\mathrm{O_2} + \mathrm{H^+} \rightarrow \mathrm{Fe^{3+}} + \frac{1}{2}\mathrm{H_2O} \quad (2)$$

$$\mathrm{FeS_2} + 14\mathrm{Fe^{3+}} + 8\mathrm{H_2O} \rightarrow 15\,\mathrm{Fe^{2+}} + \mathrm{SO_4}^{2-} + 16\mathrm{H^+} \quad (3)$$

In addition, a higher proportion of pyrite particles present in the coal fines can expedite the process of spontaneous combustion of these fines and subsequently release gaseous oxidation products (sulphur dioxide (SO_2), carbon monoxide (CO) and carbon dioxide (CO_2)) [4]. Furthermore, coal-fired power plants emit CO_2, SO_2, particulate matter (PM) and considerable amounts of nitrogen oxides (NOx) as a result of the combustion of coal. These are associated with environmental and human health risks [5]. The SO_2 and NOx emissions are associated with the inflammation and irritation of the skin and respiratory system [5]. CO_2 is responsible for global warming. Additionally, the inhalation of PM causes chronic lung diseases (pneumoconiosis and tuberculosis) and silicosis (bronchitis symptoms and asthma) [6, 7].

Chalcophile elements, especially those associated with sulphide minerals such as arsenic (As), selenium (Se), cadmium (Cd), nickel (Ni) and lead (Pd), have been linked with carcinogenic and mutation effects [8]. The propensity for releasing these toxic elements depends on their mode of occurrence, which contributes to their transformation during pyrolysis and gasification processing [9].

Constant watering of stockpiled FCR samples is needed to control dust pollution and prevent spontaneous pyrite combustion [10], requiring a high demand for water and water-polluting prevention technology. Considering South Africa is a water-scarce country and has challenges with slime dam overflow and leaks, this approach faces compliance challenges with meeting the requirements of the South Africa National Water Act 36 of 1998 and National Environmental Management Act 107 of 1998. Additionally, the legislation further requires maintenance of the slime dams even after mine shut down, resulting in additional costs.

The depletion of coal reserves and South Africa's reliance on coal for the generation of about 90% of the country's electricity [11,] highlight the need to utilise the FCR as a source of energy. In the last ten decades, the top seven coal-producing countries generated about 60 billion tonnes (Bt) of FCR. In 2013, South Africa (the seventh largest coal producer) alone reported almost 1.3 Bt of FCR in stockpiles and slime dams with an annual generation of about 60 Mt [12]. The abundance of FCR and the calorific value (CV) (15-21 MJ/kg) [13] indicate a potential economic benefit from its utilisation while alleviating the associated environmental pollution concerns.

Several researchers have studied different techniques for valorising Highveld Coalfield oxidised FCR by agglomeration [14, 15]. These authors studied the properties of agglomerated inertinite-rich FCR with various binders for their utilisation in fixed-bed gasifiers. Uwaoma et al. [16] and Meyer et al. [17] used the unoxidised coal-fine fraction derived from the run-of-mine (ROM) feed coal feeding a stockpile of a South African (SA) Highveld coal mine, as well as the unoxidised coal-fine fraction, together with microalgae blends, in the pyrolysis, gasification and liquefaction experiments. The analytical techniques used in previous studies were applied to characterise different fine coal samples and their blends with used coal-fines and microalgae. In addition, the weathered coarse coal discards sourced from the coal stockpiles of the Witbank-Highveld-Ermelo coalfields (in Mpumalanga Province, South Africa), were combusted in the Eskom (a SA Power Utility company) drop-tube furnace (DTF). This was done to understand the coal combustion behaviour [18]. Ejesieme et al. [19] studied the combustion characteristics of discard ultra-fine coal (sourced from Eskom, Mpumalanga Province, South Africa), of charcoal, and their blends with *Scenedesmus microalgae.* Furthermore, fine coal particles have also been gasified in the High-Temperature

Winkler (HTW) gasification process devolatilises which uses a fine coal discard feed coal in the size range 3 - 6 % > 0,5 mm with ash yield (48%), lignite (4% ash yield) or biomass (7% ash yield) in a bubbling fluidised-bed. This produces chemicals including methanol, ammonia, hydrogen, synthesis gas (CO and H_2), gasoline, Fischer-Tropsch liquids and chars. The process operates at 10 - 30 bar pressure and 800 - 1000 °C temperature under a steam, oxygen and carbon dioxide reactant gas environment [20].

To the authors' knowledge, no detailed characterisation studies focused on these oxidised and unoxidised FCR samples and their density-separated fractions using conventional and selected advanced analytical techniques (Raman, quantitative and qualitative XRD analyses), have been evaluated to better understand the properties of these FCR samples for utilisation in thermo-chemical processes. Moreover, thermogravimetric tests using oxidised and unoxidised FCR samples and their density-separated fractions for reactivity determination during pyrolysis and gasification have not been conducted in the past.

To close this gap, two SA Highveld coal discard samples: (1) oxidised FCR and (2) unoxidised FCR were obtained from, firstly, the oxidised FCR disposal site of a thermal export preparation plant (TEP), and secondly, from the preparation site of a steam station plant (STEM). Both samples were subjected to density separation to evaluate their washability characteristics and the association of minerals with coal macerals. This information could assist in developing coal blending strategies by providing insights into the distribution of mineral matter (MM) and their probable catalytic effects during pyrolysis and gasification. The reactivity attributes of micro-lithotypes, maceral groups and percentage ash yield or percentage MM, alkali index (AI) by mode of occurrence of MM during the pyrolysis and char-CO_2 gasification step were also evaluated. Mineralogical (X-ray diffraction (XRD)), Raman spectroscopy, chemical (proximate, ultimate and X-ray fluorescence (XRF)), petrographic, particle size distribution (PSD) and thermogravimetric analyses (TGA) were performed to accomplish these objectives. The suitability of the TEP FCR (oxidised sample) as a possible feedstock for gasification and pyrolysis applications was investigated by comparing its coal properties and reactivity with that of the STEM FCR (unoxidised sample) derived directly from the ROM feed coals currently used in operating pyrolysis/gasification and combustion plants in South Africa.

3.2 Materials and Methods

3.2.1 Sample Collection and Preparation

A total of about 250 kg of SA Highveld FCR (-1 mm +0.02 mm) was taken from the FCR disposal site of the TEP plant, and 250 kg of SA Highveld FCR (-5 mm+0.15 mm) was taken

from the FCR preparation site of the STEM ROM from an operating plant in Mpumalanga province, South Africa. The method described by the International Organisation for Standardisation (ISO), ISO 18283 and ISO 13909-4 procedures was followed. In this manuscript, the FCR samples from TEP and STEM are termed TEP and STEM samples, respectively. The TEP sample was exposed to atmospheric weathering and water treatment to prevent dust pollution. This sample was partially oxidised due to exposure to a series of chemical and physical changes occurring during its handling and storage at the disposal site. The STEM sample was obtained from a coal preparation screening plant during the blending of ROM coals from different Highveld coal sources used to prepare feed coals for thermochemical processes. The TEP sample is termed oxidised FCR, and the STEM sample is an unoxidised FCR. These FCR samples, which were characterised and evaluated in the pyrolysis and gasification study, have not previously been investigated. The bulk samples were air-dried over five days to remove excess moisture. The dried samples were homogenised to prepare 100 kg of representative samples by employing the coning and quartering method (ISO 18283 and ISO 13909-4). After this, a large proportion of the sample was subjected to density separation. Smaller representative proportions of TEP and STEM samples were prepared according to the requirements of different coal analytical techniques and TG analysis in accordance with ISO 1988 and 13909.

The prepared samples were purged with 99.995% nitrogen gas (N_2) sourced from African Oxygen (Afrox) Ltd to minimise oxidation of the samples during storage. N_2 gas was also used to create an inert atmosphere and as a sweep gas during the thermogravimetric analysis studies.

3.2.2 Density Separation Experiments

About 25 kg each of the TEP and STEM samples were beneficiated using the density separation technique to produce floats (Fl1.5) with an average density (ρ_a) of <1.5 g/cm^3, middling (Fl1.9) at 1.5 < ρ_a <1.9 g/cm^3 and sink (Sl1.9) obtained at sp.>1.9 g/cm$^{3.}$ This was done at General Society of Surveillance (SGS) Laboratories (PTY) Ltd, following procedures described in the ISO 7936 standard method. Tetrabromoethane, benzene and tetrachloroethylene, with respective ρ_a values of 2.95, 0.879 and 1.62 g/cm^3, were used as mixtures to produce 1.5, 1.5 to 1.9 and 1.9 g/cm^3 density floats and sink fractions as indicated by [21,22]. Acetone was used to wash the density-separated fractions. The washed samples were air-dried for 10 hours to remove acetone absorbed on the surface of the coal particles. The acetone-washed density-separated fractions were then dried at 80 °C for a further 24 hours to remove any remaining acetone and density-separation organic solvent residues still present on the surface of fine-coal reject samples. The density separation solvents-free

density-separated samples were subjected to pyrolysis, gasification experiments, and analyses.

3.2.3 Char Preparation

The char used for reactivity analysis was prepared by performing high-temperature pyrolysis in an Elite horizontal tube furnace (TSH12/75/610-2416CG) under an inert nitrogen environment. Figure 3-1 is a schematic diagram of the high-temperature pyrolysis unit used to prepare sufficient homogenised char samples for the CO_2-gasification experiments. The unit was equipped with a 60x900 mm Alsint work tube with a 610 mm heated zone. This preparation method was designed to produce the homogenised and representative char samples for CO_2-gasification experiments in which 5 g ±0.5 g of each FCR sample was spread into thin layers in an Alsint crucible and then heated from ambient temperature to 1000 °C at 10 °C/min under a sweeping nitrogen flowrate of 10 NL/min. The temperature was held for 30 minutes at 1000 °C to ensure complete removal of volatiles. The char samples were subsequently cooled to 30 °C under nitrogen flowing at 20 NL/min to minimise the interaction of evolved gases with the hot char layer.

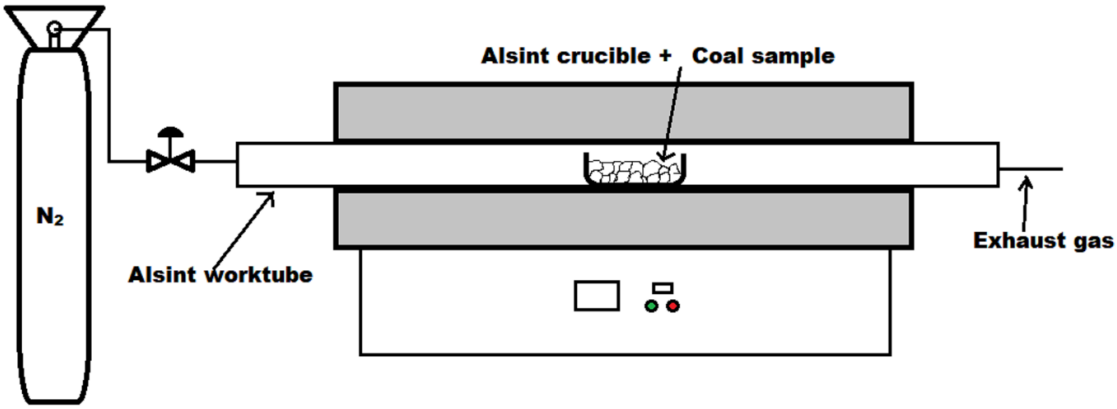

Figure 3-1: Schematic diagram of a horizontal tube furnace used for pyrolysis.

3.2.4 Particle Size Distribution (PSD) Analysis

The PSD of the TEP and STEM samples was determined using the Malvern Instrument Ltd. Mastersizer 3000 User Manual, MAN0474-07-EN-00; 2015 (Malvern Instrument Ltd 2015). This technique characterised fine and ultra-fine coal particles (<0.5 mm).

3.2.5 Coal Composition

Representative TEP and STEM samples were ground to 100% passing of a 75 µm sieve for proximate, ultimate and XRF analyses. For proximate analyses, ISO 17722, ISO 1171, ISO

526 and ISO 1928 procedures were used to determine the percentages of inherent moisture, ash yield, volatile matter (VM) and CV, respectively. The percentage of fixed carbon (FC) was calculated by difference. For the ultimate analysis, the American Society for Testing and Materials (ASTM) standard ASTM D5373-08 was used to determine the percentages of carbon (C), hydrogen (H) and nitrogen (N), while the percentages of total sulphur and oxygen were determined by following ASTM D4239 and the difference method, respectively. The distribution of sulphur was studied by adopting procedures defined by ISO 157.

The XRF analysis (ASTM D4326-13) was determined from the ashes of the FCR samples, and their density-separated fractions were followed to determine the proportions of inorganic elements contained in these samples.

3.2.6 XRD Analysis

The XRD analysis was used to characterise the pulverised FCR samples and their density-separated fractions (<75 µm) following mineralogical methods, which are developed and described by Rietveld [23] and Speakman [24]. The Scherrer equation was used to estimate the crystalline carbon sizes using the corresponding full width at half-maximum (FWHM) parameters of the graphite peak on the XRD diffractogram [25].

3.2.7 Raman Analysis

The Raman analysis of the FCR samples and their density-separated fractions was performed using a WITec Alpha300R Confocal Raman spectrometer equipped with a 532 nm laser and 50x objective. A detailed description of the equipment and the method used can be found elsewhere [26]. The Raman spectra obtained were processed using Origin Lab 2019 software. The baseline correction was performed using the second derivative approach, and the peak fitting deconvolution process was performed using the Gaussian function.

3.2.8 Petrographic Analysis

The ISO 7404-2 standard method was used to prepare polished TEP and STEM samples set in epoxy resin using a Struers Tegraforce polisher. The final polishing stage was performed using a 0.05 µm OPS lubricant. The ISO 7404-5 standard method was followed to determine vitrinite reflectance on the polished blocks using a Zeiss AxioImager M2M petrographic microscope fitted with a Fossil Hilgers system, while ISO 7404-3 was used for the maceral analysis using a semi-automated point counting stage at a magnification of x500 under oil immersion. Microlithotypes were analysed following the ISO 7404-4 standard procedures. They were reported on a volume % basis on counts of the entire surface of the polished blocks.

3.2.9 TGA

The FCR samples, chars derived from the FCR samples and their density-separated fractions, were subjected to TG analyses using an SDT Q600 TGA. The procedure followed for the TG experiments is reported in the literature [27].

3.2.10 Reactivity Analysis

A total mass of 25 mg ±1 mg of char of each sample was subjected to the TG equipment for the CO_2 gasification reactivity analysis. The conversion of residual carbon in the prepared chars was calculated using Eq. 1.

$$x = \frac{m_0 - m_T}{m_0 - m_f} \quad (1)$$

In this case, m_0 represents the initial char mass (Mass at$t = 0$), m_t represents the char mass at a specific time (Mass at $t = t$) and $m_f$represents the mass of the final residue (ash) at maximum conversion ($t = t_f$).

Bai et al. [28] demonstrated the use of an Eq.2 to define the normalised rate of gasification reactions(k).

$$k = \frac{dx}{dt} \Big/ 1 - x \quad (2)$$

Whereby, x represents the conversion of carbon as described in Eq. 1 and dx/dt represents the rate of carbon conversion (reaction rate).

3.3 Results and Discussion

3.3.1 Coal Washability Characteristics

Figure 3-2 presents the washability characteristic curves obtained for the TEP and STEM samples. Compared to the STEM sample, the TEP sample achieved a significant float fraction < 1.5 g/cm^3 (a higher percentage mass yield with a lower percentage ash yield) and a lower mass yield of its sink fraction (> 1.9 g/cm^3). According to Rautenbach et al. [22], the float fraction (< 1.5 g/cm^3) is characterised by a higher inherent mineral matter (MM) content associated with the carbon matrix and a higher vitrinite content compared to the sink fractions (> 1.9 g/cm^3) produced during density separation. The significant proportions of inherent MM and vitrinite present in the low-density float sample may contribute positively to the catalytic effects on the pyrolysis and gasification reactions and subsequently result in higher carbon

conversion. The highly reactive nature of vitrinite could imply shorter residence times and higher throughput under gasification conditions, while higher tar yields could be expected under pyrolysis conditions [21, 29]. On the other hand, the sink fraction (> 1.9 g/cm^3), which contains a higher proportion of extraneous minerals and lower vitrinite content, may resist transformation and prevent the catalytic reactions of pyrolysis and gasification. Also, as the sink fraction is characterised by a lower vitrinite content, a less reactive/semi-inert maceral group could imply longer residence times under gasification and pyrolysis conditions.

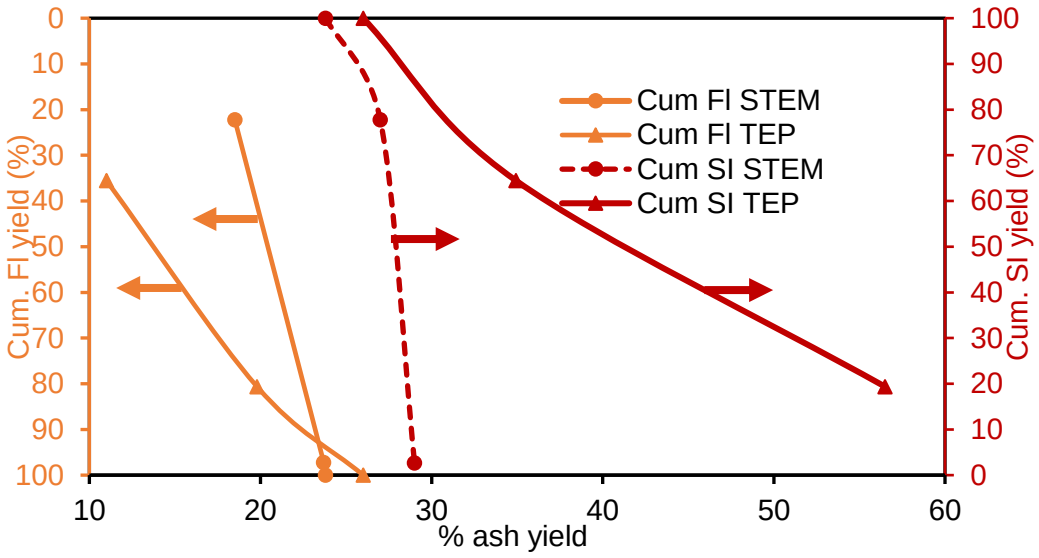

Figure 3-2: Washability characteristics of two FCR samples at 100% passing 1 mm (Cum. Fl TEP = cumulative yield of the float fractions of the TEP sample, Cum. Fl STEM = cumulative yield of the float fractions of the STEM sample, Cum.Sl TEP = cumulative yield of the sink fractions of TEP sample Cum.Sl TEP= cumulative yield of the sink fractions of the STEM sample).

The results indicate that the TEP sample is more washable than the STEM sample. The good washability characteristics of the TEP sample mean that TEP may possibly be considered as a blend coal source in thermo-chemical processes. For instance, at the density separation conditions studied, it is not possible to produce export grade 10 wt. % ash yield coal from either the TEP or the STEM sampled in the investigation. However, at 20 wt. % ash yield, which is lower than the ash percentage of typical SA feed coals to gasifiers and boilers (which are up to 35 wt. % a.d.b.) [21], 83 wt. % recovery of the TEP sample can be achieved while only 40 wt. % recovery can be achieved for the STEM sample. The blending approach could lower the amount of FCR samples in stockpiles and slime dames, subsequently alleviating environmental pollution issues associated with the current disposal methods for FCR samples.

3.3.2 PSD Analysis

The PSD results of the FCR samples presented in Figure 3-3 reveal that the TEP sample primarily comprises particles in the 40-400 µm size range. In contrast, the STEM sample contains slightly coarser particles ranging from 111 to 500 µm compared to the TEP sample. Approximately 60% of the STEM particles are below 111 µm, while about 77% of the TEP particles fall below this size, as shown in the cumulative particle size distribution in Figure 3-3. These differences in particle sizes are not expected to significantly influence the pyrolysis and gasification reactions, especially given the narrow particle size range considered in this study [30]. Liberation of MM in the finer TEP sample may contribute to enhanced washability characteristics of the coal with lower carbon content concentrated in the > 1.9 g/cm^3 sink fraction.

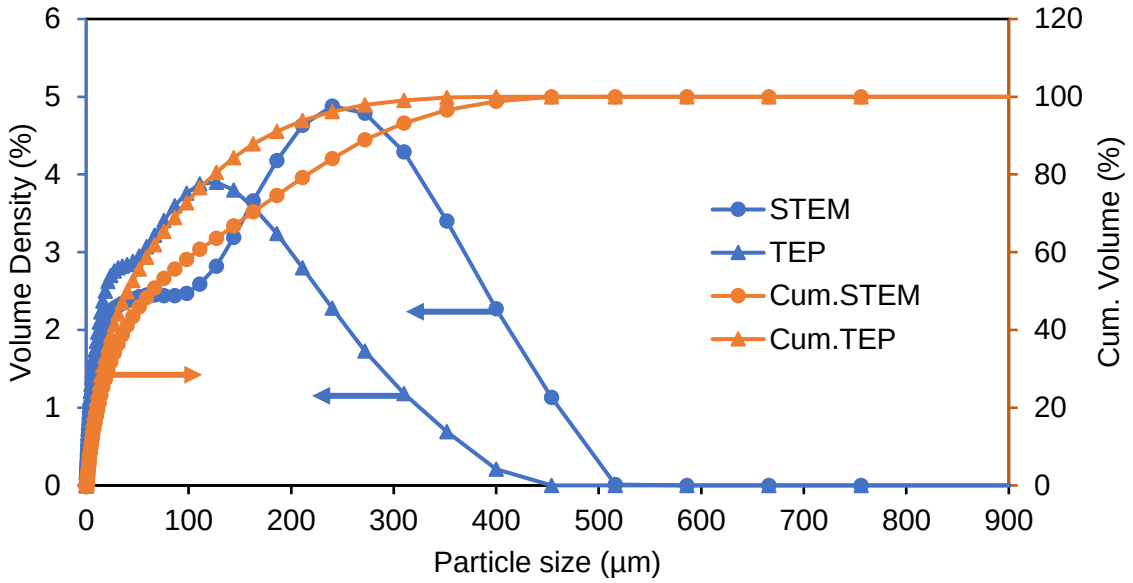

Figure 3-3: Particle size distribution results for the TEP and STEM samples (Cum.STEM = Cumulative distribution of particle sizes in the STEM sample Cum.TEP = Cumulative distribution of particle sizes in the TEP sample).

3.3.3 FCR Composition

The proximate analysis data of the two TEP and STEM samples is presented in Table 3-1. On an ash-free basis (a.f.b.), the data indicates comparable proportions of VM, FC and moisture contents. The TEP sample, on the other hand, reports a higher percentage of ash yield. Except for the higher % ash yield of the TEP sample, the chemical properties of the coals evaluated in the current study agree with the results for Highveld feed coals from different coal seams whose generic properties were evaluated by Everson et al. [21] and Henning [29].

Table 3-1: Proximate analysis results for FCR samples.

	Method	TEP	STEM	(Henning, 2017)
Inherent moisture (% a.d.b)	ISO 11722	3.7	4.1	3.7-5.2
Ash yield (% a.d.b)	ISO 1171	34.3	26.8	14.9-28.9
VM (% a.d.b)	ISO 526	22.4	21.9	21.1-28.6
FC (% a.d.b)	FC=100-IM-A-VM	39.6	47.1	38.3-53.4
Inherent moisture (%a.f.b)		5.6	5.6	4.7-7.3
FC (%a.f.b)		60.3	64.4	53.9-66.6
VM (% a.f.b)		34.1	30.0	28.3-38.8
CV (MJ/kg m.m.f)	ISO 1928	18.9	20.0	20.5-25.2

a.d.b. - air dried basis, a.f.b. - ash free basis, m.m.f. - MM free;

Density separation distributed the properties of the TEP and STEM samples across their different density fractions, including the MM, especially with the TEP sample. The distribution of these properties is presented in Figure 3-4 a-d, on an air-dried basis. The comparative analyses of FC, percentage ash yield, VM and CV for the density fractions of the TEP and STEM samples illustrate an increase in the percentage ash yields from the FI1.5 to the SI1.9 fractions, with the SI1.9 fraction of the TEP sample reporting the highest percentage ash yield. The similarities in the proportions of VM and FC of the TEP and STEM samples and the difference in their washability characteristics could imply that the difference in the chemistry of the two coals depends mainly on the mode of occurrences of MM. However, the differences in the chemical properties of the density-separated fractions of the TEP and STEM samples could also be associated with particle size differences, which indicate MM liberation differences and possibly a larger surface area exposed for the density media to interact with the coal particles. These findings on the FCR samples agree with those of three SA feed coals to SA commercial steam stations and their density-separated fractions as reported by Rautenbach et al. [31].

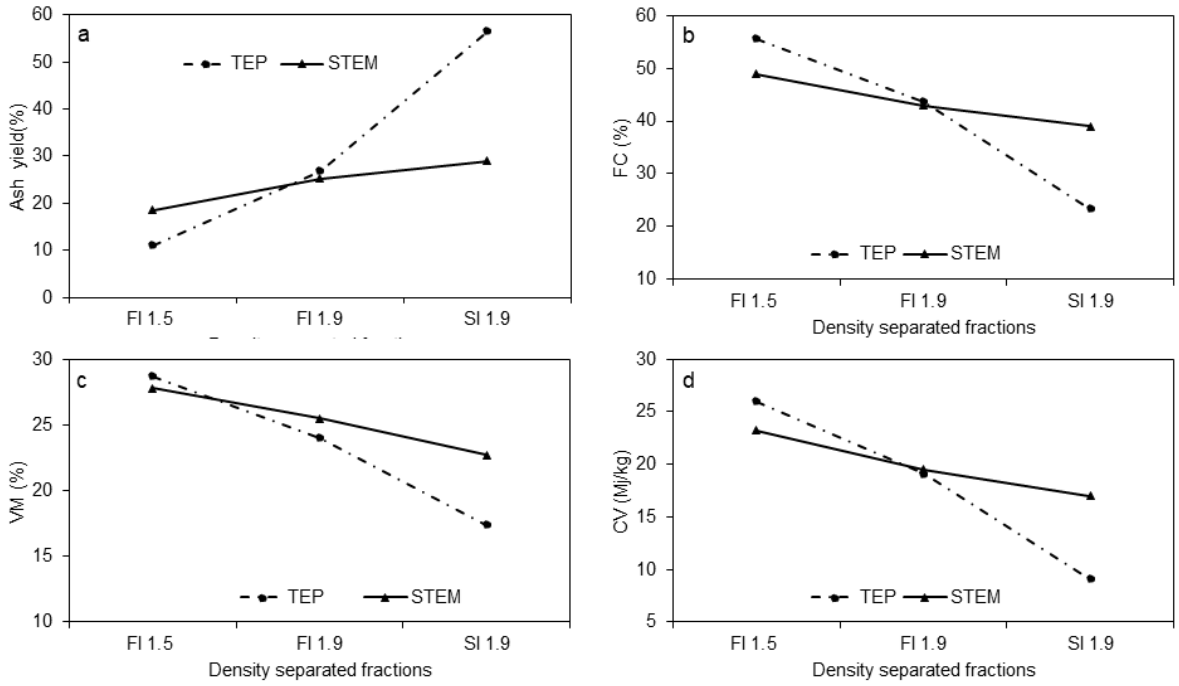

Figure 3-4: Distribution of chemical properties of FCR samples and their density-separated fractions.

The ultimate analysis results of the organic fraction of the TEP and STEM samples, along with their density-separated fractions, are reported in Table 3-2. These results indicate the predominance of carbon with lower percentages of hydrogen, nitrogen, and sulphur. The FI1.5 and FI1.9 fractions of the TEP and STEM samples comprise higher percentages of carbon, nitrogen, and hydrogen, which correlates to the increased VM in the float fractions. At the same time, the lower oxygen content in the float fractions can also be attributed to the reduced percentage of oxygen-bearing minerals, which are dominant minerals in the SA Highveld coal. These minerals tend to concentrate in the SI1.9 fraction of SA Highveld coals and could release CO_2 at high temperatures [32]. The latter could also contribute to partial oxidation of the coal carbon-matrix via the Boudouard reaction, which could improve the overall carbon conversion process. Results of the TEP and STEM samples agree well with those of Highveld coals from different seams, as reported by Henning [29]. The trend of carbon distribution agrees with that of density-separated fractions produced by Everson et al. [21].

Table 3-2: Ultimate results of FCR samples, along with their corresponding density-separated fractions (wt. % a.d.b.)

Sample Name	TEP	TEP FI 1.5	TEP FI 1.9	TEP SI 1.9	STEM	STEM FI 1.5	STEM FI 1.9	STEM SI 1.9
Carbon	48.5	66.0	50.1	28.6	54.7	58.4	50.3	44.7
Hydrogen	2.9	3.7	2.6	1.8	3.0	3.3	2.5	1.7

Sample Name	TEP	TEP FI 1.5	TEP FI 1.9	TEP SI 1.9	STEM	STEM FI 1.5	STEM FI 1.9	STEM SI 1.9
Nitrogen	1.3	1.7	1.3	0.8	1.4	1.5	1.3	1.2
Oxygen (by difference)	7.8	12.3	13.1	7.4	8.5	12.8	13.4	13.2
O/C	0.1	0.1	0.2	0.2	0.1	0.2	0.2	0.2
C/H	1.4	1.5	1.6	1.4	1.5	1.5	1.7	2.2

The percentages of total sulphur in the TEP and STEM samples presented in Table 3-3 are comparable because these FCR samples are derived from the same Highveld coal mines. However, its distribution across the density-separated fractions is expectedly more pronounced in the density-separated fractions of the TEP sample and correlates with a higher distribution of percentage ash yield (coal washability characteristics) of the same coal sample. This sulphur trend could indicate that other forms of sulphur present in the TEP sample are associated with extraneous pyrite and sulphate minerals. In contrast, sulphur distribution is almost equal across all forms in the density-separated fractions of the STEM sample. Sulphur, in the form of sulphate, was not detected in the FI1.5 fraction of the TEP sample, which illustrates its complete association with extraneous minerals. The lowest pyrite (FeS_2) percentage was reported in the FI1.5 of the TEP sample, indicating the presence of inherent pyrite in both coal samples. These results agree with those reported by Moyo et al. [3] in their sulphur speciation research reported for South African coals. Either inherent or extraneous pyrite present in the FCR stockpile oxidises and releases SO_2, which reacts with CaO from transformed inherent/extraneous calcite to form bassanite ($2CaSO_4.H_2O$) which is not contained in the ROM coal during the spontaneous combustion of pyrite [33]. In the presence of water, bassanite may gain water molecules to form gypsum ($CaSO_4.2H_2O$). Furthermore, organic sulphur and organic calcium can interact to form bassanite during the spontaneous combustion of pyrite [34, 35].

Table 3-3: Forms of sulphur in the FCR samples and distribution across their corresponding density-separated fractions.

Sample Name	TEP	TEP FI 1.5	TEP FI 1.9	TEP SI 1.9	STEM	STEM FI 1.5	STEM FI 1.9	STEM SI 1.9
Sulphate Sulphur (%)	0.3	0.0	0.1	0.1	0.1	0.1	0.1	0.1
Organic Sulphur (%)	0.4	0.4	0.3	0.4	0.4	0.4	0.4	0.3
Pyritic Sulphur (%)	0.5	0.1	0.3	1.8	0.4	0.2	0.3	0.5
Total sulphur (%)	1.2	0.5	0.7	2.3	0.9	0.7	0.8	0.9

These various reaction pathways of sulphur-bearing minerals highlight the need to fully characterise the forms of sulphur to design processes that can minimise the emission of sulphur gases.

3.3.4 XRF Analysis

3.3.4.1 Ash Compositional Analysis Results

The compositional analyses of inorganic elements present in the ashes of the TEP and STEM samples, along with their density-separated fractions, are presented in Table 3-4. This technique presents the inorganic elements in their oxide forms. The primary oxides in the ashes of the TEP and STEM samples are SiO_2 and Al_2O_3, followed by lower but significant percentages of CaO, SO_3 and Fe_2O_3. Trace amounts of TiO_2, K_2O, MgO, P_2O_5, SrO, Na_2O and MnO were also reported by the XRF analysis. These results are typical of SA Highveld coals and correlates to those reported elsewhere [34]. Inorganic elements such as Ca, K, Na, Fe and Mg have been linked with improved char reactivity in the gasification zones, especially if these elements are of intimate and are of organic association [36]. While silicon (Si) and aluminium (Al) bearing minerals could inhibit gasification reactions by coating the surfaces of the chars during their transformation, limiting the CO_2-carbon-matrix contact; these inorganic elements can also interact with calcium to form Ca-Al-silicate, which could help catalyse the gasification reactions.

The concentration of trace elements in the ashes of the density-separated fractions of the FCR samples are higher compared to the typical concentrations reported for SA Highveld ROM coals [37]. This could imply health and environmental issues during the storage of FCR samples in stockpiles and slime dams. However, they could be recovered from the gas liquors produced and the ashes derived from the gasification process, allowing for their production as saleable products [38], potentially reducing health and environmental toxicity challenges.

Table 3-4: Chemical composition of ashes of FCR samples and their corresponding density fractions.

Elements (wt.% LOI free)	TEP	TEP Fl1.5	TEP Fl1.9	TEP Sl1.9	STEM	STEM Fl1.5	STEM Fl1.9	STEM Sl1.9
SiO_2	54.1	49.2	51.7	52.8	54.6	46.4	55.8	55.5
Al_2O_3	24.9	28.7	28.5	25.9	26.0	28.3	24.1	23.5
CaO	10.4	7.2	7.6	8.6	9.3	10.8	8.5	8.6

Elements (wt.% LOI free)	TEP	TEP Fl1.5	TEP Fl1.9	TEP Sl1.9	STEM	STEM Fl1.5	STEM Fl1.9	STEM Sl1.9
Fe_2O_3	3.6	6.7	4.0	5.0	3.5	3.4	5.7	5.3
MgO	2.2	2.0	2.0	2.0	2.2	2.8	1.6	1.6
TiO_2	1.6	1.5	1.5	1.3	1.6	2.1	1.4	1.4
K_2O	1.0	1.0	1.1	1.2	0.9	0.8	0.9	1.0
Na_2O	0.7	0.8	0.7	0.8	0.5	1.8	0.4	0.4
P_2O_5	0.7	0.9	0.7	0.5	0.7	1.8	0.4	0.4
SrO	0.3	0.5	0.4	0.4	0.3	0.6	0.2	0.2
BaO	0.2	0.3	0.3	0.3	0.2	0.3	0.2	0.2
ZrO_2	0.1	0.1	0.1	0.1	0.1	0.1	0.1	0.1
MnO	0.1	0.1	0.1	0.1	0.1	0.1	0.0	0.0
SO_3	0.0	0.0	0.0	0.0	0.0	0.0	0.0	0.0
Sum of trace	n.a	0.8	1.3	0.9	n.a	0.6	0.7	1.7
Trace elements (ppm)								
Co	n.a	4751.7	6626.1	4484.9	n.a	3589.2	3663.5	6277.0
Zn	n.a	1316.9	2300.7	1901.8	n.a	1178.2	1571.9	1680.4
As	n.a	1032.3	1101.0	830.0	n.a	710.3	576.3	1829.6
Rb	n.a	303.5	374.3	284.4	n.a	160.0	172.9	3707.0
Sr	n.a	171.6	366.2	278.1	n.a	156.4	60.9	716.3
Y	n.a	151.0	175.9	126.2	n.a	53.1	57.4	352.0
Zr	n.a	146.6	473.5	545.6	n.a	373.1	377.3	973.1
Ag	n.a	49.9	74.9	41.6	n.a	12.3	6.2	102.7
Cd	n.a	32.9	52.0	41.2	n.a	37.1	35.9	128.6
In	n.a	25.2	30.5	22.0	n.a	5.1	4.9	46.5
Sn	n.a	22.2	13.2	28.1	n.a	23.3	14.5	35.6
Sb	n.a	17.8	23.5	19.5	n.a	13.7	28.6	93.5
Ba	n.a	17.8	45.3	30.9	n.a	29.8	34.4	53.9
Total	100.0	100.0	100.0	100.0	100.00	100.0	100.0	100.0

Note: L.O.I.-loss on ignition, n.a-not analysed

3.3.4.2 Ash Properties by Empirical Indices

The ash chemistry of coal could indicate the behaviour of coal and ash handling during gasification and combustion by applying empirical methods to evaluate parameters such as the alkali-index, base/acid (B/A) ratios, iron to calcium ratio, and slagging and fouling indices. Browning et al. [39] define the equations and methods for determining various empirical indices for the chemical properties of coal ashes. The ash properties of the TEP and STEM samples and their density-separated fractions are presented in Table 3-5. According to Rautenbach, et al. [31], the interaction of inherent MM with each other and coal macerals leads to the formation of slag and clinker in SA boilers during the combustion process. The empirical indices are calculated using the total inorganic elements in the coal ashes, as presented in Table 3-5. The approach of total inorganic elements disregards the mode of occurrence of MM, and it may be inaccurate in predicting the slagging behaviour of SA coals. However, the elemental composition of the ashes of the FI1.5 samples could be useful in estimating the slagging propensities of these fines. Both the TEP and STEM samples and their density-separated fractions were found to have low slagging propensity with slagging-index values below the 2.6 limit [22]. The silica and acid-base ratios of all samples fall well outside the slagging windows of 50-60 and 0.4<x>0.7. In addition, the B/A ratios of between 0.2 and 0.3 may indicate a high-ash fusibility temperature [9].

Table 3-5: Chemical ash properties of the FCR samples along with their corresponding density-separated fractions.

Ash Property	TEP	TEP FI1.5	TEP FI1.9	TEP SI1.9	STEM	STEM FI1.5	STEM FI1.9	STEM SI1.9
AI (kg/GJ)	7.6	2.5	5.0	12.3	5.4	4.7	5.3	6.1
B/A ratio	0.2	0.2	0.2	0.2	0.2	0.3	0.2	0.2
Fouling index	0.1	0.0	0.1	0.2	0.1	0.1	0.1	0.1
Slagging index	0.3	0.1	0.1	0.5	0.4	0.2	0.2	1.2
Silica ratio	77.0	75.5	79.3	77.3	78.4	73.2	78.0	78.3
Iron to Calcium	0.3	0.9	0.5	0.6	0.4	0.3	0.7	0.6

Note: Base/Acid = B/A; Alkali index (AI)

Under pyrolysis and gasification conditions, high alkali indices could imply high reaction rates and catalytic effects [36]. However, caution needs to be taken regarding carbon deficiency in the SI1.9 samples, which contain concentrated extraneous minerals that could prevent the coalescence of minerals. Pure grains of minerals such as quartz may remain unreacted at

elevated temperatures [31]. Also, confirmation of these empirical indices, especially with coal ashes reporting iron-calcium ratios greater than 0.3, using advanced analytical techniques to assess the mode of occurrence of MM is recommended before direct application of these coals to conventional thermo-chemical processing plants.

3.3.5 XRD Analysis

Table 3-6 presents the crystalline phases, amorphous organic carbon phases, MM contents, crystal carbon size of the TEP and STEM samples, and corresponding density-separated fractions. As expected, both samples contain high proportions of amorphous organic carbon with lower crystalline phase contents. Kaolinite and quartz are the primary minerals present in the TEP sample. The MM of the FI1.5 fractions of both FCR samples reduced significantly from the feed coals, while the SI1.9 sample showed an increase in MM. Similarly, kaolinite and quartz are the prevalent minerals in the STEM sample, but they had a lower percentage of kaolinite than the TEP sample. Lower proportions of fluxing minerals (dolomite, calcite, and pyrite) were also observed in both samples, ranging from 4.3 wt. % to 0.5 wt.%. Overall, both samples were dominated by kaolinite, a clay mineral, and lower contents of illite and microcline, which are typical of SA Highveld coals [31]. However, gypsum was only detected in the TEP sample as a result of (1) the presence of calcite and pyrite in this sample and (2) the interaction of calcium oxide derived from organic calcium and transformed inherent/extraneous calcite with sulphur dioxide from the partial oxidation of the inherent/extraneous pyrite particles and organic sulphur during storage of coal fines in slime dams or stockpiles. Moreover, it has been reported that organic calcium and organic sulphur interact with each other at 120-150 °C to form bassanite in the low-temperature ash samples of South African feed-coals using an International Plasma Corporation (IPC) low-temperature asher [22].

The proportions of minerals in the density-separated fractions illustrate a general incremental trend with an increase in the specific gravity of the separation medium. As expected, the SI1.9 samples contained the lowest proportions of amorphous organic carbon, while the FI 1.5 samples, especially for the TEP samples, contained the highest proportions. Although an increase in the percentage of amorphous organic carbon is observed for the FI1.5 fractions of the STEM sample, almost no difference is observed between the FI1.9 and SI1.9 samples. This behaviour could result from a lower concentration of extraneous mineral content and/or the poor washability characteristics of the STEM sample.

These XRD results illustrate that the MM of the TEP samples were comprised mainly of extraneous minerals (rock fragments) originating from roof and floor strata and possible

contamination during coal processing and handling. The Fl1.5 fractions of both FCR samples reported lower proportions of kaolinite, quartz, dolomite, calcite, and pyrite, indicating some associations with the coal carbon matrix and the prevalence of these minerals in an extraneous mode of occurrence. The microcline percentage increased slightly in the float fraction due to its prevalent intimate association with the coal carbon matrix. An anomaly is observed in the case of illite, which only increased in the float fraction of the STEM sample. In contrast, only a slight decrease was observed in the TEP sample indicating its prevalent association with the coal carbon matrix in the STEM sample. At the same time, it is mainly extraneous in the TEP sample. This confirms the presence of MM in coal in different modes of occurrence.

Furthermore, the XRD analysis indicates that the TEP and STEM samples contain 0.4 and 0.1% hematite, respectively (Table 3-6). The presence of hematite could be attributed to the corrosion product contamination from the plant's equipment during the stockpiling and handling of the FCR samples. In addition, magnetite (Fe_3O_4) media spilled into the coal-washing plant's drains, contaminating the TEP filter cake en route to the slimes dam.

Table 3-6: Mineralogical compositions and crystal carbon size of the FCR samples and their corresponding density-separated fractions.

Mineral (wt. %)	TEP	TEP Fl 1.5	TEP Fl 1.9	TEP Sl 1.9	STEM	STEM Fl 1.5	STEM Fl 1.9	STEM Sl 1.9
Kaolinite	21.5	8.3	14.8	27.3	14.3	11.0	17.2	14.4
Quartz	7.7	2.8	6.5	15.6	8.4	3.7	6.9	8.3
Dolomite	4.3	0.3	1.0	1.7	3.1	0.9	1.1	0.5
Calcite	3.0	0.4	1.7	4.8	2.0	0.9	0.7	2.6
Illite	1.0	0.9	2.6	5.5	0.5	1.0	1.7	2.0
Pyrite	0.6	0.2	0.3	0.9	0.3	0.1	0.2	0.7
Hematite	0.4	0.0	0.1	0.2	0.1	0.1	0.0	0.1
Gypsum	0.3	0.2	0.5	1.1	0.0	0.2	0.1	0.4
Microcline	0.1	0.2	0.5	1.0	0.2	0.6	0.2	0.0
Rutile	0.1	0.0	0.2	0.3	0.0	0.1	0.0	0.2
Anatase	0.1	0.0	0.2	0.2	0.1	0.0	0.1	0.2
Goyazite	0.1	0.0	0.1	0.2	0.1	0.1	0.1	0.0
Apatite	0.1	0.0	0.0	0.0	0.0	0.0	0.0	0.0
Magnetite	n.d	0.1	0.4	0.9	n.d	0.0	0.1	0.3

Mineral (wt. %)	TEP	TEP Fl 1.5	TEP Fl 1.9	TEP Sl 1.9	STEM	STEM Fl 1.5	STEM Fl 1.9	STEM Sl 1.9
Mineral Matter	39.3	13.4	28.9	59.7	29.1	18.7	18.4	29.7
AM	**60.7**	**86.6**	**71.1**	**40.3**	**70.9**	**81.3**	**71.6**	**70.3**
Total	100.0	100.0	100.0	100.0	100.0	100.0	100.0	100.0
CC size (nm)	1.1	1.5	1.4	1.3	1.0	1.6	1.4	1.2

n.d-not detected, AM–Amorphous material, CC - carbon crystal

The mode of occurrence of MM contributes to char morphology and structure, along with subsequent gasification reaction rates, downstream ash properties and handling [40]. Quartz is present in the float and sink fractions of both coals, implying a close association of quartz with the coal carbon matrix and rock fragments. Pure extraneous quartz is inert at elevated temperatures [41], while quartz associated with fluxing minerals and kaolinite could form a molten solution, and subsequently, mullite could crystallise from this molten solution in the cooler regions of either gasifiers or boilers [31].

Extraneous kaolinite has been reported extensively in the literature to undergo dehydroxylation reactions, forming a reactive meta-kaolinite ($Al_2O_7Si_2$) and subsequently mullite ($3Al_2O_3.2SiO_2$). Mullite is a hard mineral that can erode and abrade inner walls and components of gasification, pyrolysis, and combustion reactors. In addition, the reactive silica could form cristobalite (SiO_2) (a high-temperature quartz) which could end up in ash. However, meta-kaolinite could also form in the pyrolysis zone from either inherent or extraneous kaolinite associated with fluxing element-bearing minerals to form a range of Ca/Mg/Fe-aluminosilicates during coal combustion [31, 41]. This kaolinite transformation could lead to the encapsulation of unreacted carbon, resulting in reduced carbon conversion in the oxidation zone [4]. Comparably, inherent microcline, which exists in SA Highveld coals in trace amounts, could react with fluxing element-bearing minerals or melts to form a molten solution at temperatures around 1000 °C which could cause slagging [31,34], while extraneous microcline could remain unreacted.

The Inherent fluxing minerals (pyrite, dolomite, calcite) associated with coal macerals could induce the interaction of organic carbon with water vapour, which prevents the formation of heavy aromatics, subsequently increasing gasification reaction rates [42]. Under pyrolysis and gasification conditions, pure pyrite transforms into pyrrhotite, which has also been linked to catalytic effects [43].

The XRD results of STEM and TEP samples and the distribution of these minerals across their respective density-separated fractions indicate the association or mode of occurrence of these

minerals in coal. In addition, their possible effects on reaction mechanisms, reaction rates and process efficiencies, and transformation can be deduced to some extent.

3.3.6 Raman Analysis

The normalised and stacked Raman spectra of the STEM (unoxidised FCR) and TEP (oxidised FCR) samples are presented in

Figure 3-5. The observed Raman spectra of the FCR samples studied were split into three regions, namely, the minerals prominence (100 - 800 /cm), first order (800 - 1800 /cm) and second order (1800 - 3500 /cm) regions. Only the first two regions are discussed in this study due to the poor definition of peaks in the third-order region. The assignment of peaks was performed with reference to the RUFF database, CrystalSleuth software and literature [44]. The intensity of bands attributed to the disordered carbon (second order region) overpowered those of the minerals except for the very strong anatase (TiO_2) peak around 144 /cm observed for the TEP sample.

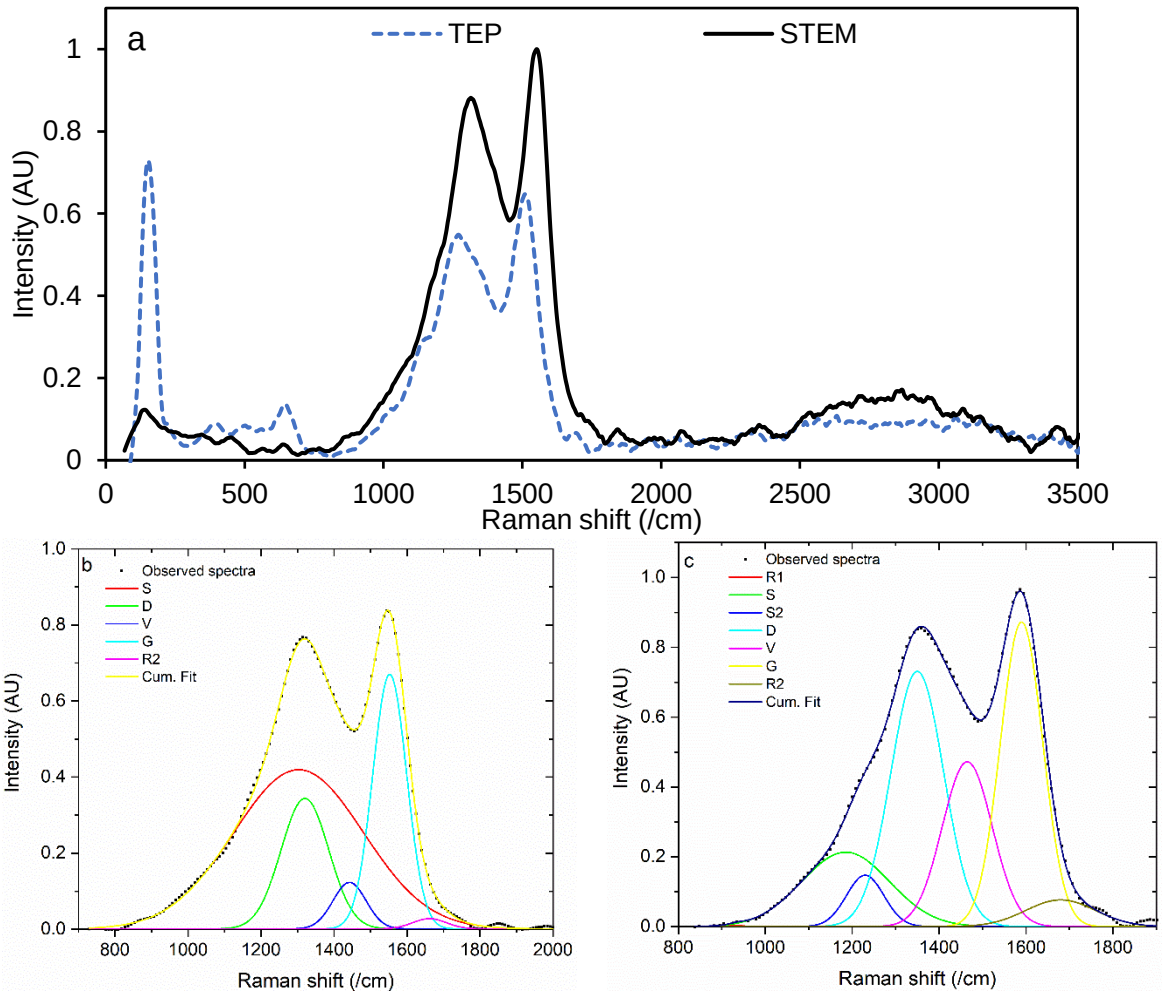

Figure 3-5: Raw Raman spectra for the FCR samples (a) and the deconvoluted Raman spectra for the STEM sample (b) and TEP sample (c).

This behaviour is caused by the high sensitivity of the Raman technique to carbon-based materials and the good Raman scattering abilities of anatase. Nonetheless, this technique is useful for confirming the XRD results, especially for minerals in low concentrations. The presence of fluxing minerals was confirmed by the peaks at 175, 299 and 339 /cm associated with dolomite peaks at 380 and 431 /cm, which could be linked to the presence of pyrite and calcite-attributed peaks at 157 and 283 /cm. These minerals have coal gasification and pyrolysis reactivity rate implications especially if they are associated with macerals. Anatase could induce hydrocracking intermediate gasification and pyrolysis products via the hot char layer [45] and was confirmed by peaks at 144, 198, 394, 514 and 638 /cm. The results confirmed the presence of low concentrations of minerals such as dolomite, calcite, anatase and pyrite, as reported by the XRD analysis.

The second-order region of the Raman spectra provides an insight into coal's maturity and the organic structures' nature. Discernment of the organic structures of the TEP and STEM samples, along with their density-separated fractions, has been performed for the second-order region by deconvoluting the Raman spectra into 5-7 peaks of the graphite-like (G) band and the defective/amorphous (D) bands. The summary of the peak parameters for the TEP and STEM samples and their beneficiated float fractions are presented in Table 3-7, while

Figure 3-5b&c illustrate the deconvoluted spectra for the TEP and STEM samples. Although a clear trend in the areas of the C-H on alkanes, cyclic alkanes and aromatic rings (R_1), C-aromatic/aliphatic ethers, C-alkyls and C-C hydroaromatic (S), para-aromatics (S_2), aromatics with >6 rings (D), amorphous carbon structures (V), graphite-like structures (G) and the C=O carbonyl groups (R_2) has not been observed, the variations clearly indicate that density separation has affected the organic structure and led to chemical differences in the float fractions of the TEP and STEM samples by separation of coal macerals having different physical properties across different density fractions. These chemical differences implicate different reaction rates for the different density-separated fractions. The area ratios of the D and the G bands (I_D/I_G) provide a summarised indication of the maturity of coal and their reactivity, whereby the lower I_D/I_G ratio indicates the maturity of the coals, while the V and S bands could be attributed to the reactive sites [46]. The float fractions of both FCR samples contributed higher areas of the S band, implying the possibility of relatively higher gasification reaction rates being achieved for these samples [47].

Table 3-7: Raman fitted peak parameters for the FCR samples and their density-separated fractions.

Peak	Position (/cm)	Peak Area		
		TEP	**TEP Fl1.5**	**TEP Fl1.9**
R_1	934	10.1 (0.3)	10.3 (0.3)	24.1 (4.1)
S	1185	54.0 (0.9)	65.0 (0.9)	73.8 (0.8)
S_2	1230	15.9 (1.4)	ud	14.2 (0.7)
D	1350	111.1 (1.6)	102.7 (1.7)	109.8 (0.8)
V	1465	68.2 (1.3)	149.5 (3.1)	67.5 (0.7)
G	1590	106.6 (0.9)	80.3 (0.9)	106.2 (0.5)
R_2	1680	15.4 (0.6)	9.4 (3.8)	13.0 (0.5)
Adj.R^2	-	0.99861	0.99894	0.99810
I_D/I_G	-	0.8	0.7	0.9
I_G/I_{ALL}		0.5	0.6	0.5
L_a (nm)		22.9	25.7	22.5
		STEM	**STEM Fl1.5**	**STEM Fl1.9**
R_1	880	5.0 (1.0)	ud	ud
S	1185	49.7 (0.9)	49.9 (1.1)	60.3 (1.0)
D	1350	161.6 (1.9)	91.3 (4.3)	118.7 (1.3)
V	1465	100.1 (3.0)	141.0 (8.8)	44.1 (1.1)
G	1590	90.1 (1.2)	80.1 (1.9)	97.0 (1.0)
R_2	1680	3.0 (11.05)	5.0 (2.0)	41.9 (1.2)
Adj.R^2	-	0.99913	0.99945	0.99971
I_D/I_G	-	0.5	0.7	0.8
I_G/I_{ALL}		0.1	0.6	0.6
L_a (nm)		37.4	28.4	23.3

Ud - undefined peak; TEP Fl1.5 is the Fl1.5 of the TEP sample; TEP Fl1.9 is Fl1.9 of the TEP sample; STEM Fl1.5 is the Fl1.5 of the STEM sample; STEM Fl1.9 is Fl1.9 of the STEM sample.

The nuclear magnetic resonance (NMR) results of the <1.5g/cm^3 float fraction of the SA coal waste and feed coals clearly indicated that this density-separated fraction contains 78% aromatic carbons and 22% aliphatic carbons [16,48]. Furthermore, the Fourier transform

infrared (FTIR) analysis of this analysed float sample detected aromatic and aliphatic functional groups. In addition, the gas chromatography-mass spectrometry (GC-MS) scan showed that the SA <1.5 g/cm^3 float fraction is comprised of aromatic and hydrocarbon compounds [48]. The Raman and XRD results for the organic matter present in the FCR samples are consistent with the NMR, FTIR and GC-MS scan data of SA feed coals and coal waste, previously reported by Uwaoma et al. [16] and Matjie et al. [48].

3.3.7 Petrographic Analysis

3.3.7.1 Rank Determination

Figure 3-6 illustrates the petrographic distribution of major maceral groups in the TEP and STEM samples and their corresponding density-separated fractions, while Figure 3-6a and b present a graphical illustration of coal maceral and maceral-mineral associations. The vitrinite reflectance analysis indicates that the TEP and STEM samples are medium-rank C/D bituminous coals with a random mean vitrinite reflectance of 0.6 RoV% (±0.057). The results further indicate, on an MM-free basis (mmf), that the STEM sample contains a higher vitrinite content than the TEP sample.

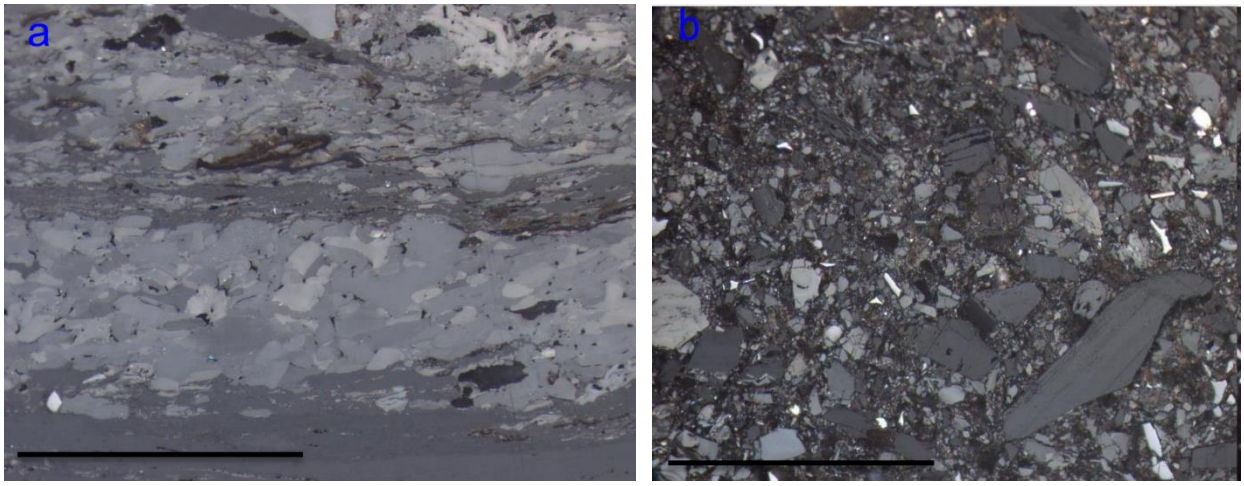

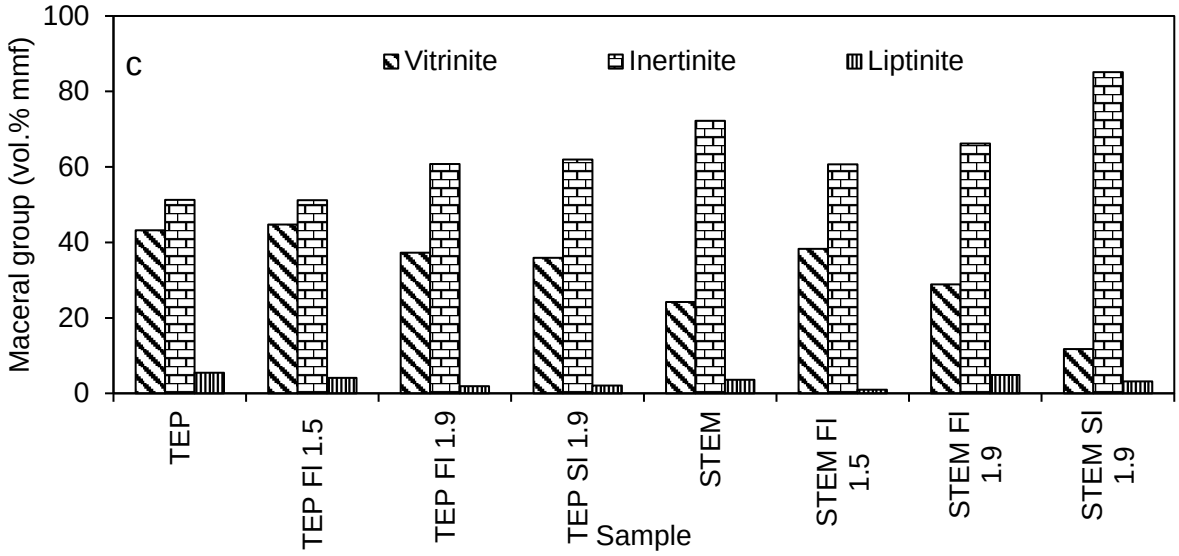

Figure 3-6: Petrographic analysis results for the TEP and STEM samples, a.) field of view of the STEM sample showing banded vitrinite and inertinite (100 µm scale), b.) field of view of the TEP sample showing distributed macerals and liberated MM (100 µm scale) and c.) distribution of macerals in the FCR samples and their corresponding density fractions (mmf-MM free basis).

As expected, the random mean vitrinite reflectance of the density-separated fractions did not change across beneficiated samples. However, significant changes were observed in the MM, vitrinite, liptinite, and inertinite maceral percentages. Vitrinite was enriched in the < 1.5 g/cm^3 float fractions of both the TEP and STEM samples, while inertinite was enriched in the >1.9 g/cm^3 sink fractions. This behaviour is attributed to the densities of these macerals' groups, with liptinite being the lightest and inertinite the heaviest. The petrography results of the TEP and STEM samples and the distribution of maceral groups across the density-separated fractions are consistent with those of the feed-coals and their density-separated fractions reported by Everson et al. [21]. The high vitrinite content in the TEP sample could imply the development of a more porous intermediate char during gasification, leading to higher gasification reactivity. In contrast, the high inertinite content in the STEM sample could shift reactions to higher temperatures, consequently increasing the residence time of the STEM sample in the pyrolysis zones of the gasifiers [49]. It is noteworthy that the MM contents detected by XRD analysis (Table 3-6) may impact the reactivity of these macerals and may, in turn, obscure the true reactivity dependence on maceral groups. Therefore, techniques for separating macerals and inherent minerals without changing the organic structure of coal are recommended to discern their behaviour. The results provide an opportunity to produce suitable blends with desired maceral groups for application in the gasification plants.

3.3.7.2 Microlithotypes

Figure 3-7 presents the distribution and association of macerals in the TEP and STEM samples. The dominance of microlithotypes and MM in both samples follows the order: monomaceral > bimaceral > rock > trimaceral carbominerites for the TEP sample and monomacera l> bimacera l> carbominerite > rock > trimaceral for the STEM sample, but with different associations and percentages of each maceral type. Vitrite and semi-fusite dominated the monomacerals in the TEP sample over their less reactive inerto-detrite and fusite counterparts. Only one-third of the vitrite was observed in the inertinite-rich STEM sample. More than double the carbominerites observed in the TEP sample occurred in the STEM sample. These variations of microlithotypes percentages, especially with reactivity implications of carbominerite and vitrite could obscure reactivity comparisons between the two samples [21]. Carbominerites, especially pyrite and ankerite associated with the carbon-matrix could catalyse gasification and pyrolysis reactions. These results associate the TEP sample with possibly higher reaction rates over the STEM sample counterpart due to the relatively higher proportions of reactive microlithotypes and the association of pyrite with the carbon-matrix in the TEP sample.

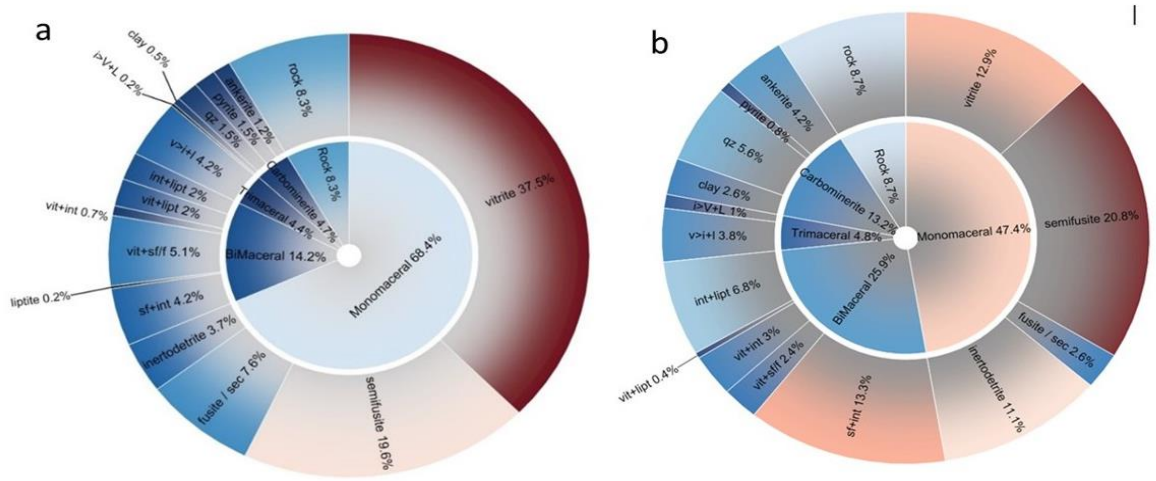

Figure 3-7: Distribution of microlithotypes in the FCR samples by petrographic analysis a) TEP sample and b) STEM sample.

3.3.8 Thermogravimetric Analysis (TGA)

3.3.8.1 Analytical Pyrolysis

The thermograms obtained from analytical pyrolysis experiments for evaluation and comparison of devolatilisation rates of the TEP and STEM samples are displayed in Figure

3-8. The TG profile of both samples followed a similar pattern. However, the devolatilisation of the STEM sample was slightly delayed until higher temperatures were reached, which could be attributed to the lower percentages of moisture, VM, and vitrinite content in the STEM sample. Three main mass loss zones were observed: 1.) linked to loss of moisture and light hydrocarbons, 2.) the main devolatilisation zone linked with thermal cracking and decomposition of VM and FC, and 3.) transformation of MM (dehydration and decarboxylation) [50].

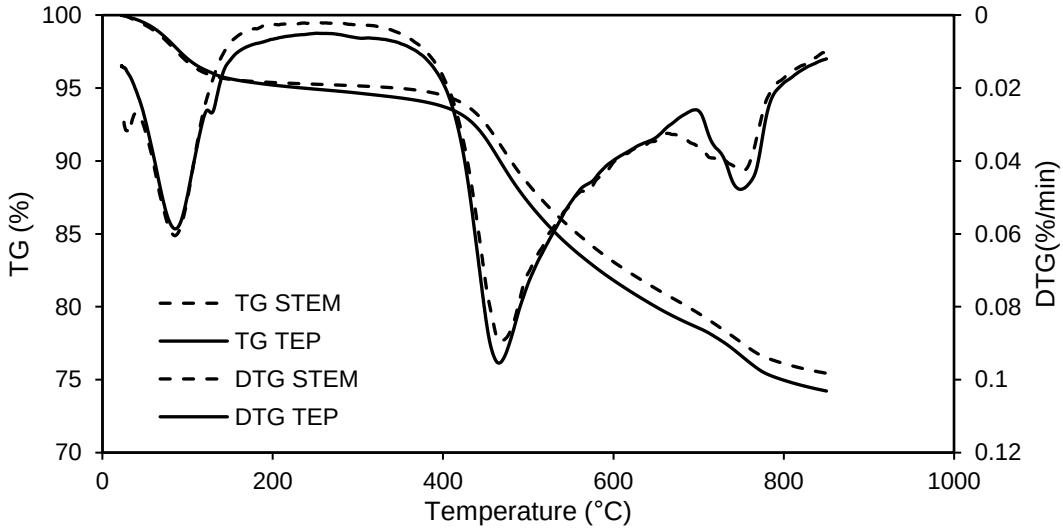

Figure 3-8: TG and derivative thermogravimetry (DTG) thermographs of the FCR samples.

Table 3-8 summarises the pyrolysis characteristics, illustrating almost no differences except for shifts in mass loss zone temperatures. This behaviour suggests that although the STEM sample may take longer to react in the pyrolysis zone, the overall decomposition rate of both samples is similar.

Table 3-8: Thermal degradation characteristic parameters of the FCR samples under inert environment at 30 °C/min.

Sample	T_i (°C)	T_m (°C)	T_f (°C)	R_p (%/min)	Ra (%/min)
STEM	340	480	670	0.088	0.038
TEP	280	472	698	0.094	0.039

T_i – temperature at which main decomposition started, T_m – the maximum decomposition peak temperature, T_f – temperature at which the main decomposition terminated, Rp – maximum rate of decomposition, R_a– average rate of decomposition.

3.3.8.2 Reactivity of Prepared FCR Chars

The isothermal gasification reaction properties of the chars prepared from the TEP and STEM samples and their corresponding density-separated fractions presented in Figure 3-9 indicate complete conversion of carbon for all samples at the studied reaction times. However, the TEP sample and its beneficiated fractions seemingly reached higher conversions (>0.8) faster than the STEM sample and its beneficiated fractions. The gasification reaction rate plots (Figure 3-9c) clearly show a sharp increase in the rate of gasification reactions leading to 0.2 conversion, followed by a gradual decrease until a complete conversion for all samples. It is difficult at this point to compare and attribute the changes in the organic structures, as illustrated by the Raman data of the TEP and STEM samples, to their reaction rates due to compensation of areas of the V and the S bands associated with the presence of aromatic and aliphatic compounds (one increases while the other decreases). In this case, this makes macerals and MM differences good indicators for predicting the reactivity of the TEP and STEM samples. As a result, the increase in gasification rates in the initial stages could be attributed to 1.) the decomposition of reactive macerals and the development of porous structures leading to a larger surface area [16] and 2.) a higher proportion of percentage ash yield or MM as indicated by the proximate and XRD analyses compared to those of STEM sample. Another explanation could be a temporary change of AI load as carbon conversion progresses. However, this does not explain the drop in the reaction rate (dx/dt) beyond 0.2 conversion. This diminution in dx/dt could be explained by reduced carbon content and the collapse of pore structures along with the coating of carbon structures by aluminium silicates (kaolinite) and quartz, which has been reported to hinder gasification reaction rates [36]. The AI load phenomena could be supported by a higher AI of 7.6 for the TEP sample compared to 5.4 for the STEM sample as presented in Table 3.5.

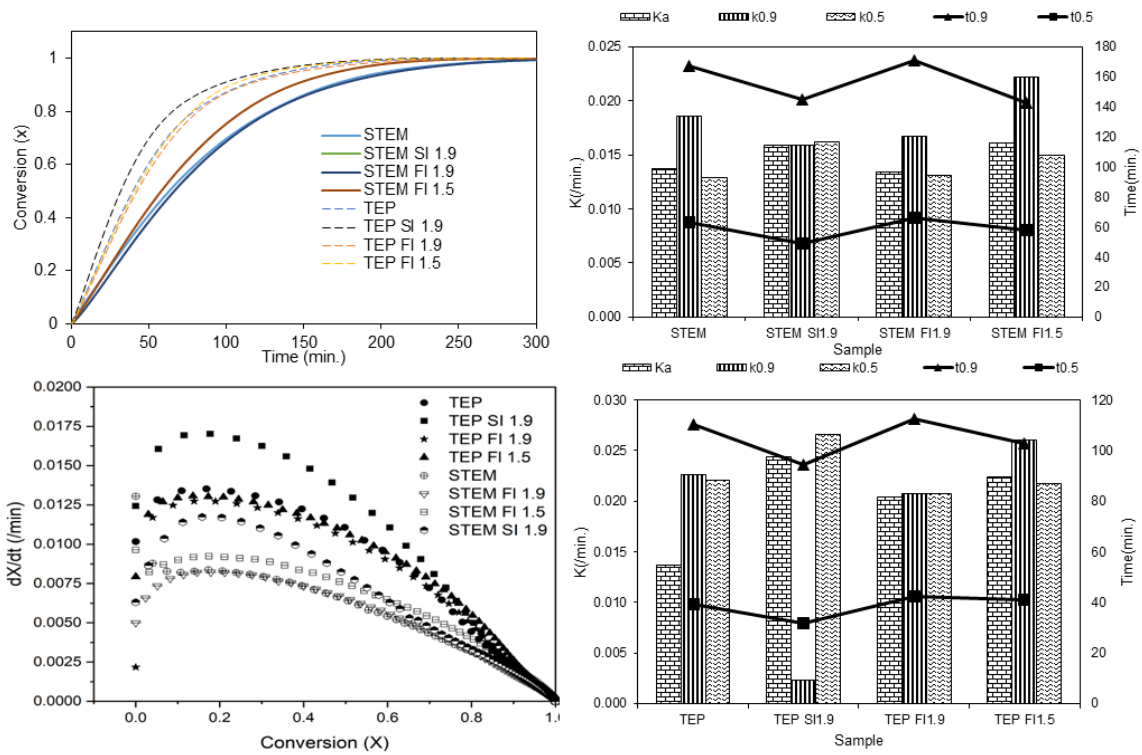

Figure 3-9: Comparison of gasification progression for chars prepared from the FCR samples and their corresponding density-separated fractions: a) conversion vs time, b) normalised gasification rate characteristics for the TEP sample, c) rate of conversion vs conversion and d) normalised gasification rate characteristics for the STEM sample.

In addition, since these coals are of the same rank, their different maceral compositions and MM contents, particularly the pure maceral and maceral-maceral and maceral-mineral associations, could contribute to the different dx/dt values. For instance, the STEM sample is rich in inertinite, which has been known to react more slowly than vitrinite [51,52]. The latter is a predominant maceral group in the TEP sample. Figure 3-9a-d illustrates that gasification reactions of the TEP sample and its density-separated fractions are completed sooner than those of the STEM sample and its density-separated fractions.

The half-life and average gasification reaction rates (k0.5 and ka, respectively) for the STEM sample are comparable to those of the TEP sample. This indicates that k0.5 can only be used to predict the average reactivity of the STEM sample. In the case of the TEP sample, the value of k0.5 is close to that of the final gasification reaction rate (k0.9). The reason for this behaviour for coal of the same rank and sourced from the same area is currently unknown. These results illustrate the contribution of different coal carbon structures and MM to gasification reaction rates and provide insight into blending and beneficiation strategies for improved reaction rates for utilisation of the TEP sample. Higher reactivity rates of the TEP sample compared to those

of the STEM sample derived from the feed coal blend to the steam generation plant could imply its suitability in thermochemical processes.

3.4 Conclusions

In this study, the TEP and STEM samples were subjected to density separation experiments to study the mode of occurrence of MM and its effects during the CO_2-gasification reactivity experiments. The FCR samples and their beneficiated fractions were characterised by both conventional and advanced analytical techniques prior to the CO_2-gasification experiments using the TGA. The analytical results for these samples revealed that the FCR samples have similar chemical properties but different mineralogical, petrographic and physical (PSD) properties. After studying the properties of the FCR samples and their density-separated fractions, the following findings and conclusions were drawn:

- On an as received basis, the STEM sample comprises a higher % fixed-carbon and calorific value than the TEP sample owing to the higher % ash yield in the TEP sample. The 1.5 g/cm^3 float fraction of the TEP sample shows the lowest percentage ash yield, a higher calorific value and a higher fixed carbon content due to the MM liberation.
- Density separation liberates extraneous and cleats minerals from the carbon matrix to yield float fractions with higher carbon content. The TEP sample shows a lower carbon content than the STEM sample. However, its float fractions comprise higher carbon content than those of the STEM float fractions, making the float fractions of the TEP sample more reactive.
- The PSD analysis shows that the TEP sample contains more fine and ultra-fine coal particles than the STEM sample. The ultra-fine nature of the TEP sample over the STEM sample contributed to a better coal washability yield due to pronounced MM liberation.
- The TEP sample comprises higher proportions of fluxing minerals (dolomite, calcite and pyrite) than the STEM sample. These higher proportions of fluxing minerals are associated with pronounced TEP CO_2-gasification reactivities.
- The spontaneous combustion of the FCR samples linked to pyrite oxidation, as well as the interaction of organic sulphur and organic calcium at 400 °C, which pose trace elements and PM release threats in the form of H_2S, CO_2, SO_2, cadmium, arsenic and selenium emissions associated with environmental and human health impacts, was described based on the forms of sulphur present in both FCR's.

- Gasification TG experiments conducted on the density-separated fractions, STEM and TEP samples demonstrated that the MM are associated with the chemical reactions and carbon-conversion rates.
- The TG experiments illustrated higher reaction rates for the TEP samples than the STEM samples. This is attributed to their differences in percentage MM, macerals-minerals association, maceral-maceral associations and maceral proportions, particularly vitrinite and inertinite.
- Raman spectra show the presence of aromatic and aliphatic compounds in the samples, which corroborated the XRD results for crystalline carbon crystallite sizes associated with these organic compounds and minerals.

This study provides a starting point for utilising the FCR blend (1:1) sample as a co-feed to the pyrolysis, fluidised-bed gasification and combustion processes.

3.5 Acknowledgements

The information presented in this paper is based on the research financially supported by the South African Research Chairs Initiative (SARChI) of the Department of Science and Technology and the National Research Foundation of South Africa (Coal Research ChairGrant No.86880 and the NRF free-standing bursary MND200715544211/UID: 136078). Any opinion, finding, conclusion or recommendation expressed in this material is that of the author(s), and the NRF does not accept any liability in this regard. Prof N. Wagner of the University of Johannesburg, Geology Department, Dr L. Kapesi of the University of Johannesburg, Department of Physics and Mr M. Van Zyl of SGS, Secunda, are thanked for assistance with different analytical techniques.

Chapter 4 reports on studies of the effect of extraneous mineral matter by the addition of composites of reactive oxides and hydroxide minerals ($Ca(OH)_2$-MgO-Fe_2O_3) to a TEP fine-coal reject sample, its density-separated fractions, and its demineralised and chemically fractionated residues. The blends were subjected to various conventional and advanced analytical techniques under pyrolysis conditions. The findings from the characterisation and pyrolysis experiments are reported in this manuscript. Comparisons of the yields and compositions of the chars and tars are also discussed.

Chapter References

[1] Tambwe O, Kotsiopoulos A, Harrison STL. Desulphurising high sulphur coal discards using an accelerated heap leach approach. Hydrometallurgy. 2020; 197:105472.

[2] Reddick Von Blottnitz H. & Kothuis BJ. A cleaner production assessment of the ultra-fine coal waste generated in South Africa. Journal of the Southern African Institute of Mining and Metallurgy. 2007; 107:811–6.

[3] Moyo A, Filho JRDA, Harrison STL, Broadhurst JL. Implications of sulfur speciation on the assessment of acid rock drainage generating potential: A study of South African coal processing wastes. Minerals. 2019; 9:776.

[4] Deng J, Ma X, Zhang Y, Li Y, Zhu W. Effects of pyrite on the spontaneous combustion of coal. International Journal of Coal Science & Technology. 2015; 2:306–11.

[5] Singh U, Sharma N, Mahapatra SS. Environmental life cycle assessment of Indian coal-fired power plants. International Journal of Coal Science & Technology. 2016; 3:215–25.

[6] Shekarian Y, Rahimi E, Shekarian N, Rezaee M, Roghanchi P. An analysis of contributing mining factors in coal workers' pneumoconiosis prevalence in the United States coal mines, 1986–2018. International Journal of Coal Science & Technology. 2021; 8:1227–37.

[7] Castranova V, Vallyathan V. Silicosis and coal workers' pneumoconiosis. Environmental Health Perspectives. 2000; 108:675–84.

[8] Nádudvari Á, Cabała J, Marynowski L, Jabłońska M, Dziurowicz M, Malczewski D, et al. High concentrations of HgS, MeHg and toxic gas emissions in thermally affected waste dumps from hard coal mining in Poland. Journal of Hazardous Materials. 2022; 431:128542.

[9] Frandsen F. Empirical prediction of ash deposition propensities in coal-fired utilities. Technical Report. 1997. Danmarks Tekniske Univ., Lyngby (Denmark). Inst. for Kemiteknik. NTIS Issue Number: 199819.

[10] Falcont RM. Spontaneous combustion of the organic matter in discards from the Witbank coalfield. Journal of the Southern African Institute of Mining and Metallurgy 1986; 86:243–50.

[11] Strydom CA, Mthombo TS, Bunt JR, Neomagus H. Some physical and chemical characteristics of calcium lignosulphonate-bound coal fines. Journal of the Southern African Institute of Mining and Metallurgy. 2018; 118:1277–83.

[12] Belaid M, Falcon R, Vainikka P, Patsa K V. Potential and technical basis for utilising coal beneficiation discards in power generation by applying circulating fluidised bed boilers. 2nd International Conference on Chemical, Ecology and Environmental Sciences (ICEES'2013), London: 2013, p. 260–5.

[13] Valdés AF, Garcia AB. On the utilisation of waste vegetable oils (WVO) as agglomerants to recover coal from coal fines cleaning wastes (CFCW). Fuel. 2006; 85:607–14.

[14] Bunt JR, Neomagus HWJP, Botha AA, Waanders FB. Reactivity study of fine discard coal agglomerates. Journal of Analytical and Applied Pyrolysis. 2015; 113:723–8.

[15] Leokaoke NT, Bunt JR, Neomagus HWJP, Waanders FB, Strydom CA. CO_2 reactivity of briquettes derived from discard inertinite-rich Highveld coal using lignosulphonate and resin as binders. Journal of the Southern African Institute of Mining and Metallurgy. 2019; 119:847–54.

[16] Uwaoma RC, Strydom CA, Bunt JR, Okolo GN, Matjie RH. The catalytic effect of Benfield waste salt on CO_2 gasification of a typical South African Highveld coal. Journal of Thermal Analysis and Calorimetry. 2019; 135:2723–32.

[17] Meyer JA, Strydom CA, Bunt JR, Uwaoma RC. Pyrolysis products derived from co-processing of coal fines and microalgae. Bioresource Technology Reports. 2022:19; 101128.

[18] Wagner NJ, Coertzen M, Matjie RH, van Dyk JC. Coal Gasification. In: Suárez-Ruiz, I., Crelling, J. C. editors. Applied coal petrology: The role of petrology in coal utilisation. 2008. p. 119–44.

[19] Ejesieme VO, Riaza J, Vorster N, Dugmore G, Zeelie B. Reclamation of ultra-fine coal with Scenedesmus microalgae and comprehensive combustion property of the Coalgae® composite. Journal of Energy in Southern Africa. 2020; 31:14–27.

[20] Toporov D, Abraham R. Gasification of low-rank coal in the High-Temperature Winkler (HTW) process. Journal of the Southern African Institute of Mining and Metallurgy. 2015; 115:589–97.

[21] Everson R, Koekemoer A, Bunt J, Neomagus H, Schwarz C. Detailed characterisation of South African high mineral matter inertinite-rich coals and density fractions and effect on reaction rates with carbon dioxide: Macerals, microlithotypes, carbominerites and minerals. South African Journal of Chemical Engineering. 2013; 18:1–16.

[22] Rautenbach R, Strydom CA, Bunt JR, Matjie RH, Campbell QP, Van Alphen C. Mineralogical, chemical, and petrographic properties of selected South African power stations' feed coals and their corresponding density-separated fractions using float-sink and reflux classification methods. International Journal of Coal Preparation and Utilisation. 2019; 39:421–46.

[23] Rietveld HM. A profile refinement method for nuclear and magnetic structures. Journal of Applied Crystallography. 1969; 2:65–71.

[24] Speakman SA. Introduction to PANalytical X'Pert HighScore Plus v3. 0. MIT Center for Materials Science and Engineering. 2012:1–19.

[25] Scherrer P. Determination of the internal structure and size of colloid particles by X-rays. Colloid Chemistry: A Textbook. 1912. p. 387–409.

[26] Kapesi L. Promoting carbon nanotube interlinking using ion implantation and high pressures in a diamond anvil cell [Master's Thesis]. Johannesburg, South Africa: University of Johannesburg; 2018.

[27] Uwaoma RC, Strydom CA, Matjie RH, Bunt JR. Influence of density separation of selected South African coal fines on the products obtained during liquefaction using tetralin as a solvent. Energy and Fuels. 2019; 33:1837–49.

[28] Bai Y, Lv P, Li F, Song X, Su W, Yu G. Investigation into Ca/Na compounds catalysed coal pyrolysis and char gasification with steam. Energy Conversion and Management. 2019; 184:172–9.

[29] Henning A. Evaluation of the gasification reactivity of Highveld coals for application in the coal to liquids process [PhD thesis]. Pretoria, South Africa: North-West University; 2017.

[30] Hanson S, Patrick JW, Walker A. The effect of coal particle size on pyrolysis and steam gasification. Fuel. 2002; 81:531–7.

[31] Rautenbach R, Matjie R, Strydom C, Bunt J. Transformation of inherent and extraneous minerals in feed coals of commercial power stations and their density-separated fractions. Energy Geoscience. 2021; 2:136–47.

[32] Bryers RW. Influence of segregated mineral matter in coal on slagging. In: Vorres KS, editor. Mineral matter and ash in coal, vol. 29, American Chemical Society; 1984, p. 353–74.

[33] Riley KW, French DH, Farrell OP, Wood RA, Huggins FE. Modes of occurrence of trace and minor elements in some Australian coals. International Journal of Coal Geology. 2012; 94:214–24.

[34] Matjie RH, Li Z, Ward CR, Bunt JR, Strydom CA. Determination of mineral matter and elemental composition of individual macerals in coals from Highveld mines. Journal of the Southern African Institute of Mining and Metallurgy. 2016; 116:169–80.

[35] Rautenbach R, Matjie RH, Strydom CA, Bunt JR, Ward CR, French D, et al. Evaluation of mineral matter transformations in low-temperature ashes of South African coal feedstock samples and their density-separated cuts using high-temperature X-ray diffraction. International Journal of Coal Preparation and Utilisation. 2020; 40:320–47.

[36] Hattingh BB, Everson RC, Neomagus HWJP, Bunt JR. Assessing the catalytic effect of coal ash constituents on the CO_2 gasification rate of high ash, South African Coal. Fuel Processing Technology. 2011; 92:2048–54.

[37] Wagner NJ, Hlatshwayo B. The occurrence of potentially hazardous trace elements in five Highveld coals, South Africa. International Journal of Coal Geology. 2005; 63:228–46.

[38] Wu G, Wang T, Chen G, Shen Z, Pan WP. Coal fly ash activated by NaOH roasting: Rare earth elements recovery and harmful trace elements migration. Fuel. 2022; 324:124515.

[39] Browning GJ, Bryant GW, Hurst HJ, Lucas JA, Wall TF. An empirical method for the prediction of coal ash slag viscosity. Energy and Fuels. 2003; 17:731–7.

[40] Sekine Y, Ishikawa K, Kikuchi E, Matsukata M, Akimoto A. Reactivity and structural change of coal char during steam gasification. Fuel. 2006; 85:122–6.

[41] Sheng C, Li Y. Experimental study of ash formation during pulverised coal combustion in O2/CO2 mixtures. Fuel. 2008; 87:1297–305.

[42] Dai S, Finkelman RB, French D, Hower JC, Graham IT, Zhao F. Modes of occurrence of elements in coal: A critical evaluation. Earth Science Reviews. 2021; 222:103815.

[43] Johannes I, Tiikma L, Luik H, Tamvelius H, Krasulina J. Catalytic thermal liquefaction of oil shale in Tetralin. ISRN Chemical Engineering. 2012; 2012:1–11.

[44] Nestler K, Dietrich D, Witke K, Rößler R, Marx G. Thermogravimetric and Raman spectroscopic investigations on different coals in comparison to dispersed anthracite found in permineralised tree fern Psaronius sp. Journal of Molecular Structure. 2003; 661:357–62.

[45] Shimada H, Sato K, Honna K, Enomoto T, Ohshio N. Design and development of Ti-modified zeolite-based catalyst for hydrocracking heavy petroleum. Catalysis Today. 2009; 141:43–51.

[46] Xu J, He Q, Xiong Z, Yu Y, Zhang S, Hu X, et al. Raman spectroscopy as a versatile tool for investigating thermochemical processing of coal, biomass, and wastes: Recent advances and future perspectives. Energy and Fuels. 2021; 35:2870–913.

[47] Sheng C. Char structure characterised by Raman spectroscopy and its correlations with combustion reactivity. Fuel. 2007; 86:2316–24.

[48] Matjie R, Bunt J, Stokes W, Bijzet H, Mphahlele K, Uwaoma R, et al. Interactions between kaolinite, organic matter, and potassium compounds at elevated temperatures during pyrolysis of caking coal and its density-separated fractions. Energy and Fuels. 2021; 35:13268–80.

[49] Megaritis A, Messenböck RC, Chatzakis IN, Dugwell DR, Kandiyoti R. High-pressure pyrolysis and CO_2-gasification of coal maceral concentrates: Conversions and char combustion reactivities. Fuel. 1999; 78:871–82.

[50] Shi L, Liu Q, Guo X, Wu W, Liu Z. Pyrolysis behaviour and bonding information of coal—A TGA study. Fuel Processing Technology. 2013; 108:125–32.

[51] Bai H, Mao N, Wang R, Li Z, Zhu M, Wang Q. Kinetic characteristics and reactive behaviours of HSW vitrinite coal pyrolysis: A comprehensive analysis based on TG-MS

experiments, kinetics models and ReaxFF MD simulations. Energy Reports. 2021; 7:1416–35.

[52] Wagner NJ. The characterisation of weathered discard coals and their behaviour during combustion. Fuel. 2008; 87:1687–97.

CHAPTER 4 CATALYTIC EFFECT OF REACTIVE EXTRANEOUS MINERAL COMPOSITE ON CHAR AND TAR DISTRIBUTION DURING PYROLYSIS OF HIGHVELD PARTIALLY OXIDISED FINE-COAL REJECT AND ITS BENEFICIATED RESIDUES.

K, Mphahlele, R. H. Matjie, J. R. Bunt

In this chapter, the effect of extraneous mineral matter was evaluated by adding composites of reactive oxides and hydroxide minerals ($Ca(OH)_2$-MgO-Fe_2O_3) to TEP fine-coal reject, its density-separated fractions, and demineralised and chemically fractionated residues. The blends were submitted to various conventional and advanced analytic techniques and subjected to pyrolysis conditions. The findings from the characterisation and pyrolysis experiments are reported in this manuscript. Comparisons of the yields and compositions of the chars and tars are also discussed.

This manuscript is published in the ACS Omega, 2023; volume 8, Pages 36479–36492. https://doi.org/10.1021/acsomega.3c05462

Abstract

In this study, a South African partially oxidised fine-coal reject sample, which is associated with human health and environmental problems, and which sustains high disposal expenses, was subjected to density-separation, chemical fractionation and demineralisation experiments to isolate and evaluate the mode of occurrence of mineral-matter effects on the fine-coal reject pyrolysis. A unique composite of two reactive oxides (i.e., MgO and Fe_2O_3) and a hydrated oxide (i.e., $Ca(OH)_2$) representing major extraneous coal-minerals were blended with fine-coal reject, demineralised fine-coal reject and its beneficiated samples, to evaluate the yields of pyrolytic products and activation energy by following a novel procedure. Different analyses determined the properties of FCR samples and their pyrolytic products. Results indicate that the reactive oxides and a hydrated oxide composite addition increased the average activation energy (332.0 to 476.5 kJ/mol) for the fine-coal reject due to the initial $Ca(OH)_2$ decomposition and Fe_2O_3 reduction that took place under pyrolysis conditions. The fine-coal reject mineral-rich sink fractions achieved the highest pyrolytic carbon conversion (char yield = 78.8%, tar yield=5.1%) compared to those of other samples evaluated (c.a. < 1.9 g/cm^3 float char yield = 87.3%, tar yield = 2.3%), due to higher proportions of calcite/dolomite/pyrite cleats and non-mineral inorganics present (Ca, Mg, Na and Fe), which catalysed the pyrolysis reactions. On the other hand, $CaCO_3$; $CaMg(CO_3)_2$ and metakaolinite formations in the char, derived from a blend of reactive oxides and a hydrated oxide composite and fine-coal reject, interfere with the pyrolysis reactions. In addition, deoxygenation reactions were impeded by oxygen present in the reactive oxides and a hydrated oxide composite. The potent catalytic effects of cleat minerals and the extraneous minerals associated with cracking heavy tars to lighter fractions provide opportunities to understand further how the mineral matter present in fine coal reject during utilisation in global pyrolysis occurs. This may reduce waste disposal costs, health hazards, air pollution, and fine-coal reject volumes, and augment feed coals.

Keywords: Pyrolysis, Fine-coal rejects, Mineral-matter, Extraneous mineral-matter, Activation energy, Inherent mineral-matter

4.1 Introduction

Mechanised mining, handling, and processing of South African (SA) run-of-mine (ROM) coals, i.e., raw coals which are extracted and transported directly from the collieries, produce more than 60 million tonnes of partially oxidised fine-coal rejects (FCRs) annually. Due to their fine nature, these are unsuitable for utilisation in some thermochemical processes [1–4]. As a result, about 1 billion tonnes of FCRs containing sulphur-bearing mineral matter (> 1%) have been disposed of in slurry ponds and stockpiles in the country. These FCRs contain ultra-fine particles (<250 µm) and coarser fine-coal particles (250 - 1000 µm), which are amenable to spontaneous combustion during storage. This results in SO_2, particulate matter (PM), nitrogen oxides (NOx), and CO_2 gaseous emissions during storage in stockpiles and slimes dams [1–4]. Literature [1–4] reports that FCRs have chemical properties similar to coals utilised in boilers and gasifiers (feed coals) but are classified as high-ash coals. The term “high-ash coals” refers to coals produced from SA collieries with a percentage ash yield (AY) greater than 30%. The similar chemical properties indicate a potential to utilise FCRs as a co-feed to thermochemical processes such as pyrolysis, gasification, and combustion without following the current waste disposal methods, which are associated with higher costs and health and environmental risks.

The SO_2 and NOx emissions associated with spontaneous combustion of FCR during storage are linked to the inflammation and irritation of the skin and respiratory system, while CO_2 is responsible for global warming [5]. Additionally, the inhalation of PM generated from conventional FCR storage causes chronic lung diseases (pneumoconiosis and tuberculosis) and silicosis (bronchitis symptoms and asthma) [6]. Chalcophile elements such as As, Se, Cd, Ni and Pd are associated with sulphide minerals present in coal [7]. These elements have been linked to carcinogenic and mutation effects [7]. The propensity to release these toxic elements depends on their mode of occurrence, which contributes to their transformation during pyrolysis and gasification processing.[8] According to Pone et al. [9], spontaneous combustion of South African coals releases toluene, benzene, xylene, bromomethane, iodomethane, trichloromethane, dichloromethane, chloromethane, methane, CO_2, CO, Hg, As, Pb, Zn, and Cu into the atmosphere. Benzene, toluene, and xylenes have carcinogenic properties.

Like feed-coal, FCR, which is generated during the preparation of Highveld feed coals comprises various types of mineral matter such as extraneous minerals (discrete mineral particles) and inherent mineral matter (sub-micron mineral cleats and non-mineral inorganics) and macerals of vitrinite, inertinite and liptinite groups, all of which undergo a chemical transformation during thermochemical treatment of coal [4,10,11]. For instance, either

extraneous fluxing minerals (such as dolomite, calcite, and pyrite) or inherent fluxing minerals, which are associated with either extraneous or inherent kaolinite in the coals, react with each other at elevated temperatures (>900 °C) to form molten solutions [11,12]. The heated rock fragments (mudstone, sandstone, and siltstone) present in the coals (roof and floor strata) are attached to the molten solution to form lump heterogeneous clinkers in commercial gasifiers or commercial boilers. The slow cooling of the molten material at lower temperatures (<340 °C) in the commercial gasifier bed allows for the formation of mullite ($Al_6Si_2O_{13}$) and anorthite ($CaAl_2Si_2O_8$) crystals and Ca/Fe/Mg-bearing aluminosilicate glasses are formed. These heterogeneous clinkers containing hard minerals (quartz and anorthite) cause deposition, blockage, erosion problems, and encapsulation of fine carbon particles, consequently lowering carbon conversion efficiencies during thermochemical processing [11].

Pyrolysis is a valuable technique for studying the reaction mechanisms involving mineral matter and carbon matrix (macerals) interaction to form precursors (such as tar, char, pyrolytic water and gas) during thermochemical processes. These reaction mechanisms form tars and gases via devotilisation, primary decomposition, secondary cracking, catalytic cracking, and isomerisation pathways upon drying, and char via carbonisation reactions.

Several researchers performed pyrolysis experiments to evaluate the catalytic effects of inherent and extraneous minerals of Chinese, Japanese, American and Middle Eastern coals [13–15]. Fu et al. [13] studied and compared the individual reactivity effects of potassium chloride (KCl), CaO and Fe_2O_3 during pyrolysis of Northern Chinese low-rank coal and reported the catalytic potency in order of Fe_2O_3> KCl > CaO. The three minerals resulted in three different reaction effects: KCl promoted tar yield, CaO promoted gas yield, and Fe_2O_3 promoted char yield. The results indicated that the mixing of potassium (ion-exchangeable), CaO and Fe2O3 reduced the bond energy of oxygenated functional groups and enhanced the pyrolysis reactions.

He et al. [14] used ion-exchangeable Na, Ca, and Mg as individual and binary mixtures with Fe to study their catalytic effects and synergies on demineralised and raw coals. Their results indicated a catalytic activity by Na, Ca, K and Mg due to the combination of these alkali and alkaline earth metals (AAEM) with the oxygenated functional groups. This facilitated the interaction of char and Fe. Furthermore, they developed an understanding that the behaviour and mode of occurrence of coal mineral matter is minimised by acid washing, and as a result, it is not well discerned during pyrolysis.

Understanding the behaviour of inherent and extraneous minerals and non-mineral inorganics in waste coal materials such as FCR could allow process operators/decision makers to take

advantage of coal mineral-matter properties to improve process efficiencies instead of using specialised catalysts. To the authors' best knowledge [11-15], there are only limited reports of the effects of ternary reactive mineral composites, representing inherent or derivatives of inherent coal cleat minerals and non-mineral inorganics present in partially oxidised coal fine waste, on product distribution during pyrolysis of this FCR.

For this reason, an in-depth understanding of the catalytic effects of Ca, Mg and Fe associated with the mode of occurrence of the mineral matter in FCR under thermochemical processing conditions is a necessity for efficient and environmentally feasible co-utilisation of these partially oxidised coal-fine wastes in global thermochemical processes. As a result, this study aims to close the gap by evaluating the effects of the mode of occurrence of coal mineral matter present in FCR on the distribution and composition of pyrolytic products. The interaction of inherent and extraneous coal mineral matter with an extraneous model composite of two commercial reactive oxides (MgO and Fe_2O_3) and a hydroxide ($Ca(OH)_2$) (ROSH) present in extraneous minerals, with an extension to their catalytic or hindrance effects, was evaluated during the pyrolysis of FCR samples.

Generally, catalysts have been applied widely in chemical production to lower operating temperatures and pressures and to facilitate product selectivity [15]. In this study, the selected ROSH only served to simulate extraneous minerals with catalytic effects to understand their nature and behaviour during the FCR pyrolysis. Furthermore, the addition of ROSH composites, which are not co-feedstock of this proposed pyrolysis to the FCR samples, may produce novel insights and perspectives that can considerably enhance understanding of the mode of occurrence of extraneous minerals on char and tar yields during the FCR pyrolysis step. Density separation, demineralisation and chemical fractionation procedures served only as techniques (they are not steps of the proposed low-temperature pyrolysis) to isolate different modes of occurrences of mineral matter and carbon matrices of FCR and to discern their effects in pyrolysis reactions. The Fischer assay experiments, mineralogical (X-ray diffraction (XRD)) and chemical (proximate, ultimate, X-ray fluorescence (XRF), Brunauer, Emmett and Teller (BET) surface area, and gas chromatography-mass spectrometry (GC/MS)) analyses, along with activation energy analysis were adopted to achieve the objectives of this novel study.

4.2 Materials and Methods

4.2.1 FCR Sampling and Preparation

The FCR sample used in this study was collected from a South African thermal export plant (TEP) disposal site situated in the Highveld coalfields of the Mpumalanga Province of South Africa. A representative sample (250 kg) of the SA Highveld FCR was collected following the guidelines provided by the International Organisation for Standardisation (ISO), ISO 18283 and ISO 13909-4 standard methods for treatment, characterisation and experiments.

4.2.2 Density Separation

A representative portion of the sample (25 kg) was submitted to the General Society of Surveillance (SGS) Laboratories (PTY) Ltd, South Africa, for the density separation procedure to produce three density-separated fractions (Fl1.5 = <1.5 g/cm^3 float; Fl1.9 = <1.9 g/cm^3 float and SI1.9 = >1.9 g/cm^3 sink) for this investigation following procedures described in the ISO 7936 standard method. Mixtures of tetrabromoethane, benzene and tetrachloroethylene, with respective densities of 2.95, 0.879 and 1.62 g/cm^3, were used to produce 1.5 and 1.9 g/cm^3 floats and sink fractions as indicated by Rautenbach et al.[4]

4.2.3 Demineralisation Experiments

A three-step demineralisation approach [16] using 10 mol/dm^3 (M) hydrochloric acid (HCl) (37%, Sigma Aldrich) and 22 M hydrofluoric acid (HF) (45%, Minema chemicals) was followed for 24 hrs to dissolve almost all of mineral-matter from the FCR sample as described in Annexure D. The acid-treated sample, without extraneous minerals and low proportions of inherent minerals, was labelled FCR D for experiments and analyses.

4.2.4 Chemical Fractionation Procedure

The chemical fractionation procedure in [17] was employed to leach non-mineral inorganics in FCR. The detailed chemical fractionation procedure is described in Annexure D. The leached FCR was labelled FCR CF, and the leachate samples were submitted for XRD, XRF, and ICP analyses. The FCR CF was evaluated in the pyrolysis experiments to investigate the catalytic effect of the mode of occurrence of mineral-matter during pyrolysis.

4.2.5 Preparation of Blends of Coal and ROSH Composites

The ROSH (Fe_2O_3, MgO and $Ca(OH)_2$) (98, 99 and 70% respectively, CC Imelmann cc) composite made up of reactive oxides and hydrated oxide minerals of extraneous minerals

(EMs) typically present in SA feed coals was prepared by combining these oxides and hydroxide of EMs at a mass ratio of 1:0.7:1 to increase proportions of reactive oxides and hydrated oxide minerals and Ca, Mg and Fe concentrations in these blends for the unique pyrolysis experiments. The composite was mixed with either FCR or FCR D separately to prepare two (2) blends with 18wt. % ROSH and 82wt. % of either FCR sample or FCR D. This ratio was chosen to ensure the saturation of mineral-matter content in FCR D and FCR samples. Each blend was ground for five minutes in a rod mill to prepare a homogenised coal sample, and ROSH blend sample with improved particle-to-particle contact. Before experiments and characterisation, the homogenised samples were stored in an airtight container under nitrogen and labelled FCR+ROSH and FCR D+ROSH.

4.2.6 Pyrolysis Experiments

The pyrolysis experiments were carried out at an average internal temperature of 500 °C and an internal heating rate of 5 °C/min using the double retort Fischer assay rig as reported by Roets et al. [18], the schematic diagram of which is presented in Figure 4-1.

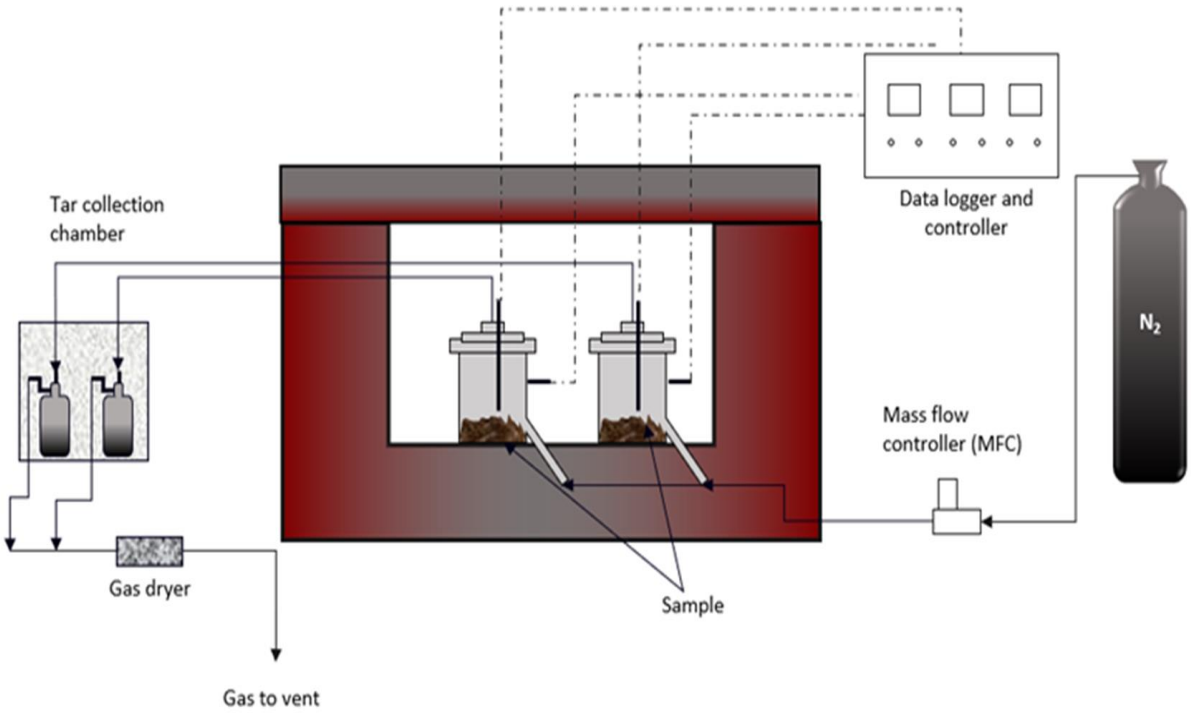

Figure 4-1: A schematic of the modified Fischer assay experimental rig used to conduct the pyrolysis experiments [18].

A previous study by Roets et al. [18] indicated that both char and tar yields for Highveld feed coal and its density-separated fractions decrease as the final pyrolysis temperatures increase from 450 °C to 900 °C [18]. On the other hand, Liu et al. [19] reported that the maximum tar yield was produced at 600 °C. Considering the insights from these two studies and the fact that the initial transformation and decomposition of coal minerals and macerals commence at temperatures above 450 °C under oxidising and nitrogen conditions, a temperature of 500 °C and time of 3 hrs were selected for the current study.

A sample of 45 g ±0.5 g was placed in a retort, allowing a 3 cm freeboard area. The retort was tightened with bolts, to which copper grease was applied, and carefully placed in the oven. In the initial stage of the experiments, nitrogen baseline 5.0 (99.995%, AFROX (PTY) Ltd) flowing at 2 NL/hr was used to purge oxygen and create an inert atmosphere. After 10 mins, the flow of N_2 was stopped, and heating was initiated. The volatiles that evolved during the process were bubbled through a toluene (99%, CC Imelmann cc) tar trap and gas washing system submerged in an ice bath. The gases produced were vented and not captured. Using a Dean-Stark distillation setup, the gas-liquor (condensate) fraction was separated from the tar and toluene mixture. The cooled tar-toluene mixture was subjected to vacuum distillation using a Buchi R100 rotor vapour setup equipped with a Buchi V100 vacuum pump at 55 °C and 75 mbar until no visible condensation of toluene was observed in the collection flask. The tar, gas-liquor and char yields were determined based on their weights and corrected using Equations 1-4. The gas yields were determined by difference according to the ISO 647 method. The pyrolysis product distribution of the various fractions (char, tar, gas, and pyrolytic water) was evaluated based on their weight. It was important to present the yields on an ash-free basis to correct for the contribution of mineral-matter to char and gas-liquor yields.

$$Y_{char} = \frac{M_{char} \times (1 - A_{char})}{M_{sample} \times (1 - A_{sample})} x100\% \qquad (1)$$

$$Y_{tar} = \frac{M_{tar}}{M_{sample} \times (1 - A_{sample})} x100\% \qquad (2)$$

$$Y_{gas\ liquor} = \frac{M_{gas\ liqour}}{M_{sample} \times (1 - A_{sample})} x100\% \qquad (3)$$

$$Y_{gas} = 100\% - Y_{char} - Y_{tar} \qquad (4)$$

In these equations, “Y” refers to yields of either char, tar, gas liquour or gas in percentage, “A” refers to the dimensionless fraction of ash yields for char and sample, and “M” to the mass of either sample, char, tar or gas liquor in grams.

After the initial calculations, the values were normalised on a gas-liquor free basis. The samples were rotated between the retorts for all repeated experiments to minimise noise and the effects of uncontrolled variables. The experiments were repeated at least three times with a 5% experimental error. The weighted averages of these samples were calculated.

4.2.7 Proximate, Calorific Value (CV), Ultimate, XRF, XRD, BET Surface Area, GC/MS, and Activation Energy Analyses

The pulverised FCR, its beneficiated samples, FCR D+ROSH and FCR+ROSH blends, and their corresponding chars (<75 µm) were submitted to the laboratories of Bureau Veritas Testing and Inspections South Africa (Pty) Ltd. for proximate, ultimate and sulphur analyses distribution respectively using the standard coal analyses standards [4].

The XRF analysis (ASTM D4326-13) [20] was followed to determine the proportions of inorganic elements contained in the ashes of the FCR, FCR D, FCR CF, FI1.5, F1.9 and SI1.9 samples and FCR D+ROSH and FCR+ROSH together with their corresponding chars.

The above pulverised samples, together with their prepared blends and their derived chars (<75 µm), were analysed by XRD using mineralogical methods, which were developed and described by Speakman [21] and Rietveld [22].

The BET surface area analysis [23] of either prepared coal samples or their corresponding char samples was performed using the North-West University (NWU) Micrometrics ASAP 2020 BET instrument.

The NWU Agilent 7890 GC-MSD gas chromatograph (GC) coupled with a 5975 Triple Axis MSD detector was used to elute, detect and identify chemical components in the pyrolytic tars [16].

The thermogravimetric analyser (SDT Q600 TGA) at NWU was used to perform analytical pyrolysis of FCR, FCR CF, FCR D, FCR D +ROSH and FCR +ROSH samples at three heating rates (10, 15 and 20°C/min). A detailed description of the activation energy analysis technique can be found elsewhere [24,25]. Equation 5 is the simplified Starink [25] technique derived from the Arrhenius equation.

$$ln\left[\frac{\beta}{T^{1.8}{}_{x}}\right] = C - 1.0037\left[\frac{E_a}{RT_x}\right] \quad (5)$$

In this equation β is the heating rate, C is the constant or x intercept, E_a is the apparent activation energy, R is the universal gas constant, and T_x is the temperature at conversion (x).

A linear plot of $ln\left[\frac{\beta}{T^{1.8}{}_{x}}\right]$ versus $\frac{1}{T}$ with $-1.0037\left[\frac{E_a}{R}\right]$ as the gradient is obtained from analytical data to estimate the E_a values.

4.3 Results and Discussion

4.3.1 Coal and Char Compositions

Proximate analysis results for the FCR, its beneficiated fractions, FCR D+ROSH and FCR+ROSH blends, and their corresponding chars are reported on an air-dried basis in Table 4-1. As expected, these results indicate a decrease in the ash yield percentage for the FCR D and FCR CF samples. Over 95 wt. % of mineral-matter removal was achieved by the demineralisation experiments, which changed the overall coal structure of FCR. On the other hand, the chemical fractionation procedure achieved only 13 wt. % mineral-matter removal in FCR. These mineral-matter removal efficiencies are consistent with those of SA Highveld coals reported by Raghoo [17]. The HF and HCl solution used in this study could remove almost all the mineral-matter excluding inherent submicron minerals, organic sulphur and carboxylate salts (organically associated inorganic elements) [10,17] accounting for 5 wt.%. The general formula of carboxylate salts is M(RCOO)n, where M represents cations such as Mg^{+}, Ca^{2+}, Na^{+} and NH_4^{+}.

After pyrolysis at 500 °C, the chars' IM and VM contents were reduced due to evaporation and devolatilisation mechanisms, respectively. On the other hand, the ash yield percent and fixed carbon contents were higher for all char samples, which is typical for SA feed coals in the pyrolysis zone of the fixed-bed gasifier (T= 500 °C).[16,17]. However, an anomaly is seen regarding the FC of the chars of the FCR CF and ROSH blends, which indicates a possible enhancement of FC conversion by the ROSH composite.

Ultimate results Table 4-1 indicates that the organic composition of macerals in the FCR and FCR D samples remains unchanged, which could suggest minimal FCR oxidation during demineralisation. In contrast, the FCR CF sample comprised slightly less carbon and higher nitrogen and oxygen percentages. The variations may be the result of slight oxidation as well as nitrogen cross-linkage by ammonium acetate during the chemical fractionation experiments. As expected, the chars exhibited decreased oxygen (O) and hydrogen (H) percentages and increased carbon and nitrogen percentages due to the pyrolysis reactions. These results are consistent with those reported by Roets et al. [16] for coal demineralisation and low-temperature pyrolytic chars after chemical fractionation of SA Highveld coals [16].

The total sulphur (TS) content increased slightly with an increase in ash yield percentage of the density-separated fractions, while it remained constant for FCR D and decreased slightly for FCR CF, indicating that the sulphur in the FCR residue produced during the chemical fractionation experiments is associated with extraneous pyrite and organic carbon matrix (organic sulphur). With the addition of ROSH, TS remained constant, which may be attributed to S capturing by $Ca(OH)_2$ to form anhydrite ($CaSO_4$), bassanite ($CaSO_4.½H_2O$) and gypsum ($CaSO_4.2H_2O$) [4].

The higher percentage ash yield values reported for the FCR, Fl1.9, Sl1.9 and FCR CF samples indicated by the proximate results could imply the presence of AAEM and metallic elements (Na, K, Ca, Mg, and Fe) associated with the cleat minerals (dolomite, calcite, pyrite), extraneous minerals (dolomite, calcite, pyrite), inherent minerals (dolomite, calcite and pyrite) and non-mineral inorganics, which could catalyse the pyrolysis reactions to yield higher carbon conversion during pyrolysis. Also, the higher proportions of H and O could imply higher carbon conversion during pyrolysis due to the presence of sufficient H for retarding free radicals and oxidation of char to form carbon gases.

Table 4-1: Proximate and ultimate results FCR, beneficiated fractions, acid-washed residues, ROSH blends and their corresponding chars.

Parameter	Proximate results (wt.% adb)				Ultimate results (wt.% daf)				
	IM	AY	VM	FC[a]	C	H	N	O[a]	TS
FCR	4.2	28.7	22.0	45.1	78.7	4.5	1.9	13.7	1.2
FCR[C]	1.1	33.3	13.5	52.2	84.8	3.2	2.3	8.7	1.1
FCR+ROSH	3.7	40.6	22.1	33.6	76.3	4.7	2.0	16.0	1.1
FCR+ROSH[C]	1.0	44.8	15.3	38.9	85.2	3.0	2.0	8.7	1.1
Fl 1.5	5.8	19.0	28.8	46.4	74.8	4.5	1.9	17.8	1.1
Fl 1.5[C]	3.7	23.2	13.8	59.3	83.6	3.1	2.2	10.4	0.7
Fl 1.9	7.0	26.2	24.0	42.8	74.1	4.0	1.9	18.7	1.2
Fl 1.9[C]	4.5	30.3	14.3	50.9	83.0	3.1	2.0	11.0	0.9
Sl 1.9	7.6	31.9	23.8	36.7	72.3	3.6	1.8	20.9	1.3
Sl 1.9[C]	4.4	32.3	14.3	49.0	83.3	3.2	2.1	10.6	0.9
FCR D	3.3	1.3	28.8	66.6	78.7	4.4	2.1	13.6	1.2
FCR D[C]	2.0	1.8	13.2	83.1	86.5	3.0	2.3	7.5	0.7
FCR D+ROSH	3.5	20.1	26.2	50.2	80.8	4.6	2.1	11.6	0.9

FCR D+ROSH[C]	1.7	22.5	14.6	61.3	86.8	2.8	2.2	7.2	0.9
FCR CF	2.8	24.8	23.5	48.9	77.6	4.6	2.2	14.5	1.1
FCR CF[C]	1.6	15.1	13.2	70.1	87.8	3.2	2.3	5.9	0.8

Daf – dry ash-free basis, adb – air-dried basis, IM – Inherent moisture, AY – Ash yield, VM – Volatile matter, FC – Fixed carbon, TS – Total sulphur, "[a]" – determined by difference, "[C]" – char

4.3.2 XRF Analysis

Table 4-2 presents the results of the XRF analysis for the ashes derived from the coal samples with and without the addition of ROSH composite, along with their corresponding chars. The ashes of these samples were comprised mainly of SiO_2, Al_2O_3, CaO, SO_3, Fe_2O_3 and MgO with minor percentages of TiO_2, K_2O, Na_2O and P_2O_5. This is consistent with the ash composition of SA feed coals to commercial gasifiers [26, 27]. Mphahlele et al. [28] found that higher concentrations of trace elements (Co, Zn, As, Rb, Sr, Zr, Ag, Cd, Ba, In and Sn) and rare earth element (Y) are concentrated in the density-separated fractions of the FCR samples as compared to the typical concentrations for SA Highveld ROM coals as reported by Wagner and Hlatshwayo [29]. This could be associated with health and environmental issues during the storage of FCR samples in stockpiles and slime dams.

According to Hower et al. [30], coal fines contain higher proportions of toxic trace elements (As, Cd, Cu, Hg, Mo, Pb, Sb, Zn, Cr, Ni, Gd) which are associated with nano-sulphide minerals. Also, these fines contain higher proportions of rare earth elements, which are linked to nano monazite, (Ce, La, Th, Nd, Y) PO_4 and nano Xenotime, (Y, Er) PO_4 [30]. Significant concentrations of trace elements and rare earth elements present in the coal fine wastes negatively impact human health and the environment. They should be recovered under suitable operating conditions from coal ash using hydrometallurgical methods before storage, disposal or utilisation in thermal processes.

A decrease in significant inorganic elements percentages in the ash of the FCR D sample (except for Fe_2O_3, TiO_2 and Na_2O) is associated with the dissolution of mineral-matter by HCl and HF, while the decrease in CaO and MgO in the FCR CF sample indicates that dolomite and calcite associated with these inorganic elements exist predominantly in coals in acid soluble form, as ion-exchangeable cation, chelates and cleat minerals [17].

As expected, variations in the composition of the ashes of coal and the ROSH composite blend samples illustrate higher proportions of CaO, Fe_2O_3 and MgO due to the addition of $Ca(OH)_2$, Fe_2O_3 and MgO to the FCR samples. In all instances, higher percentages of sulphur as SO_3

have been reported for samples containing ROSH and FCR blends. This emphasises the occurrence of sulphur encapsulation mechanisms by calcium oxide (CaO) from the dehydroxylation of $Ca(OH)_2$ and the interaction of organic sulphur, pyrite and organic Ca to form $CaSO_4$ [4]. Furthermore, the occurrence of the sulphur encapsulation by the $Ca(OH)_2$ added to the FCR samples could interfere with pyrolysis reactions and subsequently reduce the formation of pyrolytic products.

The presence of higher proportions of Ca, Mg and Fe elements in the ashes of all the FCR samples, excluding the FCR blends and the FCR CF sample, implies that these inorganic elements could potentially catalyse the pyrolysis reactions, which are linked to the dolomite, calcite and pyrite cleats inherently present in these samples.

Table 4-2: Chemical composition for FCR, beneficiated fractions, acid-washed residues and ROSH blends along with their corresponding chars.

Element (LOI free wt. %)	SiO_2	Al_2O_3	CaO	Fe_2O_3	MgO	TiO_2	K_2O	Na_2O	P_2O_5	SO_3
FCR	52.0	23.7	9.8	3.5	2.1	1.5	1.0	0.7	0.7	4.4
FCR^C	49.0	25.9	8.0	5.9	2.5	1.4	1.0	0.6	0.6	4.1
FCR+ROSH	31.6	16.1	15.1	15.9	14.4	0.9	0.7	0.4	0.4	3.9
FCR+ROSH^C	32.1	16.7	15.3	16.0	13.4	0.9	0.7	0.4	0.4	3.6
Fl 1.5	48.6	28.5	6.9	4.2	2.0	1.6	1.1	0.9	0.9	4.3
Fl 1.5^C	47.0	28.0	6.9	6.8	2.0	1.6	1.0	0.7	0.9	4.1
Fl 1.9	50.2	27.6	7.3	3.9	2.0	1.4	1.1	0.8	0.7	4.1
Fl 1.9^C	49.6	27.8	7.2	5.8	1.9	1.4	1.0	0.7	0.7	2.9
SI1.9	51.2	25.2	8.2	4.8	1.9	1.3	1.1	0.6	0.5	4.3
Sl 1.9^C	50.1	27.3	7.4	6.7	2.1	1.4	1.1	0.7	0.6	1.7
FCR D	6.3	10.1	6.2	50.4	1.6	10.0	0.1	5.0	0.4	9.9
FCR D+ROSH	4.6	1.3	23.2	31.6	29.3	0.6	0.0	0.1	0.1	8.6
FCR D+ROSH^C	5.1	1.6	22.9	32.7	28.1	0.6	0.0	dl	0.1	8.3
FCR CF	58.6	31.9	0.4	4.1	0.4	1.7	1.2	0.1	0.5	0.2
FCR CF^C	54.9	30.6	0.8	7.9	0.6	2.1	1.2	0.1	0.5	0.2

dl- below the detection limit, "^{C}" – char

4.3.3 XRD Analysis

The proportions of major and minor minerals of the FCR, treated FCR coal samples, FCR+ROSH and FCR D+ROSH, along with their corresponding chars, are presented in Figure 4-2 and Table 4-3. All samples without ROSH addition are primarily amorphous except for the SI1.9 and FCR CF samples, which showed a 40 wt.% amorphous content indicating their richness in crystalline minerals.

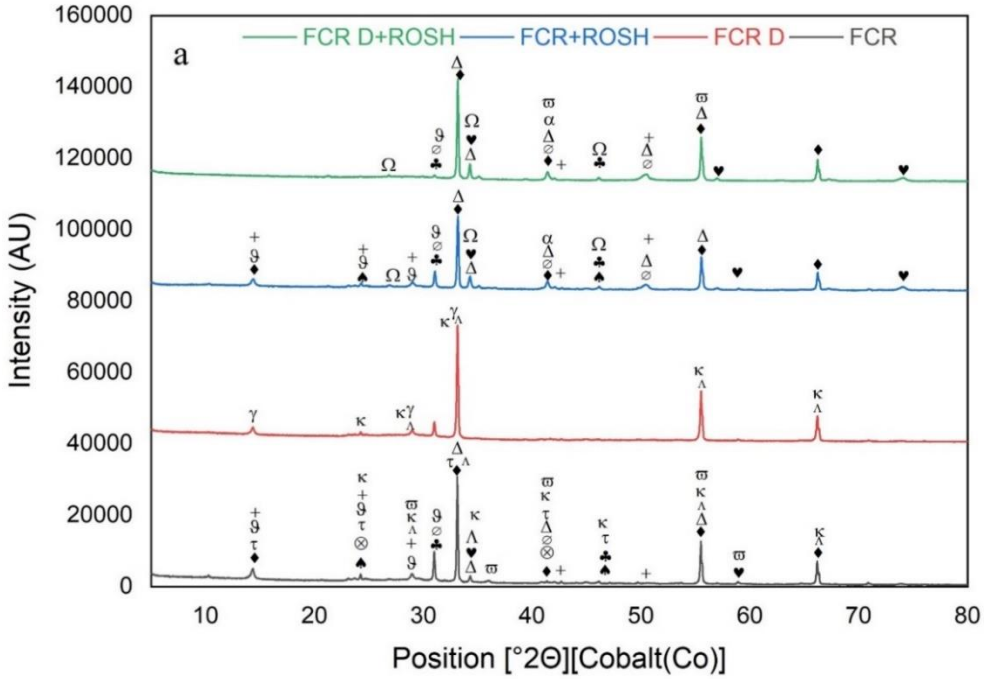

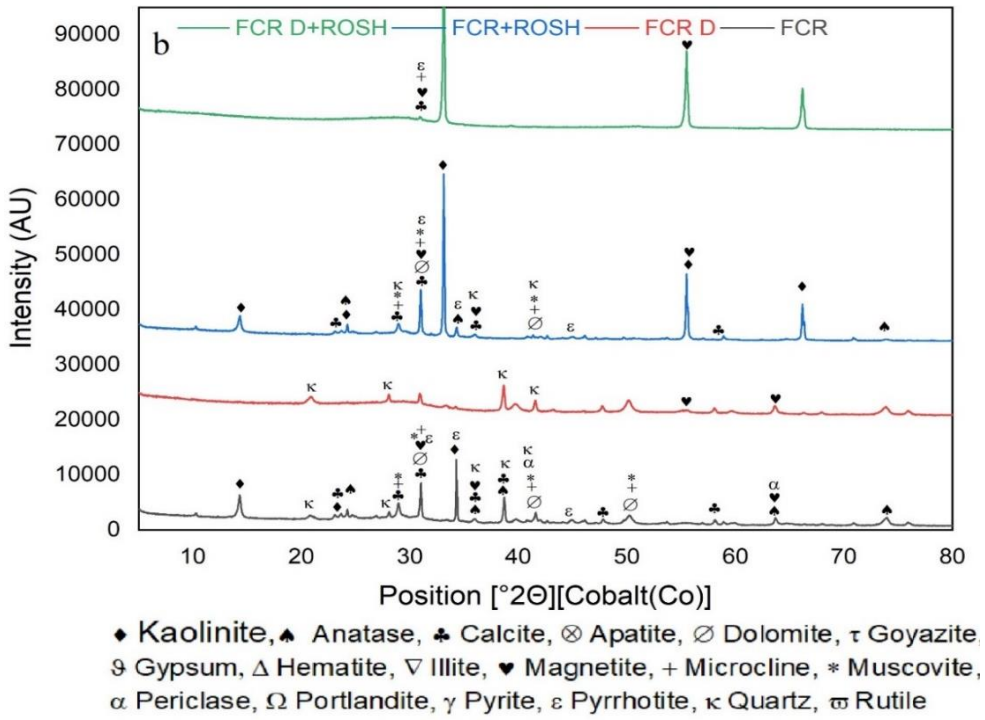

Figure 4-2: Diffractograms of a.) FCR and demineralised FCR along with their ROSH blends and b.) the chars of FCR and demineralised FCR along with their ROSH blends.

The XRD analysis for the FCR D indicates a 98% amorphous content due to the dissolution of all mineral-matter excluding inherent submicron pyrite, organic sulphur and carboxylate salts [17]. XRD results indicate that the FCR, Fl1.5, Fl1.9, Sl1.9, FCR CF and FCR D samples contain 39.3%, 13.4%, 28.9%, 59.7%, 38.7% and 1.8% mineral-matter (MM) contents respectively (Table 3). Also, the XRD detected traces of anatase (TiO_2), apatite ($Ca_5(PO_4)^{3+}$(F,Cl, or OH)), goyazite ($SrAl_3(PO_4)(PO_3OH)(OH)_6$), microcline ($KAlSi_3O_8$), rutile ($TiO_2$) and, muscovite $(KF)_2(Al_2O_3)_3(SiO_2)_6(H_2O)$ in the case of FCR CF. These results are consistent with those of SA feed coals and their density-separated fractions reported by Rautenbach et al. [14]. Raman studies performed on FCR in the previous study by Mphahlele et al. [24] confirmed the presence of minerals detected by XRD in lower proportions.

Higher proportions of MM contents in the Sl1.9 and FCR samples are associated with higher total proportions of fluxing cleat minerals (calcite, dolomite and pyrite) (>7%) compared to those of other beneficiated FCR samples. These higher cleat mineral contents are possibly responsible for the catalytic effect of pyrolysis reactions to produce higher carbon conversion values. On the other hand, the lowest or zero fluxing cleat mineral contents contained in the Fl1.5, FCR CF and FCR D samples suggest that these beneficiated samples may achieve lower carbon conversion values during pyrolysis.

Table 4-3: Mineral composition for FCR, beneficiated fractions, acid-washed residues, ROSH blends, and corresponding chars.

Mineral (wt.%)	Kao	Ana	Ap	Cal	Dol	Goy	Gyp	Hem	Ill	Mag	Mic	Mus	Per	Por	Pyr	Pyrr	Qua	Rut	Amo	MM	Total
FCR	21.5	0.1	0.1	3.0	4.3	0.1	0.3	0.4	1.0	0.0	0.1	-	-	-	0.6	-	7.7	0.1	60.7	39.3	100.0
FCR^{C}	13.1	0.2	-	1.9	1.9	-	-	-	-	0.4	0.6	1.1	0.1	-	-	0.1	9.8	0.0	71.0	29.2	100.2
FCR+ROSH	22.4	0.2	0.0	2.7	3.8	0.0	0.6	9.7	0.5	0.2	0.4	-	7.7	3.0	0.0	-	8.2	-	40.6	59.4	100.0
FCR+ROSH^{C}	11.5	0.2	-	5.8	0.8	-	-	-	-	3.8	0.3	1.2	5.0	-	-	0.3	7.1	0.0	64.1	36	100.1
Fl1.5	8.3	0.0	0.0	0.4	0.3	0.0	0.2	0.0	0.9	0.1	0.2	-	-	-	0.2	-	2.8	-	86.6	13.4	100.0
Fl1.5^{C}	7.9	0.2	-	0.0	0.0	-	-	-	-	0.2	0.1	0.9	0.0	-	-	0.1	5.3	0.1	85.2	14.8	100.0
Fl1.9	14.8	0.2	0	1.7	1.0	0.1	0.5	0.1	2.6	0.4	0.5	-	-	-	0.3	-	6.5	0.2	71.1	28.9	100.0
Fl.9^{C}	8.5	0.3	-	0.0	0.2	-	-	-	-	0.3	0.6	1.1	0.2	-	-	0.0	7.0	0.0	81.8	18.2	100.0
Sl1.9	27.3	0.2	0	4.8	1.7	0.2	1.1	0.2	5.5	0.9	1.0	-	-	-	0.9	-	15.6	0.3	40.3	59.7	100.0
Sl1.9^{C}	11.4	0.2	-	0.1	0.2	-	-	-	-	0.2	0.5	1.2	0	-	-	0.2	7.4	0.1	78.5	21.5	100.0
FCRD	-	-	-	-	-	-	-	-	-	-	-	-	-	-	1.8	-	-	-	98.2	1.8	100.0
FCRD^{C}	0	0	0	0	0	-	-	-	-	0.1	0	0	0.2	-	-	0.2	0.5	0	99	1	100.0
FCRD+ROSH	1.3	0	0	1.1	-	0	0.2	10.4	0.7	0	0.8	-	9.4	5.1	-	-	2.4	0.1	68.5	31.5	100.0
FCR	0	0	0	5.4	0	-	-	-	-	3.4	0.1	0	4.8	-	-	0.4	0.8	0	85.1	14.9	100.0
FCRCF	26.2	-	-	-	-	-	-	0.1	-	1.2	0.6	1.7	-	-	-	-	8.9	-	61.3	38.7	100.0
FCRCF^{C}	7.4	0.1	-	0	0	-	-	-	-	0.2	0	0	0.1	-	-	0.1	4.1	0	88	12	100.0

Kao-Kaolinite, Ana-anatase, Ap- apatite, Cal-calcite, Dol-dolomite, Goy-Goyazite, Gyp-gypsum, Hem-hematite, Ill-Illite, Mag-Magnetite, Mic-microcline, Mus-muscovite, Per-periclase, Por-portlandite, Pyr-pyrite, Pyrr-pyrrhotite, Qua-quartz, Rut-rutile, Amo-amorphous, "- "- not detected, ^{C}-char

Based on the XRD results, these samples are made up mainly of kaolinite ($Al_2Si_2O_5(OH)_4$) with lesser proportions of quartz (SiO_2) followed by dolomite and calcite and minor proportions of pyrite and illite ($(K,H_3O)(Al,Mg,Fe)_2(Si,Al)_4O_{10}[(OH)_2,(H_2O)]$). The presence of traces of hematite (Fe_2O_3), magnetite, anhydrite ($CaSO_4$) and gypsum ($CaSO_4.2H_2O$) in the FCR sample and its density-separated fractions are indicators that the oxidation of the FCR sample occurred as a result of the oxidation of pyrite [26] and interaction of inherent pyrite, organic sulphur and organic calcium [4] during their storage at the Highveld fine coal disposal site. These XRD results for the FCR sample and its density-separated fractions are consistent with those of SA Highveld coals [11, 16, and 17]. In the case of FCR D and FCR CF, similar trends of minerals in the demineralised and chemically fractionated samples are reported in past studies by Raghoo [17].

Calcite, dolomite, and pyrite in the FCR sample are linked to the cleats and could release Ca, Mg and Fe to catalyse the pyrolysis reactions and achieve higher pyrolytic product efficiencies. According to Rautenbach et al. [12], the >1.9 g/cm^3 sink fraction is characterised by the highest proportions of calcite, dolomite, siderite, and pyrite cleats and zero % or lowest proportion of inherent minerals compared to feed-coal and its density separated fractions. This could imply that the SI1.9 fraction evaluated in this study may achieve the highest carbon conversion value during pyrolysis based on its very low carbon content.

XRD results for the prepared chars suggest different reaction pathways for partial mineral transformation for samples both with and without ROSH composite addition. As expected, all char samples reported an increase in the percentage of amorphous materials, except for the char derived from the Fl1.5 beneficiated sample, which contains 100% inherent minerals [12]. The increase in amorphous material is associated with the partial transformation of kaolinite by losing water of hydration to form metakaolinite at 500 °C [31, 32]. While this is the case for every sample, this transformation of kaolinite is minimal for the Fl1.5 samples, which, combined with the loss of volatiles, is responsible for a decrease in the percentage of amorphous materials.

4.3.4 Chemical Fractionation Procedure

The percentage of leachable elements in FCR by de-ionised water, 1M ammonium acetate ($NH_4CH_3CO_2$) and 1M Hydrochloric acid (HCl) solutions are presented in Table 4-4. Water leaching removed the Ca, Mg, Na, K and S ions dissolved in pore waters within the FCR structure. The inorganic elements associated with salts of carboxylic acids removed by 1M $NH_4CH_3CO_2$ solution were primarily Ca with a lesser removal percentage for Na followed by Mn, Mg, K and S. 1M HCl solution leached primarily Fe, P, Mn and lesser proportions of Mg,

Ca, Al, Na. K, S and Si. The latter elements are associated with minerals and mineraloids in FCR, such as carbonates, hydroxides, oxides, organically associated inorganic elements, and submicron clays contaminated with Ti and Mn [4, 17].

The largest proportion of Na ions (ca.60%) in FCR exists as cations dissolved in pore waters. This is followed by Na, which is associated with salts of carboxylic acids, submicron clay and carbonates. Fe (ca.90%) is predominantly associated with sub-micron pyrite in the FCR sample. The absence of Fe in the water-leaching liquor illustrates minimal oxidation of pyrite during storage of FCR in slurry dams. These findings agree with Raghoo [17], who reported on the quality of SA feed coals for gasifiers. The carboxylic acid salts, submicron minerals and ions dissolved in pore waters, especially Fe and Ca, are linked with bond cleavage reactions during pyrolysis to form various aliphatic and aromatic structures [33]. As a result, their absence in the FCR CF sample could lower carbon conversion.

Table 4-4: Leachability of inorganic elements in FCR by de-ionised water, 1 M $NH_4CH_3CO_2$ and 1 M HCl Solutions.

Element	Leach liquor composition			%Leachable element		
	de-ionised water (mg/L)	1M $NH_4CH_3CO_2$ (mg/L)	1 M HCl (mg/L)	de-ionised water (wt. %)	1 M $NH_4CH_3CO_2$ (wt. %)	1 M HCl (wt. %)
Al	0.0	0.0	648.4	0.0	0.0	10.3
Ca	231.1	2726.1	2934.4	3.3	39.0	42.0
Fe	0.0	0.0	1119.9	0.0	0.0	91.0
K	7.6	15.1	13.4	1.9	3.7	3.3
Mg	39.0	139.1	605.2	3.1	10.9	47.4
Mn	0.0	6.9	30.3	0.0	14.8	65.1
Na	222.7	116.4	33.4	56.2	29.4	8.4
P	0.0	0.0	126.2	0.0	0.0	87.4
S	429.9	36.3	19.1	24.6	2.1	1.1
Si	4.9	4.5	181.3	0.0	0.0	0.7
Ti	0.0	0.0	1.0	0.0	0.0	0.1

BET Surface Area Analysis

CO_2 and N_2 surface area results of the FCR sample, the beneficiated fractions, and their corresponding chars and chars of FCR +ROSH and FCR D+ROSH are presented in Table

4-5. Samples with a high % ash yield reported the lowest mesopore structures due to the higher proportions of low porosity minerals [34]. An increase in the CO_2 and N_2 surface area of all samples illustrates the development of pores and change in the pore structures during pyrolysis due to the evolution of volatile compounds. However, the ROSH chars yielded a reduced surface area, possibly due to the dilution by Fe_2O_3, which has a low surface area. Shivakumara et al. [35] found the surface area of α- Fe_2O_3 to be less than 1m^2/g. The largest CO_2 surface area for FCR D followed by FCR CF could be attributed to the absence of minerals such as quartz. However, the N_2 surface area for the acid-washed samples was the lowest, indicating collapsing of mesopores during pyrolysis. It can be seen that the ash yield affects the structural properties of the coal and its chars. The fine nature of the added commercial MgO, Fe_2O_3 and $Ca(OH)_2$) may contribute significantly to the surface area and mesopore structures. This corresponds with the increased mesopore surface area obtained for the ROSH char samples.

Table 4-5: BET Surface area results for FCR, beneficiated fractions, acid-washed residues and ROSH blends and their corresponding chars.

Sample	CO_2 (m^2/g)	N_2 (m^2/g)
FCR	76.6	5.1
FCR^C	91.4	10.1
FCR+ROSH^C	72.7	12.0
Fl1.5	73.4	3.6
Fl1.5^C	93.3	3.3
Fl1.9	63.3	4.5
Fl1.9^C	85.6	3.9
Sl1.9	54.2	4.9
Sl1.9^C	80.9	5.8
FCRD^C	141.2	2.7
FCRD+ROSH^C	112.3	13.6
FCRCF^C	119.4	3.4

4.3.5 Pyrolytic Product Yields

4.3.5.1 Char Yield

The char yields obtained for FCR, FCR CF and FCR D samples reported in Figure 4-3 are presented on a dry ash-free basis and indicate the lowest carbon conversion (high char yield)

for the FCR CF sample due to the partial dissolution of calcite, dolomite, and pyrite cleats, non-mineral inorganics and extraneous and inherent fluxing minerals as well as carbonates and sulphate formation as the artefacts. ICP analysis of the leachates confirms the dissolution of sulphur, calcium, iron, magnesium, and potassium species by the CF procedure. These have been associated with enhancements of several carbon conversion reaction mechanisms, such as depolymerisation and dehydroxylation reactions, particularly those of intimate or organic association with the carbon matrix [36]. The presence of higher proportions of calcite, dolomite, pyrite cleats, and Ca/Mg carboxylates in the FCR sample catalysed pyrolysis reactions and may result in a higher carbon conversion. Interestingly, the FCR D sample pyrolysis yielded a lower char yield than for the FCR CF, even after almost completely removing all mineral matter.

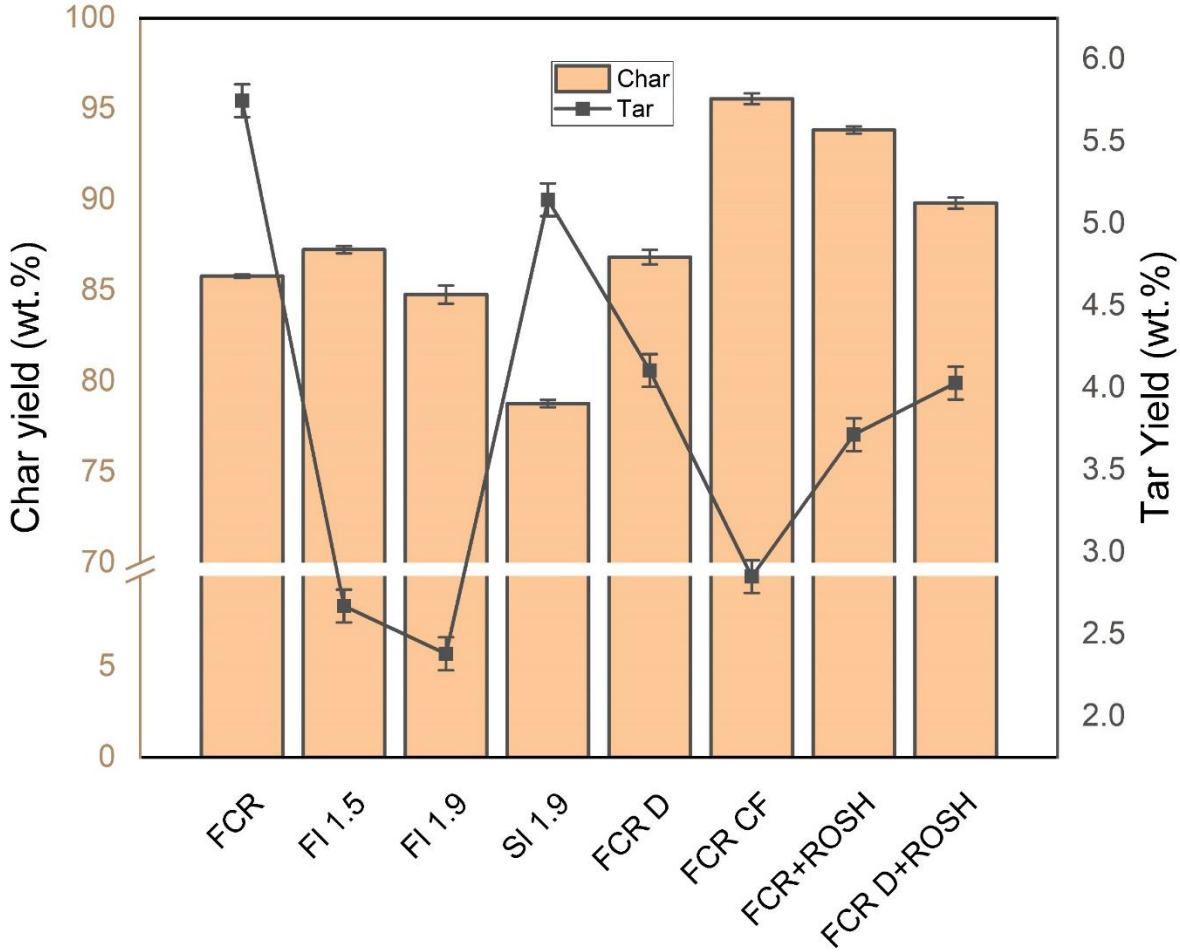

Figure 4-3: Product Distribution during Pyrolysis of FCR and Its Beneficiated Fractions, FCR/FCR D and ROSH Blends at 500 °C.

The slightly higher carbon conversion obtained for FCR D could be associated with the high surface area and recalcitrant inherent pyrite. The latter contributes to the conversion of carbon

via the catalytic Boudouard reaction (Equations. 15-17). The former allows for the transport of intermediate vapours through the developed pores with minimal secondary polymerisation reactions [37]. This illustrates that extraneous clays and quartz predominantly present in FCR CF contribute minimally to carbon conversion at 500 °C. Nonetheless, the demineralisation of FCR did not significantly increase the carbon conversion ($Y_{char}FCR \approx Y_{char}FCR\ D$). Similar findings were obtained by Roets et al. [16] during the pyrolysis of acid-washed SA coals. This can be attributed to the removal of calcite, dolomite, pyrite cleats and non-mineral inorganics, which can catalyse the pyrolysis reactions in the demineralised coal experiments of the FCR sample.

Although density separation of the FCR sample produced fractions comprising different modes of occurrences of mineral-matter, the results should be used with caution since the liberation of macerals (coal organic matrix) also took place. Maceral groups have different pyrolytic characteristic temperatures that overlap and could mask the effects of MM. Nonetheless, some inferences can be made on the effect of the mode of occurrences of MM on the distribution of pyrolysis products. The lowest char yield (highest carbon conversion) was obtained for the SI1.9 sample, followed by the FCR, FI1.5 and FI1.9 samples. Except for the FI1.9 sample, there is a better proportional relationship between the ash yield and carbon conversion of these samples.

The higher proportions of gypsum (product of the interaction of organic Ca, organic S and S released from pyrite at 400 °C [17], dolomite, calcite, apatite, and pyrite, which transform into reactive/catalytic Ca, Mg and Fe species at 500 °C), can be attributed to the higher carbon conversion produced during pyrolysis [4,34]. The XRD results of the FCR and SI1.9 samples confirmed the presence of these reactive/catalytic Mg, Ca, and Fe minerals in the FCR and SI1.9 chars. Two possibilities exist for the lower char yield obtained for the FI1.5 fraction compared to the FI1.9 fraction: 1.) the presence of low proportions of cleat minerals associated intimately with the carbon matrix in the FI1.5 sample, and 2.) the prominence of vitrinite macerals in the FI1.5 which have been associated with lower characteristic temperatures [38].

Adding the ROSH composite to the FCR and FCR D samples increased char yield percentage. A comparison between the char yields of FCR + ROSH and FCR D indicates that increasing the overall Ca and Fe contents reduced carbon conversion during pyrolysis. This can be attributed to the capturing of CO_2 by $Ca(OH)_2$ added to FCR and FCR D to form $CaCO_3$ in the blend chars during pyrolysis (Equations 8 and 9 and Table 4-6) [39]. Also, reactive Fe from the reduction of Fe_2O_3 in the blended chars can react with CO_2 to form Fe-O-C and FeC in the char samples (Equations 15-17) [39]. XRD did not detect the Fe-O-C and FeC formed in the blended chars due to their crystal size (< 2 nm) as well as the equipment detection limit of

<1% volume [4]. Mg may form amorphous MgS or react with N_2 to form Mg_3N_2 (Equations 6 and 7) [39].

The presence of magnetite in the chars of FCR + ROSH and FCR D +ROSH can be associated with the reduction of the Fe_2O_3 in these ROSH blend samples, which resulted in catalysing the pyrolysis reactions. The XRD results of the chars of FCR+ROSH and FCR D+ROSH showed the presence of calcite in these samples. This could originate from the carbonation of intermediate CaO derived from Ca(OH)2 dehydration.

Table 4-6: List of possible reactions taking place during pyrolysis of FCR, beneficiated fractions, acid-washed residues, and ROSH blends.

	MgO		$Ca(OH)_2$	
Reaction	$6MgO_{(s)} + 2N_{2(g)} \rightarrow 3O_2 + 2Mg_3N_{2(s)}$	[6]	$Ca(OH)_{2(s)} \rightarrow CaO_{(s)} + H_2O_{(g)}$	[8]
Activation reaction	$\Delta H = -462.81kj/mol, \quad T = 773K$		$\Delta H = 788.2kj/mol, \quad T = 673K$	
Reactions	$MgO_{(s)} + H_2S_{(g)} \rightarrow MgS_{(s)} + H_2O_{(g)}$	[7]	$CaO_{(s)} + CO_{2(g)} \rightarrow CaCO_{3(s)}$	[9
			$CaO_{(s)} + SO_{3(g)} \rightarrow CaSO_{4(s)}$	[10]
	Fe_2O_3		**Fe_2O_3 alternative**	
Reduction/	$3Fe_2O_3 + H_2 \rightarrow 2Fe_3O_4 + H_2O$	[11]	-	
Activation reaction	$\Delta H = 533.9kj/mol, \ T = 533K$			
Reactions	$3Fe_3O_4 + H_2S \rightarrow SO_{2(g)} + 9FeO + H_2O$	[12]	$Fe_2O_3 + CO/C \rightarrow Fe_{(s)} + FeO_{(s)} + CO_{2(g)}$	[15]
	$FeO_{(s)} + H_2S_{(g)} \rightarrow FeS_{(s)} + H_2O_{(g)}$	[13]	$Fe_{(s)} + Char_{(s)} + CO_{2(g)} \rightarrow Fe - O - C_{(s)} + CO_{(g)}$	[16]
	$Fe_{(s)} + H_2S_{(g)} \rightarrow FeS_{(s)} + H_{2(g)}$	[14]	$Fe - O - C_{(s)} \rightarrow FeC_S + CO_{(g)}$	[17]

4.3.5.2 Tar Yields

Pyrolytic tar yields indicate the highest tar yield for the FCR sample, followed by the FCR D and FCR CF samples, as shown in Figure 4-3. Roets et al. [16] linked the lower tar yields by acid-treated samples to limited hydrogen transfer usually facilitated by mineral-matter. In the case of inadequate H^+ transfer, solidification or secondary polymerisation reactions occur, leading to char formation over tar. Although FCR D has lost 98% of its minerals, including the cleat minerals, it still has a higher tar yield than FCR CF due to the higher BET surface area associated with the mineral matter removal. This is because acid washing creates active oxygen sites and scatters coal microstructures, making them unstable and susceptible to thermal scission [40]. The lower tar yield measured for FCR CF is linked to the lower carbon conversion. The tar yields of the density-separated fractions were obtained in the order of FCR>SI 1.9>FI1.5 ≈FI1.9. The tar was 10, 53 and 58 wt. % lower than that of FCR for SI1.9, FI1.5 and FI1.9, respectively. This agrees with the correlation of extraneous minerals with carbon conversion. While inherent mineral-matter contributes to bond scission of polymerised structures, the hot ash layer produced by extraneous minerals promotes secondary cracking of intermediate vapours to form low molecular weight tars, producing more tars. Rautenbach et al. [4] found that float fractions (comparable to FI1.5) of SA feed-coals are free of mineral cleats, while the sink fraction (comparable to SI1.9) is rich in rock fragments, calcite/dolomite/siderite/pyrite cleats and carbominerites. Cleat minerals and carbominerites comprising pyrite, dolomite and calcite released metallic Ca, Mg, and Fe to catalyse the pyrolysis reactions, which explains the increased tar yields for the FCR and SI1.9 samples.

The proportion of cleat fluxing minerals is higher for SI1.9 compared to FI1.9 and the FI1.5 samples (Table 4-3). MgO and CaO (derived from dehydroxylation of $Ca(OH)_2$) promote deoxygenation and cleavage of oxygen-containing bonds, while Fe, derived from the reduction of Fe_2O_3 to Fe (Equation 15), promotes deoxygenation of carboxylic functional groups via catalytic Boudouard reactions [14]. The addition of the ROSH composite to FCR D and FCR did not significantly affect the tar yields, indicating that extraneous minerals do not contribute to the evolution of tars. However, secondary reactions occur during the transport of tar precursors through the hot ash layer [41].

4.3.5.3 Tar Composition

The tar samples derived from the FCR, FCR+ ROSH and its beneficiated fractions obtained from pyrolysis tests at 500 °C were subjected to GC/MS measurements to identify the compounds present in the tars. A minimum of 100 organic compounds were detected with a 90% confidence level and were classified into six (6) chemical families (Figure 4-4) namely,

1-ring aromatic hydrocarbons (1-ringArH), aromatic and polycyclic aromatic hydrocarbons (PAHs), aliphatic hydrocarbons (aliphatic H), ethers and esters, alkylated fractions (i.e., alkyl-benzenes, alkyl-phenols, alkyl-indenes and alkyl-Naphthalenes) and nitrogen and inorganic elements containing compounds ((N, inorganic)-containing). The relative peak area percentages (RA%) of these chemical families are used as a semi-quantitative tool to compare the compositions of the obtained pyrolytic tars. In the case of the FCR, FCR D and FCR CF samples, the RA% for PAHs was obtained in the order of FCR CF ≈ FCR D > FCR. Meanwhile, the RA% for aliphatic hydrocarbons illustrated an FCR > FCR CF > FCR D trend opposite to the PAHs. This indicates that secondary reactions by mineral matter occur in increasing order of FCR D > FCR CF > FCR contributed to the secondary cracking of the complex PAHs structures into light gases and aliphatic hydrocarbons via side-chain decomposition and hydrocracking reactions. Ca, Mg and Fe, which are associated with the cleat minerals and non-mineral inorganics, have been associated with promoting such reactions during pyrolysis [14].

The higher proportions of ethers and esters obtained from the FCR CF and FCR D samples suggest that deoxygenation and dehydroxylation reactions of tars are promoted by extraneous minerals through cleavage of C-O and C-H bonds by secondary volatiles-mineral-matter interaction [42]. The proportions of all alkylated fractions are almost the same for the FCR D and FCR CF samples but lowest for the FCR sample, indicating the contribution of water-soluble cations and salts of carboxylic acids towards thermal desorption and decomposition of alkylated compounds and prevention of cross-linking reactions [43]. The proportions of (N-inorganic)-containing compounds include sulfonated compounds, which could be attributed to the higher proportions of this group in the FCR CF and FCR D samples due to the lower percentage ash yield comprising of S-capturing capable minerals.

The evolution of 1-ring aromatic compounds relates to the cleavage of ether and methylene bridges associated with the aromatic nuclei occurring at lower temperatures [44]. These are the highest in the FCR D sample and not detectable in the FCR CF sample, which could be attributed to possible significant changes in the organic structure of FCR D during pyrolysis.

In the case of the density-separated fractions, the effect of mineral-matter on tar composition is apparent between Fl1.5 and Sl1.9. This is due to the better liberation of mineral matter in the two density-separated fractions. The proportion of PAHs and oxygenated (ethers and esters) compounds was higher in the Fl1.5 fraction, while both were lowest in the tar of the Sl1.9 fraction.

Besides the suggested deoxygenation reactions by inherent minerals, SI1.9 is rich in extraneous kaolinite. Like zeolites, the acid sites associated with extraneous kaolinite or metakoalinite in coal or char promoted the decomposition of PAHs and oxygenated compounds and enhanced the formation of alkylated fractions. The SI1.9 fraction is concentrated in oxygen-carrying minerals. These oxygen carriers inhibited the deoxygenation of intermediate volatiles by reacting directly with carbon via MM-char reaction pathways (Equations 16 & 17). For instance, Fe reacts with active oxygen sites, activating carbon sites and improving carbon conversion [14]. Increased oxygen-containing aromatic compounds in the FCR +ROSH blend also support this reaction mechanism.

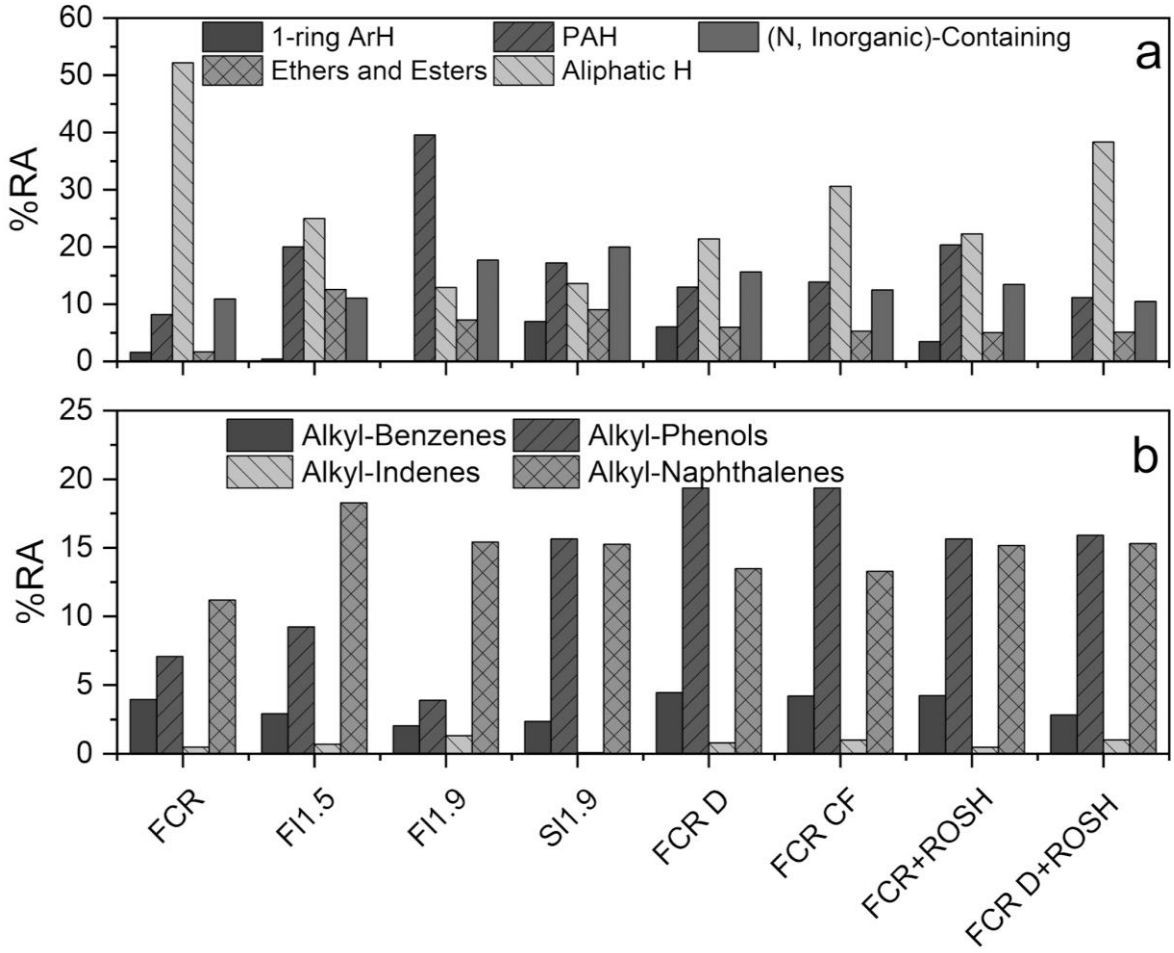

Figure 4-4: Distribution of chemical compounds during pyrolysis of FCR and its beneficiated fractions and ROSH blends at 500 °C.

The ROSH addition decreased the proportions of aliphatic hydrocarbons in the tars of the FCR sample only. However, it increased the proportions of PAHs, ether, and esters. This behaviour suggests the promotion of recombination reactions by ROSH [45]. Since PAHs evolved from the thermal cracking of the coal macromolecular structure and thermal desorption of PAHs

[46], the higher proportions of PAHs in Fl1.5, Fl1.9, Sl1.9, FCR CF and FCR D are associated with the chemical compositions of these samples. However, upon the addition of ROSH to FCR D, the PAHs proportions reduced slightly due to secondary catalytic cracking reactions of long-chain hydrocarbons and side chains associated with aromatic nuclei to form aliphatic hydrocarbons as well as dealkylated compounds [44]. Moreover, the addition of ROSH increased the proportions of alkylated compounds for both samples, illustrating the selectivity of these compounds over aliphatic hydrocarbons.

4.3.5.4 Simulated Distillation

The analysis following the simulated distillation of tars obtained from the pyrolysis of FCR, its beneficiated fractions and blends of FCR and FCR D with ROSH at 500 °C, are presented in Figure 4-5. The boiling point differences were used to group proportions of light and heavy naphtha (90-180 °C), kerosene (180-230 °C), light gas oil (230-320 °C), heavy gas oil (320-375 °C) and vacuum gas oil across samples. The results indicate increased naphtha, kerosene, light gas, and heavy gas oil fractions in all samples except for Fl1.9 when compared to the FCR sample. This behaviour can be attributed to the complex interplay of mineral matter and organic composition. The FCR D and FCR CF samples, with lower proportions of inherent mineral matter, may have different catalytic effects or reaction pathways compared to the Fl1.9 sample, which has a higher proportion of inherent minerals. These minerals might promote secondary cracking reactions, leading to a lower yield of vacuum gas oil.

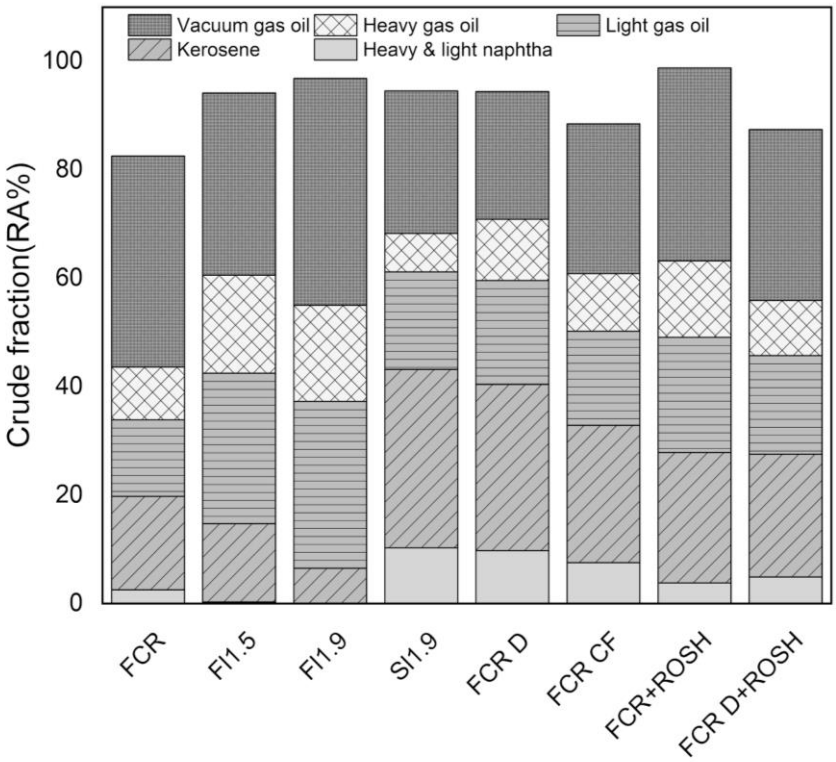

Figure 4-5: Crude fractions distribution of tars obtained during pyrolysis of FCR and its beneficiated fractions and ROSH blends at 500 °C.

The Fl1.5 and Fl1.9 samples, comprising inherent mineral-matter and a zero percent of mineral cleats, yielded the lowest fraction of naphtha, kerosene and light gas compared to SI1.9. The latter enhanced secondary catalytic cracking reactions. The addition of ROSH to the FCR sample did not increase the fraction of lower boiling point tar components, illustrating the inferiority of secondary cracking reactions. This behaviour could be attributed to the aromatisation of tar precursors promoted by higher proportions of CaO from $Ca(OH)_2$ along with $CaCO_3$ formation [34]. The formation of $CaCO_3$ resulted in an increased char yield for these samples. Increasing the overall proportions of ROSH lowered carbon conversion and increased the proportions of heavy tar fractions. This phenomenon was also seen for the FCR+ROSH sample, where the fraction of lower boiling point tar components was reduced. The reduced fractions of light tars in Fl1.5 (zero cleats) indicate that cleat minerals could have a higher potency for catalytic cracking of heavy compounds into lighter ones.

4.3.6 Activation Energy

The distribution of E_a with conversion and the average E_a of FCR and FCR D, along with their corresponding blends containing ROSH composite, are presented in Table 4-7**.** Although the average E_a is useful for understanding the general E_a requirement for the entire coal pyrolysis process, using it solely generalises pyrolysis stages while concealing their reaction mechanisms. As a result, the emphasis is placed on x vs E_a trends.

In general, pyrolysis of FCR has a higher E_a compared to coal from other regions due to the different coal properties, such as macerals and mineral-matter contents and their mode of occurrence [47]. The magnitudes of E_a varied with x, which indicates the occurrence of multiple complex reactions involved in coal pyrolysis. Using the FCR sample as a benchmark, it is seen that the E_a values increase with an increase in x and T which is ascribed to the cleavage of weaker bonds at lower temperatures due to the lower E_a required.

At $0.1 < x < 0.2$, FCR showed the lowest E_a required for carbon conversion. The residual inherent pyrite (fluxing cleat mineral) in FCR D could be associated with a lower E_a for FCR D compared to FCR CF at this conversion range. Lower coefficient of determination (R^2) values are indicative of these reactions, which is the case reported in previous studies that the occurrence of parallel reactions lowers model linearity [25]. With ROSH composite, E_a is reduced for FCR, while FCR D showed an increase of E_a at x=0.1. However, at x=0.2 the E_a values for FCR D and FCR were equal while that of FCR CF dropped.

At $0.3 < x < 0.7$, FCR required the highest E_a. This could be ascribed to the partial transformation of extraneous kaolinite, pyrite, dolomite, and calcite at $T > 500\,℃$. The contribution of these extraneous minerals to the E_a is supported by the lowest E_a values measured for the FCR D sample until $x = 0.8, \text{and}\, T = 670\,°C$. This is due to the low concentration of extraneous minerals whose transformation is highly endothermic, as indicated in Equations 8 and 11. This behaviour is more pronounced with the addition of ROSH composite, where a spike in E_a is observed for the FCR+ROSH and FCR D+ROSH at $x = 0.7, T = 610\,°C$. This is linked to the new peak found by Shi et al. [48] at T < 600 °C attributed to the presence of calcium during analytical pyrolysis of Inner Mongolia coal/CaO mixtures which increased E_a in that zone. At $T > 700\,°C$, highly endothermic reactions as indicated in Equations 15 and 16 take place. These could be associated with the overall spike in E_a. These reaction mechanisms and E_a suggest that the decomposition of minerals composite and carbon matrix occur almost parallel with minimal contribution to primary pyrolysis reactions. The change in yields and composition of pyrolytic products is ascribed to secondary pyrolysis reactions (depolymerisation, polymerisation, tar cracking and dehydroxylation) as the intermediate vapour evolves and contacts the hot ash particle derived from extraneous minerals.

Table 4-7: Activation energy distribution for FCR and its beneficiated fractions and ROSH blends.

T(K)	X	FCR		FCR CF		FCR D		FCR+ROSH		FCR D+ROSH	
		Ea	R^2	Ea	R^2	Ea	R^2	Ea	R^2	Ea	R^2
405.55	0.1	251.4	1	291.5	0.9982	276.8	0.9993	233.4	0.9984	283.8	0.999
438.25	0.2	262.7	0.9979	267.9	0.9984	254.5	0.9997	277.1	0.9997	278.6	1
463.25	0.3	279.6	0.9928	268.9	0.9997	261.8	0.9995	295.5	0.9991	319.0	0.9991
490.95	0.4	293.9	0.9770	274.6	0.9995	279.0	0.9998	316.7	0.9943	421.5	0.9890
526.25	0.5	315.3	0.9650	295.4	0.9996	301.6	0.9979	355.5	0.9771	485.1	0.9626
568.55	0.6	349.6	0.9534	332.4	0.9997	324.7	0.9970	359.2	0.9601	475.1	0.9384
610.75	0.7	413.2	0.9798	391.1	0.9988	363.4	0.9966	362.9	0.9620	361.7	0.9710
670.75	0.8	409.3	0.9956	478.1	0.9985	403.4	0.9958	378.1	0.9749	881.7	0.9944
746.85	0.9	413.0	0.9910	537.1	0.9984	445.4	0.9948	1709.8	0.8219	1394.0	0.9786
Average Ea (kJ/mol)		**332.0**	**-**	**348.5**	**-**	**323.4**	**-**	**476.5**	**-**	**544.5**	**-**

Ea – activation energy, R^2 – coefficient of determination

4.4 Conclusions

A study to evaluate the effect of reactive oxides and hydroxide composite of fluxing extraneous minerals and the mode of occurrence of mineral matter on the pyrolysis behaviour of FCR was evaluated based on the yields of tar and char, and the apparent activation energy.

Demineralisation, chemical fractionation, and density separation procedures produced samples with various modes of occurrences of mineral matter, which provided insight into their effects on pyrolysis reactions.

The highest carbon conversion (char yield=78.9 wt. % and tar yield = 5.1 wt. %) was achieved for FCR and decreased in the order FCR (char yield=78.9 wt. %, tar yield = 5.1 wt. %) > FCR D (char yield = 86.8 wt. %, tar yield = 4.1 wt. %) and FCR CF (char yield=95.6 wt. %, 2.9 wt. %) due to the prominence of extraneous, non-mineral inorganics and inherent dolomite/calcite/ pyrite cleats. Although the ROSH composites do not contribute significantly to carbon conversion, they facilitate secondary cracking reactions during the FCR pyrolysis. Artefacts of extraneous minerals (metakaolinite, calcite and dolomite (carbonation with $Ca(OH)_2$ and MgO)) with hindering effects were formed in the blended chars during low-temperature pyrolysis and navigated the reaction pathways. On the other hand, magnetite, having a catalytic effect, was formed in the blended chars due to the Fe_2O_3 reduction. The highest tar yield of 5.7 wt. % was achieved for FCR, followed by 5.1 wt. % for Sl1.9, 4.1 wt. % for FCR D while Fl1.9 achieved the lowest tar yield of 2.4 wt. % due to the prominence of non-mineral inorganics and inherent dolomite/calcite/ pyrite mineral cleats in FCR and Sl1.9 with a catalytic cracking characteristics.

The highest inherent mineral matter (non-mineral inorganics, organic Ca/Mg/Fe (carboxylate salts) and dolomite/calcite/pyrite cleats) contents in the SI1.9 fraction facilitated the conversion of the carbon matrix (low fixed carbon content) to volatile compounds during pyrolysis as shown by higher carbon conversion for the Sl1.9 fraction compared with FCR. The presence and amount of extraneous ROSH and non-mineral inorganics present in FCR facilitated secondary reactions. These mineral matters enhanced dealkylation and hydrocracking reactions to produce aromatic and aliphatic hydrocarbons.

Excess oxygen-carrying minerals inhibit deoxygenation reactions during low-temperature pyrolysis. The addition of ROSH composite to the FCR sample and the FCR D sample increased the proportions of oxygen carriers, which inhibit dehydroxylation and deoxygenation reactions but enhance secondary dealkylation and cracking to form aromatic and aliphatic compounds. The addition of ROSH composite to the FCR samples increases the average Ea

values from 332.0 to 476.5 kJ/mol for FCR and from 323.4 to 544.4 kJ/mol for FCR D due to the initial dehydration of $Ca(OH)_2$ and reduction of Fe_2O_3.

This work provides insight into the distribution and mode of occurrence of mineral matter, its effects on pyrolysis reaction mechanisms, and the effects of cleat minerals and carboxylate salts during utilisation of FCR in the global thermochemical processes. This knowledge can reduce health and environmental dangers and reduce the high FCR disposal costs. Since mineral matter and the carbon matrix may interact differently at high temperatures and in different proportions, investigations into the effects of temperature and the proportions of extraneous minerals as indigenous minerals or in their oxides and hydrated oxide forms may provide insights for future study. Furthermore, high-resolution transmission electron microscopy and QEMSCAN analyses should be used to qualify and quantify nano-minerals (micro-cleats) with catalytic and hindering effects in the pyrolytic chars. Also, the effect of mineral distribution across coal particle size on the pyrolytic product yields during pyrolysis should be investigated.

4.5 Acknowledgements

The authors would like to express their appreciation to South African Research Chairs Initiative of the Department of Science and Technology (DST) and National Research Foundation of South Africa (NRF) (Coal Research Chair Grant No. 86880) and NRF free-standing bursary MND200715544211/UID: 136078) for the financial contributions. Opinions, findings, conclusions, or recommendations expressed in any publication generated by the NRF-supported research are those of the author alone, and the NRF accepts no liability whatsoever in this regard. Dr Sabine Verryn of XRD Aanalytical and Consulting cc, Mr Morne Van Zyl of SGS, Secunda, Dr Xolisa Goso and Mr Napo Ntsasa of Mintek, Mr Willem Swanepoel of Buerua Veritas, Dr Roelf Venter of North-West University and Mr Moses Lelaka from Setpoint Llaboratories are thanked for assistance with different aspects of the analytical techniques.

Chapter 5 reports the effect of a composite addition of Ca^{2+}, Mg^{2+}, and Fe^{2+} acetates as salts of carboxylic acids simulating inherent mineral matter on the yields and composition of pyrolytic products (chars, tars, and gases) derived from TEP fine-coal reject, its Density-separated fractions, and the demineralised residues derived from the utilisation of the NWU Fischer assay set-up. The degradation profiles of samples of fine-coal rejects and their density-separated fractions during pyrolysis were also studied using a thermogravimetric analyser TGA and reported in this manuscript.

Chapter References

[1] Leokaoke NT, Bunt JR, Neomagus HWJP, Waanders FB, Strydom CA. CO_2 reactivity of briquettes derived from discard inertinite-rich Highveld coal using lignosulphonate and resin as binders. Journal of the Southern African Institute of Mining and Metallurgy. 2019; 119:847–54.

[2] Statistics SA. Mineral Accounts for South Africa: 1980-2007. 2010.

[3] Isaac K, Bada SO. The co-combustion performance and reaction kinetics of refuse derived fuels with South African high-ash coal. Heliyon. 2020; 6:e03309.

[4] Rautenbach R, Strydom CA, Bunt JR, Matjie RH, Campbell QP, Van Alphen C. Mineralogical, chemical, and petrographic properties of selected South African power stations' feed coals and their corresponding density separated fractions using float-sink and reflux classification methods. International Journal of Coal Preparation and Utilisation. 2018; 39:421–44.

[5] Singh U, Sharma N, Mahapatra SS. Environmental life cycle assessment of Indian coal-fired power plants. International Journal of Coal Science & Technology. 2016; 3:215–25.

[6] Shekarian Y, Rahimi E, Shekarian N, Rezaee M, Roghanchi P. An analysis of contributing mining factors in coal workers' pneumoconiosis prevalence in the United States coal mines, 1986–2018. International Journal of Coal Science & Technology. 2021; 8:1227–37.

[7] Nádudvari Á, Cabała J, Marynowski L, Jabłońska M, Dziurowicz M, Malczewski D, et al. High concentrations of HgS, MeHg and toxic gas emissions in thermally affected waste dumps from hard coal mining in Poland. Journal of Hazardous Materials. 2022; 431:128542.

[8] Frandsen F, Dam-Johansen K, Rasmussen P. Trace elements from combustion and gasification of coal—an equilibrium approach. Progress in Energy and Combustion Science. 1994; 20:115–38.

[9] Pone JDN, Hein KAA, Stracher GB, Annegarn HJ, Finkleman RB, Blake DR, et al. The spontaneous combustion of coal and its by-products in the Witbank and Sasolburg coalfields of South Africa. International Journal of Coal Geology. 2007; 72:124–40.

[10] Ward CR. Analysis, origin and significance of mineral matter in coal: An updated review. International Journal of Coal Geology. 2016; 165:1–27.

[11] Matjie RH, French D, Ward CR, Pistorius PC, Li Z. Behaviour of coal mineral matter in sintering and slagging of ash during the gasification process. Fuel Processing Technology. 2011; 92:1426–33.

[12] Rautenbach R, Matjie RH, Strydom CA, Bunt JR, Ward CR, French D, et al. Evaluation of mineral matter transformations in low-temperature ashes of South African coal feedstock samples and their density separated cuts using high-temperature X-ray diffraction. International Journal of Coal Preparation and Utilisation. 2020; 40:320–47.

[13] Fu Y, Guo Y, Zhang K. Effect of three different catalysts (KCl, CaO, and Fe_2O_3) on the reactivity and mechanism of low-rank coal pyrolysis. Energy & Fuels. 2016; 30:2428–33.

[14] He R, Deng J, Deng X, Xie X, Li Y, Yuan S. Effects of alkali and alkaline earth metals of inherent minerals on Fe-catalysed coal pyrolysis. Energy. 2022;238:121985.

[15] Sun B, Huang X, Huang H, Zhang X, Shang W, Sun S, et al. Preparation of iron-based catalysts by mechanical solid-phase ball milling and their applications in cohydrogenation of coal and petrochemical coking residual oil. ACS Omega. 2023; 8:25134–41.

[16] Roets L, Strydom CA, Bunt JR, Neomagus HWJP, Van Niekerk D. The effect of acid washing on the pyrolysis products derived from a vitrinite-rich bituminous coal. Journal of Analytical and Applied Pyrolysis. 2015; 116:142–51.

[17] Raghoo M. The volatilisation of aluminium and silicon species from a Highveld coal. [PhD thesis]. Potchefstroom, South Africa: North-West University; 2010.

[18] Roets L, Bunt JR, Neomagus HWJP, Van Niekerk D. An evaluation of a new automated duplicate-sample Fischer Assay setup according to ISO/ASTM standards and analysis of the tar fraction. Journal of Analytical and Applied Pyrolysis. 2014; 106:190–6.

[19] Liu Q, Hu H, Zhou Q, Zhu S, Chen G. Effect of inorganic matter on reactivity and kinetics of coal pyrolysis. Fuel. 2004; 83:713–8.

[20] Norrish K, Hutton JT. An accurate X-ray spectrographic method for the analysis of a wide range of geological samples. Geochimica et Cosmochimica Acta. 1969; 33:431–53.

[21] Speakman SA. Introduction to PANalytical X'Pert HighScore Plus v3. 0. MIT Center for Materials Science and Engineering. 2012:1–19.

[22] Rietveld HM. A profile refinement method for nuclear and magnetic structures. Journal of Applied Crystallography. 1969; 2:65–71.

[23] Okolo GN, Everson RC, Neomagus HWJP, Roberts MJ, Sakurovs R. Comparing the porosity and surface areas of coal as measured by gas adsorption, mercury intrusion and SAXS techniques. Fuel. 2015; 141:293–304.

[24] Mphahlele K, Matjie RH, Osifo PO. Thermodynamics, kinetics and thermal decomposition characteristics of sewage sludge during slow pyrolysis. Journal Environmental Management. 2021; 284:112006.

[25] Starink MJ. A new method for the derivation of activation energies from experiments performed at constant heating rate. Thermochimica Acta. 1996; 288:97–104.

[26] Moyo A, Filho JA, Harrison S, Broadhurst J. Characterising the environmental risks of coal preparation wastes: A study of fine coal slurry waste and discards from South African collieries. IMWA 2018 Annual Conference; Pretoria, South Africa, 2018.

[27] Matjie R, Bunt J, Stokes W, Bijzet H, Mphahlele K, Uwaoma R, et al. Interactions between kaolinite, organic matter, and potassium compounds at elevated temperatures during pyrolysis of caking coal and its density-separated fractions. Energy & Fuels. 2021; 35:13268–80.

[28] Mphahlele K, Matjie RH, Bunt JR, Uwaoma RC. Properties and reactivity of two oxidised and unoxidised South African Highveld fine-coal rejects and their density-separated fractions. International Journal of Coal Preparation and Utilisation. 2023; 43:1451–77.

[29] Wagner NJ, Hlatshwayo B. The occurrence of potentially hazardous trace elements in five Highveld coals, South Africa. International Journal of Coal Geology. 2005; 63:228–46.

[30] Hower JC, Dai S, Seredin V V, Zhao L, Kostova IJ, Silva LFO, et al. A note on the occurrence of yttrium and rare earth elements in coal combustion products. Coal Combustion and Gasification Products. 2013; 5:39–47.

[31] Uwaoma RC, Strydom CA, Matjie RH, Bunt JR. Influence of density separation of selected South African coal fines on the products obtained during liquefaction using tetralin as a solvent. Energy & Fuels. 2019; 33:1837–49.

[32] Matjie RH, Lesufi JM, Bunt JR, Strydom CA, Schobert HH, Uwaoma R. In situ capturing and absorption of sulphur gases formed during thermal treatment of South African coals. ACS Omega. 2018; 3:14201–12.

[33] Du Z, Li W. The catalytic effect from alkaline elements on the tar-rich coal pyrolysis. Catalysts. 2022; 12:376.

[34] Everson RC, Neomagus HWJP, Kasaini H, Njapha D. Reaction kinetics of pulverised coal-chars derived from inertinite-rich coal discards: Characterisation and combustion. Fuel. 2006; 85:1067–75.

[35] Shivakumara S, Penki TR, Munichandraiah N. High specific surface area α-Fe_2O_3 nanostructures as high-performance electrode material for supercapacitors. Materials Letters. 2014; 131:100–3.

[36] Dai S, Zou J, Jiang Y, Ward CR, Wang X, Li T, et al. Mineralogical and geochemical compositions of the Pennsylvanian coal in the Adaohai Mine, Daqingshan Coalfield, Inner Mongolia, China: Modes of occurrence and origin of diaspore, gorceixite, and ammonian illite. International Journal of Coal Geology. 2012; 94:250–70.

[37] Ahmad T, Awan IA, Nisar J, Ahmad I. Influence of inherent minerals and pyrolysis temperature on the yield of pyrolysates of some Pakistani coals. Energy Conversion and Management. 2009; 50:1163–71.

[38] Matjie RH, Li Z, Ward CR, Bunt JR, Strydom CA. Determination of mineral matter and elemental composition of individual macerals in coals from Highveld mines. Journal of the Southern African Institute of Mining and Metallurgy. 2016; 116:169–80.

[39] Binnewies M, Milke E. Thermochemical Data of Elements and Compounds, Wiley-VCH, Weinheim, 2002.

[40] Liu L, Yuan Y, Kumar S, Wang Z, He Y, Lv Y, et al. Catalytic effect of metal chlorides on coal pyrolysis and gasification part Ⅱ. Effects of acid washing on coal characteristics. Thermochimica Acta. 2018; 666:41–50.

[41] Hamel S, Hasselbach H, Weil S, Krumm W. Autothermal two-stage gasification of low-density waste-derived fuels. Energy. 2007; 32:95–107.

[42] Ban Y, Jin L, Zhu J, Liu F, Hu H. Insights into effect of Ca $(OH)_2$ on pyrolysis behaviours and products distribution of Hongshaquan coal. Fuel. 2022; 307:121791.

[43] Le J, Liu P, Liu D, Lu X, Pan T, Zhang D. Effect of catalysts on the yields of light components and phenols derived from Shenmu coal low temperature pyrolysis. Energy and Fuels. 2017; 31:7033–41.

[44] Shi Z, Jin L, Zhou Y, Li H, Li Y, Hu H. In-situ analysis of catalytic pyrolysis of Baiyinhua coal with pyrolysis time-of-flight mass spectrometry. Fuel. 2018; 227:386–93.

[45] Zheng M, Li X, Nie F, Guo L. Investigation of overall pyrolysis stages for Liulin bituminous coal by large-scale ReaxFF molecular dynamics. Energy and Fuels. 2017; 31:3675–83.

[46] Shi Z, Jin L, Zhou Y, Li Y, Hu H. Online analysis of initial volatile products of Shenhua coal and its macerals with pyrolysis vacuum ultraviolet photoionisation mass spectrometry. Fuel Processing Technology. 2017; 163:67–74.

[47] Shao S, Ma B, Wang C, Chen Y. Thermal behavior and chemical reactivity of coal gangue during pyrolysis and combustion. Fuel. 2023;331:125927.

[48] Shi X, Wu Y, Zhang J, Ding L, Wang C, Lan X, et al. Comparison of pyrolysis behaviour between pure coal and mixture of coal/CaO. Journal of Analytical and Applied Pyrolysis. 2021; 159:105311.

CHAPTER 5 EFFECT OF FLUXING INORGANIC ELEMENT-BEARING ACETATE COMPOSITE ON THE DISTRIBUTION OF PYROLYTIC PRODUCTS FROM HIGHVELD PARTIALLY OXIDISED FINE-COAL REJECT AND ITS BENEFICIATED RESIDUE

K, Mphahlele, R. H. Matjie, J. R. Bunt, A. Janse van Vuuren[b]

In this chapter, the effect of inherent mineral matter, simulated by a composite of Ca^{2+}, Mg^{2+}, and Fe^{2+} acetates as salts of carboxylic acids, on the yields and compositions of pyrolytic products (chars, tars, and gases) is evaluated. The pyrolytic products obtained from TEP fine-coal reject, their density-separated fractions, and their demineralised residues produced using NWU Fischer assay set-up are reported and discussed. The degradation profiles of fine-coal reject and their density-separated fractions during pyrolysis were studied using TGA and reported in this chapter.

This manuscript is published in Fuel journal, 2024; volume 371, Pages 131891. https://doi.org/10.1016/j.fuel.2024.131891 .

Abstract

The role of mineral matter in coal significantly influences pyrolysis, yet there is no consensus on the behavior of inherent minerals and carboxylate salts during coal or fine-coal reject (FCR) pyrolysis. This study investigates the effects of carboxylate salts ($Ca(C_2H_3O_2)_2$, $Mg(CH_3COO)_2.4H_2O$, and $Fe(C_2H_3O_2)_2$ composite (CSC) on FCR, demineralised FCR (FCRD), and demineralised >1.9 g/cm^3 FCR sink fraction (SI1.9D) in a Fischer-assay double retort set-up under the following pyrolysis conditions: 500 °C and a heating rate of 5 °C/min for 3 hours in nitrogen. Analytical techniques identified kaolinite, quartz, dolomite, siderite, and calcite and characterised tar precursors, functional groups, carbon associations, and species evolution in FCR, FCR+CSC, FCRD+CSC, SI1.9D, SI1.9D+CSC and their chars. FCR+CSC exhibited the fastest decomposition rate due to extraneous minerals and CSC interactions. FCRD+CSC and FCR+CSC achieved the highest carbon conversion, tar yield and gas yield, and the lowest char yield compared to SI1.9D and SI1.9D+CSC. The addition of CSC was expected to increase the S proportion in FCRD+CSC and SI1.9D+CSC chars due to H_2S in-situ capturing to form nano-sulfides and S-bearing amorphous phases. However, as shown in Table 5-1, the S content in FCRD+CSC char is lower than that of the FCRD char. This suggests that while some sulfur capture mechanisms are active, they do not result in a higher overall sulfur content in the char. Also, the SI1.9D+CSC blend released a higher CO_2 via inherent nano-carbonates reaction with H_3O^+ from kaolinite/illite transformation, the HF/HCl aqueous solution and acetate decomposition. Tar yield, polycyclic aromatics, alkylated phenolics, and naphthalene compounds decreased due to hydrogen transfer by CSC, inhibiting the secondary cracking of intermediate vapours. These results highlight the catalytic potential of carboxylate salts, dependency on inherent minerals and dominating maceral groups during coal pyrolysis.

Keywords: Pyrolysis, Fine-coal rejects, Mineral-matter, Inherent mineral-matter, Carboxylate salts, Thermogravimetry

5.1 Introduction

South Africa relies heavily on coal to generate over 90% of its electricity and over a third of its liquid fuels. Although South Africa is diversifying its energy mix, coal is expected to remain a significant energy source for the next 30 years [1]. It will continue to play a vital role in meeting global energy demands [2]. Clean coal utilisation is a crucial factor in meeting the carbon emission targets set by the South African (SA) Legislature for 2030, as illustrated in the National Development Framework (NDP) [1]. The valorisation of fine-coal rejects (FCRs), a by-product generated during coal handling and beneficiation, is essential for the sustainable

utilisation of coal resources. In South Africa, about 1 billion tonnes of FCRs have been disposed of in landfills or tailings dams, in colossal FCR and coal ash disposal heaps, which causes environmental nuisance and human-health risks, and incurs high costs of disposal procedures [3,4].

Given the significant reliance on coal as an energy source, it is essential to understand the thermochemical behaviour of FCRs through pyrolysis for valorisation purposes. Pyrolysis is an initial step to gasification and combustion, making it a useful technique for studying the thermochemical behaviour of coal [5]. This technique has been widely employed to study the behaviour and influence of coal properties, such as mineral matter and organic matter (macerals), on carbon conversion efficiencies and distribution of products [6].

Mineral matter in coal presents processing challenges and opportunities because its presence in different modes of occurrence leads to various coal behaviours during pyrolysis. These differences have attracted several researchers [2,4,6] to work on understanding the mode of occurrence of mineral matter in feed-coals and their partially oxidised FCRs. Alkali and alkaline earth metallic inorganic elements (AAEMIEs) (Na, K, Mg, Ca) in coal may facilitate carbon conversion and prevent the formation of heavy tars during pyrolysis [7]. The heavy tars have been linked with blockages of pipes and handling complications. As a result, there is no consensus on the limitations and effects of AAEMIE contents. Their interaction with other forms of inherent mineral matter in coal (carboxylate salts) is not well understood.

Coals of different ranks and from different regions consist of different proportions and modes of mineral matter. In a previous study [4], the influence of the mode of occurrence of mineral matter and their interactions with reactive oxides and hydroxides of extraneous minerals was investigated. The study indicated that inherent mineral matter, especially the cleat minerals, have higher catalytic potency than the reactive oxides (MgO and Fe_2O_3) and hydroxides ($Ca(OH)_2$) of extraneous fluxing minerals (dolomite, calcite, siderite and pyrite) due to the intimate association with the carbon matrix. However, it was not possible to discern the effect of carboxylate salts due to their lower proportions and overlapping decomposition profiles with the vitrinite-enriched light fractions from the FCR beneficiated float fractions. This created a gap in understanding the extent of the effects of carboxylate salts (non-mineral inorganics) and their effects on pyrolysis product distribution.

SA coals are typically comprised of up to 50 wt. % mineral matter [3, 8], whereas foreign coals such as Chinese, Russian, or Pakistani may comprise mineral matter as low as 1 wt. % [9, 10]. Sodium, calcium, magnesium, iron (II) and potassium carboxylate salts are predominantly water-insoluble, and ammonium acetate exchangeable cations are present in SA coals and

FCRs in concentrations below 1 wt. % [8,11]. In contrast, Victorian brown coals mainly comprise carboxylate salts [12]. This discrepancy poses a challenge in understanding the extent of their impact on coal pyrolysis. This limitation could hinder an accurate assessment of the effects of saturated AAEMIEs-carboxylate salts in coal samples of different ranks and origins. As a result, the use of these carboxylate salts at concentrations above the typical 2 wt. % is of needed to gain insight into the effects of AAEMIEs on coal pyrolysis mechanisms.

The AAEMIEs-carboxylate salts have been linked with hydrocarbon selectivity capabilities associated with specific AAEMIEs. Mg and Ca acetates may promote methane formation [13]. Hong et al. [14] associated the catalytic bond-breaking effect of calcium acetate during high-temperature pyrolysis with the aid of a molecular dynamic simulation technique.

These studies provide an understanding of the individual effects of AAEMIEs-carboxylate salts. However, the literature on the effects of composites of either calcium acetate, ferrous acetate, magnesium acetate or ferrous acetate on the pyrolytic product yields and distribution during the pyrolysis of partially oxidised coal fines waste is insufficient. These AAEMIEs-carboxylate salts exist in coal in ternary and quinary forms, and they may interact with each other and with inherent mineral matter at 400 °C to form artefacts [8] with diverse pyrolysis mechanisms. In addition, others could also react with the carbon matrix and extraneous minerals at elevated temperatures, further facilitating the pyrolysis reaction mechanisms.

In this investigation, the demineralisation and density separation methods only served as the physical and chemical procedures to separate distinct modes of occurrences of mineral matter and organic matter of FCR for application in the pyrolysis experiments to determine their effects in the pyrolysis mechanisms. As a result, a study was conducted to evaluate the effects of a composite of three carboxylate salts (calcium, ferrous and magnesium acetates) on the distribution of pyrolytic products of Highveld partially oxidised FCR and its selected beneficiated residue. This study extends to evaluating interactions between the carboxylate salts in FCR, demineralised FCR (FCRD), and demineralised >1.9 g/cm^3 sink fraction (SI1.9D). Moreover, the addition of a suitable ratio of these acetate salts could be utilised as co-feedstock of this suggested pyrolysis process to the FCR samples in order to assist in better understanding the effects of the carboxylate salts on pyrolytic product yields and distribution during the pyrolysis of FCR. To achieve the objective of this novel study, Fischer assay experiments [4] of these selected samples were conducted along with mineralogical analyses (X-ray diffraction (XRD) and high-resolution transmission electron microscopy (HRTEM)), chemical analyses (proximate, ultimate, Inductively coupled plasma-mass spectroscopy (ICP-MS), ^{13}C nuclear magnetic resonance (^{13}C NMR), gas chromatography-

mass spectrometry (GC-MS), GC-MS scan, Fourier transform infrared (FTIR)) and thermogravimetric (TG) analyses.

5.2 Materials and Methods

5.3 FCR Sampling and Preparation

Sample preparation procedures [4, 15] were followed to take 250 kg FCR of a representative sample from a South African thermal export plant (TEP) disposal site in the Highveld coalfield of the Mpumalanga Province, South Africa. The 1.9 g/cm^3 sink fraction (Sl1.9) was obtained by performing density separation of the FCR [4, 15]. The Sl1.9D and FCRD samples were obtained by subjecting the Sl1.9 and FCR samples to sequential leaching using 10 mol/dm^3 (M) HCl and 22 M HF sourced from Minema Chemicals, as described in a previous study [4]. This was done to obtain FCRD and Sl1.9D with varying contents of carboxylate salts for pyrolysis experiments. FCR contains carboxylate salts lower than 1 wt. % [16]. The samples dried at 105 °C were stored in a nitrogen environment before pyrolysis experiments and characterisation.

5.4 Preparation of Blends of Coal and Ca/Fe^{2+}/Mg-acetate Composite

Analytical grade calcium acetate monohydrate ($Ca(C_2H_3O_2)_2$), magnesium acetate tetrahydrate ($Mg(CH_3COO)_2.4H_2O$) and ferrous (Fe (II)) acetate ($Fe(C_2H_3O_2)_2$) supplied by Sigma Aldrich were used to prepare a composite material in a Ca: Mg: Fe mass ratio of 1:1:1. The composite was mixed with either FCR, FCRD or Sl1.9D to obtain three samples with 18 wt. % of Ca/Mg/Fe-acetate composite (CSC) and 82 wt. % of either FCR, FCRD or Sl1.9D by grinding them to obtain homogenised <75 µm particles. The Ca/Mg/Fe-acetate composite samples were labelled FCR+CSC, FCRD+CSC, or Sl1.9D+CSC. They were stored in a nitrogen environment before use.

5.5 Pyrolysis Experiments

Figure 5-1 below summarises the steps taken during this investigation. The pyrolysis experiments were carried out using a Fischer-assay double retort set-up at an average internal temperature of 500 °C and an internal heating rate of 5 °C/min for 3 hours. Char and tar yields of SA Highveld feed coals decrease with an increase in temperature from 450 to 900 °C [4, 17]. Therefore, in the current study, the pyrolysis temperature of 500 °C was selected based on the results obtained from these two studies [4, 6]. The full description of the Fischer-assay set-up and the start-up procedure can be found elsewhere [4, 17]. In summary, each retort was filled with 35 g ±0.5 g of sample, sealed, and carefully placed in the oven. Oxygen was

expelled from the retorts by purging with nitrogen baseline 5.0 (99.995%) supplied by AFROX (PTY) Ltd. Nitrogen gas was allowed to flow at 2 NL/hr for 10 minutes and was stopped once heating was initialised to minimise dilution of evolved gases. This procedure was repeated for each sample and their repeat runs.

The tar collection chamber comprised of four Dreshel bottles (2 for each retort) submerged in ice and filled with toluene (99%, CC Imelmann cc). The condensed water containing traces of volatile organic compounds (VOCs) and semi-volatile organic compounds (SVOCs) (gas-liquor) was separated from the tar and toluene mixture using a Dean-Stark distillation set-up. A Buchi R100 rotor vapour set-up equipped with a Buchi V100 vacuum pump was used to separate the tar-toluene mixture at 55 °C and 75 mbar for 30 minutes or until no toluene condensation was visible in the receiving chamber. The char, gas, tar, and gas-liquor proportions were calculated using their masses and presented on a dry ash-free basis (daf) [4].

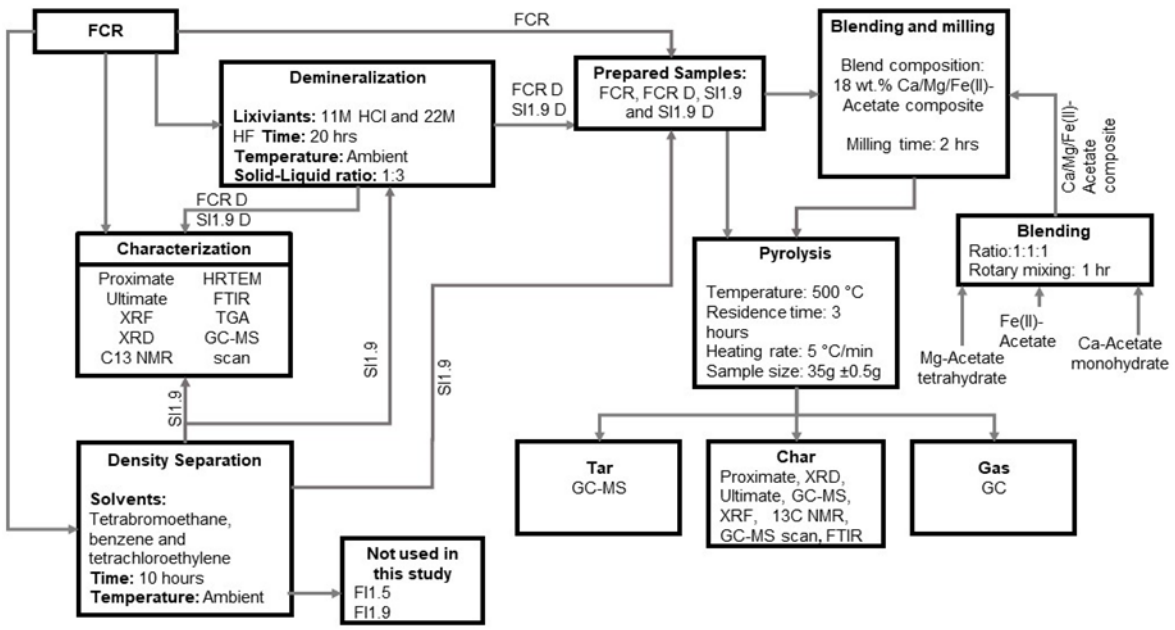

Figure 5-1: A schematic diagram of the sampling and preparation, and experimental procedure (note: Fl1.5 = <1.5 g/cm^3 float and F1.9 = <1.9 g/cm^3 float).

5.6 Analytical Methods and Sample Characterisation

FCR+CSC, FCRD+CSC, Sl1.9D+CSC and SI1.9D, along with their corresponding chars, were pulverised to <75 µm and submitted to Bureau Veritas Testing and Inspections South Africa (Pty) Ltd. for proximate, ultimate, and sulphur analyses using the ISO standard methods: ISO 17246:2010, ISO 17247:2020 and ISO 334:2020 for coal analyses, respectively. The proportions of inorganic elements in the ashes derived from the blends and SI1.9D samples,

along with their corresponding chars, were determined by SGS-South Africa (Pty) Ltd ICP-MS in accordance with ASTM D6349-1. The chemical, mineralogical and TGA results for FCR, FCRD, SI1.9 and their chars are presented and discussed elsewhere [4,15].

The analytical procedures developed and described by Speakman [18] and Rietveld [19] were adopted to determine the proportions of crystalline and amorphous phases in the SI1.9D sample and blended composites as well as their derived chars using an XRD analytical instrument. The FCR microstructural analysis was conducted using a JEOL JEM 2100 LaB6 HR-TEM operated at 200 kV, which included elemental analysis with an attached Oxford Instruments energy dispersive spectroscopy (EDS) detector at Nelson Mandela University [20].

The composition of pyrolytic tars was measured by an Agilent 7890 GC-MSD gas GC coupled with a 5975 Triple Axis MSD detector [21]. The composition of non-condensable gases was characterised by a Perkin Elmer Clarus 500 GC coupled with a sample loop/valve and a TCD cell. Only chemical components (hits) with detection quality above 89% were considered. The analysis was performed in triplicates, and the averages of the relative peak areas were considered.

The structural parameters of FCR and its char were determined by a ^{13}C (solid-state) NMR technique using a Varian VNMRS 500 MHz two-channel spectrometer coupled with 4 mm zirconia rotors in length aided with a 4 mm probe (Chemagnetics TM T3 HX Y magic angle spinning (MAS)) at the University of the Western Cape. The detailed method adopted for the analyses has been published elsewhere [22, 23]. The GC-MS scan analysis (i.e. solvent extraction followed by GC-MS measurements) [8] was followed to characterise VOCs and SVOCs in FCR and its derived chars. The ground samples (FCR, FCRD or SI1.9D) were subjected to a Brukker Vertex 70 FTIR analysis to determine their major functional groups. The FTIR measurements of samples mixed with potassium bromide at a 1:100 ratio was performed from 4500 to 500 cm^{-1} at a resolution of 4 cm^{-1}. A total of 25 scans were performed for the background analysis, and another 25 scans were performed for the sample analysis.

5.7 Results and Discussion

5.7.1 Proximate, Ultimate, and ICP Analyses

The proximate and ultimate results of samples labelled FCR, FCRD, FCRD+CSC, SI1.9D+CSC and SI1.9D, along with their corresponding chars, are presented in Table 5-1. The results for FCR have been published and can be found elsewhere [15]. The ash yield (AY) in the FCRD and SI1.9D samples was 3.0 wt. %, suggesting that only a small proportion of

inherent nano-mineral-matter (nano-inherent minerals and carboxylate salts) [8] is insoluble in HF and HCl solutions. Also, HF reacts with aluminium from the kaolinite lattice to form insoluble non-crystalline solid phases (hydrated fluoro-complex) containing Al^{3+}, $Al(OH)_2^+$, Si^{4+} and H_3O^+ on the leached kaolinite surface [24]. These proximate analysis results in Table 1 are consistent with those of South African coals and their density-separated fractions [8, 15]. Expectedly, the inherent moisture (IM), ash yield (AY), and fixed carbon (FC) contents increased with the addition of CSC to the FCR samples. The volatile matter (VM) content in the FCR blends decreased, while the chars comprised higher proportions of FC and AY and lower contents of IM and VM compared to their unheated counterparts because of dehydration, devolatilisation, and decomposition of organic functional groups to produce light organic compounds [21,25].

The ultimate results indicate that the proportions of C in the FCR+ CSC and SI1.9D +CSC blends increased by 3% in the corresponding chars and decreased by 7% in the FCRD+CSC char. The H content decreased in the chars of all samples, while the N content in the blends and their chars remained similar. A decrease in carbon content in the FCR D+CSC blended char, as well as an increase in C content in FCR/SI1.9D+CSC blended chars, could be attributed to the reactions of remnant mineral acids with carboxylic acid functional groups to release CH_4, H_2, CO, CO_2 and C_2H_6 during pyrolysis [10]. Also, calcium acetate thermally decomposes at between 170 °C and 180 °C compared to magnesium acetate (285 - 365 °C) and ferrous acetate (260 - 328 °C) to produce CaS, MgS, FeS, ketones, CO_2 and H_2, respectively under nitrogen [26–28].

Table 5-1: Proximate and ultimate results for FCR, FCRD, SI1.9D and their blends with CSC, and their corresponding chars.

Sample	Proximate results wt.% (adb)				Ultimate results wt.% (daf)				
	IM	AY	VM	FC*	C	H	N	S	O*
FCR	2.0	29.9	22.7	45.5	78.7	4.5	1.9	2.0	12.6
FCR Char	1.1	33.3	13.5	52.2	84.8	3.2	2.3	8.7	1.1
FCR+CSC	4.6	32.9	24.9	37.7	82.7	7.0	1.6	n.a	8.7#
FCR+CSC Char	0.8	39.7	13.9	45.6	85.6	1.2	1.4	n.a	11.8#
SI1.9D	5.1	3.0	28.5	63.4	75.2	4.2	2.0	1.1	17.5
SI1.9D Char	0.7	4.4	11.7	83.2	82.8	2.4	2.1	0.9	10.9
SI1.9D+CSC	8.1	7.3	29.3	55.2	79.9	6.7	1.6	0.9	10.9
SI1.9D+CSC Char	1.2	10.4	11.9	76.5	73.6	2.5	2.0	1.0	20.9

Sample	Proximate results wt.% (adb)				Ultimate results wt.% (daf)				
	IM	AY	VM	FC*	C	H	N	S	O*
FCRD	3.9	3.0	26.7	66.4	78.7	4.4	2.1	1.2	13.6
FCR D Char	2.0	1.8	13.2	83.1	86.5	3.0	2.3	7.5	0.7
FCRD+CSC	6.6	9.3	28.7	55.5	82.7	6.9	1.7	0.8	7.9
FCRD+CSC Char	1.7	12.7	12.0	73.6	75.5	2.4	2.1	0.8	19.2

*Note: adb – air dry basis, daf – dry ash free basis, n.d. – not analysed, * – calculated by difference (O=100-C-H-N-S), CSC – carboxylate salts composite, IM – inherent moisture, AY – ash yield, VM – volatile matter, FC – fixed carbon, # – residual (Oxygen+sulphur).*

The composition of inorganic elements (in their oxide forms) in the ashes of FCRD, FCRD, FCR+CSC, SI1.9D+CSC and SI1.9D, along with their derived chars, is presented in Table 5-2. The SI1.9D sample contains a higher proportion of Fe than other samples, indicating the presence of insoluble Fe-bearing mineral matter in the SI1.9 sample. As expected, the addition of CSC increased the Fe, Mg, and Ca proportions in FCR, SI1.9D and FCRD blend samples. The proportion of Fe increased only in the FCRD+CSC sample, while a reduced Fe content was obtained for SI1.9D+CSC and FCRD+CSC. This anomaly in Fe contents can be attributed to the oxidation of Fe^{2+} to form Fe^{3+} by the solubilised Fe^{2+} from Ferrous acetate and the subsequent formation of $FeCl_3$ and FeF_3 [29]. The ferric chloride and ferric fluoride formed possibly volatilised during the ashing of FCRD+CSC and SI1.9D+CSC at 1000 °C for ICP analysis [30, 31]. As a result, caution must be taken when assessing the proportions of Fe in these samples. In addition, Ferrous in the blends of CSC and either FCRD or SI1.9D oxidised to form ferric ions at pH values > 4.5 during the preparation of these blends [32, 33]. These ions can also react with OH^- (produced from the hydrolysis of either acetate or coal moisture) to form colloidal precipitates (FeOCl, $FeCl_3/F_3$, $Fe(OH)_3$) at pH values >4.5 during the sample preparation for the ICP analysis. The ICP analysis cannot detect these ferric colloids, resulting in lower proportions of Fe in the ashes of FCRD/SI1.9D+CSC blends.

Minor proportions of Mg, Na, K, Ti, Mn, and S are reported in all samples and seemingly increased in the chars due to the devolatilisation of the organic fractions. Due to sample limitations, S was not analysed for FCR+CSC FCR+CSC Char samples (Table 5-1). Also, the CSC significantly increased the proportion of S in the FCRD+CSC and SI1.9D+CSC blend chars, due to the reactions of Ca/Mg/Fe(II) species from the decomposition of either $Ca(C_2H_3O_2)_2$ or $Mg(CH_3COO)_2.4H_2O$ or $Fe(C_2H_3O_2)_2$ and H_2S at 500 – 900 °C to form nano-CaS, nano-MgS, nano-FeS, and S-bearing non-crystalline solid phases formed on the blend char surfaces (Table 5-2), together with the evolution of H_2 and CO_2 respectively under

nitrogen [34,35]. The size of sulphides formed ranged between 0.03 µm and 10 µm. As a result, the CSC addition, which contains Fe, Ca and Mg, is surmised to increase carbon conversion and gas yield during earlier stages of pyrolysis.

Table 5-2: ICP results of the ashes for FCR, FCRD, SI1.9D and their blends with CSC and their corresponding chars.

Elements	SiO_2	Al_2O_3	CaO	Fe_2O_3	MgO	TiO_2	K_2O	Na_2O	P_2O_5	SO_3
FCR	48.6	27.9	7.6	4.3	2.0	1.3	1.1	0.8	0.7	5.6
FCR Char	48.5	27.3	7.4	4.2	2.0	1.2	1.1	1.1	0.7	6.5
FCR+CSC	37.7	21.4	11.8	9.6	6.7	1.0	0.8	0.7	0.6	9.6
FCR+CSC Char	38.5	19.5	14.3	9.3	6.8	1.0	0.8	0.9	0.5	8.5
SI1.9D	10.0	14.2	4.8	44.3	4.2	7.7	0.2	3.7	0.7	10.2
SI1.9D Char	4.4	19.5	4.6	47.6	6.0	8.2	0.1	3.7	0.5	5.2
SI1.9D+CSC	2.2	1.8	19.2	23.8	17.6	1.1	0.0	0.6	0.1	33.5
SI1.9D+CSC Char	1.5	1.5	20.3	28.8	17.9	1.6	0.0	0.5	0.1	27.6
FCRD	5.3	16.6	5.8	51.6	1.7	7.3	0.1	2.0	0.7	8.9
FCR D Char	4.8	16.5	6.1	49.3	1.9	6.9	0.0	2.3	0.6	11.6
FCRD+CSC	0.8	1.8	22.6	29.1	19.5	0.9	0.0	0.5	0.1	24.8
FCRD+CSC Char	1.4	1.7	18.5	26.4	16.6	0.9	0.0	0.6	0.1	33.7

Note: CSC – carboxylate salts composite

5.7.2 XRD Analysis

XRD results for samples labelled FCR, FCRD, SI1.9D+CSC, FCR D+CSC and SI1.9D and their corresponding chars are presented in Table 5-3. FCR comprised 30 wt. % crystalline phases, while FCRD and SI1.9D, as expected, are comprised mainly of amorphous phases up to 94 wt. %. The diffractograms of the samples are presented in Figure 5-2. As expected, SI1.9D and its char are comprised mainly of amorphous phases (94% and 95%). A higher proportion of amorphous phases in SI1.9D result from kaolinite/quartz/ microcline/illite distortion and dissolution in the HF/HCl aqueous solution to form amorphous phases [24] during demineralisation. The presence of trace mineral matter (MM) is associated with insoluble inherent pyrite/siderite/kaolinite cleats, AAEM-carboxylate salts, and organic sulphur, as reported in a previous study [4]. As expected, the addition of CSC diluted the MM in FCR, but had little effect on the traces of MM proportions in FCRD and SI1.9D. As shown in Table 5-3, FCR+CSC and its char are comprised mainly of kaolinite ($Al_2Si_2O_5(OH)_4$) and

quartz (SiO_2) with lesser proportions of dolomite ($CaMg(CO_3)_2$), microcline ($KAlSi_3O_8$), calcite ($CaCO_3$), magnetite, gypsum ($CaSO_4.2H_2O$) and pyrite (FeS_2). Traces of goyazite ($SrAl_3(PO_4)(PO_3OH)(OH)_6$), illite ($(K,H_3O)(Al,Mg,Fe)_2(Si,Al)_4O_{10}[(OH)_2,(H_2O)]$) and anatase ($TiO_2$) were also detected by XRD. Upon pyrolysis, pyrrhotite ($Fe_{(1-x)}S$) and periclase (MgO) traces were detected in the chars, possibly due to the transformation of pyrite or H_2S in-situ capturing by CSC and dolomite respectively [36].

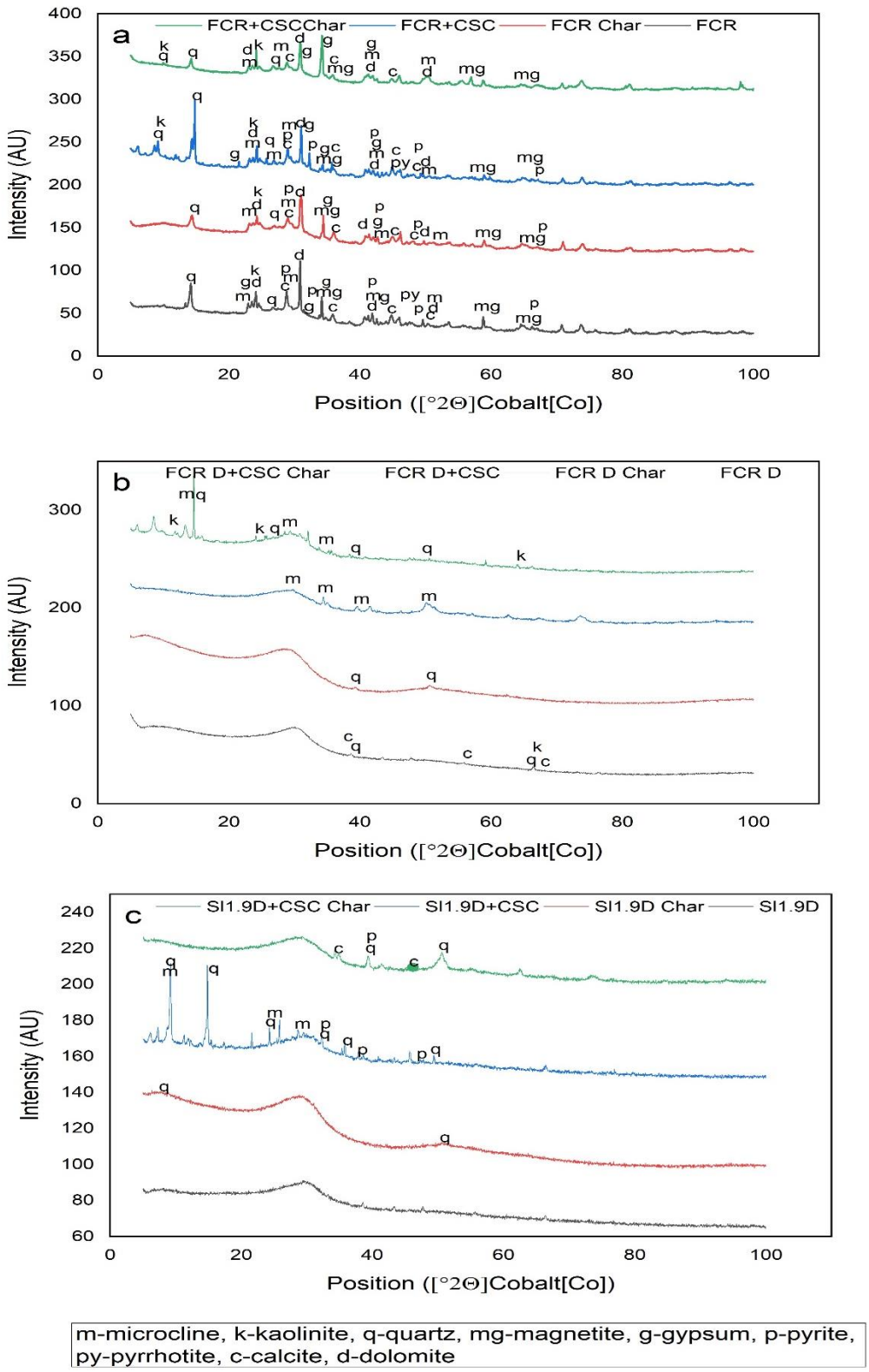

Figure 5-2: Diffractograms of FCR, FCRD, SI1.9D, their blends with CSC, and their corresponding chars.

Table 5-3: Proportions of crystalline and amorphous phases of the CSC blends and SI1.9 D, and their chars.

Mineral (wt. %)	Kao	Qua	Dol	Mic	Cal	Mag	Gyp	Pyr	Goy	Ill	Ana	Per	Pyrr	OC	Total Amo	MM	Tot
FCR	18.3	6.6	1.6	1.5	1.4	0.4	0.3	0.3	0.1	0.1	0.1	0.0	0.0	55.5	13.9	30.6	100.0
FCR Char	16.4	7.8	3.1	1.4	1.9	0.3	0.1	0.0	0.0	0.5	0.2	0.0	0.1	58.5	9.7	31.8	100.0
FCR+CSC	15.9	6.0	1.0	3.1	0.5	0.3	0.2	0.3	0.2	0.6	0.3	0.0	0.0	40.3	31.4	28.2	100.0
FCR+CSC Char	10.3	4.8	1.6	1.2	2.2	0.5	0.0	0.0	0.1	0.2	0.1	0.7	0.3	43.5	34.5	22.0	100.0
SI1.9D	0.0	0.0	0.0	0.0	0.0	0.0	0.0	0.0	0.0	0.0	0.0	0.0	0.0	6.5	93.5	0.1	100.0
SI1.9D Char	0.0	0.1	0.0	0.0	0.0	0.0	0.0	0.0	0.0	0.0	0.0	0.0	0.0	4.5	95.3	0.2	100.0
SI1.9D+CSC	0.0	0.1	0.0	0.2	0.0	0.0	0.0	0.1	0.0	0.0	0.0	0.0	0.0	7.9	91.8	0.4	100.0
SI1.9D+CSC Char	0.0	0.1	0.0	0.0	0.1	0.0	0.0	0.0	0.0	0.0	0.0	0.1	0.2	13.5	85.9	0.6	100.0
FCRD	-	0.2	-	-	-	-		0.1	-	-	-	-	-	5.8	93.8	0.4	100.0
FCRD Char	0.0	0.2	0.0	0.0	0.1	0.0	0.0	0.0	0.0	0.0	0.0	0.0	0.1	8.6	90.9	0.5	100.0
FCRD+CSC	0.2	0.1	0.0	0.1	0.0	0.0	0.1	0.0	0.0	0.1	0.0	0.0	0.0	12.7	86.7	0.7	100.0
FCRD+CSC Char	0.0	0.0	0.0	0.1	0.0	0.1	0.0	0.0	0.0	0.0	0.0	0.0	0.0	15.2	83.9	0.9	100.0

Note: Kao-Kaolinite, Qua-quartz, Dol-dolomite, Mic-microcline, Cal-calcite, Mag-Magnetite, Gyp-gypsum, Pyr-pyrite, Goy-Goyazite, Ill-Illite, Ana-anatase, Rut-rutile, Per-periclase, Pyrr-pyrrhotite, Total Amo- total amorphous phases (organic carbon(OC) + metakoalinite + illite/microcline amorphous), MM-mineral-matter, Tot-total.

5.7.3 HRTEM Analysis

The FCR sample was subjected to HRTEM measurements to study the presence of fine crystalline phases and their association with the carbon matrix. The presence of the major coal minerals reported by XRD, such as kaolinite and quartz, was confirmed by HRTEM analysis across 33 selected test spots with nano-minerals. Figure 5-3 illustrates the position of nano-minerals (200-500 nm) associated with coal-macerals [8, 11, 15], while Table 5-4 presents the mineral-element matrix and detection counts for each mineral. Minor minerals such as dolomite, calcite, microcline, rutile/anatase, pyrite, gypsum, and hematite (Fe_2O_3) were also observed. Also, nano-siderite ($FeCO_3$) traces were observed in the HRTEM analysis but not in the XRD. This behaviour could be associated with nano-$FeCO_3$, which the XRD analysis cannot detect. The HRTEM detected nano-cleat minerals with intimate association with macerals (vitrinite, inertinite) [15], especially dolomite, calcite, and pyrite cleats, which may catalyse pyrolysis reactions, leading to high carbon conversion [4].

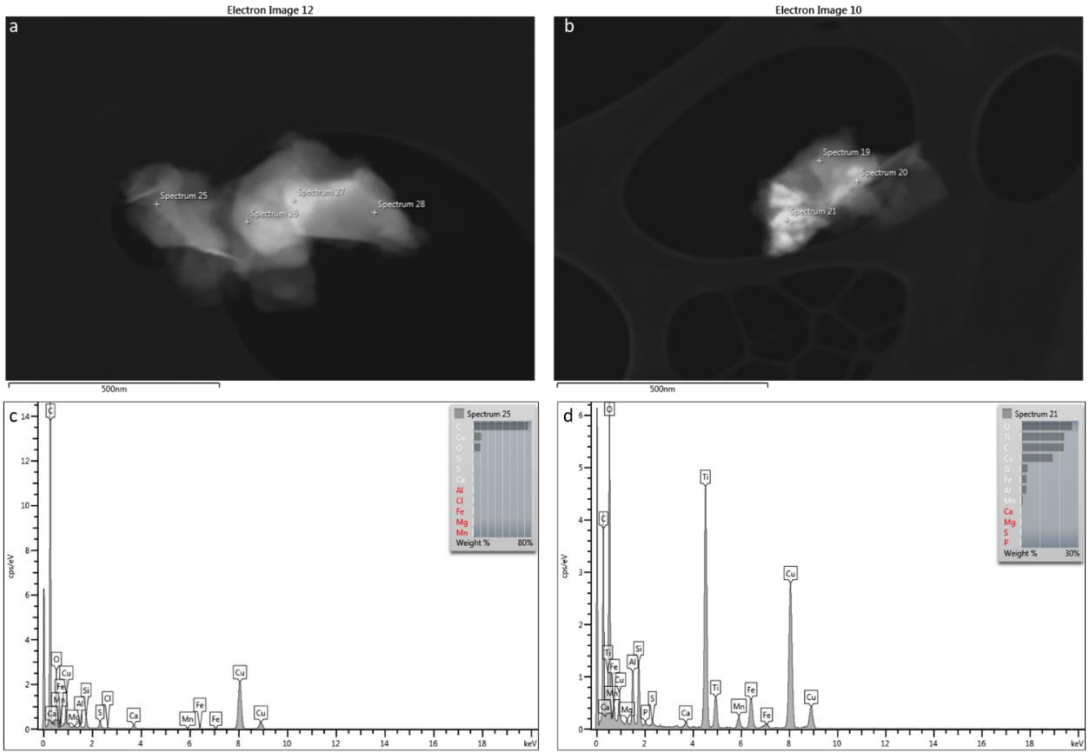

Figure 5-3: HRTEM (a&b) images of FCR showing nano-mineral particles and selected detection spots and (c&d) the spectra of 2 points presenting major elements.

Table 5-4: Mineral-element matrix based on HRTEM spectra counts for FCR.

Mineral	**Kao**	**Qua**	**Cal**	Dol	**Pyr**	**Gyp**	**Hem**	**Rut/Ana**	**Mic**	**Sid**
Al	√								√	
Si	√	√							√	
Ca			√	√		√				
Mg				√						
Ti								√		
Fe					√		√			√
K									√	
S					√	√				
C			√	√						√
O	√	√	√	√		√	√	√	√	√
Counts	33	33	10	10	2	5	10	2	1	11

Note: √ - present, *Kao-Kaolinite, Qua-quartz, Dol-dolomite, Mic-microcline, Cal-calcite, hem-hematite, Gyp-gypsum, Pyr-pyrite, Ana-anatase, Rut-rutile, Sid-siderite.*

5.7.4 Organic Matrix Analysis

5.7.4.1 GC-MS scan (Solvent Extraction)

The GC-MS scan results provide information about solvent-extractable VOCs and SVOCs present in FCR and FCR char. As presented in Table 5-5, low to mid-boiling range organic compounds such as toluene, tribromoethene, naphthalene and 1-methylnaphthalene were detected in the FCR extract. The lower boiling range organic compounds observed in the char consisted of toluene, tetrachloroethylene, benzaldehyde and tribromoethene. Naphthalene and 1-methylnaphthalene were devolatilised during pyrolysis of FCR and reported to tar. As a result, there were no observable peaks of naphthalene and 1-methylnaphthalene in the FCR char extract. Furthermore, tetrachloroethylene and benzaldehyde were not detected in FCR, but observed in its char. The former compound may derive from Cl addition pathways to intermediate acetyl radicals [37] and the latter from cleavage of phenylacetaldehyde, respectively [38].

Table 5-5: GC-MS scan results for FCR and its pyrolytic char.

Compound name	Retention time	FCR	FCR char
Toluene	4.34	√	√
Tetrachloroethylene	5.5		√
Benzaldehyde	11.61		√
Tribromoethene	11.96	√	√
Naphthalene	17.97	√	
Naphthalene, 1-methyl	19.13	√	

Note: √ - present

5.7.4.2 FTIR Analysis

The major peaks of the FTIR spectra in Figure 5-4 for the chars obtained from pyrolysis of FCR, FCRD, SI1.9D and their blends with CSC were interpreted and assigned in accordance with the literature [39–42]. A summary of the peak assignments and the centre points associated with every peak is presented in **Table C3** (Annexures C). The FCRD and FCR spectra show major differences in the 3700-3600 /cm and the 1200-900 /cm regions. The strong peak at 3700-3600 /cm is caused by the OH from kaolinite/illite/gypsum, while the strong peak at 1200-900 is caused by Si–O–Si vibrations in quartz for the FCR sample [42,43]. These peaks were not recorded for the SI1.9D and FCRD due to the distortion and dissolution of minerals by HF and HCl. The XRD and FTIR results are in good agreement in this regard. A small peak at around 3100-2980 /cm associated with the =C-H in aromatic and unsaturated hydrocarbon is observed across all samples. The broad band at 1740-1658 /cm was ascribed to the C=O-O stretching vibrations by carboxylic acids, aldehydes, amides and esters. The sharp peaks at 1600-1500 /cm were associated with the C=C by alkenes and benzenes in cyclic aromatics compounds such as naphthalene, reported by the GC-MS scan results. The peaks at 1450-1400 /cm are associated with the bending vibrations of the -CH_3 of the aliphatic compounds.

While peak intensities varied, the positions of peaks in the organic matrix of all samples remained nearly consistent, implying a limited impact of the demineralization by HCl/HF lixiviants on the organic matrix of the coals. The association of the C=O–O peak with aldehydes agrees with the GC-MS scan results of the FCR char, which showed the presence of benzaldehyde. The carboxylic acids, unsaturated hydrocarbons, benzenes, aldehydes and esters are the precursors of organic compounds in the pyrolytic tars.

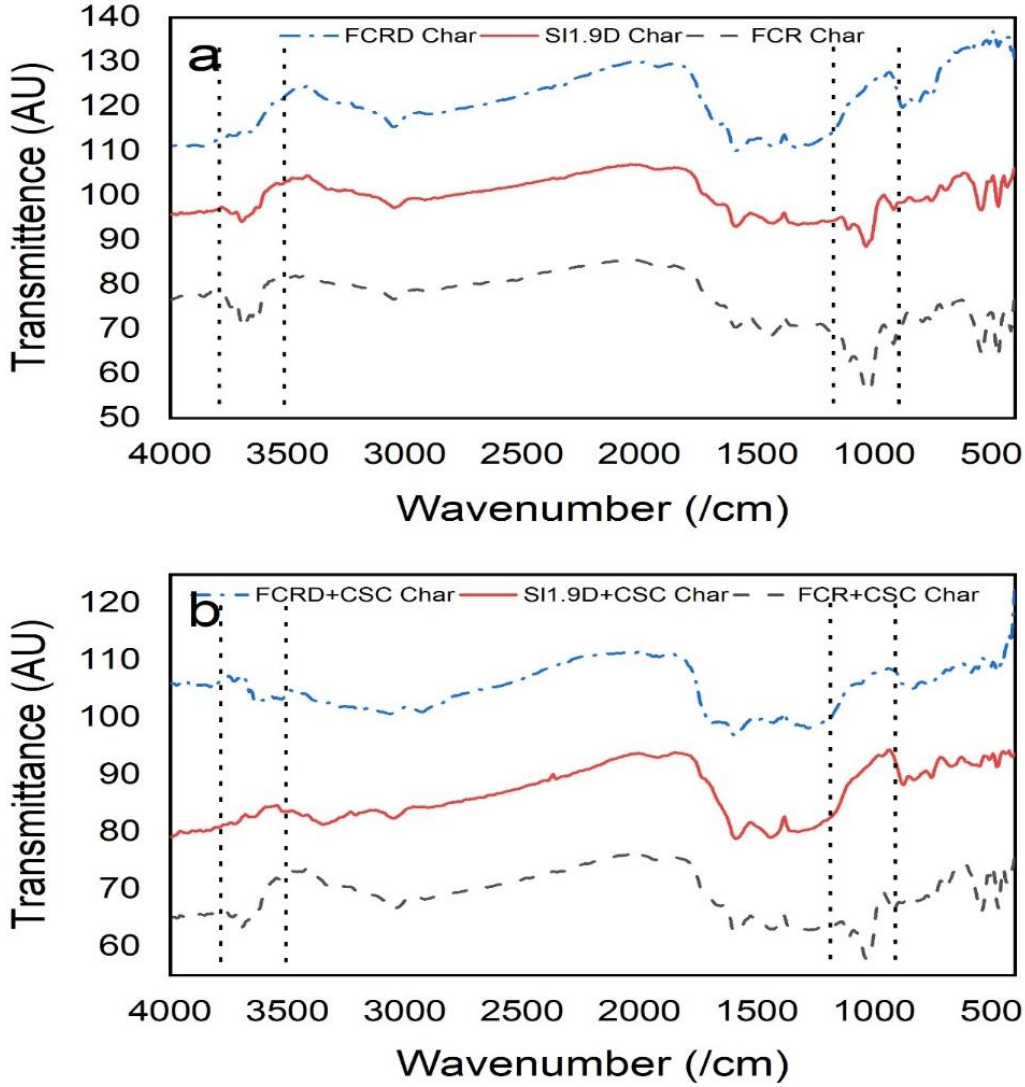

Figure 5-4: FTIR spectra of (a) FCR, FCRD and SI1.9D chars, and (b) FCR+CSC, FCRD+CSC and SI1.9D+CSC chars obtained at 500 °C.

5.7.5 ^{13}C Nuclear Magnetic Resonance

The structural parameters obtained from solid-state NMR analysis of FCR and its derived char obtained at 500 °C are presented in Table 5-6. The structural parameters indicate that FCR consists mainly of aromatic carbons (64%) and only 34% aliphatic. These proportions are common amongst SA vitrinite-rich coals, which have been investigated in the past [42-44]. This technique also estimated the presence of carbonyl, phenolic and alkylated aromatic carbons. The char comprises lesser fractions of aliphatic, phenolic, and alkylated carbons due to the devolatilisation and decomposition of these organic structures during pyrolysis. The ^{13}C NMR spectra of the char shifted towards a Lorenztian characteristic peak, which illustrates the

aromatisation of the carbon matrix. Similar to the study by Strydom et al. [42] no measurable differences were observed for the protonated and bridgehead carbons between FCR and its derived char; therefore, these structural parameters were not reported. These results provide insight into the transformation of the coal organic matrix during pyrolysis.

Table 5-6: Structural parameters obtained by ^{13}C NMR of FCR and FCR Char.

Parameter	FCR	FCR Char
f_a	0.64	0.74
f_a*	0.51	0.54
f_{al}	0.36	0.26
f_{al}^O	0.01	0.01
f_a^{CO}	0.01	0.02
f_a^P	0.03	0.02
f_a^S	0.08	0.07

*Note: f_a – total fraction of aromatic carbon, f_a *- fraction of aromatic carbons excluding carbons bonded to oxygen, f_{al} – total fraction of aliphatic carbons, f_{al}^O – aliphatic carbons bonded to oxygen, f_a^{CO} – fraction of carbons bonded to oxygen, f_a^P – fraction of phenolics, f_a^S – fraction of alkylated carbons.*

5.7.6 TGA

The thermal decomposition profiles for the samples labelled FCR+CSC, SI1.9D+CSC and SI19 D, presented in Figure 5-5, illustrate a change in the pyrolysis mechanisms and rates of decomposition. Sample SI1.9D had a 33.4 wt.% mass loss. Table 5-7 summarises the characteristic parameters estimated from the analytical pyrolysis experiments. A significant increase in mass loss was obtained for the FCR+CSC and SI1.9D+CSC blend samples compared to a 1 wt. % decrease for the FCRD+CSC blend sample. Although Ca/Mg/Fe-acetate salts decompose at temperatures ranging from 170 °C to 370 °C [26–28], their contribution to the overall mass losses of the samples labelled FCR+CSC, SI1.9D+CSC and FCRD+CSC is not obvious. In addition, the in-situ capturing of H_2S by CSC form Ca/Mg/Fe sulphides, S-bearing amorphous phases, C, CH_4 and CO can be associated with mass loss/increase during pyrolysis [34, 35]. As a result, these reported increases in mass loss obtained upon the addition of CSC to FCR and SI1.9D could not solely be associated with the catalytic effect of Ca, Mg and Fe from the CSC, but the possible change in the physical structure of the inertinite in the SI1.9D sample by demineralisation [45] and synergy between the mineral matter in FCR and CSC [46]. In the

presence of Fe, Ca facilitates the removal of water and nitrate compounds, which could lead to an increased mass loss [47]. The FCRD and SI1.9D samples comprise different modes of occurrence of inherent mineral matter associated with different proportions of macerals. The decomposition of pyrite, dolomite, calcite cleats and carboxylate salts and their association with vitrinite and inertinite [11, 15] could account for the differences observed in the mass loss of these samples.

The derivative thermogravimetry (DTG) graphs in Figure 5-5d illustrate this behaviour clearly. This behaviour could be associated with the change in the chemical composition and structure of the FCRD and SI1.9D samples by the lixiviants used during demineralisation. Mineral matter in coal has been associated with the clogging of surface pores, which impedes the transport of intermediate vapours [48]. Also, the interaction of the intermediate vapours with the hot ash layer and intermediate char may lead to secondary repolymerisation, consequently reducing mass loss percentages. This phenomenon is especially true in the case of the samples studied because a previous study [4] revealed that removing extraneous minerals and non-mineral inorganics increased the CO_2 surface area of FCR, which creates channels for vapour transport.

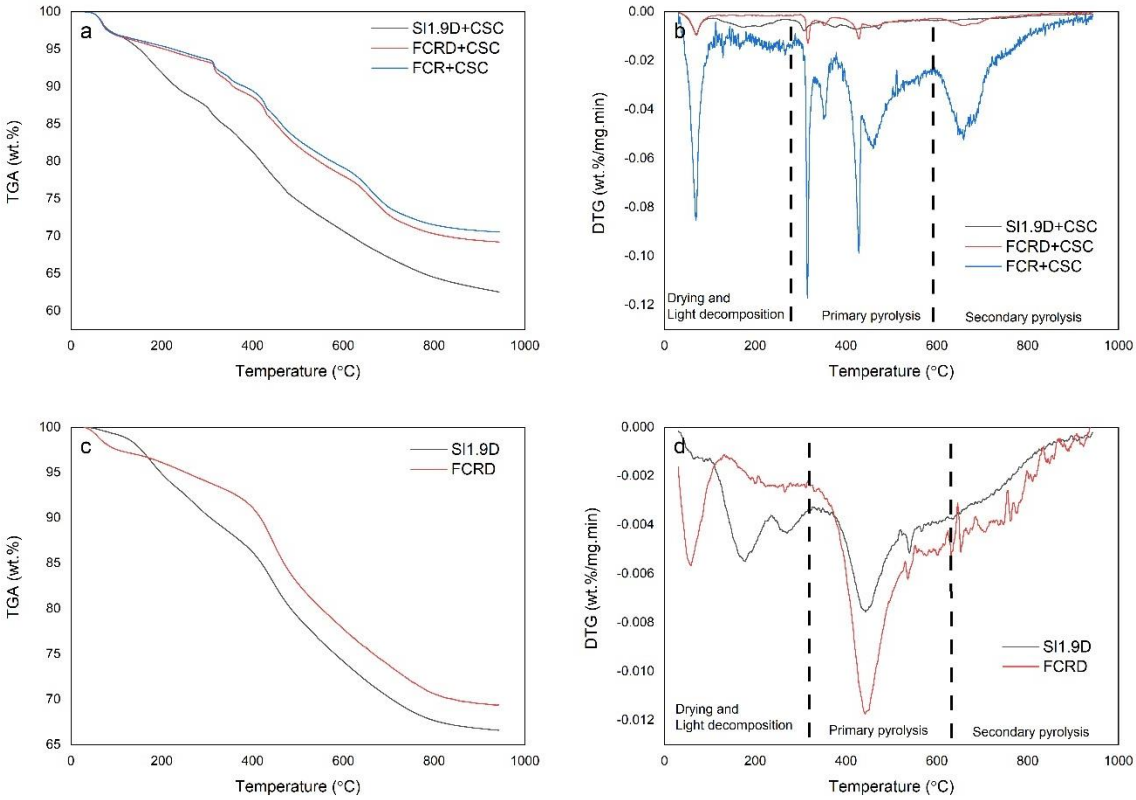

Figure 5-5: The (a & c) thermogravimetry and (b & d) derivative thermogravimetry plots for the CSC blends and SI1.9D.

The addition of CSC led to a significant change in the decomposition rates due to possible interaction with extraneous minerals and non-mineral inorganics in the FCR, SI1.9D and FCRD samples along with in-situ capturing of H_2S. Acetate decomposition exhibits a deficiency in mineral matter and demonstrates the lowest values of mass loss, which are closely comparable. The DTG graphs in Figure 5-5c also show the highest decomposition rate for FCR+CSC, which hints at possible synergistic interactions between CSC and extraneous minerals, non-mineral inorganics, and inherent cleat minerals. These findings suggest that CSC improves the rate of decomposition and pyrolysis reactions.

Table 5-7: Pyrolysis characteristic parameters for CSC blends and Sl1.9D.

Sample	Temperature (°C)						Rate of decomposition (1000x%/mg.min)					ΔW (wt.%)
	T_i	T_{m1}	T_{m2}	T_{m3}	T_{m4}	T_f	R_{m1}	R_{m2}	R_{m3}	R_{m4}	R_{av}	
FCR	316	444	-	-	-	605	9.3	0.0	0.0	0.0	2.4	-
FCR+CSC	288	316	351	428	460	592	116.9	43.8	98.7	55.9	24.3	5.6
Sl1.9D	349	443	-	-	539	519	7.6	5.2	-	-	3.3	-
Sl1.9D+CSC	288	308	375	421	471	592	7.8	6.3	7.1	6.9	3.8	5.6
FCR D	315	442	-	-	536	530	11.7	6.2	0.00	0.00	3.7	-
FCR D+CSC	299	316	351	428	467	592	12.9	5.6	11.1	5.9	2.8	-1.0

Note: Ti - the temperature at which the main decomposition started, T_{m1} – first peak temperature in the main pyrolysis zone, T_{m2} – second peak temperature in the main pyrolysis zone, T_{m3} – third peak temperature in the main pyrolysis zone, T_{m4} - fourth peak temperature in the main pyrolysis zone, R_{m1} – the first peak rate of decomposition, R_{m2} – the second peak rate of decomposition, R_{m3} – the third peak rate of decomposition, R_{m4} – the fourth peak rate of decomposition, Rav – the average rate of decomposition, ΔW – change in mass loss (e.g.

$\Delta W = W_{FCR+CSC} - W_{FCR}$).

5.7.7 Pyrolytic Product Yields

The char yields generated from pyrolysis of the FCR+CSC, SI1.9D+CSC, FCRD+CSC and, SI1.9D samples are presented in Figure 5-6a on a dry ash-free basis. The extraneous minerals in FCR, removed by the demineralisation method, reduced the carbon conversion, leading to a higher char yield. This behaviour suggests the contribution of the inherent mineral matter to catalyse pyrolysis reactions. To be precise, adding CSC lowered char yield and increased carbon conversion, confirming the catalytic action of carboxylate salts during coal pyrolysis. A previous study [4] on the effect of extraneous minerals revealed a decrease in carbon conversion with the addition of calcium hydroxide, magnesium oxide, and ferric oxide. This comparison indicates that inherent carboxylate salts catalyse carbon conversion reactions while extraneous minerals impede the process. Although the highest carbon conversion was obtained for the FCRD+CSC blend, the highest carbon conversion gain of 15.9% was obtained for FCR+CSC, versus 2.8% for FCRD+CSC. This behaviour suggests the presence of synergy between the CSC and mineral matter in FCR towards coal carbon recovery.

The highest tar yield was obtained for sample FCRD+CSC, as shown in Figure 5-6b. Inversely, the highest gas yield was recorded for FCRD+CSC due to CSC decomposition and in-situ capturing of H_2S by CSC. The higher surface area obtained by demineralising FCR improves the transport of intermediate vapours, favouring the formation of gas products over char and tar [4]. These results are in agreement with other studies on SA coals [21]. The SI1.9D sample produced higher gas yields due to the decomposition of kaolinite, calcite, and dolomite by residual HCl/HF (Figure 5-6c). Coal mineral matter, especially AAEM associated with inherent mineral matter, is beneficial for impeding repolymerisation reactions by the protonation of free radicals, which leads to the formation of stable tar components [49-51]. HRTEM results in Figure 5-3 and Table 5-4 confirmed the presence of these AAEM associated with the coal carbon matrix, which supports the retardation of free radicals by coal mineral matter. The absence of extraneous minerals (kaolinite, dolomite, calcite, quartz) in the FCRD sample is linked to the increased gas yield and reduced tar yield during pyrolysis [4]. The decrease in tar yields in the FCR+CSC and FCRD+CSC blends further confirms the above claim. Comparing the SI1.9D and SI1.9D+CSC samples shows an insignificant difference in the tar yields. The gas yield increases, which supports the view that kaolinite, calcite, and dolomite retard free radical formation. These results suggest that adding a suitable amount of CSC can influence pyrolysis mechanisms, improve carbon conversion, and gas yields, and reduce tar yields, potentially lowering the risk of blockages in downstream processes.

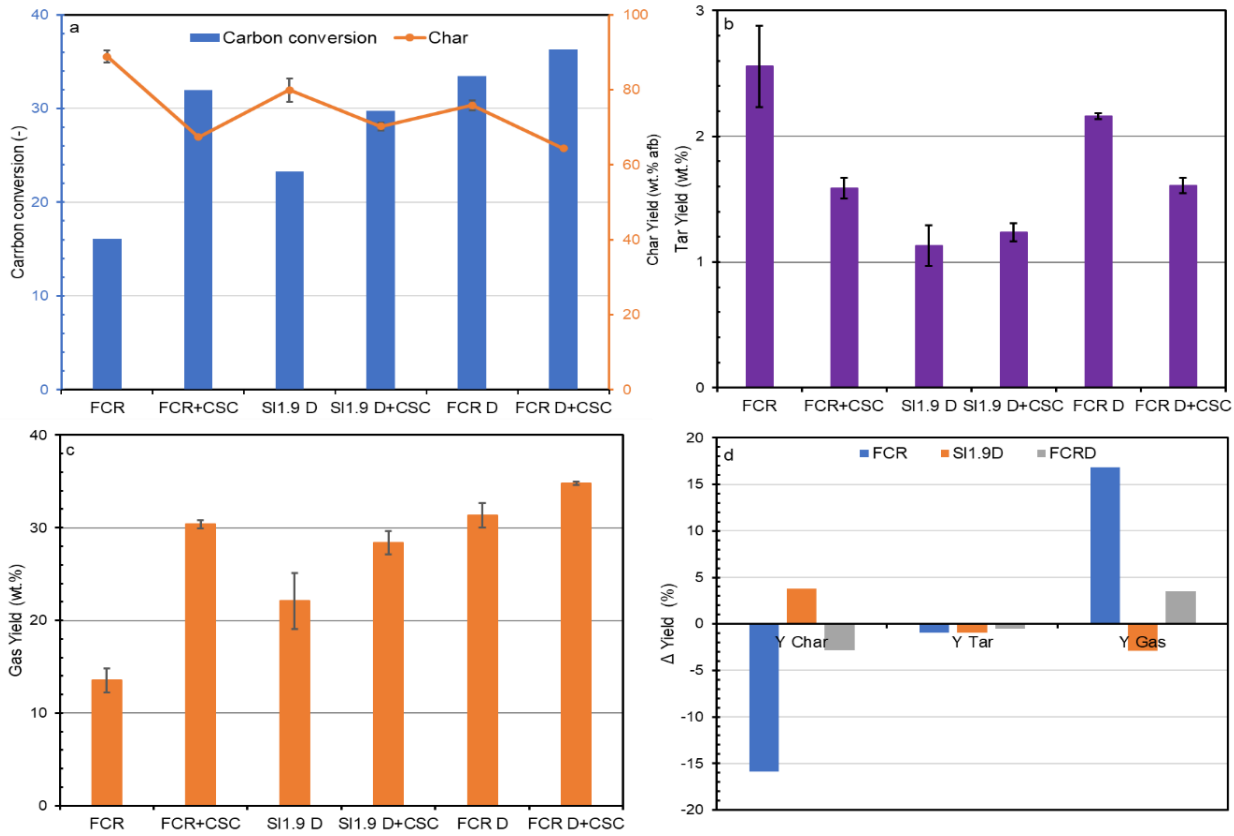

Figure 5-6: Yields of (a) char, (b) tar, (c) gas and (d) change in product yield from pyrolysis of CSC blends and SI1.9 D. Note: ΔY – change in product yield (e.g., ΔY_char=Y_(char FCR+CSC)-Y_Char FCR).

These findings agree with literature studies on the influence of AAEM and carboxylate salts [52–54]. The interaction between different minerals and non-mineral inorganic components such as CSC in coal, can promote or hinder decarboxylation and repolymerisation, affecting the types of products formed during pyrolysis processes [55]. According to [51–53], the sulphur, Fe, Ca and Mg contribute to reaction pathways by forming free radicals and undergoing transformations during heating or pyrolysis.

5.7.7.1 Tar Composition

The composition of tars obtained from pyrolysis of the CSC blends and SI1.9D at 500 °C were investigated by GC-MS measurements. Only compounds with a fit quality greater than 89% were considered. The relative peak area percentages (RA %) were used to compare tar components. The compounds were grouped into chemical families, as indicated in Figure 5-7a&b. The proportions of aliphatic hydrocarbons were unaffected by demineralisation, but the addition of CSC increased their proportions in all samples. The increase in aliphatic hydrocarbons could be

associated with the decomposition of CSC to produce aliphatics, ketones, CO_2, H_2 and Ca/Mg/Fe-oxides [47, 56]. Polycyclic aromatic hydrocarbons were higher in the demineralised samples, highlighting the minimisation of repolymerisation reactions by mineral matter in FCR. These polycyclic aromatic hydrocarbons increased upon the addition of CSC to FCR but decreased for the SI1.9D+CSC and FCRD+CSC samples. This behaviour narrows the promotion of polycyclic aromatic hydrocarbons to extraneous minerals, which agrees with the findings from previous work on extraneous minerals [4]. As a result, inherent mineral matter, such as carboxylate salts, inhibits the formation of polycyclic aromatic hydrocarbons by catalysing the scission of aliphatic esters to form radicals. These radicals are retarded by H^+ to form aliphatic compounds during SI1.9D+CSC and FCRD+CSC pyrolysis. In addition, Strydom et al. [42] reported changes in the surface morphology of the organic matrix of SA coals due to the mineral acid leaching. These changes contribute to the different pyrolytic product distributions that are obtained.

The presence of naphthalene and alkyl-naphthalenes in the tars can be ascribed to devolatilisation mechanisms more than precursor transformation due to their presence in FCR, as indicated by the GC-MS scan results. The highest proportion of alkyl-phenols and alkyl-naphthalene in the tar of the SI1.9D+CSC blend sample could be associated with the interaction between CSC and inertinite macerals. This conclusion is based on the fact that a smaller change in RA% of alkyl-phenols and alkyl-naphthalene is observed in the case of FCRD+CSC. The RA% of Alkyl-Benzenes was low in the SI1.9D sample and disappeared almost entirely for the FCR+CSC, SI1.9D+CSC, and FCRD+CSC blends, indicating the suppression of benzyl radical attack by CSC to form polycyclic aromatic compounds [57]. Yu et al. [53] report the reforming of alkyl groups by AAEM, which causes delays in the evolution of coal carbon conversion. This behaviour may affect the char structure and increase carbon conversion.

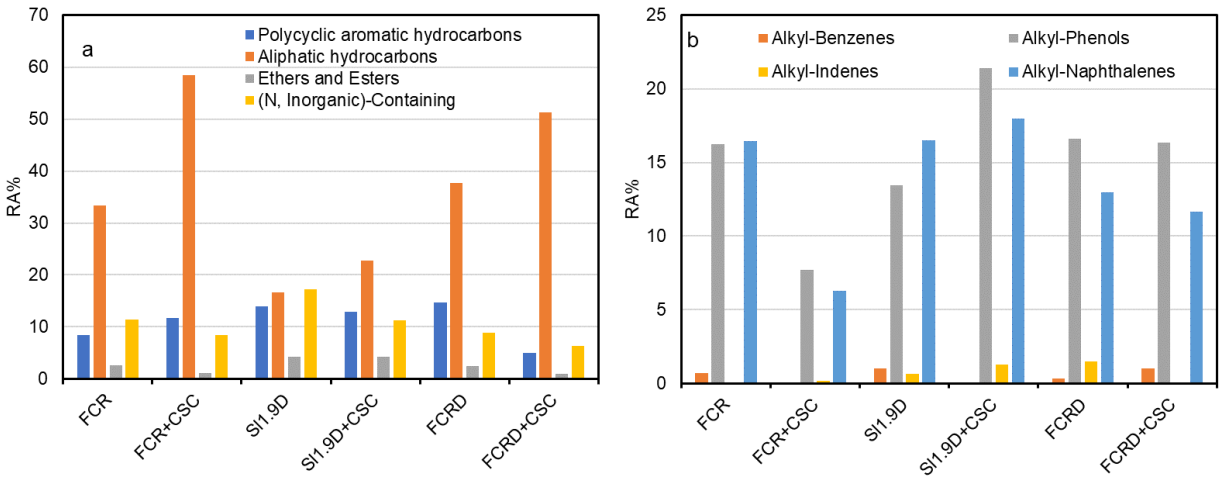

Figure 5-7: Distribution of chemical compounds in pyrolytic tars of CSC blends and SI1.9D.

5.7.7.2 Gas Composition

The proportions of non-condensable gases represented in Figure 5-8 illustrate the effect of CSC addition on FCR, FCRD and SI1.9D pyrolysis reaction pathways. The major pyrolytic gas products comprised CH_4, H_2, CO, CO_2 and C_2H_6. The SI1.9D sample produced a higher proportion of CH_4, CO and CO_2, but lower H_2 and C_2H_6 compounds than the FCRD data [4]. This behaviour is associated with the catalytic cracking of intermediate vapour by transforming inherent kaolinite and nano-mineral carbonate cleats [4, 8]. The improved transport of intermediate vapours without secondary interaction with extraneous clays and carbonates in the demineralised samples is also a contributor [21]. Also, higher gas (CH_4, CO, CO_2) yields are associated with in-situ capturing of H_2S to form S-bearing amorphous phases [34, 35] and decomposition of acetates [26–28] in the CSC blends during pyrolysis.

The addition of CSC to the SI1.9D sample increased the proportions of CH_4 and CO_2 while reducing the CO, H_2, and C_2H_6, possibly due to the breakdown of C_2H_6 followed by methanation reactions. Although previous studies [58] linked the decomposition of CSC and its interaction with extraneous kaolinite to CO_2 generation, this was not the case in this study. This behaviour could be associated with the interaction between intermediate volatiles and free $H^{\bullet}$ radicals to form CH_4. This observation was similar for the FCR [4] and SI1.9D samples, indicating that the addition of CSC promotes the formation of CH_4 over H_2 via possible interaction with inherent cleat minerals

and acetate decomposition [59, 60]. The decrease in CO_2 generation for FCRD+CSC and FCR+CSC is attributed to the CSC addition to the FCR and FCRD samples.

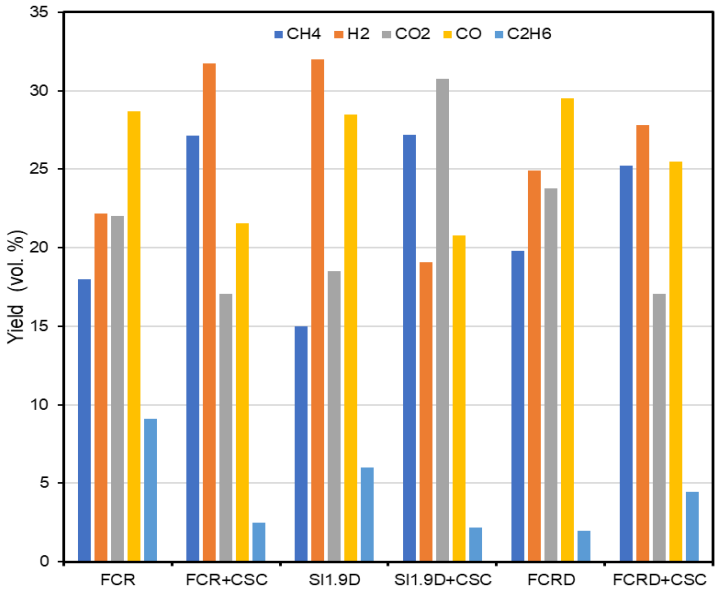

Figure 5-8: Distribution of non-condensable gases during pyrolysis of CSC blends and SI1.9D.

5.8 Conclusions

A study was conducted to assess the impact of carboxylate salts on pyrolysis by introducing CSC. In summary, inherent carboxylate salts catalyse carbon conversion while extraneous minerals impede it. The following points summarise the conclusions drawn from this study.

- HRTEM confirmed the presence of siderite, calcite and pyrite cleats in FCR, along with kaolinite/quartz proportion reduction by demineralisation to form a non-crystalline solid phase with Al^{3+}, $Al(OH)_2^+$, Si^{4+} and H_3O^+.
- The coal char produced at 500 °C exhibits reduced fractions of aliphatic carbons, attributed to devolatilisation and decomposition mechanisms that take place during pyrolysis. Furthermore, FTIR, GC-MS scans, and ^{13}C NMR analyses complement one another in determining tar precursors, their functional groups, and carbon associations in coal.
- Carboxylate salts interact with coal-inherent minerals and H_2S to improve carbon conversion during pyrolysis.

- The diverse modes of occurrence of inherent pyrite, kaolinite, siderite, dolomite, calcite, and carboxylate salts present in the SI1.9D sample contribute to variations in mass loss during heating. The primary decomposition temperature of the SI1.9D sample suggests changes in chemical composition and structure induced by HF/HCl to form an amorphous phase during demineralisation. The removal of extraneous kaolinite and quartz facilitates channels for vapour transport. It minimises secondary repolymerisation, which could explain the observed differences in mass loss percentages among the studied samples.
- Carboxylate salts increase carbon conversion and gas yield but decrease tar and char yields due to in-situ capturing of H_2S by $Ca(C_2H_3O_2)_2$, $Fe(C_2H_3O_2)_2$ and $Mg(CH_3COO)_2$ to form nano-CaS/nano-MgS/nano-FeS and S-bearing amorphous solid phase, and increase C, CO, CH_4 and H^+ transfer which retards intermediate radicals.
- The pyrolysis of carboxylate salts-saturated coal reduces levels of polycyclic aromatic compounds and alkylated phenolic and naphthalene compounds.
- The addition of CSC to the FCR and SI1.9D samples increases CH_4 and CO_2 formation in the gas phase. However, it decreases CO, H_2, and C_2H_6, possibly due to the C_2H_6 breakdown followed by methanation reactions and decomposition of acetates. As a result, these trends are associated with the potential breakdown reactions of C_2H_6 followed by methanation by inherent pyrite, calcite, and siderite cleats.

This study demonstrates that the behaviour of carboxylate salts depends on the presence of other mineral matter and the dominating maceral groups. Also, higher carbon conversion can be expected upon the addition of CSC, along with a decrease in phenolics and naphthalene compounds. These results provide insight into the pyrolytic effects of the mode of occurrence of mineral matter in coal and FCRs. The results may be helpful for coal blending strategies and the utilisation of coal with high concentrations of inherent mineral matter, especially carboxylate salts. A study on the effects of pyrolysis temperature, the concentration of salts of carboxylic acids and the individual effects of Ca, Fe and Mg acetates on pyrolytic product yields, artefacts crystallisation, and composition is recommended.

5.9 Acknowledgements

The authors would like to express their appreciation to Dr Sabine Verryn of XRD analytical and consulting cc, Morne Van Zyl of SGS, Secunda, Dr Xolisa Goso and Napo Ntsasa of Mintek, Willem Swanepoel of Bureau Veritas, Dr Roelf Venter and Louisa Hattignh of North-West University, and Prof. Edith Antunes of the University of the Western Cape for their assistance with different aspects of the analytical techniques used in this study. This work was financially supported by the National Research Foundation (NRF) [Coal Research Chair Grant no. 86880] and the NRF free-standing bursary MND200715544211/UID: 136078). Opinions, findings, and conclusions or recommendations expressed in any publication generated by the NRF supported research is that of the author(s) alone, and the NRF accepts no liability whatsoever in this regard.

The next chapter is a summary of conclusions drawn from this study, the contributions made to science and engineering, and recommendations for future studies.

Chapter References

[1] The Presidency, National Planning Commission. National Development Plan 2030: Our future - make it work. 2012.

[2] Liu Y, Cheng L, Zhao Y, Ji J, Wang Q, Luo Z, et al. Transformation behaviour of alkali metals in high-alkali coals. Fuel Processing Technology. 2018; 169:288–94.

[3] Isaac K, Bada SO. The co-combustion performance and reaction kinetics of refuse derived fuels with South African high-ash coal. Heliyon. 2020; 6:e03309.

[4] Mphahlele K, Matjie RH, Bunt JR. Catalytic effect of reactive extraneous mineral composites on char and tar distribution during pyrolysis of Highveld partially oxidised fine-coal reject and Its beneficiated residues. ACS Omega. 2023; 8:36479–92.

[5] Bin Saidin HS. Reduction of Malaysian iron ore pellet by using coal as reductant [Masters Thesis]. Penang, Malaysia: Universiti Sains Malaysia; 2013.

[6] Pretorius GN, Bunt JR, Gräbner M, Neomagus H, Waanders FB, Everson RC, et al. Evaluation and prediction of slow pyrolysis products derived from coals of different rank. Journal of Analytical and Applied Pyrolysis. 2017; 128:156–67.

[7] He R, Deng J, Deng X, Xie X, Li Y, Yuan S. Effects of alkali and alkaline earth metals of inherent minerals on Fe-catalysed coal pyrolysis. Energy. 2022; 238 Part C: 121985.

[8] Rautenbach R, Matjie RH, Strydom CA, Bunt JR, Ward CR, French D, et al. Evaluation of mineral matter transformations in low-temperature ashes of South African coal feedstock samples and their density separated cuts using high-temperature X-ray diffraction. International Journal of Coal Preparation and Utilisation. 2020; 40:320–47.

[9] Ali J, Kazi TG, Baig JA, Afridi HI, Arain MS, Ullah N, et al. Monitoring of arsenic fate with proximate parameters and elemental composition of coal from Thar coalfield, Pakistan. J Geochem Explor. 2015; 159:227–33.

[10] Kou JW, Bai ZQ, Bai J, Guo ZX, Li W. Effects of mineral matter and temperatures on conversion of carboxylic acids and their derivatives during pyrolysis of brown coals. Fuel Processing Technology. 2016; 152:46–55.

[11] Matjie RH, Li Z, Ward CR, Bunt JR, Strydom CA. Determination of mineral matter and elemental composition of individual macerals in coals from Highveld mines. Journal of the Southern African Institute of Mining and Metallurgy. 2016; 116:169–80.

[12] Grigore M, Sakurovs R. Inorganic matter in Victorian brown coals. International Journal of Coal Geology. 2016; 154:257–64.

[13] Nisar J, Awan IA, Iqbal M, Abbas M. Pyrolysis–gas chromatography of lakhra coal: Effect of temperature and inorganic matter on the product distribution. Iranian Journal of Chemistry and Chemical Engineering 2019; 38:297–305.

[14] Hong D, Cao Z, Guo X. Effect of calcium on the secondary reactions of tar from Zhundong coal pyrolysis: A molecular dynamics simulation using ReaxFF. Journal of Analytical and Applied Pyrolysis. 2019; 137:246–52.

[15] Mphahlele K, Matjie RH, Bunt JR, Uwaoma RC. Properties and reactivity of two oxidised and unoxidised South African Highveld fine coal rejects and their density-separated fractions. International Journal of Coal Preparation and Utilisation. 2023; 43:1451–77.

[16] Raghoo M. The volatilisation of aluminium and silicon species from a Highveld coal [PhD thesis]. Potchefstroom, South Africa: North-West University; 2010.

[17] Roets L, Bunt JR, Neomagus HWJP, Van Niekerk D. An evaluation of a new automated duplicate-sample Fischer Assay setup according to ISO/ASTM standards and analysis of the tar fraction. Journal of Analytical and Applied Pyrolysis. 2014; 106:190–6.

[18] Speakman SA. Introduction to PANalytical X'Pert HighScore Plus v3. 0. MIT Center for Materials Science and Engineering. 2012:1–19.

[19] Rietveld HM, IUCr. A profile refinement method for nuclear and magnetic structures. Urn: Issn: 0021-8898 1969; 2:65–71.

[20] Janse van Vuuren A, Mutali A, Ibrayeva A, Sohatsky A, Skuratov V, Akilbekov A, et al. High-energy heavy ion tracks in nanocrystalline silicon nitride. Crystals. 2022; 12:1410.

[21] Roets L, Strydom CA, Bunt JR, Neomagus HWJP, Niekerk D Van. The effect of acid washing on the pyrolysis products derived from a vitrinite-rich bituminous coal. Journal of Analytical and Applied Pyrolysis. 2015; 116:142–51.

[22] Solum MS, Sarofim AF, Pugmire RJ, Fletcher TH, Zhang H. ^{13}C NMR analysis of soot produced from model compounds and a coal. Energy and Fuels. 2001; 15:961–71.

[23] Pugmire RJ, Solum MS, Grant DM. ^{13}C Solid-state NMR of Argonne premium coals. Energy & Fuels. 1989; 3:187–93.

[24] Semmens B, Meggy AB. The reaction of kaolin with fluorides. II. Effect of aqueous hydrofluoric acid. Journal of Applied Chemistry. 1966; 16:125–8.

[25] Solomon PR, Serio MA, Suuberg EM. Coal pyrolysis: Experiments, kinetic rates and mechanisms. Progress in energy and combustion science. 1992; 18:133–220.

[26] de Souza AO, Biondo V, Ivashita FF, de Souza Nunes GC, Paesano Jr A. Structural and magnetic characterisation of nanostructured iron acetate. Orbital: The Electronic Journal of Chemistry. 2017:261–5.

[27] Landoll M. Ketone production from the thermal decomposition of carboxylate salts [PhD thesis]. Texas, USA: Texas A&M University; 2012.

[28] Galwey AK, Brown ME. Thermal decomposition of ionic solids: chemical properties and reactivities of ionic crystalline phases. Amsterdam, The Netherlands: Elsevier; 1999.

[29] Rezaei SE, Sadrnezhaad SK. Fluoride precipitation of Cu over Fe in a selected pH window. International Journal of Engineering. 2019; 32:424–9.

[30] Wang Y, Liu R, Wan Y. Thermal reaction properties of aluminum/iron fluoride nanothermites. Journal of Thermal Analysis and Calorimetry. 2023; 148:5297–308.

[31] Šima J. Structure-related melting and boiling points of inorganic compounds. Foundations of Chemistry. 2016; 18:67–79.

[32] Hem JD, Skougstad MW. Coprecipitation effects in solutions containing ferrous, ferric, and cupric ions. Washington DC: US Government Printing Office; 1960.

[33] Matjie RH, Bunt JR, Van Heerden JHP. Extraction of alumina from coal fly ash generated from a selected low rank bituminous South African coal. Minerals Engineering. 2005; 18:299–310.

[34] Nimmo W, Agnew J, Hampartsoumian E, Jones JM. Removal of H_2S by spray-calcined calcium acetate. Ind Eng Chem Res. 1999; 38:2954–62.

[35] Reed JJ. The NBS tables of chemical thermodynamic properties: Selected values for inorganic and C1 and C2 organic substances in SI units; 1989.

[36] Matjie RH, Lesufi JM, Bunt JR, Strydom CA, Schobert HH, Uwaoma R. In situ capturing and absorption of sulphur gases formed during thermal treatment of South African coals. ACS Omega. 2018; 3:14201–12.

[37] Taylor PH, Dellinger B. Pyrolysis and molecular growth of chlorinated hydrocarbons. Journal of Analytical and Applied Pyrolysis. 1999; 49:9-29.

[38] Fong LC, Yaylayan VA. Model studies on the oxygen-induced formation of benzaldehyde from phenylacetaldehyde using pyrolysis GC-MS and FTIR. Journal of Agricultural and Food Chemistry. 2008; 56:10697–704.

[39] Lambert JB. Introduction to organic spectroscopy. New York: MacMillan; 1987.

[40] Mphahlele K, Matjie RH, Osifo PO. Thermodynamics, kinetics and thermal decomposition characteristics of sewage sludge during slow pyrolysis. Journal of Environmental Management. 2021; 284:112006.

[41] Qian L, Xue J, Tao C, Ma C, Jiang X, Guo F. Effect of demineralisation on pyrolysis characteristics of LPS coal based on its chemical structure. International Journal of Coal Science & Technology. 2023; 10:21.

[42] Strydom CA, Bunt JR, Schobert HH, Raghoo M. Changes to the organic functional groups of an inertinite rich medium rank bituminous coal during acid treatment processes. Fuel Processing Technology. 2011; 92:764–70.

[43] Koech L, Everson RC, Hattingh B, Rutto H, Lerotholi L, Neomagus HW. Comparative study of sorbents for spray dry scrubbing of SO_2 from flue gases. ACS Omega. 2023; 8:23401–11.

[44] Phiri Z, Everson RC, Neomagus HWJP, Wood BJ. Transformation of nitrogen functional forms and the accompanying chemical-structural properties emanating from pyrolysis of bituminous coals. Appl Energy. 2018; 216:414–27.

[45] Song Q, Zhao H, Jia J, Yang L, Lv W, Gu Q, et al. Effects of demineralisation on the surface morphology, microcrystalline and thermal transformation characteristics of coal. Journal of Analytical and Applied Pyrolysis. 2020; 145:104716.

[46] Hattingh BB, Everson RC, Neomagus HWJP, Bunt JR. Assessing the catalytic effect of coal ash constituents on the CO_2 gasification rate of high ash, South African coal. Fuel Processing Technology. 2011; 92:2048–54.

[47] Clayton TW, Britt PF, Buchanan AC. Decarboxylation of salts of aromatic carboxylic acids and their role in cross-linking reactions. ACS Division of Fuel Chemistry, Preprints 2001; 46.

[48] Ahmad T, Awan IA, Nisar J, Ahmad I. Influence of inherent minerals and pyrolysis temperature on the yield of pyrolysates of some Pakistani coals. Energy Conversion and Management. 2009; 50:1163–71.

[49] He W, Liu Z, Liu Q, Ci D, Lievens C, Guo X. Behaviors of radical fragments in tar generated from pyrolysis of 4 coals. Fuel. 2014; 134:375–80.

[50] Yao Q, Ma M, Liu Y, He L, Sun M, Ma X. Pyrolysis characteristics of metal ion-exchanged Shendong coal and its char gasification performance. Journal of Analytical and Applied Pyrolysis. 2021; 155:105087.

[51] Wang W, Lemaire R, Bensakhria A, Luart D. Review on the catalytic effects of alkali and alkaline earth metals (AAEMs) including sodium, potassium, calcium and magnesium on the pyrolysis of lignocellulosic biomass and on the co-pyrolysis of coal with biomass. Journal of Analytical and Applied Pyrolysis. 2022; 163:105479.

[52] Shi Z, Jin L, Zhou Y, Li Y, Hu H. Online analysis of initial volatile products of Shenhua coal and its macerals with pyrolysis vacuum ultraviolet photoionisation mass spectrometry. Fuel Processing Technology. 2017; 163:67–74

[53] Yu J, Guo Q, Ding L, Gong Y, Yu G. Study on the effect of inherent AAEM on char structure evolution during coal pyrolysis by in-situ Raman and TG. Fuel. 2021; 292:120406

[54] Ward CR. Analysis and significance of mineral matter in coal seams. International Journal of Coal Geology. 2002; 50:135–68.

[55] Zhang C, Yan A, Guo H, Lei Y, Hao H, Liu F. DFT combined with XPS to investigate sulphur removal and sulphur-fixation mechanisms of copper oxide during coal pyrolysis and semi-coke combustion. Fuel. 2022; 317: 123482

[56] Jiang Y, Chen H, Mu X, He Z. Thermal decomposition of magnesium acetate in nitrogen. J. Phys.: Conf. Ser. 2020; 1653 012057

[57] Li W, Li WY, Wang XB, Feng J. Radical-induced pyrolysis mechanism in Cal–O and Cal–Cal bond cleavage. Fuel Processing Technology. 2022; 238:107494.

[58] Cheng H, Li K, Liu Q, Zhang S, Li X, Frost RL. Insight into the thermal decomposition of kaolinite intercalated with potassium acetate: An evolved gas analysis. Journal of Thermal Analysis and Calorimetry. 2014; 117:1231–9.

[59] Domazetis G, Raoarun M, James BD. Low-temperature pyrolysis of brown coal and brown coal containing iron hydroxyl complexes. Energy and Fuels. 2006; 20:1997–2007.

[60] Yang Y, Lin X, Chen X, Guo W, Wang Y, Zhang J, et al. Investigation on the effects of different forms of sodium, chlorine and sulphur and various pre-treatment methods on the deposition characteristics of Na species during pyrolysis of a Na-rich coal. Fuel. 2018; 234:872–85.

CHAPTER 6 SUMMARY OF CONCLUSIONS AND RECOMMENDATIONS.

6.1 Concluding Remarks

In this study, the mode of occurrence of coal mineral matter and the effects of mineral matter on coal pyrolytic product yields, mechanisms and product compositions have been investigated during pyrolysis. An investigation on the mineral matter liberation, mineral-maceral associations and the presence of nano-minerals has also been conducted. The discernment of different modes of occurrence of coal mineral matter was achieved by performing density separation, chemical fractionation, and demineralisation, which successfully separated extraneous minerals, inherent mineral matter, and dissolved all mineral matter (ions) except for cleat minerals, respectively. A simulation of extraneous minerals and the inherent mineral matter was done using reactive oxides and hydroxides composite, as well as via acetate salts composite. This study focused mainly on FCRs and the general conclusions and key findings derived from this study are discussed below.

6.1.1 Mode of Occurrence of Mineral Matter

The fuel properties of STEM and TEP samples are similar to those of South African feed coals to gasification and combustion units, except for the higher mineral matter content of up to 40%. Both samples contain fine and ultra-fine particles, with more than 60% of the particles smaller than 0.2 mm. Liberation of extraneous and cleat minerals from the carbon matrix by density separation to yield float fractions with up to 66 wt.% carbon content was achieved. The highest mineral matter liberation of 70% at an 83 wt. % recovery through density separation, is obtained for the TEP and STEM samples respectively. The prominence of kaolinite and quartz in the TEP, STEM and density-separated fractions was confirmed by XRD and Raman analyses. The XRD analysis further confirmed that TEP comprised higher proportions of fluxing minerals (i.e., dolomite, calcite, and pyrite) than the STEM sample. The TEP sample comprised half the carbominerite in STEM, but twice the vitrinite content, which obscured the reactivity implication of maceral groups. Also, cleat minerals, carbominerite and inorganic elements were confirmed by HRTEM analysis, which indicates the presence of siderite, calcite, and pyrite cleats in FCR. Demineralisation of FCR leads to the reduction of kaolinite/quartz, forming a non-crystalline solid phase with Al^{3+}, $Al(OH)^{2+}$, Si^{4+} and H_3O^+.

The 3 wt. % of ash yield obtained after demineralisation of TEP and TEP Sl1.9 density separated samples is associated with non-mineral inorganics and acid-recalcitrant cleat minerals. These residual inorganic materials led to higher carbon conversions during pyrolysis in the Fischer Assay

rig. Chemical fractionation of TEP produced a sample mainly of extraneous minerals, which provided insight into their effects on pyrolysis reactions. Furthermore, FTIR, GC-MS scans, and ^{13}C NMR analyses mutually complemented one another in determining tar precursors, their functional groups, and carbon associations in coal.

The contribution of all mineral matter towards carbon conversion is made evident by the lowest char yield of 78.8 wt. % for TEP, followed by its demineralised (86.5 wt. %) and chemical fractionated (95.2 wt. %) derived counterparts. The prominence of extraneous, non-mineral inorganics and inherent dolomite/calcite/ pyrite cleats in the TEP and chemically fractionated TEP samples support this statement.

6.1.2 Pyrolysis and CO_2-Gasification Reactivity

The high proportions of fluxing minerals (dolomite, calcite, and pyrite) in the TEP sample contribute to the 0.23 /min reaction rates which is slightly higher than the 0.18 /min for the STEM sample which makes TEP desirable as a feed material to gasifiers. The different maceral-maceral associations and maceral-mineral associations also contribute to superior reaction rates for TEP. The cleat minerals and extraneous minerals in TEP Sl1.9, STEM Sl1.9, TEP and STEM samples have faster initial gasification reaction rates which are associated with the catalytic activity of these mineral matter. Additionally, the prominence of non-mineral inorganics and inherent dolomite/calcite/ pyrite mineral cleats in FCR and Sl1.9 led to the highest tar yield of 5.7 and 5.1 wt. %, respectively. A higher carbon conversion is associated with the cleat minerals and inherent mineral matter in the Sl1.9 fraction. The primary decomposition temperature of the Sl1.9D sample suggests changes in chemical composition and structure induced by HF/HCl to form amorphous phases during demineralisation. The removal of extraneous kaolinite and quartz facilitates channels for vapour transport and minimises secondary repolymerisation, which could explain the observed differences in mass loss percentages among the studied samples.

6.1.3 The effects of Reactive Oxides and Hydroxide Composite

The pyrolysis behaviour of FCR, particularly on the yields and compositions of the derived pyrolytic tars and chars, as well as the apparent activation energy, is affected by the addition of 18 wt. % reactive oxides and hydroxide composite. Magnetite with catalytic effect was formed in the chars containing ROSH due to the Fe_2O_3 reduction. The XRD results showed the presence of artefacts of extraneous minerals (metakaolinite, calcite and dolomite (carbonation with $Ca(OH)_2$ and MgO)) in the ROSH blended chars during low-temperature pyrolysis. These artefact minerals have hindering effects leading to low tar yields. Pyrolysis of coal+ROSH blends produce tars with

lower molecular weight, indicating secondary cracking, dealkylation and hydrocracking of heavy tar components.

The highest inherent mineral-matter (non-mineral inorganics, organic Ca/Mg/Fe (carboxylate salts) and dolomite/calcite/pyrite cleats) contents in the SI1.9 fraction facilitated the conversion of the carbon matrix (low fixed carbon content) to volatile compounds during pyrolysis as shown by higher carbon conversion for the SI1.9 fraction compared with FCR.

Secondary reactions were facilitated by the presence and amount of extraneous ROSH and non-mineral inorganics present in FCR. The addition of ROSH composite to the FCR sample and FCR D sample increases the proportions of oxygen carriers, which inhibits dehydroxylation and deoxygenation reactions, but enhances secondary dealkylation and cracking to form aromatic and aliphatic compounds. The addition of ROSH composite to the FCR samples increases the average Ea values from 332.0 to 476.5 kJ/mol for FCR and from 323.4 to 544.4 kJ/mol for FCR D due to the initial dehydration of $Ca(OH)_2$ and reduction of Fe_2O_3.

6.1.4 The effects of Carboxylate Salts on Pyrolysis

Carboxylate salts interacted with coal-inherent minerals and H_2S to improve carbon conversion during pyrolysis. However, this behaviour of carboxylate salts depends on the presence of extraneous minerals and non-mineral inorganics along with the dominating maceral groups. With the addition of 18 wt. % of carboxylate salts composite (i.e., $Ca(C_2H_3O_2)_2$, $Fe(C_2H_3O_2)_2$ and $Mg(CH_3COO)_2$), the gas yield and carbon conversion increase while H_2S capturing is initiated. The in-situ H_2S capturing promotes the formation of nano-CaS/nano-MgS/nano-FeS and S-bearing amorphous solid phases and increases C, CO, and CH_4 and H^+ transfer which retards intermediate radicals.

Saturating FCR with a composite of acetate salts reduces the levels of polycyclic aromatic compounds and alkylated phenolic and naphthalene compounds in the pyrolytic tars and increases CH_4 and CO_2 formation in the gaseous phases derived from FCR and SI1.9D. Additionally, blending CSC with FCR and SI1.9D samples increases CH_4 and CO_2 formation in the gas phase, but decreases CO, H_2, and C_2H_6, possibly due to the C_2H_6 breakdown followed by methanation reactions and decomposition of acetates. As a result, these trends are associated with the potential breakdown reactions of C_2H_6 followed by methanation by inherent pyrite, calcite, and siderite cleats.

6.1.5 Achievements of Objectives and Aims

South African oxidised and unoxidised fine coal rejects comprise mineral matter composed of extraneous minerals, inherent minerals, non-mineral inorganics and organically associated inorganic elements. The majority of mineral matter in South African coals is associated with coal by static forces. This is because most of the mineral matter was liberated by density separation, despite the fine and ultra-fine nature of the FCRs. Also, the chemical fractionation method provided a clear discernment of these modes of occurrence by selective leaching.

The hypothesis of the ROSH addition to FCR to reduce carbon conversion percentages and increase activation energy values via carbonation reaction in the char was successfully proved during pyrolysis. The presence of extraneous minerals, reactive oxides, and hydroxides, along with non-mineral inorganics in FCR promote secondary reactions.

The addition of carboxylate salts to FCR successfully increased carbon conversion and gas yields, while producing chars with higher gasification reactivities and improving pyrolysis thermal efficiencies through the in-situ sulfur capturing reaction. Carboxylate salts such as calcium acetate, ferrous acetate and magnesium acetate inhibit the formation of polycyclic aromatic compounds and alkylated phenolic and naphthalene compounds in the pyrolytic tars. This is due to the retardation of free radicals and cracking of complex intermediate organic compounds during pyrolysis of a blend of coal and carboxylate salt composite. Methane and carbon dioxide gas formation is also promoted by the presence of carboxylate salt composite.

The aim and specific objectives of this study were carried out successfully and used to draw the final conclusions. The experimental procedures and techniques, along with the results, can be used for evaluating the mode of occurrence of coal mineral matter and their impact on pyrolysis reactions and pyrolytic products.

6.2 Contribution to Science

This work provides insight into the distribution and mode of occurrence of mineral matter and their effects on pyrolysis reaction mechanisms, along with the effects of cleat minerals and carboxylate salts during the utilisation of FCR in the global thermochemical processes. The following points are viewed as new contributions to understanding mineral matter, mode of occurrence and valorisation of fine-coal rejects:

- Fundamental differences in maceral and mineral matter differences between oxidised and unoxidised fine-coal rejects were discerned.

- Novel insights into decomposition profiles and gasification reactivities of unoxidised and oxidised fine-coal rejects, along with their density-separated fractions were obtained.
- The proposal of oxidised ultra-fine coal rejects recovery by density separation was evaluated.
- Discernment of the mode of occurrence of mineral matter in Highveld fine-coal rejects was elucidated.
- Yields and properties of product obtained from pyrolysis of fine-coal rejects and reactions facilitating carbon conversions was measured.
- The effects of carboxylate salts and reactive forms of major coal minerals during pyrolysis of fine-coal rejects was explained.
- Association and presence of nano-minerals and REEs by high-resolution transmission emission microscopy clarified.

6.3 Prospects and Recommendations

Although progress has been made in understanding the distinct nature of the mineral matter in SA Highveld fine-coal rejects from the thermal export plant, there is still an opportunity to advance this technology before commercial utilisation of fine-coal rejects in conventional boilers and gasifiers. The suggested next steps in fine-coal rejects research can involve;

Further studies on the effects of pyrolysis temperature, concentration of carboxylate salts, and individual effects of Ca, Fe, and Mg acetates on pyrolytic product yields are recommended.

- Further studies are needed on the effects of temperature, mineral proportions, and concentration of extraneous or inherent minerals on pyrolytic product yields.
- A study using a large particle/mass gasification of fine-coal rejects to evaluate gasification regimes and thermodynamic properties should be considered.
- The evaluation of fine ash and coarse ash particles obtained from the gasification of fine-coal rejects to assess the potential recovery of LREEs and HREEs present in these materials is needed.
- Blending strategies with feed coals and optimisation of blending ratios for maximum carbon conversion and energy recovery should be conducted.
- Research to evaluate the mechanisms driving the effects of mineral matter on coal pyrolysis, particularly focusing on extraneous minerals and their interactions with each other is an area that needs further attention.

By addressing these recommendations, it is possible to enhance the efficiency and sustainability of coal utilisation in thermochemical processes, mitigating environmental impacts and reducing disposal costs associated with fine-coal rejects.

ANNEXURES A: CHAPTER 3 SUPPLEMENTARY DATA

Table A1: Raw results for proximate and ultimate analyses for TEP and STEM samples, and their density-separated fractions

SGS

Address	4 Paul Kruger Road Trichardt 2311
Tel:	0826053903
Contact Persons	Kobus Janse van Rensburg

Client	North West University
Address	Potchefstroom
Contact Person	Dr. Henry Matjie
Contact Number	
Subject	TEP & STEM analysis
Date reported	12/01/2022

Test Report: Job number- 768/21-1

				Sample ID	TEP +0.5mm	TEP +0.5mm	TEP +0.5mm		STEM +0.5mm	STEM +0.5mm	STEM +0.5mm	
				Laboratory number	1402539	1402540	1402541		1402569	1402570	1402571	
				Amount of bags								
				Original mass (kg)								
	Analysis		Unit	Method / Standard								
Washing	Yields	In Coal	%	ISO 7936	36.61	46.45	16.94		22.23	75.06	2.71	
Analysis (air dried basis)	Calorific Value	In Coal	Mj/kg	ISO 1928	25.96	19.10	9.11		23.25	19.52	17.00	
	Inherent Moisture	In Coal	%	ISO 5068-2	4.7	5.5	2.7		4.8	6.4	9.3	
	Ash	In Coal	%	ISO 1171:1997(E)	11.0	26.8	56.5		18.5	25.2	29.0	
	Volatile	In Coal	%	ISO 562	28.7	24.0	17.4		27.8	25.5	22.7	
	Fix Carbon	In Coal	%	By Calculation	55.6	43.7	23.4		48.9	42.9	39.0	
	Total Sulphur	In Coal	%	ASTM D 4239	0.48	0.58	1.97		0.62	0.63	0.70	
	*Carbon	In Coal	%	ASTM D 5373-08	66.00	50.07	28.62		58.37	50.32	44.74	
	*Hydrogen	In Coal	%	ASTM D 5373-08	3.72	2.55	1.75		3.34	2.54	1.73	
	*Nitrogen	In Coal	%	ASTM D 5373-08	1.72	1.30	0.78		1.52	1.32	1.18	
	Oxygen	In Coal	%	By Calculation	12.41	13.20	7.70		12.89	13.59	13.35	

COMPILED BY: Joseph Tema
Client Liaison Officer

APPROVED BY: Kobus Janse van Rensburg
Manager: Geology (Technical Signatory)

Results marked "*" in this report are not included in the SANAS schedule of Acreditation for this laboratory
Results marked "**" in this report were outsourced to other testing facilities within SGS

This document is issued by the Company under its General Conditions of Service accessible at http://www.sgs.com/terms and conditions.htm. Attention is drawn to the limitations of liability, indemnification and jurisdiction issues defined therein.

sanas Testing Laboratory T0581

Table A2: Ash chemical composition of ashes of TEP and STEM samples, and their corresponding density fractions by XRF

Sample name		TEP F1 1.5	STEM F1 1.9	TEP F1 1.9	STEM S1 1.9	TEP S1 1.9	STEM F1 1.6
Sum of concentration	(%)	99.7	99.6	100.1	100.1	98.0	99.8
Na_2O	(%)	0.1	0.4	0.1	0.2	0.3	0.2
MgO	(%)	0.0	0.3	0.0	0.0	0.0	0.0
Al_2O_3	(%)	0.0	1.3	0.0	0.1	0.0	0.0
SiO_2	(%)	7.8	19.7	16.6	12.4	15.8	16.5
P_2O_5	(%)	0.3	0.3	0.3	0.3	0.3	0.7
SO_3	(%)	0.0	0.0	0.0	0.0	0.0	0.0
K_2O	(%)	0.1	0.2	0.7	0.9	0.6	0.6
CaO	(%)	2.4	2.9	3.4	4.1	3.7	6.7
TiO_2	(%)	0.6	1.0	0.8	0.7	0.7	2.2
V_2O_5	(%)	0.1	0.1	0.1	0.1	0.0	0.2
Cr_2O_3	(%)	0.0	0.0	0.0	0.0	0.0	0.0
MnO	(%)	0.1	0.1	0.1	0.1	0.1	0.1
Fe_2O_3	(%)	3.2	1.9	3.3	1.6	2.8	6.2
Sum of Concentration Major Elements		14.6	28.2	25.3	20.3	24.1	33.3
Co	(ppm)	17.8	45.3	30.9	29.8	34.4	53.9
Zn	(ppm)	0.0	16.9	0.0	0.0	0.0	0.0

Sample name		TEP F1 1.5	STEM F1 1.9	TEP F1 1.9	STEM S1 1.9	TEP S1 1.9	STEM F1 1.6
As	(ppm)	3.8	10.1	9.9	6.3	7.5	12.7
Rb	(ppm)	17.8	23.5	19.5	13.7	28.6	93.5
Sr	(ppm)	1316.9	2300.7	1901.8	1178.2	1571.9	1680.4
Y	(ppm)	32.9	52.0	41.2	37.1	35.9	128.6
Zr	(ppm)	303.5	374.3	284.4	160.0	172.9	3707.0
Ag	(ppm)	1032.3	1101.0	830.0	710.3	576.3	1829.6
Cd	(ppm)	22.2	13.2	28.1	23.3	14.5	35.6
In	(ppm)	0.1	0.1	0.1	0.1	0.1	0.1
Sn	(ppm)	0.0	23.0	13.1	11.5	0.0	0.0
Sb	(ppm)	3.5	5.9	3.8	2.2	2.2	3.4
Ba	(ppm)	4751.7	6626.1	4484.9	3589.2	3663.5	6277.0
La	(ppm)	171.6	366.2	278.1	156.4	60.9	716.3
Ce	(ppm)	146.6	473.5	545.6	373.1	377.3	973.1
Pr	(ppm)	49.9	74.9	41.6	12.3	6.2	102.7
Nd	(ppm)	151.0	175.9	126.2	53.2	57.5	352.0
Sm	(ppm)	25.3	30.5	22.0	5.1	4.9	46.5
Eu	(ppm)	1.5	1.5	1.7	1.3	1.4	3.2
Dy	(ppm)	1.9	1.9	3.7	0.4	2.3	5.2

Sample name		TEP F1 1.5	STEM F1 1.9	TEP F1 1.9	STEM S1 1.9	TEP S1 1.9	STEM F1 1.6
Er	(ppm)	3.9	4.1	4.1	3.9	4.0	7.8
Hf	(ppm)	0.5	0.8	0.6	0.3	0.3	6.4
Au	(ppm)	1.8	3.0	2.4	1.6	1.8	2.2
Th	(ppm)	0.0	14.9	9.9	0.0	0.0	8.9
Sum of Concentration Trace Elements	(ppm)	8056.4	11739.0	8683.6	6369.1	6624.3	16046.2
Sum of Concentration Trace Elements	(%)	0.8	1.2	0.9	0.6	0.7	1.6
Loss on ignition	(%)	84.3	70.2	74.0	79.1	73.3	64.8

Table A3: Distribution of microlithotypes in the density fractions of TEP and STEM samples.

THESE RESULTS RELATE ONLY TO THE SAMPLES ANALYSED													
Sample no:		2295		2296		2297		2298		2299		22300	
Sample identification:		STEM F1 1.5		STEM F1 1.9		STEM S1 1.9		TEM F1 1.5		TEM F1 1.9		TEM S1 1.9	
		inc. mm	mmf	inc. mm	mmf	inc. mm	mmf	inc. mm	mmf	inc. mm	mmf	inc. mm	mmf
MACERAL GROUP	MACERAL (vol%)	vol%	vol%	vol%	vol%	vol%	vol%	vol%	vol%	vol%	vol%	vol%	vol%
Vitrinite	telinite	0,2	0,2	0,0	0,0	0,0	0,0	0,0	0,0	0,0	0,0	0,0	0,0
	collotelinite	10,2	10,9	3,3	3,9	8,7	17,9	22,1	25,9	12,7	19,2	15,1	20,2
	vitrodetrinite	0,0	0,0	0,0	0,0	0,0	0,0	0,0	0,0	0,0	0,0	0,0	0,0
	collodetrinite	24,4	26,2	6,2	7,3	4,7	9,8	16,1	18,8	11,7	17,7	10,3	13,8
	corpogelinite	0,6	0,6	0,0	0,0	0,0	0,0	0,0	0,0	0,3	0,4	0,8	1,1
	gelinite	0,4	0,4	0,4	0,5	0,4	0,8	0,0	0,0	0,0	0,0	0,6	0,8
	pseudovitrinite	0,0	0,0	0,0	0,0	0,2	0,4	0,0	0,0	0,0	0,0	0,0	0,0
Inertinite	fusinite	6,7	7,2	3,9	4,6	3,2	6,5	10,4	12,2	9,0	13,6	5,4	7,2
	reactive semifusinite	3,1	3,3	0,8	0,9	0,4	0,8	2,5	3,0	0,5	0,8	1,8	2,4
	inert semifusinite	34,6	37,1	42,3	50,2	20,1	41,5	22,1	25,9	18,0	27,1	23,4	31,4
	micrinite	0,6	0,6	0,0	0,0	0,0					0,0	0,6	0,8
	macrinite	0,4	0,4	0,4	0,5	0,2					0,0	0,2	0,3
	secretinite	0,0	0,0	2,5	3,0	1,2	2,4	0,6	0,7	0,5	0,8	1,0	1,3
	funginite	0,0	0,0	0,0	0,0	0,0	0,0	0,0	0,0	0,0	0,0	0,0	0,0
	inertodetrinite R	0,2	0,2	0,8	0,9	0,4	0,8	0,4	0,5	0,2	0,4	0,0	0,0
	inertodetrinite I	11,1	11,9	21,1	25,0	6,7	13,8	7,2	8,5	12,0	18,1	13,9	18,6
Liptinite	sporinite	1,0	1,0	2,7	3,2	2,4	4,9	3,5	4,1	1,2	1,9	1,6	2,1
	cutinite	0,0	0,0	0,0	0,0	0,0	0,0	0,0	0,0	0,0	0,0	0,0	0,0
	resinite	0,0	0,0	0,0	0,0	0,0	0,0	0,0	0,0	0,0	0,0	0,0	0,0
	alginite	0,0	0,0	0,0	0,0	0,0	0,0	0,0	0,0	0,0	0,0	0,0	0,0
	liptodetrinite	0,0	0,0	0,0	0,0	0,0	0,0	0,0	0,0	0,0	0,0	0,0	0,0
	suberinite	0,0	0,0	0,0	0,0	0,0	0,0	0,0	0,0	0,0	0,0	0,0	0,0
	exsudatinite	0,0	0,0	0,0	0,0	0,0	0,0	0,0	0,0	0,0	0,0	0,0	0,0
Mineral matter	clay	2,1		4,2		16,4		6,1		12,2		15,1	
	quartz	1,7		6,2		17,9		4,7		10,2		6,8	
	pyrite	0,2		0,4		5,7		0,8		2,0		1,2	
	carbonate	2,5		4,4		10,0		2,7		9,0		2,0	
	other	0,0		0,4		1,4		0,4		0,5		0,2	
SUMMARY TABLE													
MACERAL GROUP	VITRINITE	35,8	38,3	9,9	11,7	14,0	28,9	38,2	44,7	24,7	37,3	26,8	35,9
TOTALS (vol%)	INERTINITE	56,7	60,7	71,8	85,1	32,2	66,2	43,6	51,2	40,2	60,8	46,3	62,0
	LIPTINITE	1,0	1,0	2,7	3,2	2,4	4,9	3,5	4,1	1,2	1,9	1,6	2,1
	MINERAL MATTER	6,5		15,6		51,4		14,7		33,9		25,3	
	TOTAL INERTINITE	56,7	60,7	71,8	85,1	32,2	66,2	43,6	51,2	40,2	60,8	46,3	62,0
	TOTAL REACTIVE MACERALS	40,1	42,8	14,2	16,7	17,2	35,4	44,6	52,3	26,6	40,4	30,2	40,4

Graphical user interface, application, table
Description automatically generated

Total inertinite = all the inertinite macerals
Total reactive macerals = vitrinite + liptinite + reactive semifusinite + reactive inertodetrinite

Table A4: A list of macerals and their associations based on microlithotypes analysis present in TEP and STEM samples

	Maceral	TEP	STEM
Monomaceral	vitrite	37.5	12.9
	semifusite	19.6	20.8
	fusite / sec	7.6	2.6
	inertodetrite	3.7	11.1
BiMaceral	sf+int	4.2	13.3
	liptite	0.2	0
	vit+sf/f	5.1	2.4
	vit+int	0.7	3
	vit+lipt	2	0.4
	int+lipt	2	6.8
Trimaceral	TRIMAC dc v>i+l	4.2	3.8
	TRIMAC cd i>V+L	0.2	1
	TRIMAC vl L>V+I	0	0
Carbominerite	cbm arg clay	0.5	2.6
	cbm silicate qz	1.5	5.6
	cbm pyrite	1.5	0.8
	cbm ankerite	1.2	4.2
	poly	0	0
Rock	rock	8.3	8.7

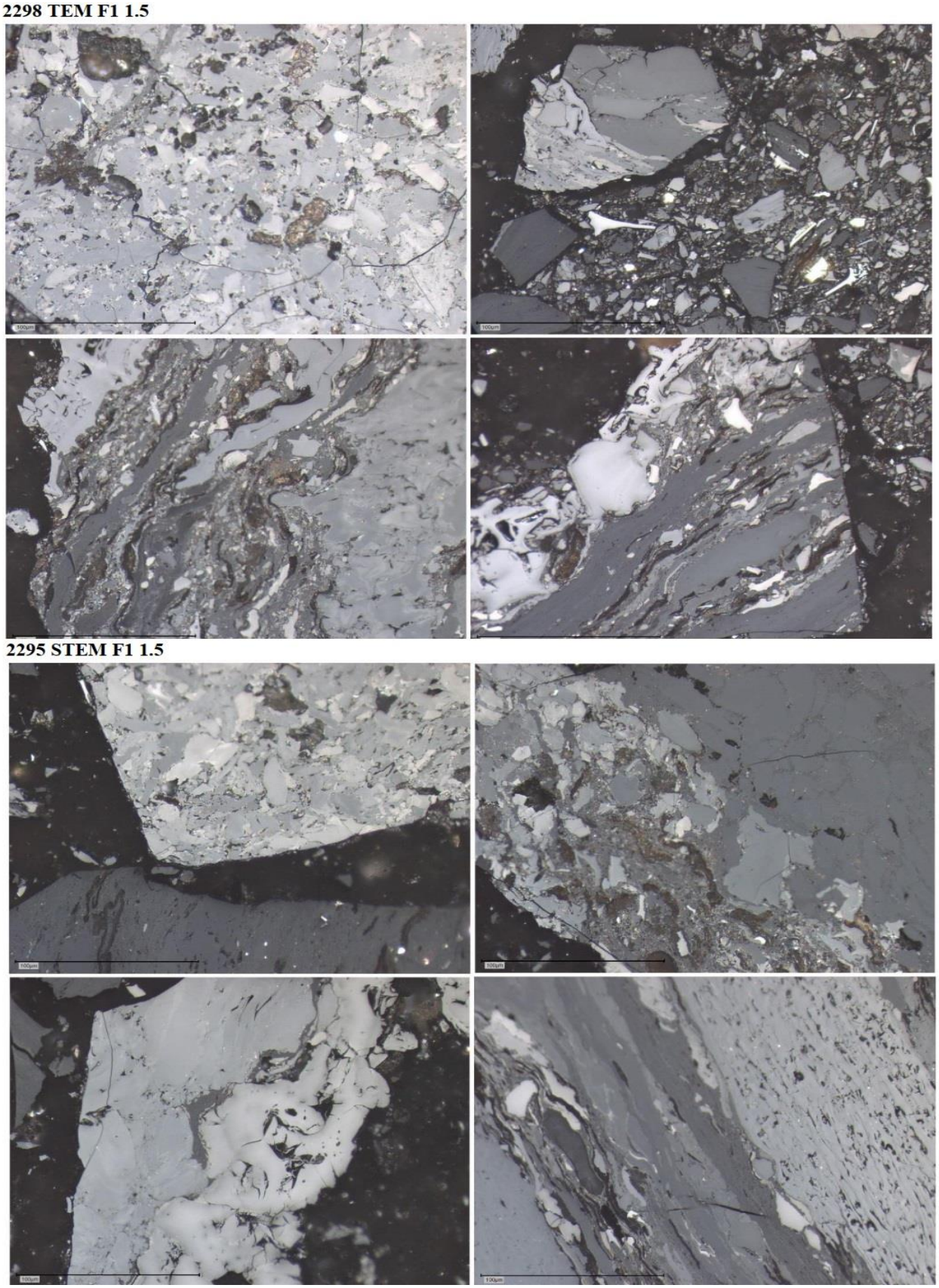

Figure A1: Micrographs of Float fractions <1.5 g/cm^3 for TEP (TEM) and STEM samples.

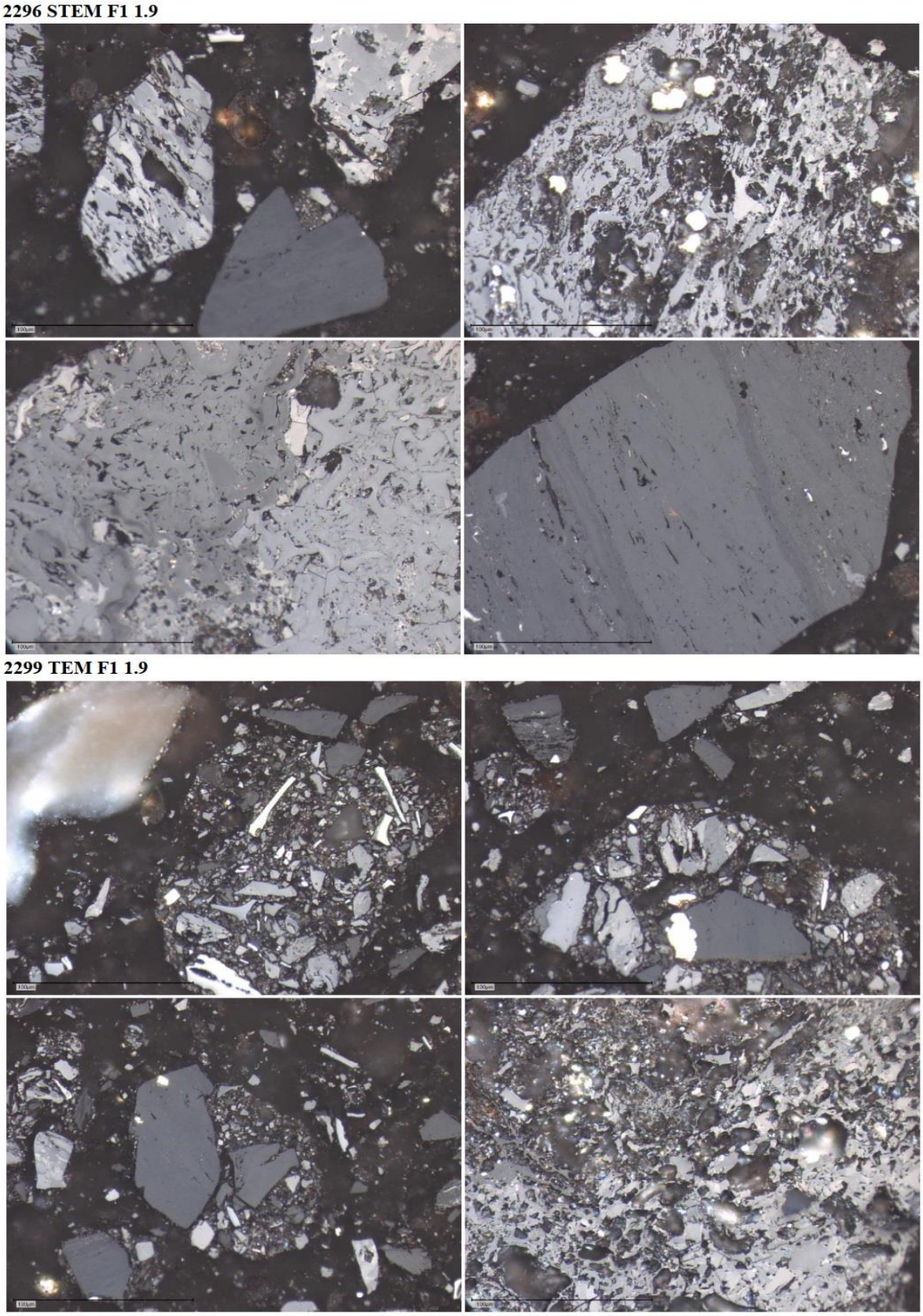

Figure A2: Micrographs of Middling fractions <1.9 g/cm^3 for TEP (TEM) and STEM samples.

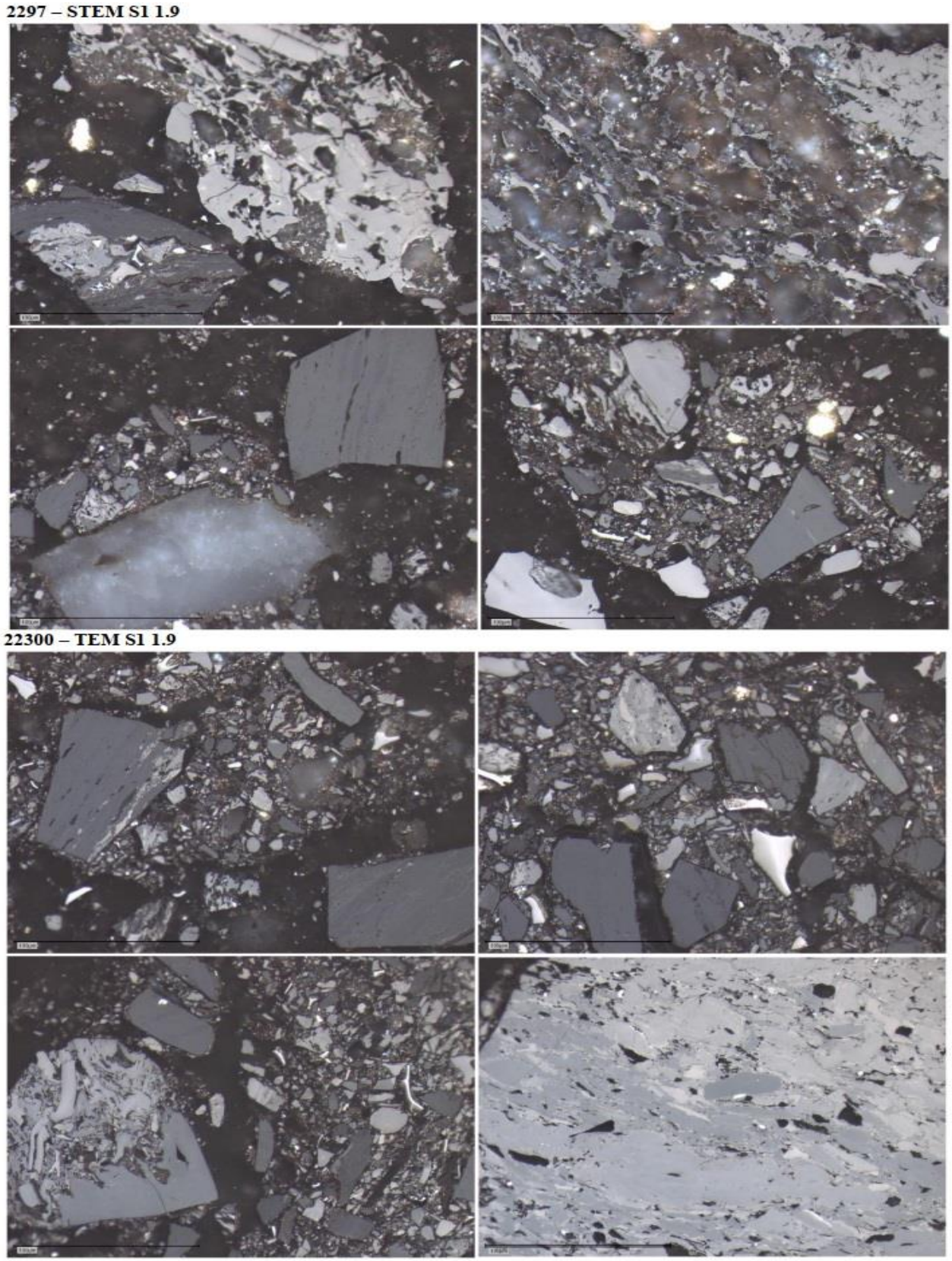

Figure A3: Micrographs of Sink fractions >1.9 g/cm^3 for TEP (TEM) and STEM samples.

ANNEXURES B: CHAPTER 4 SUPPLEMENTARY DATA

Table B1: Pyrolytic product yields for FCR+ROSH

Sample	Run 1	Run 2	Run 3	AVG	Std.dev	Relative Std.dev
Sample mass (g)	42.16	39.30	41.53	41.0	1.5	3.6
Char(g)	38.16	34.60	36.36	36.4	1.8	4.9
Tar (g)	0.66	0.70	0.84	0.7	0.1	12.9
Gas L(g)	2.50	2.80	3.30	2.9	0.4	14.1
Gas (g) calculated	0.7	1.2	1.0	1.0	0.2	23.5
Yields (wt. %)						
Y Char	84.4	81.9	81.4	82.5	1.6	1.9
Y Tar	2.6	3.0	3.4	3.0	0.4	12.7
Y Gas Liquor	0.1	0.1	0.1	0.1	0.0	14.4
Y Gas	12.9	15.0	15.1	14.3	1.2	8.6
Total conversion	84.4	81.9	81.4	82.5	1.6	1.9
Yields (wt.%) water-free basis						
Y Char	84.4	82.0	81.5	82.6	1.6	1.9
Y Tar	2.6	3.0	3.4	3.0	0.4	12.7
Y Gas	12.9	15.0	15.1	14.3	1.2	8.6
Total conversion	84.4	82.0	81.5	82.6	1.6	1.9

Table B2: Pyrolytic product yields for Sl1.9+ROSH

Sample	Run 1	Run 2	Run 3		AVG	Std.dev	Relative Std.dev
Sample mass (g)	42.12	41.08	46.80	44.99	43.7	3.0	7.0
Char(g)	35.90	35.87	39.49	38.20	37.4	2.1	5.6
Tar (g)	0.71	0.53	0.45	0.52	0.6	0.1	24.1
Gas L(g)	3.43	3.24	3.34	3.44	3.4	0.1	2.8
Gas (g) calculated	2.1	1.4	3.5	2.8	2.5	1.1	43.2
Yields (wt. %)							
Y Char	78.2	80.1	77.4	77.9	78.4	1.4	1.8

Sample	Run 1	Run 2	Run 3		AVG	Std.dev	Relative Std.dev
Y Tar	2.1	1.6	1.2	1.4	1.6	0.5	28.5
Y Gas Liquor	0.1	0.1	0.1	0.1	0.1	0.0	6.8
Y Gas	19.6	18.2	21.3	20.5	19.9	1.6	7.8
Total conversion	78.2	80.1	77.4	77.9	78.4	1.4	1.8
Yields (wt.%) water-free basis							
Y Char	78.3	80.2	77.5	78.0	78.5	1.4	1.8
Y Tar	2.1	1.6	1.2	1.4	1.6	0.5	28.5
Y Gas	19.6	18.2	21.3	20.6	19.9	1.6	7.8
Total conversion	78.3	80.2	77.5	78.0	78.5	1.4	1.8

Table B3: Pyrolytic product yields for Fl1.5+ROSH

Sample	Run 1	Run 2	Run 3	AVG	Std.dev	Relative Std.dev
Sample mass (g)	43.83	41.02	40.89	41.9	1.7	4.0
Char(g)	36.27	34.04	34.14	34.8	1.3	3.6
Tar (g)	1.15	1.00	1.18	1.1	0.1	8.7
Gas L(g)	3.12	3.22	3.25	3.2	0.1	2.1
Gas (g) calculated	3.3	2.8	2.3	2.8	0.5	17.4
Yields (wt. %)						
Y Char	76.8	77.1	77.5	77.1	0.4	0.5
Y Tar	4.0	3.7	4.4	4.0	0.3	8.5
Y Gas Liquor	0.1	0.1	0.1	0.1	0.0	5.9
Y Gas	19.1	19.2	18.0	18.8	0.6	3.5
Total conversion	76.8	77.1	77.5	77.1	0.4	0.5
Yields (wt.%) water-free basis						
Y Char	76.9	77.1	77.6	77.2	0.4	0.5
Y Tar	4.0	3.7	4.4	4.0	0.3	8.5
Y Gas	19.1	19.2	18.0	18.8	0.6	3.5
Total conversion	76.9	77.1	77.6	77.2	0.4	0.5

Table B4: Pyrolytic product yields for FCRD+ROSH

Sample	Run 1	Run 2	Run 3	AVG	Std.dev	Relative Std.dev
Sample mass (g)	40.21	45.16	43.59	43.0	2.5	5.9
Char(g)	34.02	38.42	36.83	36.4	2.2	6.1
Tar (g)	1.20	1.33	1.17	1.2	0.1	6.9
Gas L(g)	3.14	3.55	3.42	3.4	0.2	6.2
Gas (g) calculated	1.9	1.9	2.2	2.0	0.2	9.3
Yields (wt. %)						
Y Char	82.1	82.5	82.0	82.2	0.3	0.4
Y Tar	3.7	3.7	3.4	3.6	0.2	5.7
Y Gas Liquor	0.1	0.1	0.1	0.1	0.0	0.3
Y Gas	14.1	13.7	14.6	14.1	0.4	3.2
Total conversion	82.1	82.5	82.0	82.2	0.3	0.4
Yields (wt.%) water-free basis						
Y Char	82.2	82.6	82.1	82.3	0.3	0.4
Y Tar	3.7	3.7	3.4	3.6	0.2	5.7
Y Gas	14.1	13.7	14.6	14.1	0.4	3.2
Total conversion	82.2	82.6	82.1	82.3	0.3	0.4

Table B5: Pyrolytic product yields for FCRCF+ROSH

Sample	Run 1	Run 2	Run 3	AVG	Std.dev	Relative Std.dev
Sample mass (g)	42.69	41.07	42.04	41.9	0.8	1.9
Char(g)	38.33	36.52	37.18	37.3	0.9	2.5
Tar (g)	0.75	0.76	0.66	0.7	0.1	7.6
Gas L(g)	2.73	2.86	2.97	2.9	0.1	4.2
Gas (g) calculated	0.9	0.9	1.2	1.0	0.2	18.7
Yields (wt. %)						
Y Char	64.2	63.6	63.3	63.7	0.5	0.8
Y Tar	2.2	2.3	2.0	2.2	0.2	8.3
Y Gas Liquor	0.1	0.1	0.1	0.1	0.0	5.3

Sample	Run 1	Run 2	Run 3	AVG	Std.dev	Relative Std.dev
Y Gas	33.5	34.0	34.7	34.1	0.6	1.8
Total conversion	64.2	63.6	63.3	63.7	0.5	0.8
Yields (wt.%) water-free basis						
Y Char	64.3	63.7	63.3	63.8	0.5	0.8
Y Tar	2.2	2.3	2.0	2.2	0.2	8.3
Y Gas	33.5	34.0	34.7	34.1	0.6	1.8
Total conversion	64.3	63.7	63.3	63.8	0.5	0.8

Table B6: Pyrolytic product yields for FCRCF+ROSH

Sample	Run 1	Run 2	Run 3	AVG	Std.dev	Relative Std.dev
Sample mass (g)	44.217	41.42	41.60	42.4	1.5	3.6
Char(g)	38.03	35.63	35.97	36.5	1.3	3.6
Tar (g)	0.80	0.79	0.78	0.8	0.0	1.3
Gas L(g)	2.49	2.20	2.90	2.5	0.4	13.9
Gas (g) calculated	2.9	2.8	1.9	2.5	0.5	20.0
Yields (wt. %)						
Y Char	79.0	79.0	79.4	79.1	0.2	0.3
Y Tar	3.3	3.4	3.4	3.4	0.1	2.6
Y Gas Liquor	0.1	0.1	0.1	0.1	0.0	14.7
Y Gas	17.6	17.5	17.1	17.4	0.3	1.4
Total conversion	79.0	79.0	79.4	79.1	0.2	0.3
Yields (wt.%) water-free basis						
Y Char	79.1	79.0	79.5	79.2	0.2	0.3
Y Tar	3.3	3.4	3.4	3.4	0.1	2.6
Y Gas	17.6	17.5	17.1	17.4	0.2	1.4
Total conversion	79.1	79.0	79.5	79.2	0.2	0.3

Table B7: Compositions of the leachates obtained from the chemical fractionation experiments

Water Analysis Report

Sample name			A_A	AA_2	AA_CF	AA_CF2	HCL	HCL_2	HCL_CF	HCL_CF2	H2O_2	H2O_CF	H2O_CF2
Sample date			2022/11/24	2022/11/24	2022/11/24	2022/11/24	2022/11/24	2022/11/24	2022/11/24	2022/11/24	2022/11/24	2022/11/24	2022/11/24
Sample container description			Glass Container	Glass Container	Glass Container	Glass Container	Glass Container	Glass Container	Glass Container	Plastic Container	Glass Container	Glass Container	Glass Container
Submission date			2022/11/24	2022/11/24	2022/11/24	2022/11/24	2022/11/24	2022/11/24	2022/11/24	2022/11/24	2022/11/24	2022/11/24	2022/11/24
Sample type			Water	Water	Water	Water	Water	Water	Water	Water	Water	Water	Water
Set Point ID			WAT/23/06 77-0001	WAT/23/06 77-0002	WAT/23/06 77-0003	WAT/23/06 77-0004	WAT/23/06 77-0005	WAT/23/06 77-0006	WAT/23/06 77-0007	WAT/23/06 77-0008	WAT/23/06 77-0009	WAT/23/06 77-0010	WAT/23/06 77-0011
Visual inspection			N/A	N/A	N/A	N/A	N/A	N/A	N/A	N/A	N/A	N/A	N/A
Method no	Determinand	Unit											
Chemical Properties and Parameters													
M474	Aluminium (Al)	mg/L	<0.15	<0.15	<0.15	<0.15	<0.15	<0.15	367	930	<0.15	<0.15	<0.15
M474	Calcium (Ca)	mg/L	4.29	<0.50	2178	3279	1.51	0.77	3370	2501	0.89	231	233
M474	Iron (Fe)	mg/L	<0.10	<0.10	<0.10	<0.10	0.17	<0.10	562	1678	<0.10	<0.10	<0.10
M474	Potassium (K)	mg/L	0.31	0.31	13.8	17.0	0.06	0.10	8.49	18.4	0.11	7.64	7.68
M474	Magnesium (Mg)	mg/L	0.39	0.25	99.8	179	0.28	0.23	629	582	0.38	39.4	39.3
M474	Manganese (Mn)	µg/L	0.03	<0.02	5.38	8.43	0.02	<0.02	30.3	30.4	0.02	0.02	<0.02
M474	Sodium (Na)	mg/L	1.42	1.37	94.5	141	1.09	1.56	50.0	19.4	1.80	223	226
M474	Phosphorus (P)	mg/L	<0.20	<0.20	<0.20	<0.20	<0.20	<0.20	91.8	161	<0.20	<0.20	<0.20
#	Sulphur (S)	mg/L	0.57	0.34	43.5	30.1	0.08	0.13	18.9	19.6	0.11	425	435
M474	Silicon (Si)	mg/L	<0.25	<0.25	3.64	5.91	<0.25	<0.25	145	218	<0.25	5.19	5.14
M474	Titanium (Ti)	mg/L	<0.04	<0.04	<0.04	<0.04	<0.04	<0.04	0.93	1.13	<0.04	<0.04	0.11

Johannesburg (A Part of Synerlytic Services (Pty) Ltd Reg. No. 1989/000201/07 - Vat No. 4520131816)
A: 55 Angus Crescent, Longmeadow Business Park, Johannesburg, 1610
P: PO Box 856, Isando, 1600, Gauteng, South Africa
T: +27 (0) 11 923 7100 **W:** www.setpointlabs.co.za

Note: AA – Ammonium acetate, HCl – Hydrochloric acid

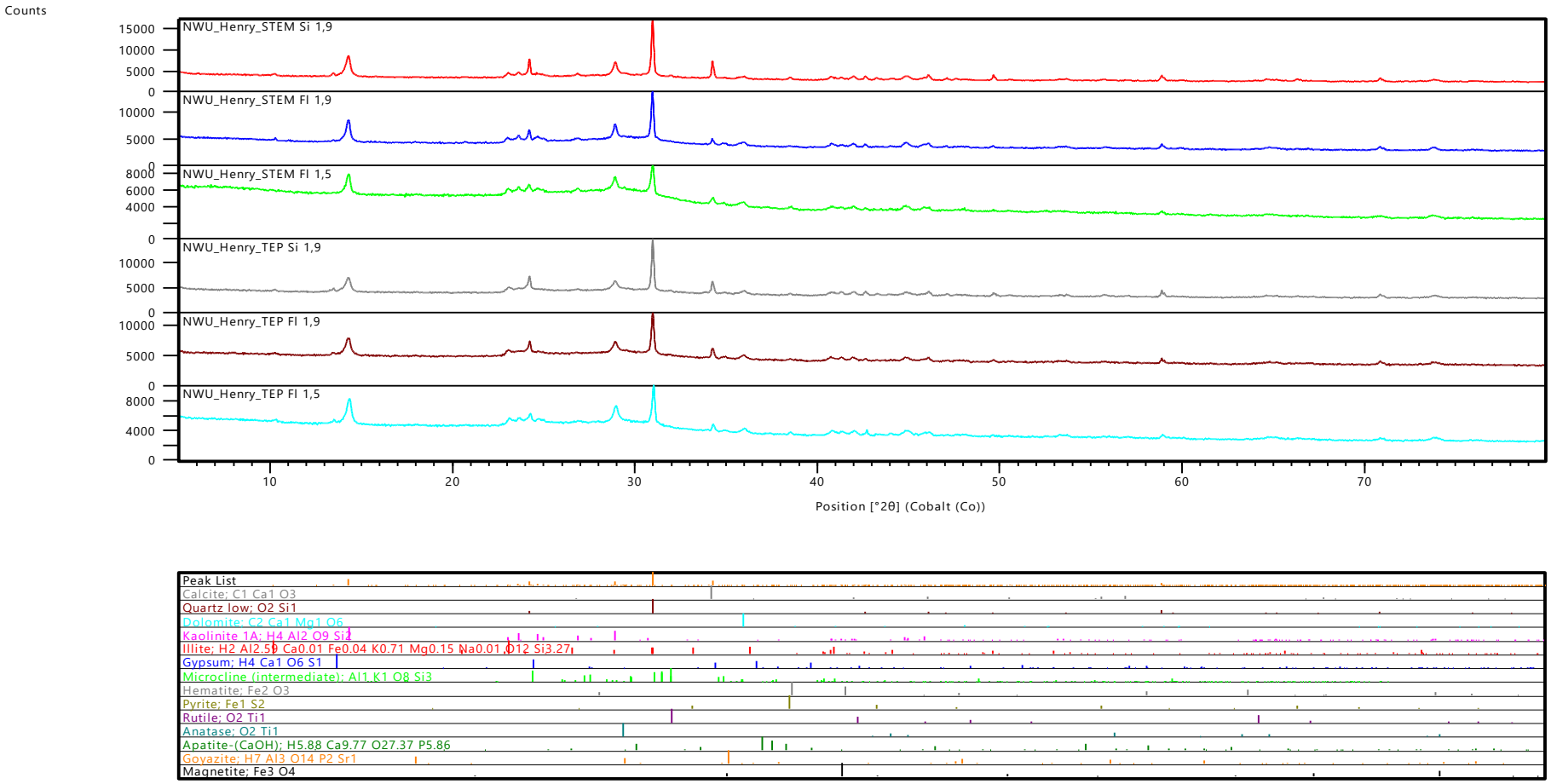

Figure B2: Diffractograms and mineral identifications for TEP and STEM density separated fractions.

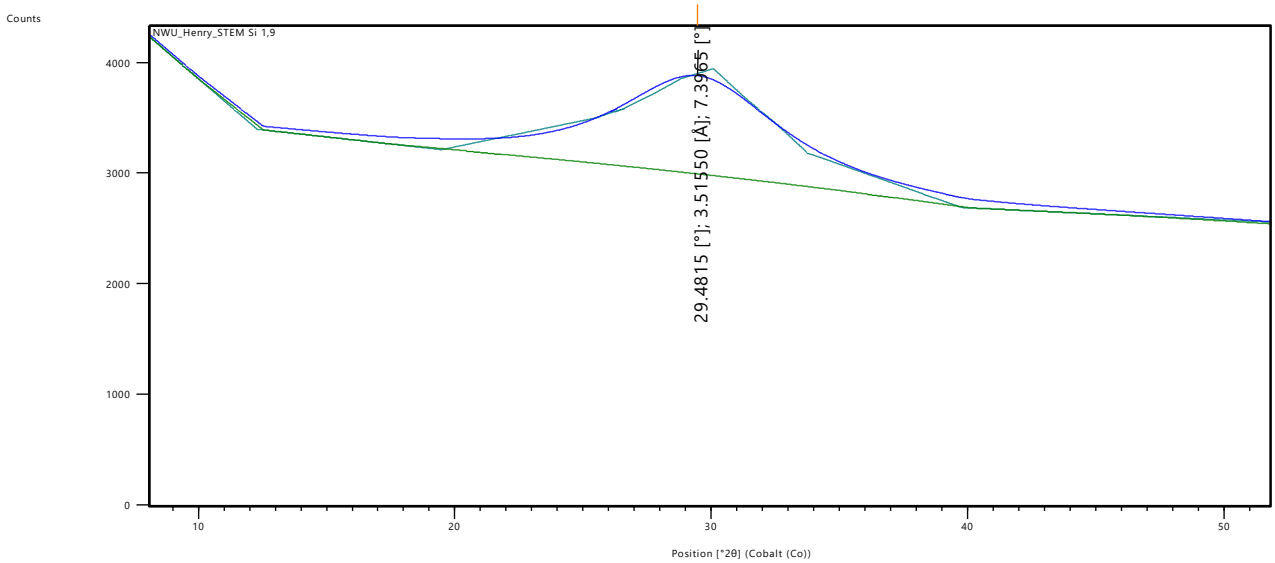

Figure B3: Crystalline carbon size peak parameters for STEM SI1.9.

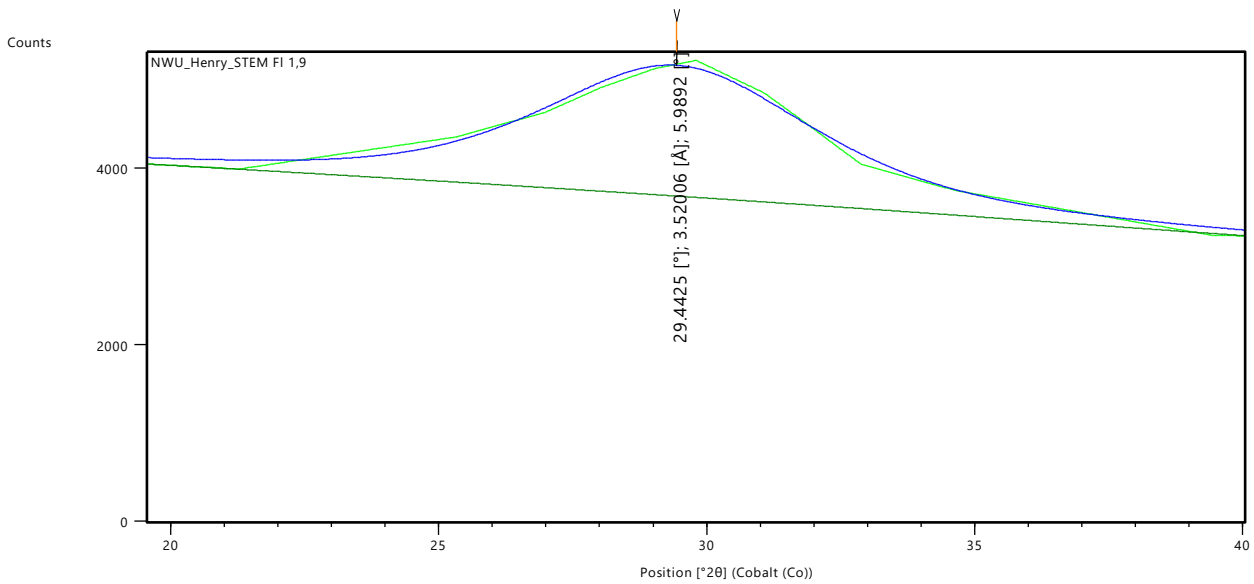

Figure B4: Crystalline carbon size peak parameters for STEM FI1.9.

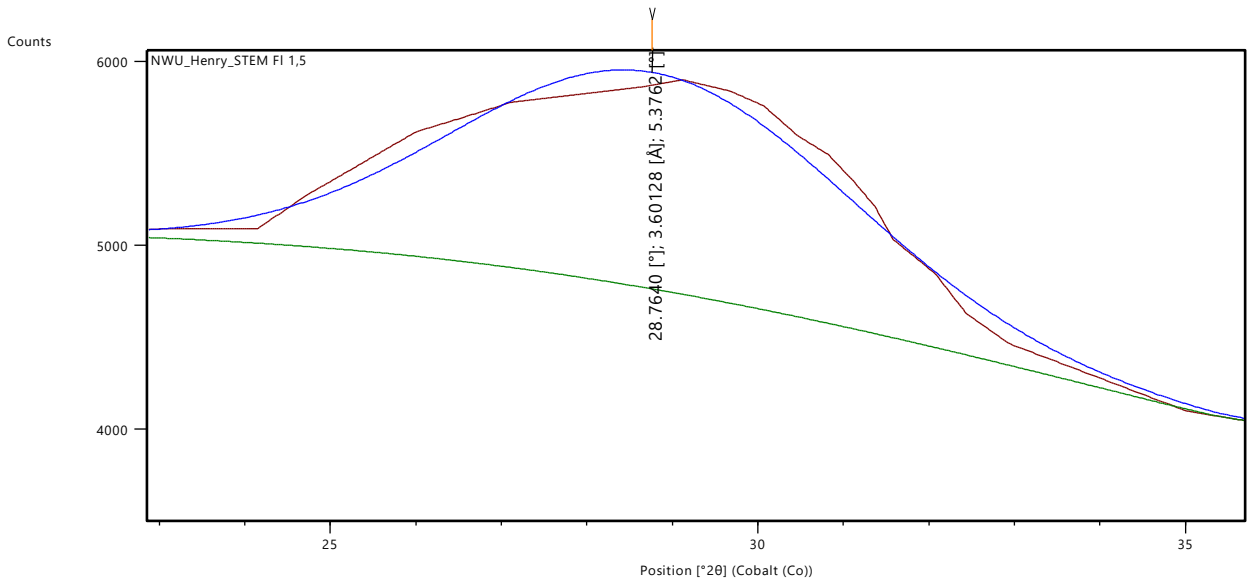

Figure B5: Crystalline carbon size peak parameters for STEM Fl1.5.

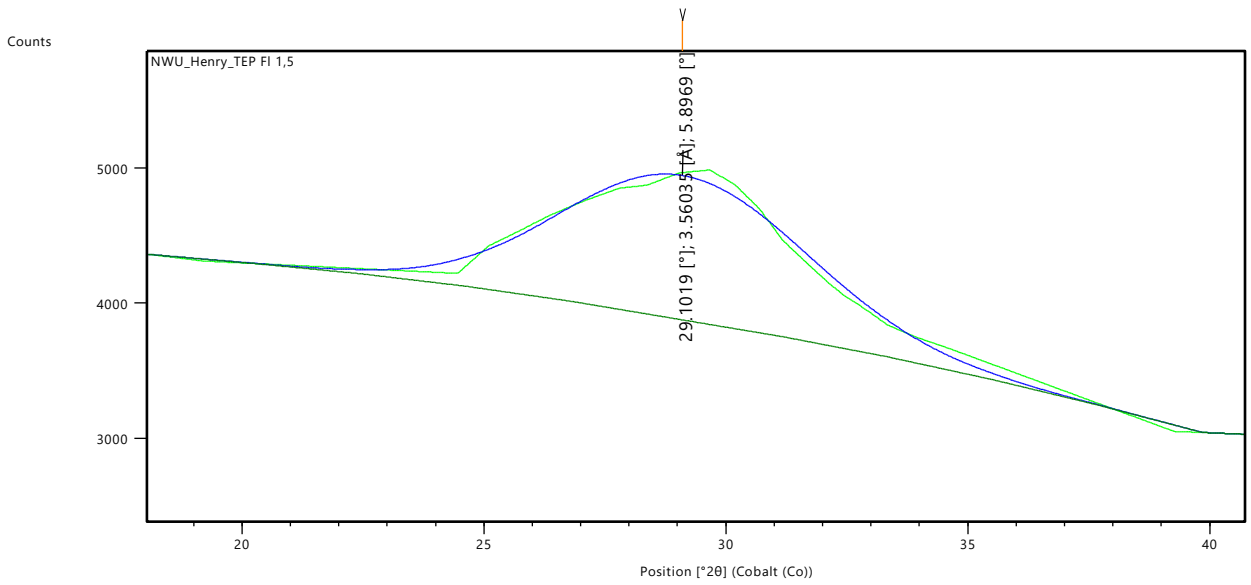

Figure B6: Crystalline carbon size peak parameters for TEP Fl1.5.

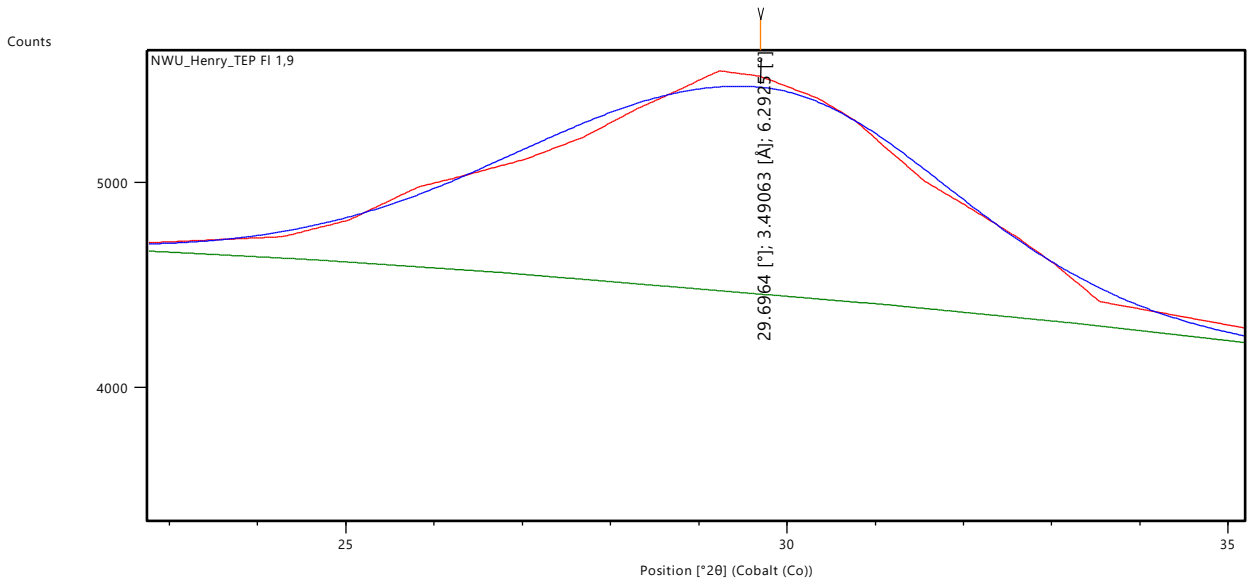

Figure B7: Crystalline carbon size peak parameters for TEP Fl1.9.

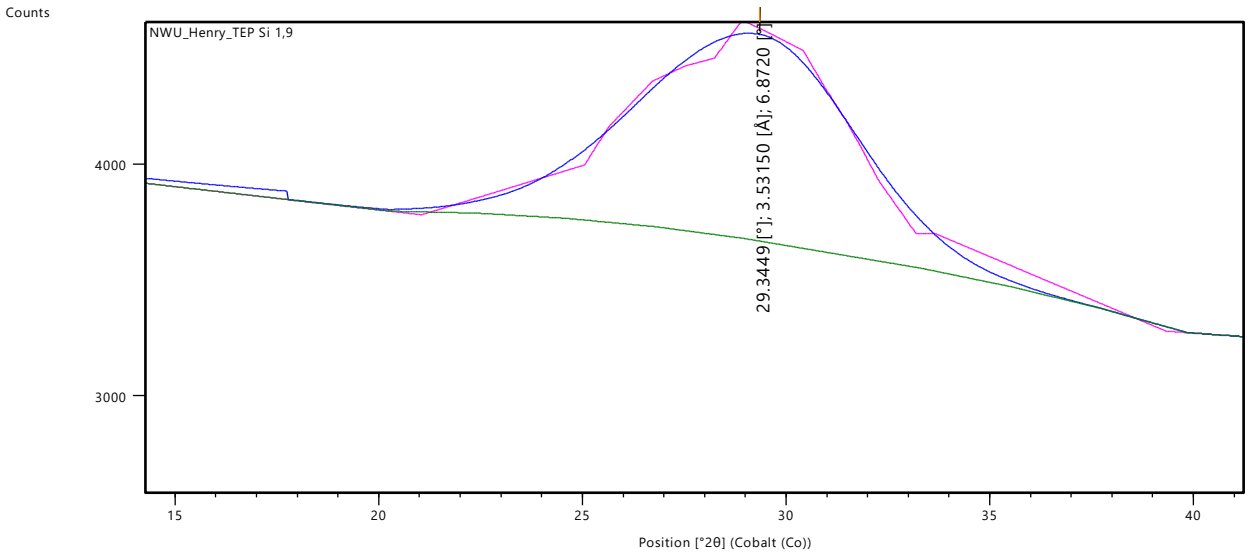

Figure B8: Crystalline carbon size peak parameters for TEP Sl1.9.

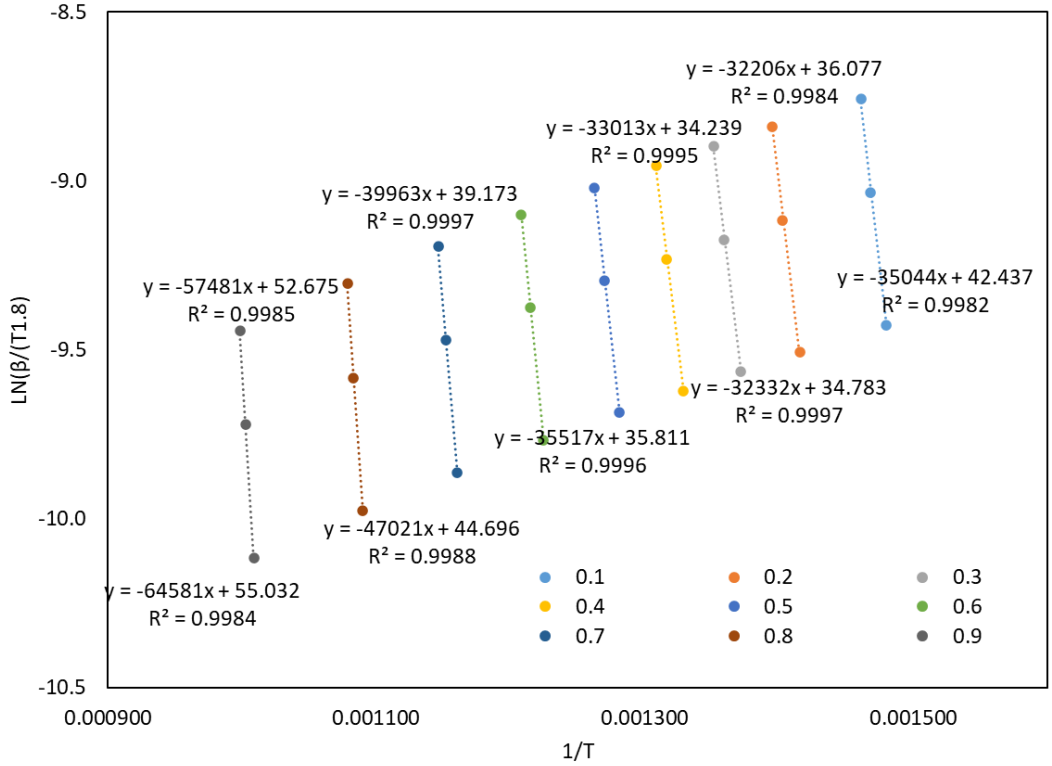

Figure B9: Arrhenius plot for TEP CF.

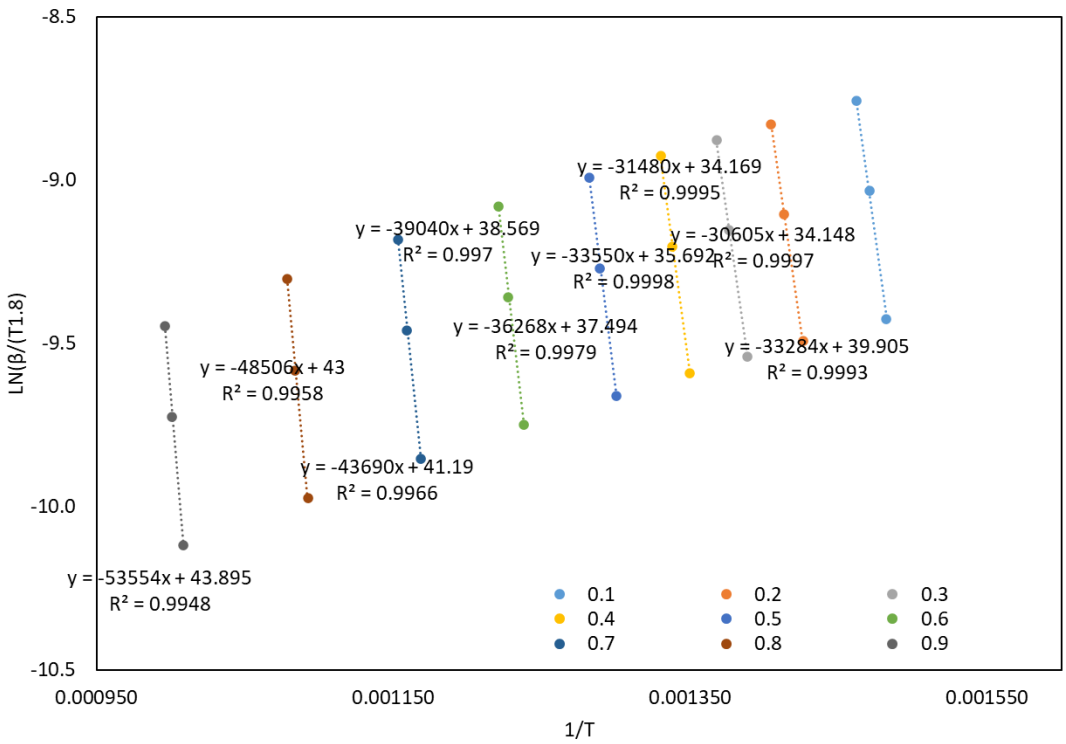

Figure B10: Arrhenius plot for TEP D.

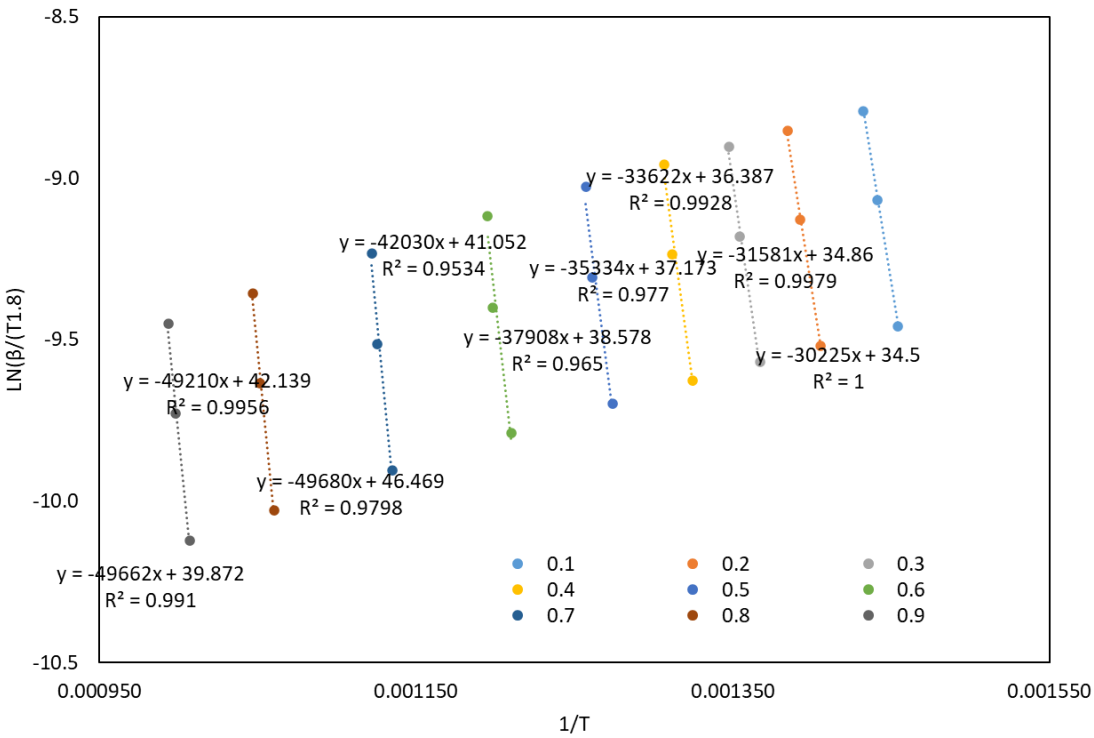

Figure B11: Arrhenius plot for TEP.

ANNEXURES C: CHAPTER 5 SUPPLEMENTARY DATA

Table C1: Pyrolytic product yields for FCR+Fe acetate

Sample	Run 1	Run 2	Run 3	Run 4	AVG	Std.dev	Relative Std.dev
Sample mass (g)	24.53	24.69	24.19	24.76	24.5	0.3	1.0
Char(g)	20.06	20.13	19.56	19.97	19.9	0.3	1.3
Tar (g)	0.60	0.62	0.64	0.65	0.6	0.0	3.5
Gas L(g)	1.97	2.17	2.04	2.08	2.1	0.1	4.0
Gas (g) calculated	1.9	1.8	2.0	2.1	1.9	0.1	6.3
Yields (wt. %)							
Y Char	69.2	69.0	68.4	68.3	68.9	0.4	0.6
Y Tar	3.5	3.6	3.7	3.7	3.6	0.1	4.0
Y Gas Liquor	0.1	0.1	0.1	0.1	0.1	0.0	4.5
Y Gas	27.2	27.3	27.7	27.9	27.4	0.3	0.9
Total conversion	69.2	69.0	68.4	68.3	68.9	0.4	0.6
Yields (wt.%) water-free basis							
Y Char	69.3	69.1	68.5	68.4	69.0	0.4	0.6
Y Tar	3.5	3.6	3.8	3.7	3.6	0.1	4.0
Y Gas	27.2	27.3	27.7	27.9	27.4	0.3	0.9
Total conversion	69.3	69.1	68.5	68.4	69.0	0.4	0.6

Table C2: Pyrolytic product yields for FCR+Ca acetate

Sample	Run 1	Run 2	Run 3	Run 4	AVG	Std.dev	Relative Std.dev
Sample mass (g)	24.06	25.06	25.29		24.8	0.7	2.6
Char(g)	19.71	20.62	19.70		20.0	0.5	2.6
Tar (g)	0.58	0.62	0.61		0.6	0.0	3.5
Gas L(g)	2.00	2.23	2.43		2.2	0.2	9.7
Gas (g) calculated	1.8	1.6	2.6		2.0	0.5	25.9
Yields (wt. %)							
Y Char	79.0	79.3	75.1		77.8	2.3	3.0

Sample	Run 1	Run 2	Run 3	Run 4	AVG	Std.dev	Relative Std.dev
Y Tar	3.6	3.7	3.6		3.6	0.1	1.5
Y Gas Liquor	0.1	0.1	0.1		0.1	0.0	7.3
Y Gas	17.3	16.9	21.2		18.4	2.4	12.8
Total conversion	79.0	79.3	75.1		77.8	2.3	3.0
Yields (wt.%) water-free basis							
Y Char	79.1	79.4	75.2		77.9	2.3	3.0
Y Tar	3.6	3.7	3.6		3.6	0.1	1.5
Y Gas	17.3	16.9	21.2		18.5	2.4	12.8
Total conversion	79.1	79.4	75.2		77.9	2.3	3.0

Table C3: Pyrolytic product yields for FCR+Mg acetate

Sample	Run 1	Run 2	Run 3	Run 4	AVG	Std.dev	Relative Std.dev
Sample mass (g)	24.88	25.63	24.73		25.1	0.5	1.9
Char(g)	19.78	19.43	19.81		19.7	0.2	1.1
Tar (g)	0.58	0.57	0.59		0.6	0.0	1.7
Gas L(g)	1.48	2.17	1.72		1.8	0.4	19.6
Gas (g) calculated	3.0	3.5	2.6		3.0	0.4	14.0
Yields (wt. %)							
Y Char	74.7	71.2	75.2		73.7	2.2	3.0
Y Tar	3.3	3.2	3.4		3.3	0.1	3.6
Y Gas Liquor	0.1	0.1	0.1		0.1	0.0	17.8
Y Gas	21.9	25.5	21.3		22.9	2.3	10.0
Total conversion	74.7	71.2	75.2		73.7	2.2	3.0
Yields (wt.%) water-free basis							
Y Char	74.7	71.3	75.3		73.8	2.2	2.9
Y Tar	3.3	3.2	3.4		3.3	0.1	3.5
Y Gas	21.9	25.5	21.3		22.9	2.3	10.0
Total conversion	74.7	71.3	75.3		73.8	2.2	2.9

Table C4: Pyrolytic product yields for FCR+CSC

Sample	Run 1	Run 2	Run 3	Run 4	Run 5	AVG	Std.dev	Relative Std.dev
Sample mass (g)	25.06	24.82	21.50	24.36	23.96	23.9	1.4	6.0
Char(g)	18.99	18.65	16.31	18.52	16.48	17.8	1.3	7.2
Tar (g)	0.28	0.25	0.23	0.39	0.36	0.3	0.1	23.1
Gas L(g)	2.71	2.65	2.29	2.53	2.27	2.5	0.2	8.1
Gas (g)	3.1	3.3	2.7	2.9	4.9	3.4	0.9	25.7
				Yields (wt. %)				
Y Char	68.1	67.5	68.1	68.3	61.8	67.9	0.4	0.5
Y Tar	1.7	1.5	1.6	2.4	2.2	1.6	0.1	5.2
Y Gas Liquor	0.2	0.2	0.2	0.2	0.1	0.2	0.0	0.8
Y Gas	30.1	30.8	30.1	29.2	35.8	30.4	0.4	1.4
Total conversion	68.1	67.5	68.1	68.3	61.8	67.9	0.4	0.5
				Yields (wt.%) water-free basis				
Y Char	68.2	67.6	68.3	68.4	61.9	68.0	0.4	0.5
Y Tar	1.7	1.5	1.6	2.4	2.2	1.6	0.1	5.2
Y Gas	30.2	30.9	30.2	29.2	35.9	30.4	0.4	1.4
Total conversion	68.2	67.6	68.3	68.4	61.9	68.0	0.4	0.5

Table C5: Pyrolytic product yields for FCRD+CSC

Sample	Run 1	Run 2	Run 3	Run 4	Run 5	AVG	Std.dev	Relative Std.dev
Sample mass (g)	24.92	24.65	23.12	24.19	23.39	24.2	0.8	3.3
Char(g)	16.44	16.14	15.23	16.16	18.39	16.0	0.5	3.3
Tar (g)	0.24	0.35	0.31	0.39	0.45	0.3	0.1	19.8
Gas L(g)	4.63	4.85	4.28	4.07	2.67	4.5	0.3	7.8
Gas (g)	3.6	3.3	3.3	3.6	1.9	3.4	0.2	4.8

Sample	Run 1	Run 2	Run 3	Run 4	Run 5	AVG	Std.dev	Relative Std.dev
				Yields (wt. %)				
Y Char	63.5	63.0	63.4	64.3	75.7	63.6	0.3	0.4
Y Tar	1.1	1.6	1.5	1.8	2.1	1.5	0.3	18.3
Y Gas Liquor	0.2	0.2	0.2	0.2	0.1	0.2	0.0	3.5
Y Gas	35.2	35.2	34.9	33.7	22.1	34.8	0.2	0.5
Total conversion	63.5	63.0	63.4	64.3	75.7	63.6	0.3	0.4
				Yields (wt.%) water-free basis				
Y Char	63.6	63.2	63.5	64.4	75.8	63.7	0.2	0.4
Y Tar	1.6	1.6	1.5	1.8	2.1	1.6	0.1	3.8
Y Gas	35.3	35.3	35.0	33.8	22.1	34.8	0.2	0.5
Total conversion	63.1	63.2	63.5	64.4	75.8	63.6	0.2	0.4

Table C6: Characteristic parameters for pyrolysis of FCR, FCR D, Sl1.9 D, and their blends with CSC.

Compound name	RT	Fit %
FCR		
Toluene	4.3	90
Tribromoethene	12.0	91
Naphthalene	18.0	83
Naphthalene, 1-methyl	19.1	80
FCR Char		
Toluene	4.3	96
Tetrachloroethylene	5.5	89
Benzaldehyde	11.6	92
Tribromoethene	11.96	92

Table C7: A list of FTIR band positions and assignments for FCR, FCR D, SI1.9 D, and their blends with CSC.

Assignment	Position (/cm)	Centre positions (/cm)					
		FCR	FCRD	FCR+CSC	FCRD+CSC	SI19D	SI1.9D+CSC
OH from clay minerals (kaolinite and illite)	3700-3600	3691	-	3694	-	-	-
		3617	-	3620	-	-	-
C–H stretching vibrations: low-molecular aliphatic structures, probably alkanes, aromatic structures	2980-3100	3046	3046	3047	3063	3048	3044
COH stretching vibrations: by C═O–O carboxylic acids, aldehydes and amides	1740-1658	1658	1670	1665	1695	1658	1733

Assignment	Position (/cm)	Centre positions (/cm)					
		FCR	FCRD	FCR+CSC	FCRD+CSC	SI19D	SI1.9D+CSC
C=C and C ··· C: Alkenes and Benzene ring in aromatic hydrocarbons	1500-1600	1591	1587	1593	1595	1589	1584
CH_3 in aliphatic compounds	1450-1400	1443	1426	1446	1454	1433	1435
Si–O–Si vibrations: quartz and silica-based minerals	900-1200	1162	-	1113	-	-	-
		1111	-	1105	-	-	-
		1032	-	1029	-	-	-
Si-C organosilicon compounds	860-720	880	879	886	875	873	877
C-H vibrations by aromatic compounds	850-700	-	814	820	830	819	820

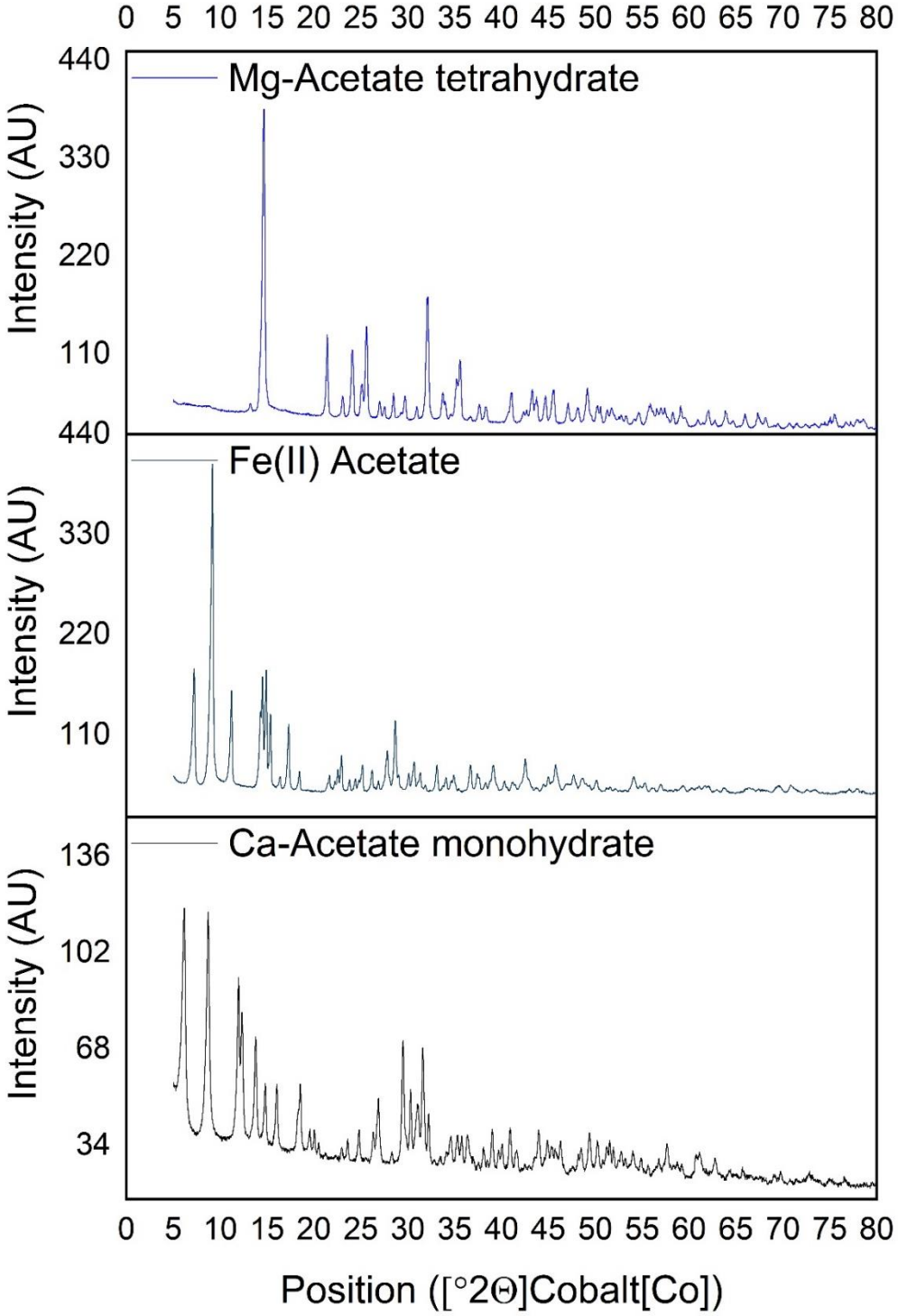

Figure C1: Diffractograms and assignments for the three acetates used in this study.

ANNEXURES D: LEACHING PROCEDURES

D-1: Chemical Fractionation procedure

Chemical fractionation procedure comprised of sequential leaching steps using deionised water, 1 M NH_4OAc and 1M HCl, in that order. In the first step, about 800 g of 100% passing 75 µm coal sample was leached in 2400 mL deionised H_2O at 20 °C ±2 °C for 18 h, agitated at 600 rpm. After leaching, the water and residue were separated via vacuum filtration using a Whatman no 1 filter paper, and the residue was washed with 5 L deionised H_2O or until the pH of the washing water was around 6. The washed filter cake of leached coal was at 105 °C ±5 °C for 24 h. The pH and mass of the leachate were recorded, and a portion was analyzed by ICP-OES. Approximately 60 g dissolved in the water leaching stage.

The residual coal (about 700 g) underwent the second step of leaching with 2100 mL of 1 M NH_4OAc solution at 70 °C ±2 °C for 18 h. After leaching, the water and residue were separated via vacuum filtration using a Whatman no 1 filter paper, and the residue was washed with 5 L deionised H_2O or until the pH of the washing water was around 6. The washed filter cake of leached coal was at 105 °C ±5 °C for 24 h.

Finally, 400 g of H_2O and NH_4OAc-treated coal was leached with 1200 mL of 1 M HCl solution at 70 °C ±2 °Cfor 18 h. After leaching, the water and residue were separated via vacuum filtration using a Whatman no 1 filter paper, and the residue was washed with 5 L deionised H_2O or until the pH of the washing water was around 6. The washed filter cake of leached coal was at 105 °C ±5 °C for 24 h. The final masses, pH, and the leachates were recorded.

D-2: Demineralisation procedure

Demineralisation procedure comprised of sequential leaching steps using 10 M HCl, 22 M HF and 10 M HCl, in that order. In the first step, about 800 g of 100% passing 75 µm coal sample was leached in 2400 mL 10 M HCl at 20 °C ±2 °C for 18 h, agitated at 600 rpm placed in an acid resistant fume hood. After leaching, the HCl and residue were separated via vacuum filtration using a Whatman no 1 filter paper, and the residue was washed with 10 L deionised H_2O. The washed filter cake of leached coal was at 105 °C ±5 °C for 24 h. The pH and mass of the leachate were recorded, and a portion was analyzed by ICP-OES. Approximately 90 g dissolved in the water leaching stage.

The residual coal (about 650 g) underwent the second step of leaching with 2000 mL of 22 M HF solution at 20 °C ±2 °C for 18 h. After leaching, the water and residue were separated via vacuum filtration using a Whatman no 1 filter paper, and the residue was washed with 10 L deionised H_2O. The washed filter cake of leached coal was at 105 °C ±5 °C for 24 h.

Finally, 400 g of H_2O and HCl-treated coal was leached with 1200 mL of 1 M HCl solution at 20 °C ±2 °C for 18 h. After leaching, the water and residue were separated via vacuum filtration using a Whatman no 1 filter paper, and the residue was washed with 50 L deionised H_2O or until the pH of the washing water was around 6. The washed filter cake of leached coal was at 105 °C ±5 °C for 24 h. The final masses, pH, and the leachates were recorded.

ANNEXURE E: KINETIC TRIPLET DERIVATIONS

E-1. Kinetic triplet

The thermal decomposition of coal involves multiple reactions that occur simultaneously. This makes it challenging to describe the reaction mechanism by assessing individual reactions. A simple approach uses overall mass loss or degree of conversion (x) which can be determined using Equation E-1.

$$x = \frac{m_0 - m_T}{m_0 - m_\infty} \tag{E-1}$$

Where m_0 is the initial sample mass, m_T is the sample mass at temperature (T) and m_∞ is the sample mass at the final pyrolysis temperature. The thermogravimetric study is carried out under non-isothermal conditions with a constant heating rate $\beta = {dT}/{dt}$, the rate of decomposition is defined by both the conversion function $f(x)$ and the temperature function $k(T)$. The relationship is depicted in Equation E-2;

$$\frac{dx}{dt} = f(x)\,k(T) \tag{E-2}$$

From the Arrhenius equation, the temperature dependency of the reaction is defined by the rate constant (Equation E-3);

$$k(T) = Ae^{\left(-\frac{E_a}{RT}\right)} \tag{E-3}$$

Where:

k(T) is the reaction rate constant (s^{-1});
A is the frequency factor (s^{-1});
E_a is the activation energy (J/mol);
R is the universal gas constant (J/mol.K); and
T is the temperature (K).

Now, incorporating the heating rate (β) and substituting Equation E-3 into Equation E-2, Equation E-4 is obtained.

$$\frac{dx}{dT} = \frac{A}{\beta}\exp\left[-\frac{E_a}{RT}\right] f(x) \qquad \text{(E-4)}$$

After integrating Equation E-4, we obtain Equation E-5.

$$g(x) = \int_0^x \frac{dx}{f(x)} = \frac{A}{\beta}\int_{T_0}^{T} \exp\left[-\frac{E_a}{RT}\right] dT = \frac{AE_a}{\beta R}\, p(u) \qquad \text{(E-5)}$$

Whereby, $p(u) = \int_0^\infty \exp(-u)/u^2 \quad u = E_a/RT$, and $g(x)$ is the integral from of $f(x)$. The limits of the temperature integral is based on the assumption that no reaction occurs at $T = 0$ and the point where pyrolysis starts ($T = T_0$).

Since there is no explicit solution for $p(u)$, KAS, FWO and Starink methods were developed based on different techniques for approximations of $p(u)$ (Dhyani and Bhaskar, 2018). Substituting the value of $p(u)$ into Equation E-5 and linearising leads to a simplified correlation (Equation E-6), which incorporates the various approximations in the form of constants (S and B).

$$\text{In}\left[\frac{\beta}{\mathrm{T}_x^{\mathrm{s}}}\right] = C_s - \left[\frac{BE_a}{RT_x}\right] \qquad \text{(E-6)}$$

Whereby:

$S = 0$ and $B = 0.457$ for FWO,

$S = 2$ and $B = 1$ for KAS,

$S = 1.8$ and $B = 1.0037$ for Starink.

A plot of $\ln\left|\frac{\beta}{T_x^s}\right|$ against $\frac{1}{T}$ should be linear with $-\frac{E_a}{R}$ as the slope and constant (Cs).

The activation energy (E_a) can be calculated from the slope, but a high coefficient of determination (R^2) must be obtained for satisfactory confidence in the calculated value E_a.